CRYSTAL ALIGNMENT IN SEA ICE

Patricia Jean Langhorne

A dissertation submitted for the degree of

Doctor of Philosophy

in the University of Cambridge

Clare Hall

Cambridge

May 1982

SUMMARY

The c-axes of grains in a sheet of sea ice not only lie in the plane perpendicular to the direction of heat flow but also may align about a particular axis in that plane. It has been suggested that the existence of horizontal temperature gradients or the current at the ice-water interface are likely driving forces for this ordering. In addition to making relevant field observations, we have carried out experiments to discover which factor exerts the greatest influence on the resulting distribution of c-axes.

Apparatus to grow NaCl ice in the presence of a water current has been constructed in the cold room at the Scott Polar Research Institute. Two lengthy experiments have been performed in saline water (34‰), one with a current of $3 cms^{-1}$ beneath the growing ice and a corresponding "null" experiment in which there was no forced flow. Two similar experiments were carried out with brackish water (20‰). The growth rate of the ice and the shape of the ice-water interface at the completion of the experiment were found in all four cases. Vertical and horizontal temperature gradients were measured during the saline experiments and the vertical gradients correlate well with those predicted by a theory for growth rate. Horizontal gradients for all experiments may then be deduced from a knowledge of the slope of the interface and the vertical temperature gradient. No correlation was found between the observed mean c-axis direction and the predicted or measured horizontal temperature gradients. In the presence of a current the mean of the c-axes was found to lie in the direction of the forced flow. In addition, in the saline experiment the columnar grains were tilted upstream into the current, a feature which has been described for metals solidifying in a flowing melt. Where there was no fluid motion the c-axis distribution was significantly less aligned.

As the growth velocity of the ice decreased during the forced flow experiment with a brackish solution, a cellular to planar transition took place at the ice-water interface. The conditions under which this occurred

are in reasonable agreement with a theory for interfacial stability in fluid flow.

The experimental and field observations follow a simple, empirical equation relating the fraction of c-axes aligned in the direction of the current to the time at which the ice solidified. This yields an alignment relaxation time which has been related to the fluid velocity outside the boundary layer. Thus it is possible to predict the direction and strength of the c-axis alignment from knowledge of the mean current. Alternatively, the effective current can be found from the fabrics of the sea ice.

PREFACE AND ACKNOWLEDGEMENTS

The project described in this dissertation was carried out at the Scott Polar Research Institute, initially under the supervision of Dr. P. Wadhams. I am grateful for his support, enthusiasm and encouragement. Latterly, Dr. G. de Q. Robin took charge and I particularly thank him for his guidance and good judgement and for painstakingly wading through the original drafts of this manuscript.

I acknowledge the support of the Natural Enviromental Research Council in providing a research studentship for the first three years of this project. The subsequent two years have been generously supported by a grant from the Office Of Naval Research, U.S.A..

Thanks are also due to past and present members of staff at the Institute who kept night vigil over me while I worked in the cold room and who were pressganged into helping lift slabs of ice, buckets of brine and into mopping floors! I was also touched by the way in which many have rallied to help in the final stages of this dissertation and a special thanks is due to Jill Fredston.

Much of the equipment used in the experiments was borrowed and I am grateful for the generosity of Mr. Williams of Dept. of Anatomy who lent a microtome, Mr.N. Smith of the Institute of Oceanographic Sciences, Wormley, who lent an electromagnetic current meter and Mr Peck of the Dept. of Engineering who lent the electronics for the vane current meter. Mr. Peck also assisted with the running of the laminar flume which was kindly made available for my use by Dr. J. Hunt of Engineering. I am indebted to the laboratory staff at the Dept. of Applied Mathematics and Theoretical Physics who helped me to calibrate the electromagnetic current meter and to Dr. P. Linden for permission to use the wave tank. Iain Hutchison of Dept. of Earth Sciences allowed me to calibrate thermistors on his apparatus.

Many members of the above departments have given their time to talk over my problem and I extend my gratitude to them.

Field work was carried out under the auspices of C-CORE. I am grateful to the members of the field party who supported me, not only in the field, but also while data processing and who helped make Newfoundland a second home. Dr. J. Rossiter, Terry Ridings, Ken Butt and Brian Gamberg deserve a special mention. Members of the SURSAT team and others at Tuktoyaktuk also helped to make this a successful and enjoyable trip.

My laboratory work benefited from observing the experimental procedures of Dr. S. Martin of the University of Washington, Seattle who also allowed me to perform an experiment in his wave tank. I am grateful to Dr. W.F. Weeks of Cold Regions Research and Engineering Laboratory, Hanover, New Hampshire for keeping me on my toes by threatening to perform the same experiment and for supplying me with unpublished papers.

Dr. D.T.J. Hurle introduced me to the world of the materials scientist and sent me off in the right direction in the maze of available literature. He involved me in a seminar and introduced me to workers on similar problems on different materials which, profited me greatly. To him my thanks.

Thanks also to Vernon Squire who struggled to make me a friend of the computer's, who helped with the typing and who has patiently endured life with an experiment. Rob Massom transformed my untidy diagrams into figures of great merit. I am grateful for his skill and paricularily for the cheerfulness with which he coped with my mistakes.

There is no doubt that this dissertation was vastly improved by the sustained interest of Dr. W. Robinson, Dept. of Science and Industrial Research, New Zealand, who brought with him laboratory experience and many new ideas on the approach to my problem. For the many, many hours he has spent, I am very, very grateful.

Finally, it is a pleasure to thank Mr. S. Moore, on whom this project has depended most crucially. He was responsible for keeping my hope alive in the first stages of the experiment, for teaching me the rudiments of

workshop practice, for dealing with cold room breakdowns on any day, at any time and for building the apparatus, with my help. He has also printed the photographs in this thesis.

I declare that this dissertation does not exceed the regulations on length and, unless otherwise stated, is my own work. It has not been submitted for a degree at any other university.

This dissertation is the result of my own work and includes nothing which is the outcome of work done in collaboration.

Patricia Jean Langhorne

CONTENTS

CONTENTS

1. INTRODUCTION AND REVIEW

1.1 Introduction

The addition of salts to water has two effects on the freezing properties which cause the resulting sea ice to differ, quite considerably, from pure ice. Firstly, the freezing point is depressed and becomes a function of salinity. Secondly, sea water freezes over a range of temperatures and the liquid phase may exist within the solid. In addition, salt is rejected at the ice-water interface during freezing and diffuses into the bulk of the liquid at a slower rate than the diffusion of heat to the interface. This causes the brine immediately ahead of the interface to be below its liquidus temperature and the liquid is said to be constitutionally supercooled. In these circumstances, the planar interface is unstable and develops into an array of 2-dimensional cells (also called platelets), the crystal c-axis lying perpendicular to the long axis of the cell (see figure 1.1). Liquid brine is trapped between the platelets and the resulting sea ice laminate consists of alternating layers of pure ice and brine. In sea ice, this fragile region at the interface is frequently called the skeletal layer.

In this thesis we consider the most important factors influencing the orientation of the crystal c-axes of sea ice with an aim to understanding the mechanism by which the c-axes of large areas of sea ice in the Arctic and Antarctic become aligned in a particular direction in the horizontal plane. This alignment is of interest since the mechanical and electromagnetic properties of sea ice are highly sensitive to the inclusion of brine which is controlled by the orientation of the platelets, and thus by the direction of the c-axis. At the time this project commenced, the related field data were extremely inconclusive. This has been rectified, to a large extent, due mainly to the efforts of Weeks and Gow who consider the current at the ice-water interface to be

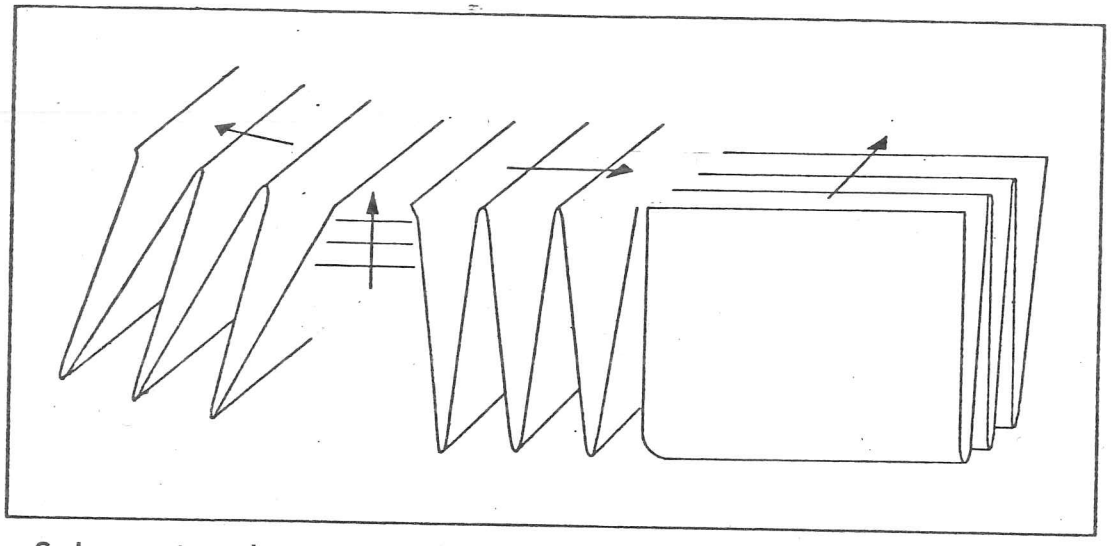

Schematic diagram of cellular interface and the relationship of c-axis to the cells.

FIGURE 1.1(a) Separation between cell tips approximately 0.05cm. C-axis shown by arrow.

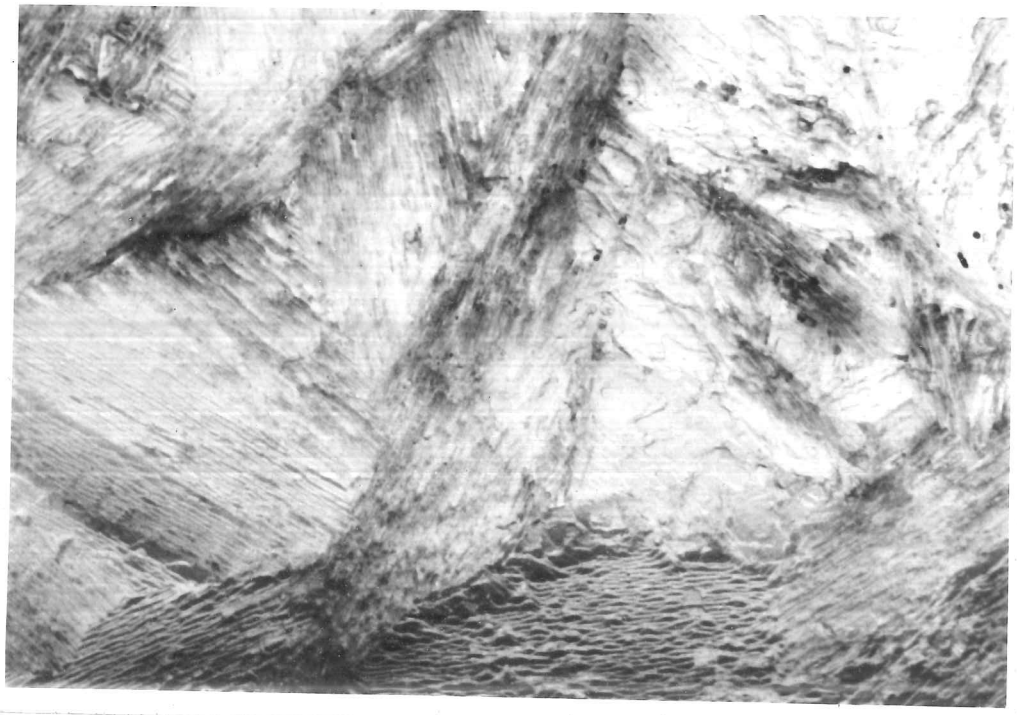

FIGURE 1.1(b) Photograph of the skeletal interface of laboratory NaCl ice, shortly after it was removed from the brine. Spacing between platelets is approx. 0.05cm.

the primary influence. The results of our experiments are in agreement with their conclusions.

In the present chapter we review the development of a sea ice cover and the processes at a cellular interface. Field observations of preferred orientation of c-axes, including our own data, are discussed in chapter 2. Patterns of natural convection and forced flow at the ice-water interface are also examined in this chapter. The kernel of the thesis is contained in chapter 3, where we describe our laboratory experiments on the alignment of c-axes in sea ice. In chapter 4 the results of these experiments are discussed in relation to studies on other materials and in terms of a simple model of the alignment process.

1.2 The formation of an ice cover

The coastline of much of the Arctic and sub-Arctic is ice-free for the short summer months. In the autumn air temperatures drop below freezing and the sea surface begins to cool. However sea ice cannot form until the temperature of the water column above the pycnocline has been reduced to the freezing point since, at salinities greater than 24.7‰, the temperature of maximum density lies below the freezing point. The cooler surface water is thus denser and will sink while warmer, deeper water rises to replace it. In regions, such as the Russian coast, where large rivers have drained into the sea during the summer making the coastal waters brackish (less than 24.7‰), no mixing takes place and freezing can proceed more rapidly (Cherepanov, 1972).

Although there is no doubt that supercoolings of up to 20°C can be achieved in small volumes of calm, dust-free sea water in the laboratory (Farrar and Hamilton, 1965), the existence of supercooling in the ocean is still a matter of some controversy and the presence of thermal convection decreases this possibilty. Reports of thermal supercooling at depth (for example Coachman, 1966) are now viewed with scepticism since small errors in the salinity measurement, neglect of the dependence of freezing point on pressure, and inaccuracies in the expressions for the freezing point as a function of salinity can all lead to apparent supercooling when there is

none. [1] In regions where the water surface is open to the atmosphere, for example in the polynyas of the Antarctic (Chikovskii, 1978), supercooling is more likely and has been directly measured at the surface of an Arctic lead (Katsaros, 1973). Experiments indicate, however, that even in these locations thermal supercooling will be transitory (Bennington, 1963b; Lewis and Lake, 1971; Farhadieh and Tankin, 1972) and once a complete cover has formed the potential for the production of supercooled water is greatly reduced. Nevertheless in laboratory ice grown at low velocities, Wakatsuchi (1974) and Bennington (1963b) have noted a layer of supercooled water which has been formed by the rejection of brine.

The first sign of the formation of ice is the damping of capillary waves by a flexible, almost transparent skim of ice on the water surface. On closer examination we would find that this frazil ice [2] consists of thousands of crystals which have spread out rapidly across the surface, quenching any thermal supercooling. The crystallites will be similar to those which nucleate on the surface of pure water where they take the form of needles or discs, developing into shapes with hexagonal symmetry (for example Arakawa, 1955; Hobbs, 1974). In the ocean this nucleation will occur heterogeneously due to the presence of undissolved matter. A theoretical account of the nucleation of ice is given in reviews by Fletcher (1970) and Hobbs (1974).

The orientations of the crystals in the initial skim depends on their shapes, on the turbulence in the water, and on the possible presence of a thin layer of supercooled water. The initial seeds will expand parallel to their fastest growing direction which, for ice, is perpendicular to the c-axis (Hillig, 1958). In calm conditions, the disc-shaped crystals average 2.5cm in diameter and 0.01-0.1cm in thickness (Weeks, 1958) and float with their c-axes perpendicular to the water surface (Doronin and Kheysin, 1975). When rapid freezing takes place on an undisturbed surface

---

[1] Two determinations of freezing point as a function of salinity differ by approximately 5×10^{-3}°C for typical Arctic salinities (Doherty and Kester, 1974; Fujino et al, 1974)

[2] All terminology used in this thesis follows the descriptions given in the World Meteorological Organisation publication on Sea-Ice Nomenclature (1970).

needle crystals are formed (Bennington, 1968) and, according to Doronin and Kheysin (1975), the c-axes lie in the plane of the water surface.

Under the influence of wind and waves the skim of frazil ice develops in thickness and density to form a suspension up to 30cm thick, called grease ice. The original crystals are rounded by abrasion against each other into tiny plates of ice, 0.1-0.4cm in diameter and 1-100μm thick. They rapidly sinter together in groups, called flocs, which are 0.3-1.0cm across (Martin, 1981). The subsequent conglomerate is equigranular and the c-axes are randomly oriented. If the effects of wind and waves are not substantially dampened by this cover of grease ice, then pancake ice will form (Weeks and Lee, 1958; Martin et al, 1976) or, in more extreme conditions, the crystals will be herded downwind and under the edges of floes in a manner described by Martin (1981). It is common to find consolidated frazil or grease ice in the top few centimeters of any ice sheet but in areas of considerable wind mixing and free ice drift it occupies a much larger proportion of the cover. For example frazil ice comprises a large fraction of the lower portion of the sea ice cover in the marginal ice zone [3] such as the coastal waters of Newfoundland and Labrador (Winsor and LeDrew, 1978), the Greenland Sea (Weeks, 1982), the Bering Sea (Martin and Kauffman, 1981) and in the Weddell Sea (Gow et al, 1982.).

Underwater ice is also a common feature of the Antarctic sea ice. This forms when all the sensible heat has been removed from the water column and consists of large lamellar plates, typically 2-15cm wide and 0.1-0.2cm thick. These protrude downwards from the ice-water interface forming a mesh which traps brine. The c-axis of these crystals is perpendicular to the plane of the plates. The structure and formation of this ice are described by Lewis and Weeks (1970) and Lewis and Milne (1977).

Stalactites have also been observed under sea ice by a number of authors (e.g. Lewis and Milne. 1977) and their formation has been simulated in the laboratory and explained theoretically by Martin (1974).

---

[3] The marginal ice zone is defined by Wadhams (1980) as the ice cover which is close enough to open water to be influenced by its presence.

Having acknowledged the existence of consolidated grease and frazil ice and of underwater ice, a more detailed description of congelation ice [4] will now be given. This type of ice is extremely common in the Arctic where the "crystallinity factor", defined as the ratio of the thickness of congelation ice to the thickness of the entire cover (Buynitskiy, 1967), is 0.90 to 1.0. In the Antarctic this coefficient can have values between 0.15 and 0.87.

Once the initial skim has formed, the growing crystals are no longer able to expand laterally and grains begin to compete for survival during the subsequent downward growth. In the 5-30cm immediately below the initial layer, grains with their c-axis in the plane of the ice-water interface become rapidly predominant. Any preference for the a-axis to lie in the horizontal plane is not nearly so striking (Kawamura and Ono, 1980). The growth velocity decreases because the thickening ice sheet acts as an insulating layer to the cold air temperatures. The grain size increases with the decreasing growth rate and through this thin, so-called transition layer, the grains increase from sizes of the order of millimeters, if there is an initial frazil layer, to sizes of the order of a centimeter. Figure 1.2(a) is a horizontal thin section, photographed under crossed polaroids, showing sea ice close to the base of the transition layer. [5]

Beneath the transition layer,in the columnar zone, the grains become elongated in the direction of the heat flow, as shown in the vertical thin section in figure 1.3, and may extend many tens of centimeters to the bottom of the ice sheet. The c-axes now lie perpendicular to this long axis and are generally only a few degrees off the horizontal plane. The grain size viewed in the horizontal plane also increases, though more slowly than in the transition layer. Paige (1966) and Weeks and Assur (1967) report a roughly linear increase in mean grain length [6] with depth. In

---

[4] By congelation ice we mean ice which has increased in thickness only by freezing at the ice-water interface.

[5] All thin section photographs in this chapter were prepared by the author from sea ice from the coastal waters of the Beaufort Sea.

[6] Grain length is generally measured perpendicular to the c-axis and width is measured parallel to it.

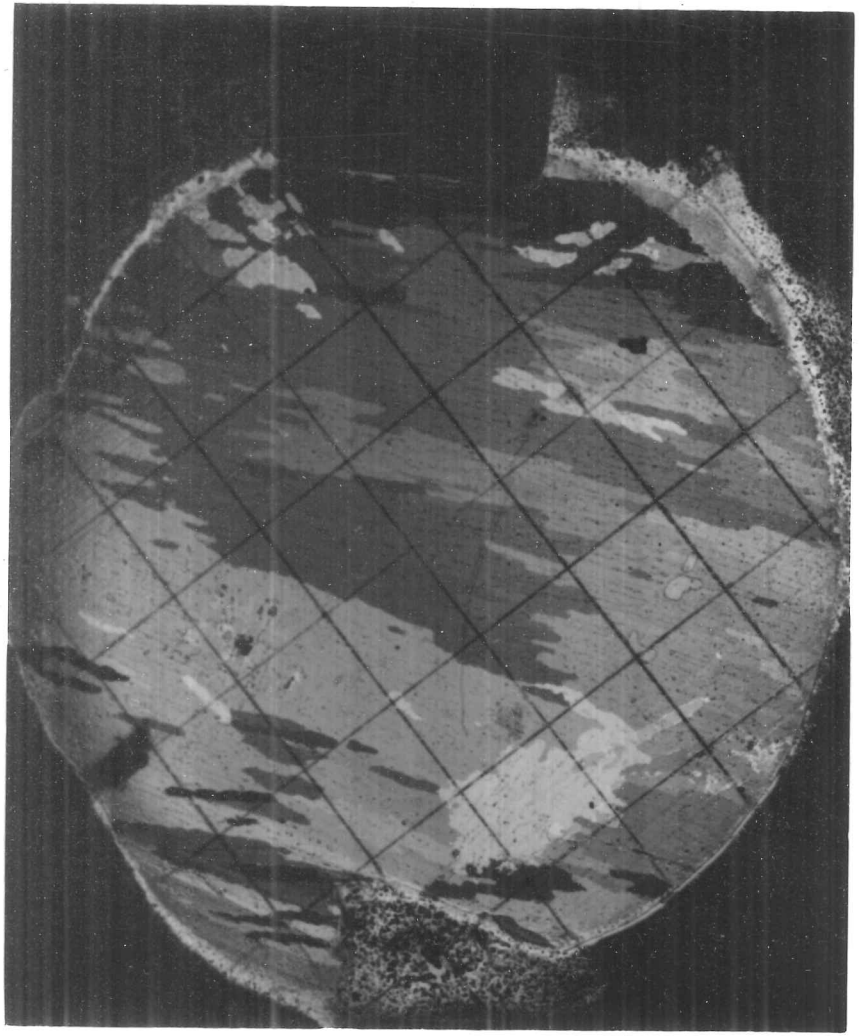

FIGURE 1.2 (b) Horizontal thin section from 100cm below the ice surface near Tuktoyaktuk, Beaufort Sea. Fine black lines separating platelets are brine inclusions. Grid is 1cm square.

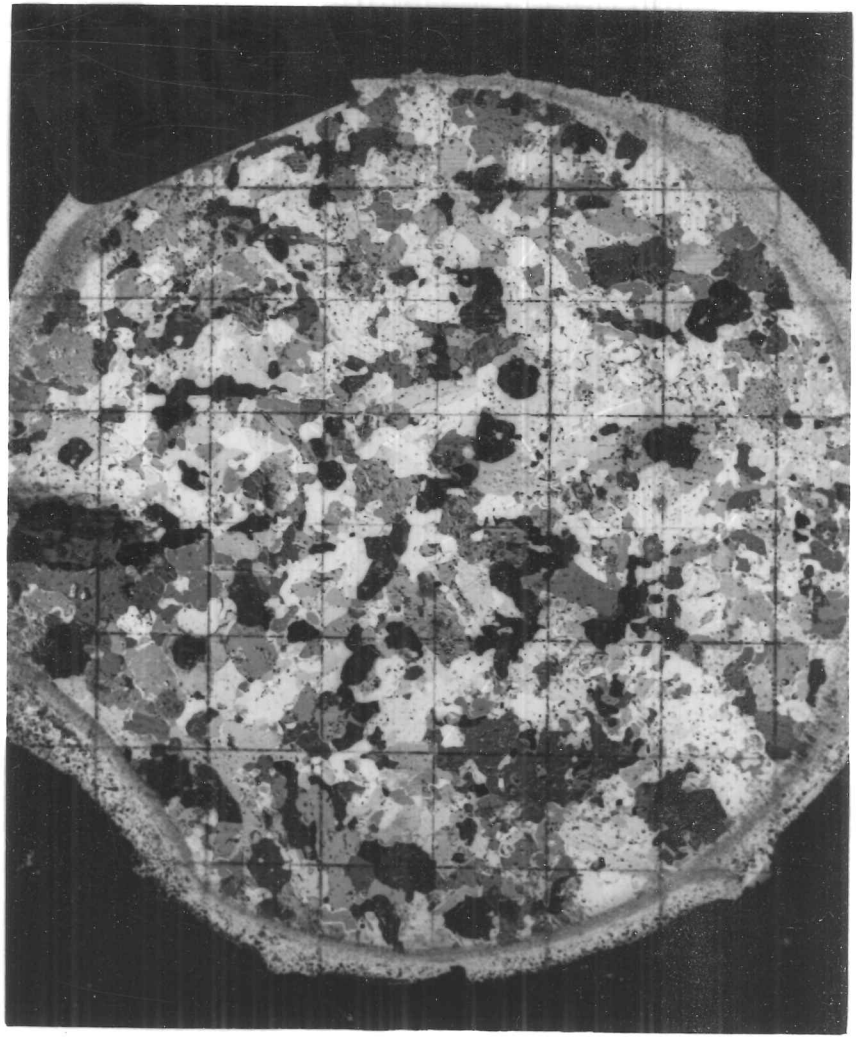

FIGURE 1.2 (a) Horizontal thin section from 10cm below the upper ice surface near Tuktoyaktuk, Beaufort Sea. Sample is near the base of the transition layer. 1cm grid covering section.

Typical crystal size = 0.3 X 0.3 C-axes lie within 30^{o} of the direction of growth.

Noted that all cores broke approximately 15 cm from the surface. At this point, there is a distinct change in the numbers and sizes of air bubbles. Above, the bubbles are roughly spherical, uniformly distributed and occupy a high percentage of the total ice volume. Below the break to the bottom of the core the inclusions are of a variety of irregular shapes, highly localised and much less prevalent. This distinct change is not accompanied by any change in crystal size or c-axis direction, although axes are slightly more randomly distributed.

Typical crystal size = 0.7 X 0.3 C-axes lie both in vertical and horizontal directions. Crystals are now beginning to lengthen in growth direction.

Typical crystal size = 1.6 X 0.3 Maximum crystal size = 3.0 X 0.3 C-axes lie closer to horizontal than vertical but still no distinct preference.

Typical crystal size 3.0 X 0.3 Maximum crystal size = 4.0 - 8.0 X 1.5 The c-axis of the larger crystals now beginning to lie close to the horizontal. Ice now evidently forming columnar crystals elongated along the direction of growth. A number of small crystals interrupt this morphology.

Typical crystal size = 2.0 X 0.3

Typical crystal size = 6.0 X 0.4 C-axes generally close to the horizontal and constant down the length of the section.

Brine inclusions separating platelets of pure ice can be seen running parallel to the long axis of the sample. The number of small randomly orientated crystals has decreased.

Typical crystal size = 10 X 0.5 - 0.7 C-axes almost all very close to the horizontal. Numbers of small, randomly orientated crystals now very small.

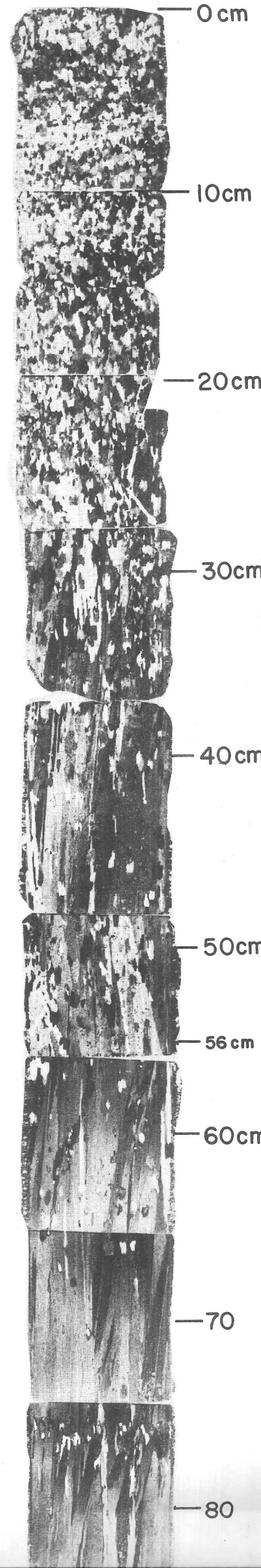

of the total ice volume. Below the break to the bottom of the core the inclusions are of a variety of irregular shapes, highly localised and much less prevalent. This distinct change is not accompanied by any change in crystal size or c-axis direction, although axes are slightly more randomly distributed.

Typical crystal size = 0.7 X 0.3 C-axes lie both in vertical and horizontal directions. Crystals are now beginning to lengthen in growth direction.

Typical crystal size = 1.6 X 0.3 Maximum crystal size = 3.0 X 0.3 C-axes lie closer to horizontal than vertical but still no distinct preference.

Typical crystal size 3.0 X 0.3 Maximum crystal size = 4.0 - 8.0 X 1.5 The c-axis of the larger crystals now beginning to lie close to the horizontal. Ice now evidently forming columnar crystals elongated along the direction of growth. A number of small crystals interrupt this morphology.

Typical crystal size = 2.0 X 0.3

Typical crystal size = 6.0 X 0.4 C-axes generally close to the horizontal and constant down the length of the section.

Brine inclusions separating platelets of pure ice can be seen running parallel to the long axis of the sample. The number of small randomly orientated crystals has decreased.

Typical crystal size = 10 X 0.5 - 0.7 C-axes almost all very close to the horizontal. Numbers of small, randomly orientated crystals now very small.

At 75 cm there is the sudden appearance of a large number of small, randomly oriented crystals. This causes many of the subsequent crystals to grow downwards with long axis about 10^{o} to the vertical for a distance of about 5 cm. The effect of the disturbance is still apparent about 17 cm below its occurrence.

Typical crystal size = 20 X 0.5 C-axes not only lie in the horizontal plane but typically lie in one particular direction in this plane. There is one exception which lies in the horizontal plane but at 90^{o} to the other c-axes.

Typical crystal size = 20 X 1.0 C-axes horizontal and 15^{o} - 30^{o} from the plane of the section.

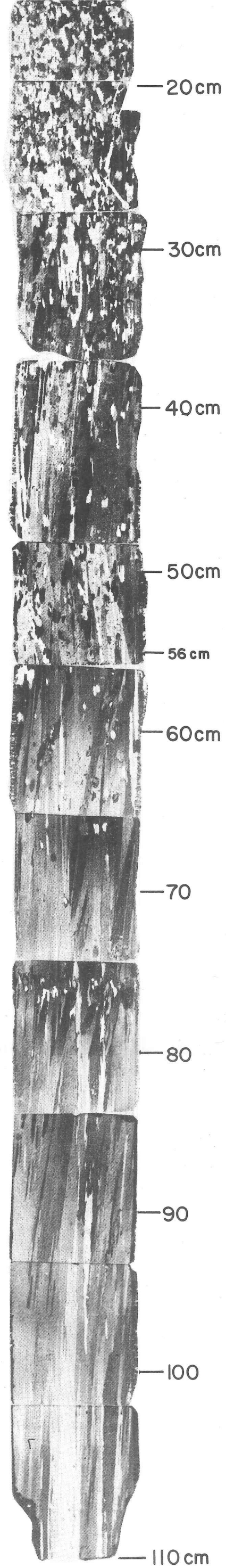

FIGURE 1.3 Vertical thin section through entire ice thickness at Tuktoyaktuk. Crystal dimensions in centimetres. (Reproduced X 0.4)

addition, Weeks and Hamilton (1962) found in 30cm thick Arctic sea ice, that the maximum grain length was approximately twice the maximum width. Similar results were obtained in Antarctica (Paige, 1966) at levels above 120cm, but deeper in the ice the length to width ratio increased to 5:1, indicating that the length increases more rapidly with depth than the width. Indeed it is common, at depths of greater than 100cm, for the grain length in the horizontal plane to be greater than 5cm (figure 1.2(b)). However, as illustrated in figure 1.2(b), determination of the exact size or shape of a sea ice grain is a difficult task since the grains are fragmented and interlocking.

Ice grain structure has been classified according to its size and mode of formation (Michel and Ramseier, 1971; Cherepanov, 1972) but these schemes are not widely used.

A highly idealised picture has been described. In nature there are frequently bands superimposed on the basic structure which may consist of alternating layers of c-axis vertical and c-axis horizontal grains, zones of high porosity or so-called "corrosion bands" formed by brine pocket expansion (Bennington, 1963b).

1.3 The theory of geometric selection

Two of the most striking features of sea ice are the rapid increase in grain size and the tendency for the c-axes to lie predominantly in the horizontal. The development of these features is generally attributed to the process of geometric selection (Shumskii, 1955; Perey and Pounder 1958). The basic postulate is that grains with a growth advantage project slightly further into the melt and are therefore able to grow at the expense of those in unfavourable orientations. In principle, this idea is simple and convincing but it has not been conclusively verified from experimental studies on pure or saline ice and the major factors which cause a grain to be favoured are not well understood.

Given the consistency with which c-axis horizontal fabrics develop in sea ice, it is not surprising that several mechanisms have been identified which select this orientation. The four most important are as follows;

(i)Kinetics of growth Crystallisation on the prism faces takes place considerably faster than on the basal plane. This is common to both sea and pure ice and the differences in the resulting fabrics suggest that this is not the only significant factor.

(ii)Anisotropy of the thermal conductivity The anisotropy of the thermal conductivity in sea ice (Anderson, 1958, 1960) will favour the growth of those grains with their direction of highest conductivity lying in the direction of heat flow (Weeks, 1958); that is, the growth of grains with the c-axis normal to the vertical heat extraction through the sheet of sea ice.

(iii)Transport of solute from the interface Bennington (1963b) pointed out that the interchange of salt-rich brine at the interface is not inhibited by the cells which are oriented vertically. Cells at a large angle to the plane of the interface will form a trap for impurities. This means that the concentration, and hence the temperature, at the surface of a grain are dependent on its orientation.

(iv)Supercooling In the presence of constitutional supercooling, grains with directions of "easiest" growth extending into the melt are at an advantage. However if the supercooling decreases ahead of the interface, then vertically oriented grains become predominant (Shumskii, 1955[64]). Knight (1962a) was able to confirm this hypothesis in pond ice, where impurity build-up caused a planar to cellular transition to take place which was accompanied by a transition from vertically to horizontally oriented c-axes.

Laboratory studies on ice growth in dilute solutions (Kvajic and Brajovic, 1971; Kvajic et al, 1973) suggest that the relative geometry of the basal planes is the most important in determining the survival of certain grains. Although this suggests the growth kinetics may be dominating the resulting orientations, the dependence of the rate of elimination of unfavoured grains on the growth velocity and solution concentration indicates that the supercooling ahead of the interface is also of consequence. The importance of the relative orientations of the cells is illustrated by figure 1.4 which is a photograph of the ice-water interface in the early stages of the growth of NaCl ice in the laboratory. The almost planar face of the c-axis vertical grain grows more slowly than

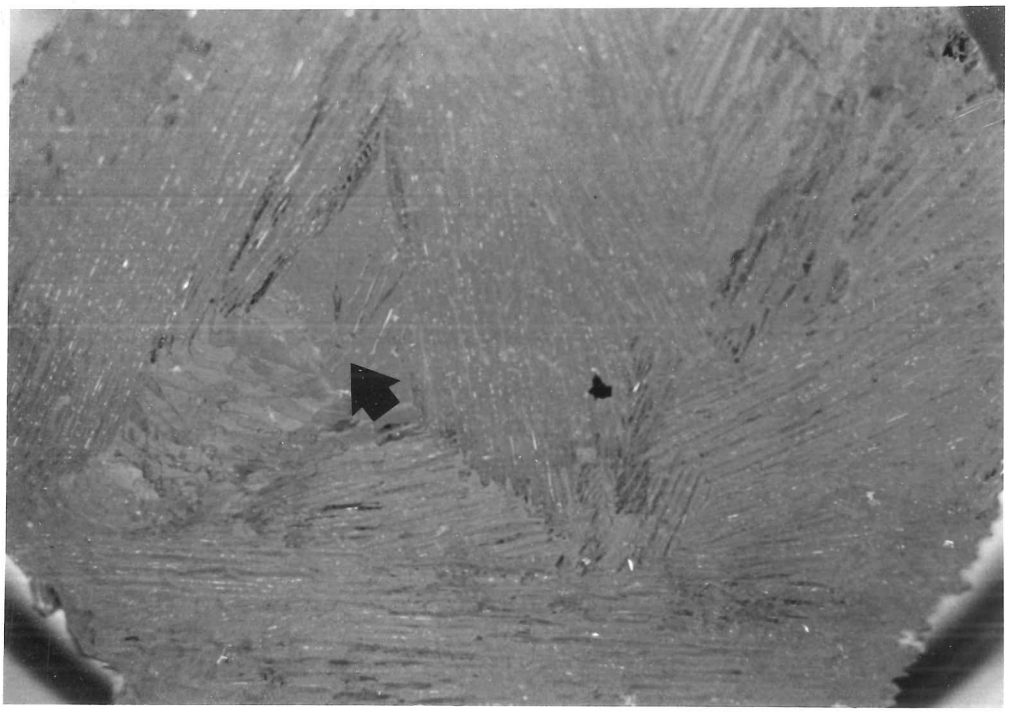

FIGURE 1.4 Photograph showing c-axis horizontal grains with almost vertically oriented cells, encroaching on the planar ice-water interface of the c-axis vertical grain (shown by an arrow).

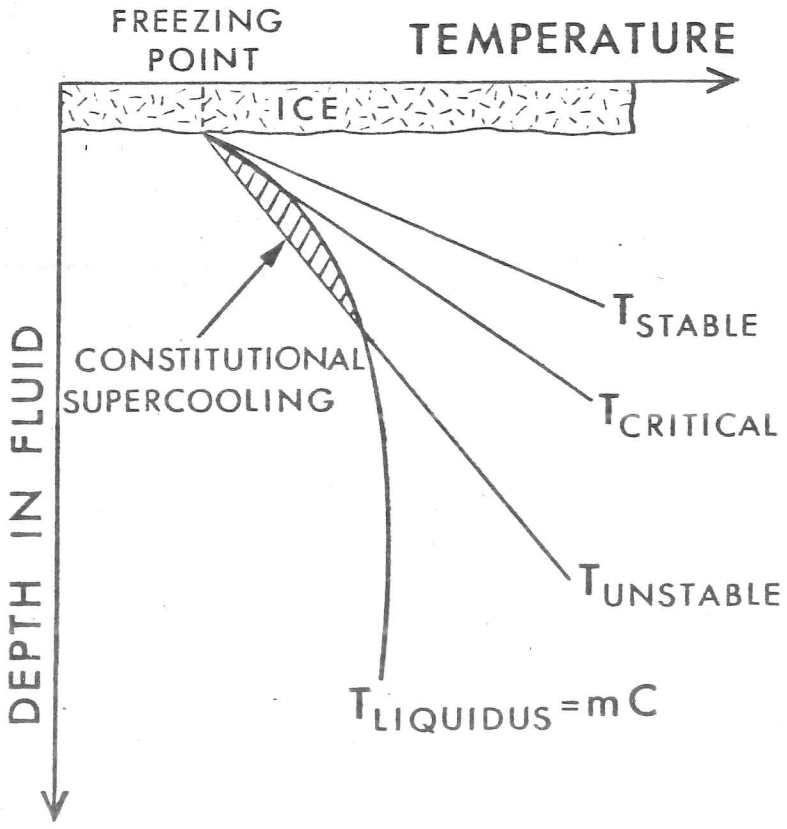

FIGURE 1.5 Diagram showing the temperature profiles in the liquid underneath growing sea ice, which inhibit (T_{STABLE}) and produce ($T_{UNSTABLE}$) constitutional supercooling

the tilted or c-axis horizontal grains which protrude into the constitutionally supercooled region ahead of the interface. The rate of encroachment on the former grain depends on the orientation of its neighbours. Kolmogorov (1949) has formulated geometric selection mathematically and has obtained (Shumskii, 1964),

$$n = A \left(\frac{n_0}{z}\right)^{\frac{1}{2}} . \qquad [1.1]$$

In equation [1.1], n_o and n are the number of grains at the origin and at a depth z from the origin. The constant A depends on the magnitude of the anisotropy in crystal growth. This has never been tested for the growth of grains in sea ice.

However, the observations of a number of authors suggest that the principle of geometric selection is not the complete explanation (for example, the review by Doronin and Kheysin (1975) gives a number of counterexamples). Bennington (1963b) rarely found evidence of selective growth taking place either in the upper 10cm of sea ice or at the boundaries of bands of grains of differing orientations. He concludes that the orientation of a grain depends on the fast growth direction and on the availability of growth material. Cherepanov (1973) also feels that the rules of geometric selection are not obeyed at salinities above 24.7‰ but that they predict the growth of grains in a stable water column. This latter statement is, however, difficult to reconcile with observations on lake ice.

The preferred orientation of the c-axes in pure ice is complicated because the mechanisms governing which grains grow most rapidly do not favour grains of the same orientation as they did in the case of sea ice. That is, the growth kinetics prefer c-axis horizontal grains, while the lack of solute rejection, and hence constitutional supercooling, favours vertically oriented grains. The latter orientation is also predicted from heat flow considerations since the thermal conductivity is slightly greater parallel to the c-axis, if there is any anisotropy at all (Landauer and Plumb, 1956). Thus on frozen lakes, horizontally or vertically oriented c-axes may predominate (Cherepanov, 1968; Knight, 1962a). Knight (1962a) reports that, although his findings on lake

ice are generally in agreement with the theory of geometric selection, he was unable to find any direct evidence of the process occurring. On the contrary, he discovered one instance where a crystal with a tilted c-axis at the ice-water interface was taking over from a c-axis horizontal crystal, despite the fact that the rippled interface of the latter protruded further into the melt.

The earliest experiments to determine the processes involved in the geometric selection of pure ice (Pounder, 1963) yielded inconclusive results. Knight (1966) was also unable to find firm evidence for the wedging-out process and suggested that, in his 3cm thick laboratory ice, fabric development is controlled by grain boundary migration, driven by a reduction in interfacial free energy or by stress of unknown origin. In further experiments, Ketcham and Hobbs (1967) measured slight differences in the interface position of crystals growing in an aggregate. Although they observed that the grain which protruded further into the melt generally encroached upon its neighbour, they were unable to find a systematic relationship between this distance of projection and the relative orientation of the grains. A requirement of the theory of geometric selection is that such a relationship exists. As an alternative, Ketcham and Hobbs (1967) postulate an anisotropy in surface tension and suggest that asymmetrical grain boundary grooves are formed when one grain exposes its low energy basal plane at the growing interface, while its neighbour with a different orientation, exposes a higher energy surface. Accretion then takes place at this boundary in such a way that the grain boundary moves, causing one grain to grow at the expense of another. Ramseier (1968) has proposed a general rule to describe this process. More recently, Jones (1978) has shown that it is not necessary to postulate an anisotropy in solid-liquid interfacial free energy to explain the motion of grain boundaries. If the boundary is inclined to the interface then the grain boundary groove will be asymmetrical and the unequal curvatures will cause freezing on one side of the groove and melting on the other.

1.4 Constitutional supercooling and interface stability

The relative importance of factors influencing the solidification of sea water is rather confusing and to clarify this it is necessary to take a more detailed look at the processes at the interface. As we have seen, the interface of growing sea ice is cellular (see figure 1.1). The conditions under which such an interface develops were originally described by Rutter and Chalmers (1953) and Weeks (1966), among others, has applied the experience of the metallurgists to the case of sea ice.

Solute rejected at the interface diffuses into the liquid, forcing the freezing point of the fluid to follow the salinity profile. However, because the ratio of thermal to solute diffusivity is typically of the order of 370 for Arctic sea water at its freezing point, the actual temperature profile in the liquid can be considered linear over the region that the liquidus temperature is changing rapidly. As shown in figure 1.5, two situations are possible. In the case of the steep temperature profile, T_{stable}, the liquid is above its freezing point everywhere and a planar interface is stable. However, if the actual temperature profile is $T_{unstable}$, then the brine ahead of the interface is below its liquidus temperature and is said to be constitutionally supercooled. The mathematical expression of these ideas follows simply and, where there is no mixing in the liquid, states that constitutional supercooling will be present if

$$mG_{ci} - G_{li} > 0 \quad , \qquad [1.2]$$

that is

$$G_{li}V^{-1} < m(C_{li} - C_{si})D^{-1} \quad , \qquad [1.3]$$

~~where there is no mixing in the liquid.~~ G_{li} and G_{ci} are the vertical temperature gradient and concentration gradient in the liquid at the interface respectively. C_{li} and C_{si} are the concentrations in the liquid and the solid at the interface, D is the diffusivity of solute in the liquid, V is the growth velocity of the ice and m is the slope of the liquidus. Therefore if a projection forms on the interface it encounters a region of constitutionally supercooled water. These projections grow to a

length determined by lateral solute diffusion from the cell tip and heat flow at the cell base (Rutter and Chalmers, 1953). However Mullins and Sekerka (1964) and Sekerka (1965) have shown that the existence of constitutional supercooling is necessary, but not sufficient for the formation of a cellular interface. They have developed a more rigorous theory of interface stability by considering the growth rate of infinitesimal perturbations on the plane surface. Again solute transport equations contain only terms in diffusion. The result of the analysis is that instability is predicted when

$$mG_{ci} - G_{li} > \frac{2K_l}{K_s + K_l} \left\{ \frac{LV}{2K_l} + G_{li} \right\} \zeta - G_{li} \,, \qquad [1.4]$$

where ζ is a stability function which has been shown graphically in Sekerka (1965). K_l and K_s are the thermal conductivities in the liquid and the solid and L is the latent heat of fusion per unit volume.

The linear morphological stability theory of Mullins and Sekerka (1964) has been confirmed indirectly [7] in a series of elegant experiments (Hardy and Coriell, 1968; 1973) on the growth rate of perturbations on ice cylinders. For the case of perturbations of larger amplitude and with coupling between modes, they found it necessary to develop a non-linear morphological stability theory and again they obtained quantitative agreement with experiment. However Weeks (1966) and Lofgren and Weeks (1969) have not been so successful in their attempts to fit their data to theory, since they found instability was predicted in low salinity lakes where a smooth, planar interface was observed. They attribute this discrepancy to the effects of free and forced convection which may delay the onset of morphological instability (Weber, 1977). The influence of the intensity of convection on the solute accumulation ahead of the interface, and hence on the interface stability, has been directly observed in the laboratory (Kvajic et al, 1968). In further experiments, Kvajic and others (1971) were also unable to confirm morphological stability theories but, in this case, they observed the initial features of

---

[7] These experiments predicted values of ice-solution surface tension which agree with those from other sources

instability where a planar interface was expected. To explain this they suggest that stability may not be independent of the crystallography.

We may conclude that the theories for constitutional supercooling and morphological stability are successful, but that their application to sea ice is complicated by the presence of natural convection and by grains growing parallel to the c-axis. However, under almost all conditions, the ice-water interface in sea ice is unstable and a cellular structure develops.

1.5 The segregation coefficient at a planar interface

The development of a cellular interface hinges on the fact that there is a salt enriched region just ahead of the freezing interface. This salt is rejected at the freezing interface which we assume to be planar in the present section. In the next section we consider the inclusion of brine in pockets when a cellular interface develops.

The rejection of salt at the interface is governed by the equilibrium segregation coefficient [8] which is defined as

$$k_e = {}^{C_{si}}/_{C_{li}} \quad . \qquad [1.5]$$

This assumes that equilibrium exists between the phases. The segregation coefficient is a measure of the distortion which the solute imposes on the molecular arrangement of the solid, values close to 1 indicating little distortion (Hobbs ,1974). It depends critically on impurity (Burton et al, 1953) and we might expect different values for each of the ions in sea water. For example, the chloride ion enters the lattice substitutionally (Gross et al, 1977) and a segregation coefficient, which is slightly higher than that of the sodium ion is anticipated. This dissimilarity can cause large electrical potential gradients to build up at the ice-brine interface in dilute NaCl solutions

---

[8] The segregation coefficient can also be called the partition or distribution coefficient

(10^{-6} - 10^{-4} molar) [9] and is termed the Workman-Reynolds effect (see Hobbs (1974) and Gross et al (1977) for further discussion of this effect).

In general, k_e is a function of concentration (Gross et al, 1975) unless the liquidus and solidus lines on the phase diagram are straight and emanate from the freezing point of the pure liquid. The phase diagram of NaCl does not satisfy this condition, but the experiments of Gross and co-workers (Gross et al, 1977) have shown that, for 10^{-6} to 10^{-2} molar solutions, this concentration dependence may be ignored. In these experiments the segregation coefficients were found in the presence of forced flow and the results are thus free from the apparent concentration dependence which natural convection can introduce (Seidensticker, 1972). The molarity was sufficently low for the ice to grow with a planar interface, giving

$$k_e = 2.7 \times 10^{-3} \quad .$$

This is remarkably similar to the value deduced by Weeks and Lofgren (1967),

$$k_e = 2.5 \times 10^{-3} \quad ,$$

from extrapolation of their results on the velocity dependence of the effective redistribution of brine during cellular growth, to the limit of infinitesimally small growth rates.

Generally it is not possible to measure the concentration at the interface and it is therefore useful to define an effective distribution coefficient,

$$k_{eff} = {}^{C_{si}}/_{C_\infty} \quad , \qquad [1.6]$$

where C_∞ is the concentration in the bulk of the liquid. The value of k_{eff} is not a constant but depends on the mode of transport of solute from the interface to the bulk of the liquid. Burton and others (1953) have found

---

[9] Sea water in Arctic regions is equivalent to 0.5 molar solutions.

the expression

$$k_{eff} = \frac{k_e}{k_e + (1-k_e)\exp(-V\delta_c/D)} \quad , \qquad [1.7]$$

relating k_{eff} to k_e. This assumes that stirring in the liquid is such that the concentration is constant outside a solute boundary layer, δ_c, while solute transport is purely diffusive within this zone.

1.6 Solute redistibution in cellular growth

1.6.1 Brine pocket formation

In all but the purest lakes, the major portion of the salt content of the ice is enclosed in pockets and channels containing brine. Brine pockets can be seen, in figure 1.2(b), in rows parallel to the (0001) planes of the almost pure ice platelets. This dependence of brine inclusion on the crystallography is explained with reference to figure 1.6 which illustrates the skeletal layer of a growing ice sheet. Since the equilibrium segregation coefficient is very small, most of the salt from the solidifying solution is rejected at the platelet boundary. Although it can be quite readily transported away from the tip, higher up in the intercellular groove the brine becomes trapped. If we assume that the ice and brine at the interface are at the equilibrium freezing point and that the freezing point is a linear function of salinity, then the concentration must increase towards the root of the groove. This increase can only be achieved by freezing on the cell walls and, as a result, the grooves shrink. According to Anderson and Weeks (1958) and Assur (1958), a critical groove width is reached at which surface tension forces cause "necking" to occur and the brine layer forms a cylindrical tube and finally a pocket, as demonstrated in figure 1.6 . As the ice thickens, the brine within the pockets becomes colder and freezing occurs on the inner walls, making the solution more saline. As the eutectic temperatures of each of the species is reached, solid salts will crystallise out of solution. Anderson and Weeks (1958), Lake and Lewis (1970) and others have

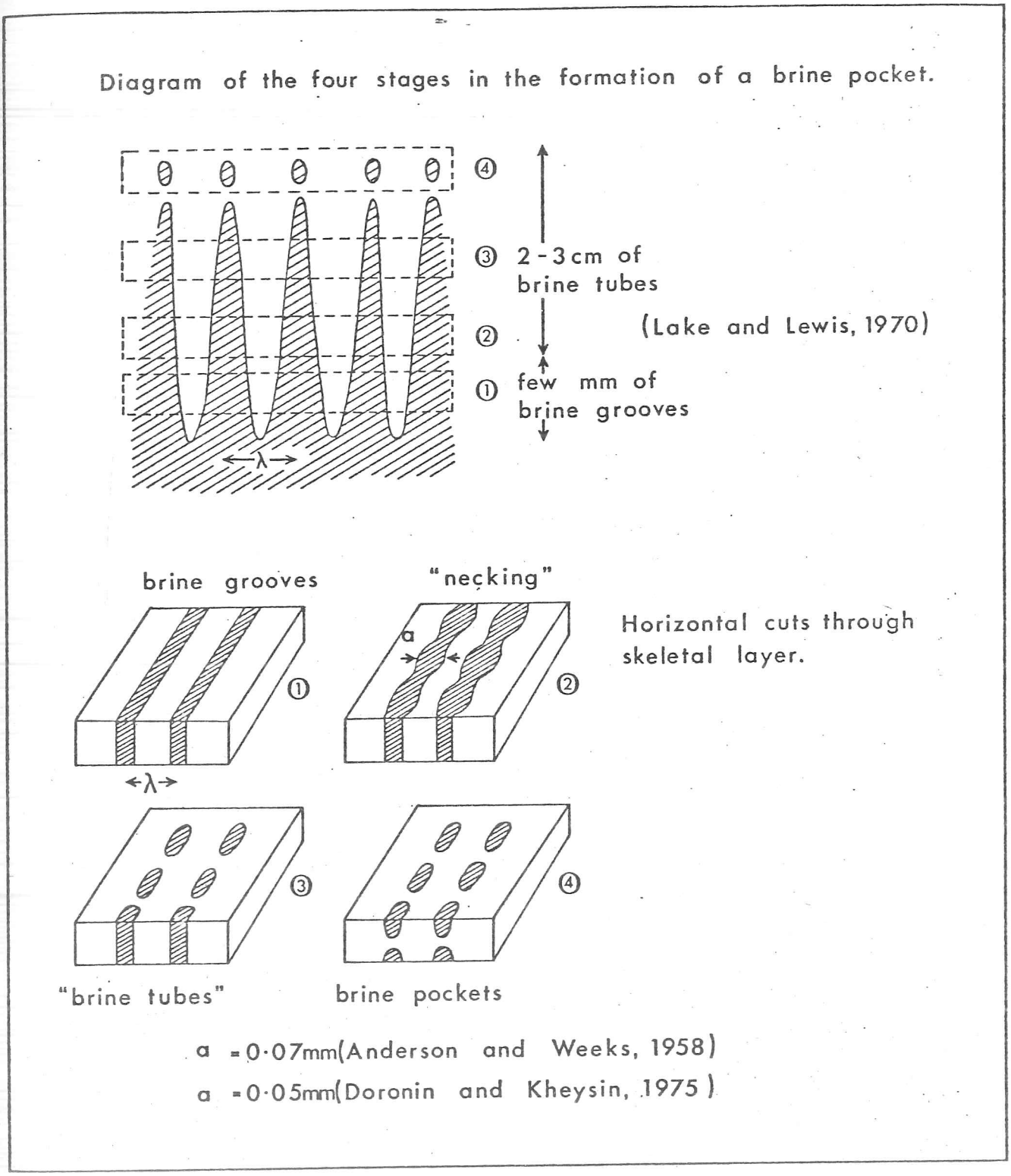

FIGURE 1.6 The skeletal layer is pictured in the top half of the figure with the horizontal cuts, (1) to (4), shown by dotted lines. The proportion of brine present in (1) to (4) is shown in the lower portion of the figure. Regions of brine are shaded.

made a number of measurements on the geometry of these grooves, tubes and pockets and some of these are given in the figure 1.6. This is a highly idealised picture and in reality the majority of the brine inclusions are irregular in shape and are present at boundaries parallel to the c-axis as well as perpendicular to it (Sinha, 1977). Sinha (1977) gives good examples of these features at high magnification and, by examining replicas of thin section surfaces with a scanning electron microscope, has succeeded in producing impressive photographs of the crystallisation of salts in a brine pocket.

Considering only solute diffusion, the prediction for the depth of the cell boundary groove in sea ice is excessively large unless the existence of the eutectic at the root of the cell is postulated. This is rather an unrealistic assumption which may be unnecessary if convection within the skeletal layer is considered. Lake and Lewis (1970) have observed temperature fluctuations within the bottom few centimeters of a growing ice sheet which they attribute to such convection. They suggest that this overturning is responsible for the formation of brine pockets, hypothesising that each tube has a stagnant end cap which will be sealed off when the cold, dense, descending brine is replaced by water of higher freezing point. However this fails to explain brine pocket formation in the upward growth of saline ice (Kvajic et al, 1973) and, although overturning may be important in certain circumstances, we do not believe it is primarily responsible for brine enclosure. While studying convection in the region of the ice-water interface, Niedrauer and Martin (1979) have directly observed the formation of brine pockets from brine tubes but they do not discuss the method of formation.

1.6.2 The segregation coefficient during cellular growth

The problem of quantifying impurity inclusion during cellular solidification is much more complex than its counterpart for a planar interface. The equilibrium partition coefficient is no longer a useful parameter since C_{li} will vary around the cell boundary and we are forced to use the effective distribution coefficient. Even if macrosegregation (such as the formation of brine pockets), convection in the fluid and the

interaction between cells are ignored, it is found that k_{eff} is a function of interface curvature and growth velocity (Harrison and Tiller, 1963a). If the latter restriction is lifted, the concentration in the solid will increase from the cell centre out to the boundary which is a reflection of the fact that the fluid in the intercellular grooves becomes more concentrated as the grooves shrink. When a brine pocket forms, the inhomogeneities in solute concentration in the solid increase further, as shown schematically in figure 1.7.

It is not surprising that experiments, designed to find a relationship between the effective segregation coefficient and the growth parameters, have firstly, averaged over a number of intercellular grooves and secondly, made no attempt to describe the mechanism of salt entrapment. Weeks and Lofgren (1967) have fitted ice salinity and growth velocity data to the expression of Burton et al (1953) (equation [1.7]). The agreement between theory and experiment is surprisingly good considering that the theory describes the segregation at a planar interface and the data were collected in a cellular regime.

A weakness of the experiments of Weeks and Lofgren is that the measured salinities were not the values at the time of formation because of brine drainage from the ice. This difficulty was overcome by Cox and Weeks (1975) who, by tagging the solution with radioactive Na, have recorded salinity profiles at specified times and positions without destroying the sample. Again the data were in good agreement with equation [1.7], yielding a value of " δ_c/D" which is higher than that found by Weeks and Lofgren ~~authors~~. These are

$$k_{eff} = \frac{0.26}{0.26 + (1-0.26)\exp(-\frac{V\delta_c}{D})} \quad , \qquad [1.8]$$

$$\delta_c/_D = 5090 \text{scm}^{-1}, \quad 10^{-5} > V > 5\text{x}10^{-3} \text{cms}^{-1}$$

Weeks and Lofgren (1967)

$$\delta c/_D = 7243 \text{scm}^{-1}, \quad 3\text{x}10^{-4} > V > 2\text{x}10^{-5} \text{cms}^{-1}$$

Cox and Weeks (1975)

These expressions are useful in the calculation of initial salinity

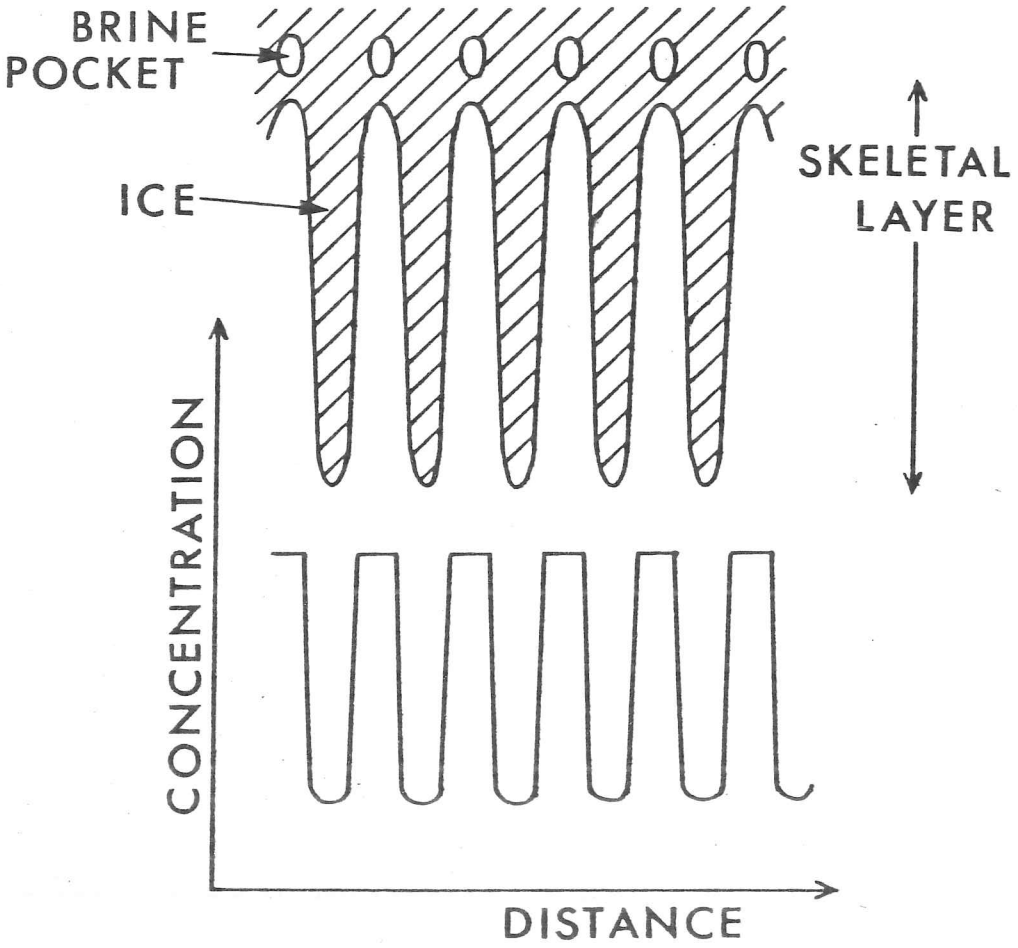

FIGURE 1.7 Schematic representation of the concentration of solute in a horizontal cut through the solid, just above the roots of the intercellular grooves. There is a sharp increase in concentration from the centre of the cell, out towards the edge.

profiles but the parameters derived from fitting data and theory are of little physical significance.

However the situation is not so simple as the preceding expressions might imply. Using radioactive Cs as a dopant, Kvajic and others (1968) and Kvajic and Brajovic (1970) studied the effects of freezing ice both upwards and downwards and found that, in some complicated manner, the effective segregation coefficient was dependent on the growth velocity, the initial concentration in the liquid and the intensity of convection. The picture is made still more baffling by reports of a relationship between effective segregation coefficients and the temperature gradient in the liquid (Fertuck et el, 1972) and by the observation that salinity differences of 1-2‰ can occur because of the dependence of brine entrapment in crystallography (Bennington, 1968).

Therefore we conclude that the expressions in [1.8] are extremely useful as an approximate description of solute entrapment, provided we recognise that they are a simplification of an extremely complex process and provided we do not require an accuracy greater than a few parts per thousand.

1.7 Growth kinetics and surface tension

In the ~~preceding chapters~~ preceding sections we have concentrated on some of the peculiarities that the presence and motion of impurities introduce during the freezing of sea water. In contrast two properties of the ice-water interface which are not severely influenced by the presence of impurities will now be discussed.

1.7.1 The kinetics of growth

The manner in which atoms attach themselves to a solidifying surface is determined by the roughness of the interface on the atomic scale, the imperfections in the crystal and the rate of growth. In ice, the diffuseness of the interface depends on the crystallographic plane

presented at the interface and the kinetics of solidification on the c and a-axes may therefore differ. In principle, the mechanism of attachment can be deduced from the functional relationship between the growth velocity and the supercooling in the liquid, the rate being given by the kinetic coefficient. The results of numerous experiments on pure ice (see Fletcher (1970) and Hobbs (1974) for reviews) suggest that growth perpendicular to the c-axis proceeds by the propagation of layers across the crystal surface, atoms attaching themselves at the step where a screw dislocation emerges at the interface. Direct observation by Ketcham and Hobbs (1968) of spiral steps on the ice-water interface further support this conclusion, although some features of their experiment are difficult to explain. Hillig (1958) and Michaels and others (1966) have examined growth parallel to the c-axis and have found growth velocities of the order of 100 times smaller than those in the perpendicular direction. This led them to hypothesise that two-dimensional nucleation, requiring the formation of an embryo of critical size, may be limiting growth in this direction. However if the crystal is imperfect, a screw dislocation mechanism is again operative.

The addition of solute unexpectedly gives rise to an enhancement in the growth rate of a single crystal in a quiescent melt. It has been speculated that solute adsorbtion on the crystal faces could increase the kinetics of solidification (Hobbs, 1974). However the experiments of Huang (1975) show that this anomalous effect disappears when freezing takes place in the presence of a forced flow of sufficiently high velocity. This suggests that natural convection is the dominant factor, swamping all other possible effects.

Attempts have been made to measure the interface kinetic coefficient for solutions, including NaCl, by experiments on the migration of liquid droplets through ice (Jones and Chadwick, 1971, Jones, 1973a) and on the stability of ice cylinders (Hardy and Coriell, 1973). However these workers have assumed different kinetic laws and no conclusions can be drawn from these studies.

It is now generally accepted that there is a large anisotropy in growth kinetics of ice, despite the fact that attempts to measure the resultant difference in interfacial temperature of grains oriented at right angles have failed (Ketcham and Hobbs, 1969a). It follows that the kinetics of growth will play a major role in the formation of the horizontal girdle distributions of c-axes which are characteristic of lake and sea ice. Nevertheless this will not be true when the rate limiting process is the transport of heat or solute.

1.7.2 The ice-water interfacial energy

Early values of the solid-liquid interfacial energies for pure water were deduced from nucleation data. However recent theoretical developments have allowed investigators to arrive at it by more direct means, such as the measurement of grain boundary grooves (Ketcham and Hobbs, 1969b; Jones, 1973b; Hardy, 1977) and by employing morphological stability theory (Hardy and Coriell, 1968; 1973). In addition to the experimental results, two indirect methods of estimating the ice-water surface energy exist (see for example Pruppacher and Klett, 1978), both of which yield values within the spread of experimental observations and both of which predict that the surface energy is less on the basal plane. This has been tentatively confirmed in measurements of the asymmetry of grain boundary grooves (Ketcham and Hobbs, 1967).

The ice-water-NaCl system has been studied by Hardy and Coriell (1973) and Jones (1973b) and Jones reports a linear increase in ice-solution surface energy with concentration of $2 \times 10^{-8} Jcm^{-2} ‰^{-1}$.

The ice-solution surface energy is particularly important at the cell tip and root where the curvature is large and is required in stability calculations. From consideration of the above sources, we shall subsequently take an ice-NaCl solution surface energy of $3 \times 10^{-6} Jcm^{-2}$ in this thesis.

1.8 Cell shape and spacing

Having provided some of the physical concepts behind the formation of the skeletal layer, these ideas shall now be applied towards an understanding of the shape and separation of the cells.

Although it has been shown that the platelet length and width increase simultaneously, the scatter in the data makes it difficult to determine a functional relationship between these two quantities (Weeks and Hamilton, 1962). However the length is 2 to 3 times greater than the width (see figure 1.2(b)) and this elongation is easily explained in terms of the growth kinetics since any perturbation on the surface will rapidly expand in the plane perpendicular to the c-axis. Dendritic side-branching on these cells has been noted in the laboratory but not in samples from the ocean and is thus characteristic of unnaturally large, experimental temperature gradients (Harrison and Tiller, 1963b) or concentration gradients (Rohatgi and Adams, 1965). Likewise cells on c-axis vertical grains have never been observed in nature, although they have also developed on laboratory ice in rather extreme conditions (Harrison and Tiller, 1963b).

As discussed in section 1.7.1, the depth of the intercellular grooves seems to be determined either by the overturning of brine or by spherodisation due to surface tension. The latter occurs some distance from the cell tip where the groove has reached a critical minimum width. This distance, in turn, should be determined by the temperature gradient. However, Weeks and Anderson (1958) were unable to find any relationship between skeletal layer thickness and vertical temperature gradient. The thickness of this layer as a function the growth parameters has never been systematically studied.

The shape of the cells has been calculated by Bolling and Tiller (1960), neglecting fluid motion, but again there are no experimental results with which to compare the theory.

In comparison with the other dimensions of the cell, platelet spacing [10] has received a great deal of attention. This is partly because a single core preserves a record of these values throughout the growth season and because it is a measure of the spacing between brine layers and is therefore of fundamental importance in the structural models of the mechanical properties of sea ice (Weeks and Assur, 1963). It has been frequently measured as an adjunct to other studies. However we shall discuss only the investigations which have attempted to relate this spacing to the growth parameters. There is general agreement that the platelet spacing increases as the growth velocity decreases but the exact form of this dependence has not been resolved.

One of the earliest studies (Weeks and Hamilton, 1962) which brings together data from NaCl ice and sea ice, gives a linear dependence of platelet spacing, λ, on growth velocity, that is

$$\lambda = A' + AV \qquad [1.9]$$

where A and A' are constants which will take different values in the expressions presented here. However from the work of the metallurgists the expected relationship is of the form (Assur and Weeks, 1964)

$$\lambda V^{\frac{1}{2}} = A \qquad [1.10]$$

The NaCl-ice data of Assur and Weeks (1964) fitted this latter expression reasonably well but, least squares regression yielded

$$\lambda V^{\frac{1}{2.7}} = A \qquad [1.11]$$

Assur and Weeks (1964) derived a very simple expression giving λ as a function of the depth below the ice surface, z, to the power of 0 or $\frac{1}{2}$, ~~respectively~~ for the thin or thick ice limits respectively. From measurement, Weeks and Assur (1963) determined

---

[10] The platelet spacing is measured parallel to the direction of the c-axis from the centre to centre of adjacent pure ice plates.

$$\lambda = A\, z^{\frac{1}{6}} \qquad [1.12]$$

It is of little significance that the empirical power of z lies between the calculated bounds. In thick Antarctic sea ice, Paige (1966) found that the platelet spacing increased in a roughly linear manner with depth from the top of the ice sheet where λ = 0.04cm to λ approximately equal to 0.1cm at 300cm depth.

The most detailed studies to date are those of Rohatgi and co-workers (Rohatgi and Adams, 1965; Rohatgi and Adams, 1967a,b,c; Rohatgi et al 1968) and Lofgren and Weeks (1969).

Rohatgi and Adams (1965) observed that the platelet spacing responds to the conditions at the time of formation either by divergent growth, which coarsens the structure, or by branching, which results in a finer platelet spacing. They therefore suggest (Rohatgi and Adams, 1965, 1967a,c) that the spacing evolves in such a way that the constitutional supercooling, ΔT, in the intercellular grooves does not exceed a certain value, given by

$$\Delta T = m\Delta C = \frac{\lambda^2 m C_o}{8D} \cdot \frac{dS}{dt} \quad . \qquad [1.13]$$

C_o is the initial concentration in the fluid and $\frac{dS}{dt}$ is the rate of change of the fraction solid at a given level. From heat conduction analysis, Rohatgi and Adams (1967b) find that each depth in the ice is subjected to a spectrum of freezing rates and that

$$\left(\frac{dS}{dt}\right)^{max} \propto \frac{1}{z^2} \quad . \qquad [1.14]$$

In NaCl ice, they have also shown experimentally that

$$\lambda \propto z \quad , \qquad [1.15]$$

and

$$\lambda \propto C_o$$

Combining equations [1.13] to [1.15] leads to the conclusion that the

intercellular supercooling is independent of freezing rate [11] but increases rapidly as the concentration increases.

Lofgren and Weeks (1969) found it physically unrealistic to allow the spacing to be controlled by the supercooling deep in the groove and instead favoured the theory of Bolling and Tiller (1960), which focuses attention on the motion of the cell tip under diffusion. In simplified form the predictions are

$$\lambda V = A \text{ for small velocities}$$

$$\lambda V^{\frac{1}{2}} = A \text{ for large velocities}$$

In fact, for all but high velocities, the predictions of Bolling and Tiller are close to those of Rohatgi and co-workers. However, the experimental data of Lofgren and Weeks confirm the theory only in cases where convection is thought to be minimal. Instead, the best fit to their data is given by the expression

$$\log(\lambda V) = \log A + A'(\log \frac{1}{V})^2 \qquad [1.16]$$

The conclusion of Lofgren and Weeks reflects the theme that recurs in this chapter; viz that convection under-ice cannot be ignored. Indeed, the mathematical formulation of cell spacing, even in cases of pure diffusion, has not been undisputedly resolved.

---

[11] The freezing rate, $\frac{dS}{dt}$, is a function of the growth velocity, V and the temperature gradient in the liquid, G_{li}, through

$$\frac{dS}{dt} = \frac{V}{C_o} \frac{G_{li}}{m}$$

1.9 The bulk properties of sea ice

Most of our discussion has focused on processes at the ice-water interface. However, for the remainder of this chapter we shall provide a background in some of the bulk properties of sea ice. The phase diagram is fundamental to the understanding of these properties.

1.9.1 The phase relations in sea ice

At a given temperature, sea ice in equilibrium will contain certain proportions of ice, brine and solid salts. Assuming that the ratios of the impurities in sea ice are the same as in standard sea water, Assur (1958) and Anderson (1958) have independently constructed a phase diagram for sea ice. The assumption of species-independent brine entrapment has subsequently been confirmed by Bennington (1963a) and Addison (1977). Assur has used this diagram to deduce a table of the volume of brine in sea ice, at a given temperature and salinity from which Frankenstein and Garner (1967) have formulated equations for brine volume. Since the work of Assur, the liquid brine content within saline ice has been measured directly by means of a nuclear magnetic resonance spectrometer (Richardson and Keller, 1977; Richardson, 1977; Mel'nichenko et al, 1979) and brine volumes have been revised for temperatures below -23° (Nazintsev, 1974). The brine volume is the most important variable in determining the mechanical (Weeks and Assur, 1967) and electromagnetic (Vant, 1976) properties of sea ice. To calculate it the salinity and temperature within the sea ice sheet must be found. Much effort has therefore been directed towards measuring and understanding the form of the salinity profile.

1.9.2 Salinity and desalination

In cold conditions [12] the salinity, which decreases rapidly during the first week after ice formation at any level, reaches a value at which

---

[12] By this we mean air temperatures below about -10°.

it subsequently remains (Nakawo and Sinha, 1981). [13] Young sea ice is typically between 5 and 10‰ increasing towards the top and bottom of the ice sheet to form the characteristic C-shaped profile (Malmgren, 1927; Weeks and Lee, 1958; 1962). However the exact form of this profile not only depends on age but also varies with location and ice type. For example, the salinity distribution is dependent on ice topography (Cox and Weeks, 1974) and, even if measurements are taken at closely-spaced locations there is considerable scatter in the results (Weeks and Lee, 1962).

A limited number of the features can be explained by equation [1.8], describing the initial entrapment of brine. For instance, the high salinity close to the upper ice surface is predicted by [1.8] because of the large growth velocity at the time this ice solidified. However desalination is the major influence on the distribution of brine. The mechanisms by which this occurs are described in detail in Untersteiner (1967) and Cox and Weeks (1975) and three are briefly dealt with below. The fourth, gravity drainage, is investigated more thoroughly since it contributes to under-ice water motion.

(1)Brine pocket migration; historically this was the first method of desalination to be recognised. Brine pockets move up the temperature gradient at a rate determined by the diffusion of solute in the brine, melting occurring on the warmer side of the enclosure and freezing on the colder. Subsequent studies have shown that the droplet's velocity is rather complicated (Harrison, 1965) and that this migration is a very minor contributor to the reduction in the salinity of sea ice (Kingery and Goodnow, 1963).

(2)Brine expulsion; this mecanism was first suggested by Bennington (1963b), who realised that, because of expansion due to freezing within the brine pockets, tiny cracks appear in the ice. Brine can then escape both upwards and downwards, frequently causing a high salinity surface layer on young sea ice (Cox and Weeks, 1974; Martin, 1979).

---

[13] Fluctuations of the order of ± 1‰ take place around the mean stable salinity, which is observed to decrease at approximately 0.5‰ per month.

it subsequently remains (Nakawo and Sinha, 1981). [13] Young sea ice is typically between 5 and 10‰ increasing towards the top and bottom of the ice sheet to form the characteristic C-shaped profile (Malmgren, 1927; Weeks and Lee, 1958; 1962). However the exact form of this profile not only depends on age but also varies with location and ice type. For example, the salinity distribution is dependent on ice topography (Cox and Weeks, 1974) and, even if measurements are taken at closely-spaced locations there is considerable scatter in the results (Weeks and Lee, 1962).

A limited number of the features can be explained by equation [1.8], describing the initial entrapment of brine. For instance, the high salinity close to the upper ice surface is predicted by [1.8] because of the large growth velocity at the time this ice solidified. However desalination is the major influence on the distribution of brine. The mechanisms by which this occurs are described in detail in Untersteiner (1967) and Cox and Weeks (1975) and three are briefly dealt with below. The fourth, gravity drainage, is investigated more thoroughly since it contributes to under-ice water motion.

(1)Brine pocket migration; historically this was the first method of desalination to be recognised. Brine pockets move up the temperature gradient at a rate determined by the diffusion of solute in the brine, melting occurring on the warmer side of the enclosure and freezing on the colder. Subsequent studies have shown that the droplet's velocity is rather complicated (Harrison, 1965) and that this migration is a very minor contributor to the reduction in the salinity of sea ice (Kingery and Goodnow, 1963).

(2)Brine expulsion; this mecanism was first suggested by Bennington (1963b), who realised that, because of expansion due to freezing within the brine pockets, tiny cracks appear in the ice. Brine can then escape both upwards and downwards, frequently causing a high salinity surface layer on young sea ice (Cox and Weeks, 1974; Martin, 1979).

---

[13] Fluctuations of the order of ± 1‰ around the mean stable salinity, which is observed to decrease at approximately 0.5‰ per month.

(3)Flushing; this only occurs during the summer months. Thawing at the surface produces a hydrostatic head which forces the meltwater to percolate downwards, driving brine from the ice. It is believed that this is important in determining the salinity profiles of multiyear ice (Untersteiner, 1967).

(4)Gravity drainage; the importance of gravity drainage in the elimination of salt from young ice was originally recognised by Kingery and Goodnow (1963) and their conclusions have subsequently been confirmed by Bennington (1967) and Cox and Weeks (1975). The size and distribution of brine drainage channels, through which the solute finds a route to the underlying sea water, [14] depends critically on the sea ice temperature (Martin, 1979) and growth rate but is independent of grain size (Saito and Ono, 1980). Brine drainage channels leave a mass of tiny crystals in their wake (Lake and Lewis, 1970) which have either been sheared from the fragile skeletal layer by the flow or have been nucleated around descending brine streamers (Bennington, 1963b). Bennington (1967) classified brine drainage channels found in growing ice into two types. The first type which is not related to the crystallography, appears to be a relic of the dense brine streamers associated with under-ice convection. The second of these forms at crystal boundaries and is surrounded by feeder channels which converge on these main channels in a conical pattern (Bennington, 1963b, 1967; Lake and Lewis, 1970). ~~grain size (Saito and Ono, 1980).~~ In a series of ingenious laboratory experiments, Eide and Martin (1975) and Neidrauer and Martin (1979) observed that drainage channels are not stationary features but move in response to the thermal gradients, sloping in the direction of the isotherms. Niedrauer and Martin (1979) believe that the lateral migration of the channels can be explained by convective exchange of the fluid within the channel with the underlying sea water. This overturning is important since it is responsible for the percolation of oil within an ice sheet (Martin, 1979). Eide and Martin (1975) and Neidrauer and Martin (1979) have examined the physics of this convective process.

---

[14] They typically occur with a frequency of one large channel every 200cm^2 and may be almost 1cm in diameter (Lake and Lewis, 1970).

Some of the features of the observed salinity profiles can now be explained in terms of the brine drainage mechanisms. For example, consider the rate of desalination of grease ice where the crystals are small and chaotically oriented. The intergranular brine thus has poorer vertical connection with the underlying sea water than slab of columnar ice of the same thickness and is therefore more saline (Weeks and Lee, 1958). Hence the dependence of sea ice salinity on crystallography and ice type is explained. The existence of brine drainage channels explains the local scatter in salinity that we have mentioned. The initial rapid decrease in salinity is, primarily, due to gravity drainage, brine expulsion also being important in the first few hours of growth (Cox and Weeks, 1975). As the ice at a given level becomes colder, the channels become narrower or close altogether and the desalination rate consequently decreases. This, of course explains the tendency of the ice to approach a stable salinity. The warmer weather of the melt season will not only widen the brine drainage channels but also allow flushing to occur. The dependence of flushing on freeboard explains the dependence of salinity on topography.

2. THE ALIGNMENT OF CRYSTAL C-AXES

2.1 Previous observations

For many years much of the interest in the crystallography of sea ice was concentrated on the upper portions of the cover, where the c-axes were found to be essentially random in the horizontal plane (e.g. Weeks, 1958; Weeks and Assur, 1963). Because the increase in grain size with depth made it difficult to collect a large sample of crystal c-axis measurements from thick ice, it was often assumed that this randomness persisted through the ice (e.g. Tabata and Ono, 1957).

Nevertheless in the early 1960's Peyton (1963, 1966, 1968) had begun to use a classification, "bottom ice", for a particular sea ice type which he often found at depths greater than 70cm. The bottom ice had a preferential, azimuthal c-axis direction in the horizontal plane over areas of the order of meters. This alignment occurred in the fast ice off Barrow, Alaska, in seasonal floes, refrozen leads, and old polar floes in the Chukchi and Bering Seas and in the Central Arctic. As an explanation, Peyton (1966; 1968) observed that all cores exhibiting bottom ice had been collected from regions of thermal cracking and that the c-axes were parallel to any crack around its entire perimeter. This suggested to him that thermal stress within the ice sheet produced some co-operative effect between the crystals. Certainly we cannot explain this observation by recognising that the crystallography controls the direction of failure in an omnidirectional thermal stress field, since this would result in c-axes which were normal to the crack (Anderson and Weeks, 1958). Weeks and Lee (1958) have also noted that the c-axes within a healed crack lay along its length but in this case lateral heat transfer during refreezing supplied an obvious explanation. An alignment of c-axes has also been found within sea ice which showed other evidence of stress due to the movement of the M^{c}Murdo Ice Shelf (Paige, 1966).

An earlier observation of a very similar feature had been made on multiyear ice by Schwarzacher (1959). He reported that the crystal c-axes of a 25cm x 20cm horizontal sample taken from the polar pack, were grouped in three particular directions in the horizontal plane. One of these directions was preferred by most of the axes, while the other two were at 45° on either side. He also found that each grain was likely to have an orientation such that it differed from its neighbour by 45° or 90°. When the specimen size was increased to 50cm x 50cm, the preferential orientation disappeared, though the intergrain relationship remained. This suggested to Schwarcher that the arrangement of brine pockets caused an anisotropic thermal conductivity in the plane containing the c-axes. Schwarcher also noted that the tilting of floes could produce a very pronounced alignment of c-axes along the axis of tilt. He explained this convincingly by pointing out that these axes alone will remain in the horizontal plane when the floe is repositioned.

Since this preferred orientation is a peculiarity of sea ice from depth, it is not surprising that the phenomenon was observed on the saline, 10 - 12 m thick sea ice formation, SP-6, by Cherepanov (1964). Walker and Wadhams (1979) suggest that this type of floe has grown for many years as fast ice in a constricted channel at high latitudes. Over the entire 80km of SP-6 the c-axes lay close to 50° - 60° from magnetic north. In the opinion of Cherepanov this high degree of azimuthal alignment may have been established at the time of initial ice formation by a non-uniform distribution of air temperatures at the water surface. Further observations of such ordering were made over extensive areas of the sea ice portion of the ice island ARLIS II by Smith (1964).

Cherepanov continued to study this phenomenon and presented evidence of c-axis alignments covering hundreds of square kilometers of the fast and pack ice of the Kara Sea, noting the direction of the c-axes with respect to a geographical datum (Cherepanov, 1971). In this work he drew a comparison between the structure of sedimentary rocks laid down in a magnetic field and the aligned sea ice structure. He felt this suggested that some interaction between the earth's magnetic field and the gradients of electrical potential produced at the freezing interface (see section 1.5) was responsible for the sorting of the c-axes. He proposed then

rejected, the orienting influence either of currents or of the prevailing meteorological conditions at the time of initial ice formation. He felt that both effects were too chaotic to account for such an ordered phenomenon. However neither the application of static or oscillating magnetic fields nor of an electric field have been found to have any measurable effect on the uni-directional solidification of NaCl solution (Rohatgi et al, 1974). Solution concentrations similar to those found in nature were used but field strengths were many orders of magnitude larger. It seems reasonable, that if some interaction between magnetic field and grain structure exists, that it should have been observed by Rohatgi and his colleagues.

Using NaCl ice grown under calm conditions in the laboratory (Weeks, 1962), Knight and Knight (1968) have shown that there is a strong tendency for the orientation of neighbouring grains to differ by a small angle. This will, of course, lead to anisotropic masses of sea ice As mechanisms for this intergrain preference they have proposed the nucleation of new grains by stress effects due to volume change when brine pockets freeze and the reduction of interfacial free energy at the freezing interface by recrystallisation.

Similar measurements were made by the present author on sea ice from the Mackenzie Delta, Beaufort Sea, in March 1979. Figure 2.1 shows the results of measuring differences in c-axis orientation between each pair of grains encountered in linear traverses across a thin section. These traverses were performed parallel and perpendicular to the mean c-axis direction. Ice from 60cm depth was sampled at a number of intersection points in the 10m x 10m grid at our field site (see figure 2.2). Below the 60cm level, our results are in agreement with those of Knight and Knight (1968), the most frequently occurring angle between adjoining grains being approximately zero. In addition, our data show the development of the intergrain relationship with depth. Close to the upper ice surface, the peak in angular difference is centred on 45°, as observed by Schwarzacher (1959) but no peak at 90° was found at any level in this study. A minimum at angles less than 5° is expected, since differences in orientations between platelets comprising a grain can be of this order of magnitude.

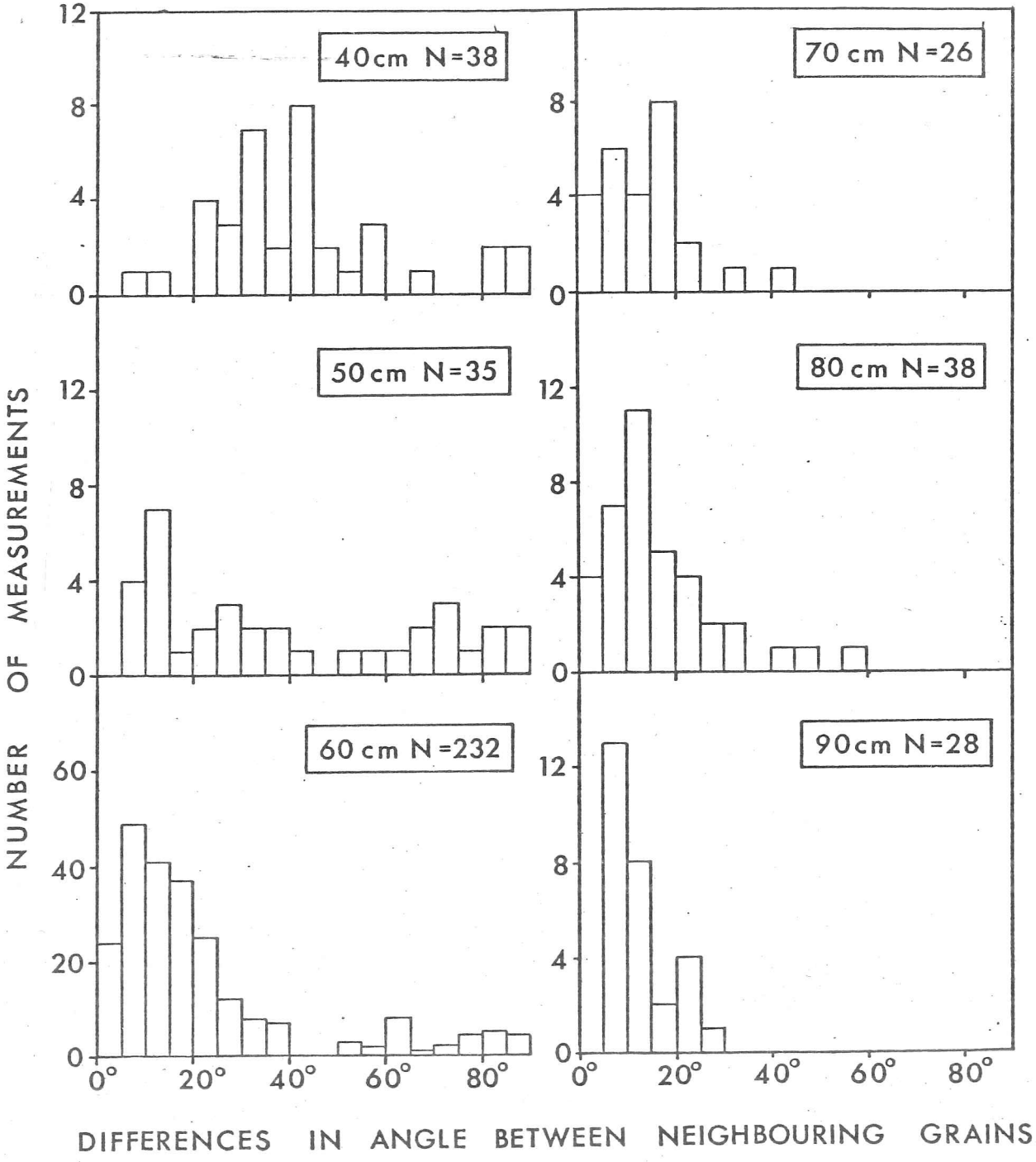

FIGURE 2.1 Frequency of occurrence of c-axis orientation differences between adjoining grains. Data at 6 levels beneath the ice surface at site C4, near Tuktoyaktuk, Beaufort Sea. Number of measurements for each level given by N.

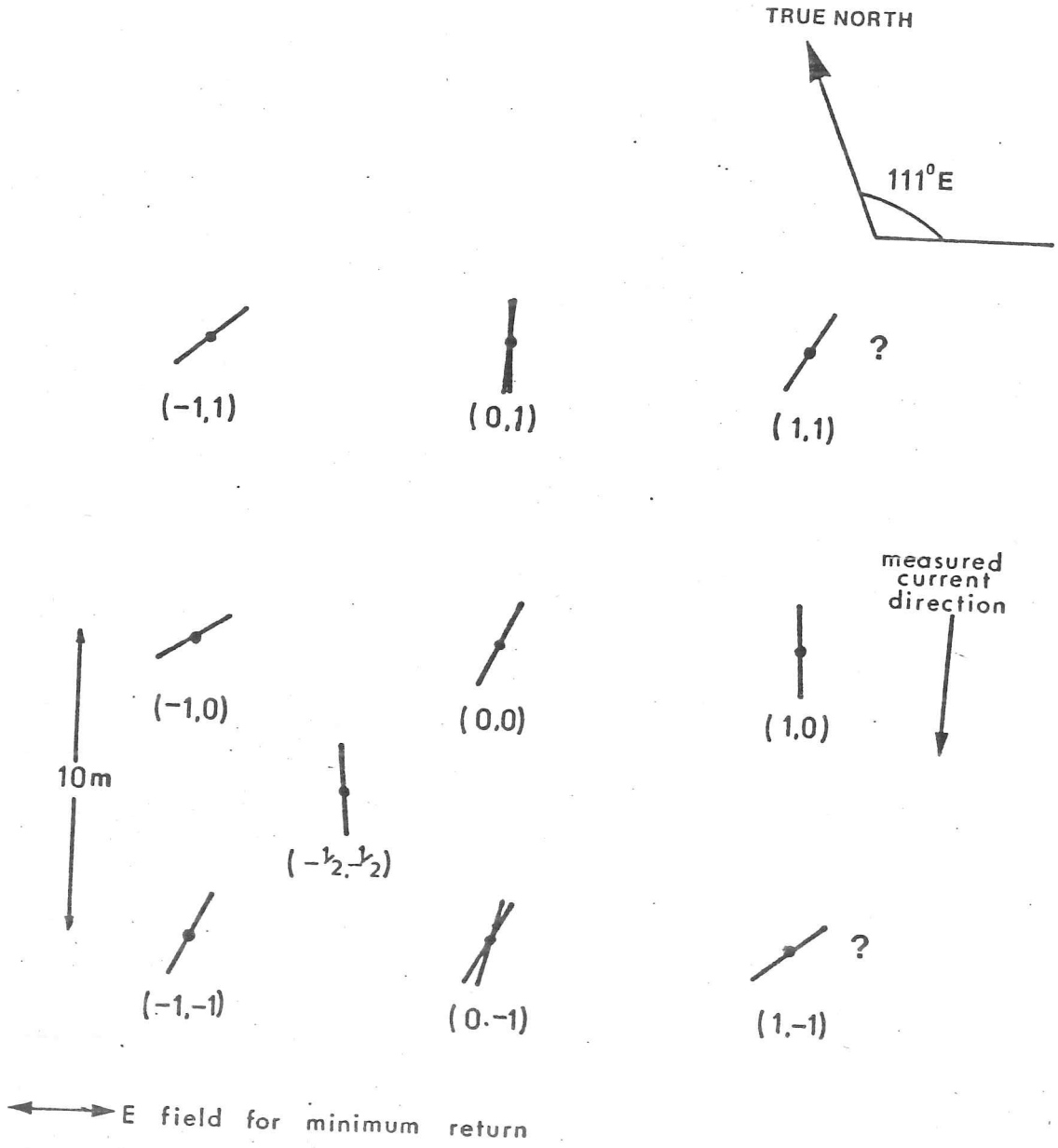

FIGURE 2.2 Diagram of the grid at C4, showing mean c-axis directions 100cm below the ice surface. The orientation of the impulse radar antenna E-field for a minimum reflected signal (see section 2.3) is also shown. Locations on grid are given by coordinate pairs.

More recently, Gow and Weeks (1977) found this c-axis alignment near Narwhal Island, Beaufort Sea, Alaska. Unsatisfied that these observations were made only on a 1m block of ice, the following year they carried out a more extensive study over an area 1400km^2 on the fast ice in the same vicinity (Weeks and Gow, 1978). Crystal c-axis data were collected from a variety of depths between 15cm and 185cm and clearly show the following;

(i) that at depths only 15cm from the surface, the grains show a tendency to align;

(ii) that at different levels in the ice at one location variations in mean c-axis directions are usually less than 20°;

(iii) that there is a systematic decrease in standard deviation about this mean as the depth increases.

Weeks and Gow also noted that the c-axes tended to lie along the expected ocean current directions. In addition the mean current directions, measured on the previous year with meters deployed 10m below the ice-water interface, [1] correlate well with the mean c-axis orientation. Kovacs and Morey (1978) simultaneously confirmed this correspondence between currents and crystal c-axes in the same geographical location. They measured current speed (2 - 5cms^{-1}) and direction, 10cm below the ice-water interface in a region of aligned sea ice grains. At sites where there was no current they found no orientation and at a station with an abnormally high velocity the current vector and c-axis direction were perpendicular. The latter observation should be treated with some scepticism since there may have been a change in current direction.

On the basis of their measurements, both Weeks and Gow (1978) and Kovacs and Morey (1978) favour some current-governed mechanism of orientation. The explanation for this was originally suggested by the work of Harrison and Tiller (1963b) who noted that convection under ice would probably be sensitively related to interface morphology. The interfacial temperature of a grain would then depend on its orientation, producing an orientation-dependent "step" between crystals. Following their ideas, Weeks and Gow (1978) propose the following method by which fluid flow at

---

[1] The Ekman turning angle was subtracted from the current measurements at 10m to give the current close to the interface.

the ice-water interface can favour crystal growth in a particular direction. The cells of the skeletal layer are elongated perpendicular to the c-axis and a different interface morphology will be seen by a current parallel or perpendicular to the general c-axis direction. The rejection of brine during freezing forms a salinity boundary layer which, in the presence of advection, depends on interface shape. They suggest that this boundary layer is smaller when the flow is perpendicular to the long axis of the cells. Thus growth is favoured with the current and c-axis aligned.

According to this picture, c-axis alignment would not be predicted during the growth of pure ice since the planar interface cannot interact anisotropically with the fluid motion. In view of this, it is difficult to explain the preliminary report of the c-axes of river ice grains which are perpendicular to the direction of the current (Lasca, 1971).

The most extensive field study of the phenomenon of alignment has been carried out by Weeks and Gow (1980). They surveyed sea ice along the coasts of Kotzebue Sound, the Beaufort Sea and the Chukchi Sea. Their measurements were made close to shore (within the 50m isobath) and from 42 measurements, they found that the most common deviation between the instantaneous current direction just under the ice-water interface, and the mean c-axis orientation was less than 10^{o}. In addition, 52% of the c-axis orientations (including the data of Gow and Weeks (1977) and Weeks and Gow (1978)) lay parallel to the coastline which, in most cases, is the expected current direction. A seven hour average of the current vector was taken at one site and this differed from the mean c-axis by only 4^{o}. In addition a similarity was found between the mean c-axis directions at the same site but on different years. All measured current speeds were low, typically ranging between 2 and $4 cms^{-2}$. However they also report anomalies to these typical observations, for example, samples showing weak or no preferential alignment, or a mean c-axis direction which differs from the current direction. The existence of these anomalies precludes any relationship between grain alignment and the inherent properties of the material.

Observations of preferred c-axis alignment in sea ice are now being accumulated from distant locations and diverse ice types. Gow et al (1982)

have sampled the high salinity ice of McMurdo Sound, Antarctica and found ordered c-axes in the bay-fast site. Well-aligned grains have been noted in the 6m thick sea ice layer at the bottom of the Ross Ice Shelf (Zotikov et al, 1980). There are reports of c-axis alignment in the brackish waters of the Mackenzie Delta, Beaufort Sea (Vittoratos, 1979; Langhorne, 1980). Vittoratos has observed that the c-axes around the artificial ice island, Isserk E-27, followed the expected streamlines. His measurements were made after the rubble field had stabilised and the deformation was < 1m over approximately six months (Vittoratos, personal communication).

The results of our own field studies have largely been described in Langhorne et al (1980) and Langhorne (1980), but we shall reiterate the most important points here.

The sea ice at the study site had formed on brackish water (21‰), the low salinity being caused by the flux of fresh water from the Mackenzie River. Our site was located on fairly flat, first year sea ice and typical examples of the grain structure are shown in figure 1.2 and 1.3. A 10m x 10m grid (figure 2.2) was laid out on the ice and cores were taken at the grid intersections. The current, 20cm from the ice-water interface, was measured at a site 15km shoreward from the previous position. The mean speed, from a 26 hour record, was $1 cms^{-1}$, and its direction is shown on figure 2.2. This flow is probably tidally induced, although a small component of the motion may be driven by the refreezing of a lead a few kilometers to the north (see section 2.2.4). The measured current direction is within the estimated bounds on the current direction from the available literature (Herlinveaux et al; Herlinveaux and de Lange Boom, 1976). Figure 2.2 shows that the deviation between the measured current direction and the mean of the c-axis orientations, was 17^{o} which was well within the standard deviation between c-axis orientations from different locations. 40 sets of c-axis measurements were made and a typical example of the development of the c-axis alignment at 40, 60 and 100cm from the ice surface, is shown in figure 2.3. Fabric strengths were calculated for each of these c-axis samples, using a method to be described in section 3.8.1. These data are compared with our laboratory results in section 4.7.5. Comparison of figure 2.3(a) with figure 2.1 indicates that, although there was no obvious preference between grains at a depth of 50cm, an alignment

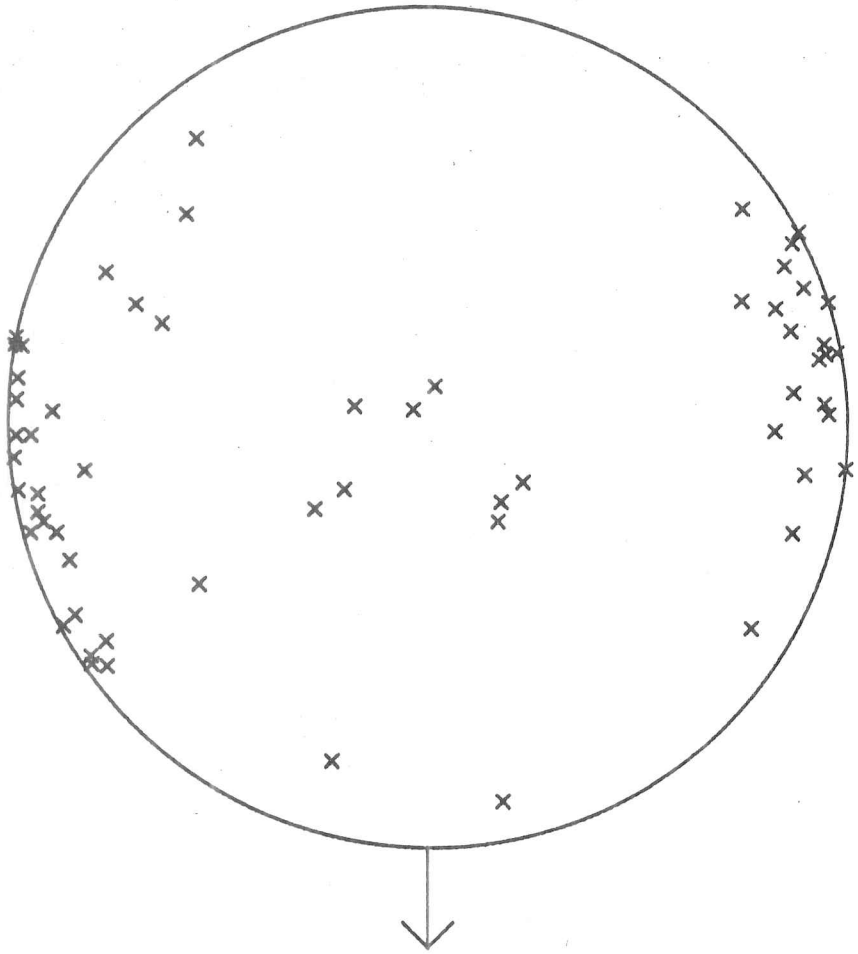

SAMPLE C4-15-42/43

FIGURE 2.3(a)

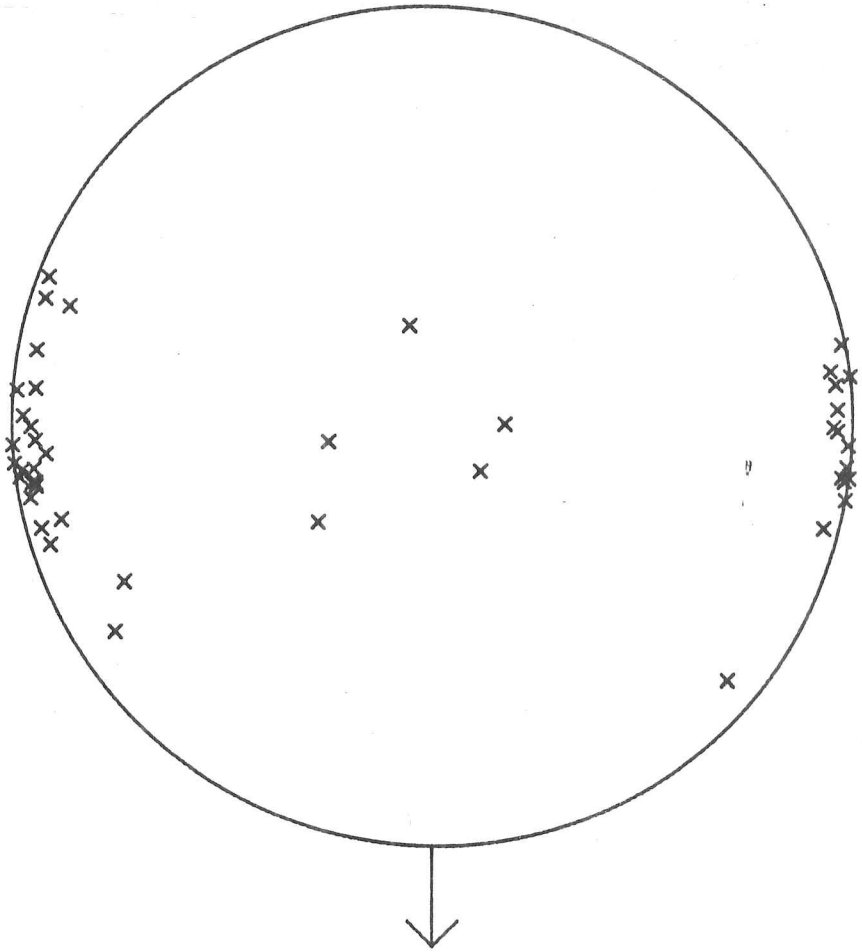

SAMPLE C4-15-62/63

FIGURE 2.3(b)

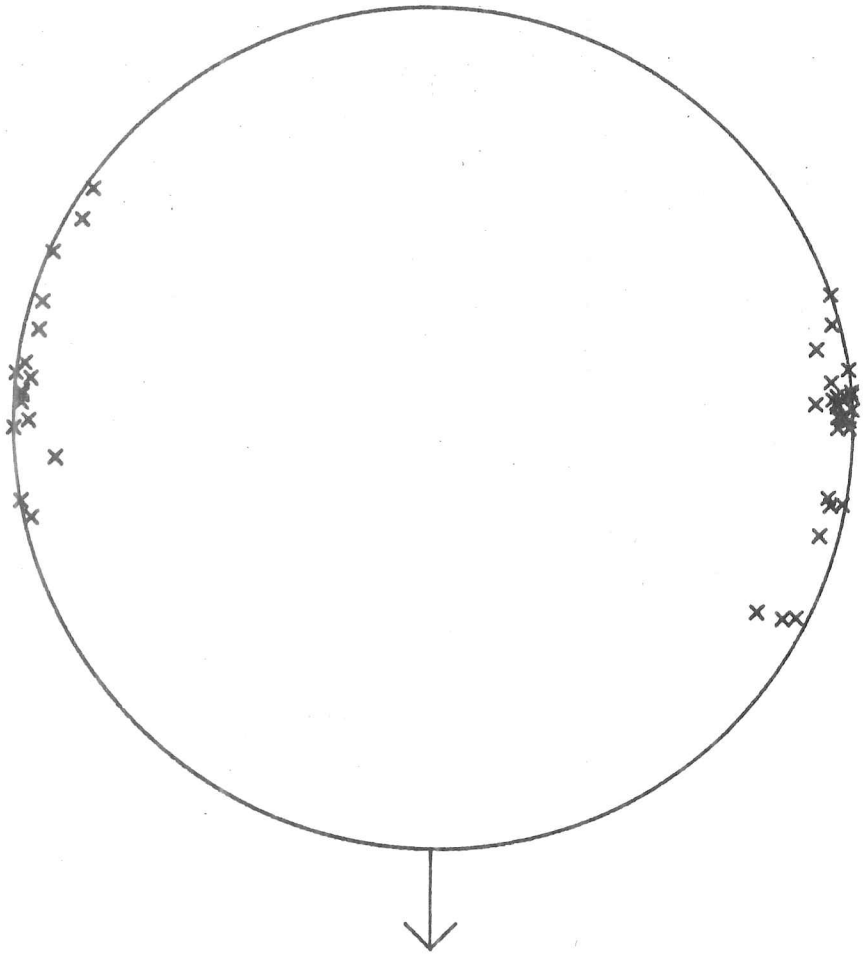

SAMPLE C4-15-102/103

FIGURE 2.3(c)

CAPTION for FIGURE 2.3

Equal-area projection diagrams of c-axis directions for (a) 40cm, (b) 60cm and (c) 100cm below the ice surface. Projection diagrams are explained in section 3.8.1. Arrow shows the direction of the impulse radar E-field orientation for minimum reflected signal.

was already apparent in the fabric diagram. This gives us additional grounds for believing that the mechanism responsible for the alignment is not a property of the material.

Stander and Gidney (1980) have interpreted existing observations in terms of recrystallisation under non-hydrostatic stress or strain. In view of the abundant literature on experimental, theoretical and field studies on the recrystallisation of pure ice we were surprised to find only a single experiment in which the movement of grain boundaries under deformation in sea ice has been explored (Sprenger, 1972). The most remarkable feature of this experiment was that no structual changes were observed until the melting point was reached. Polygonisation then took place but the grain boundaries retained their identities. This is in direct contrast to the requirements of Stander and Gidney if stress or strain is to explain c-axis alignment. In addition, Weeks and Gow (1982) have critised Stander's arguments because the fabrics of sea ice result from growth from the melt and are not established after solidification. We feel these objections are sound.

However, since the application of a non-hydrostatic stress can produce an orientation-dependant chemical potential in the solid (Kamb, 1959a), then it may be possible that stress could bring about the anisotropic formation of grains at the time of freezing. Shear or compressive stresses might be exerted on the outer edge of the fast ice by the moving pack but because of the isotropic nature of thermal stresses we do not find Peyton's arguments for alignment under thermal stress compelling. Although we consider this an unlikely mechanism of alignment we shall not reject the possibility immediately.

We have summarised the discussion of this chapter in table 2.1, indicating which mechanisms, in our opinion, may be immediately rejected. Of the nine suggestions, we feel that only stress, horizontal temperature gradients, tilting and currents warrant any further investigation. We have already discussed the available information on how the first three might be generated within the ice sheet and how they might operate to bring about an alignment of crystal c-axes. However, although we have indicated how currents could favour the growth of certain grains, we have said

Mechanism	Comments	Possible?
Stress	May be thermal or externally imposed.	Yes
Horizontal temperature gradients	Well-known to align if large enough. No measurements in the field. Estimates only from Lewis (1967).	Yes
Tilting	Mainly important in deformed ice. In fast ice tidal action or changes in sea level may produce small tilts.	Yes
Alignment in initial layer	There is a good deal of evidence to suggest the initial skim is disordered.	No
Earth's magnetic field	Mechanism of alignment is not clear and higher field strengths shown to have no effect on solidification.	No
Nucleation due to stress when brine pockets freeze	Nucleation events are relatively rare after the transition layer and these increase the disorder.	No
Recrystallisation driven by reduction in interfacial freezing energy	Material property and does not explain alignment with respect to a geographical datum. No evidence of recrystallisation.	No
Grain boundary migration driven by surface tension or asymmetric grain boundary grooves	Does not explain alignment with respect geographical datum or observations of no alignment.	No
Currents	Under-ice currents to be examined in more detail in the next section.	Yes

TABLE 2.1

nothing about the water motion under a sheet of sea ice. This will be the subject of the next section.

2.2 Flow at the ice-water interface

2.2.1 Introduction

Although observations of c-axis alignment have mainly been made on nearshore, fast ice, measurements also exist on moving, pack ice. Undoubtedly, the major factors influencing the flow in these two situations are significantly different. In addition, the magnitude and direction of the mean oceanic current will vary seasonally. In the ice-free summer months, the wind controls the flow in the Arctic (Healey, 1971; Wilson, 1974). However, when ice partially isolates the ocean from the atmosphere in the winter, the motion is determined by the relative magnitudes of the tides (Matthews, 1981b), the flux of water from large rivers (Herlinveaux et al, 1976; Herlinveaux and de Lange Boom, 1976), buoyancy-driven convection (Hunkins, 1972) and a number of other effects.

In this section, we give a general description of the fluid motion at the ice-water interface under a broad range of conditions. A basic review of the dynamics of a turbulent boundary layer is given in section 2.2.2. In section 2.2.3 we describe the motion when forced flow is virtually absent and buoyancy-driven convection dominates the motion. However, shear is frequently more important than buoyancy and there are many possible regimes and very little data.

2.2.2 The near-surface boundary layer

The boundary layer immediately below an ice cover is shown schematically in figure 2.4. The region in which the flow "feels" the effect of the ice is called the planetary boundary layer and unless the flow is extremely slack ($<0.1 cms^{-1}$), this zone is turbulent (Wimbush and Munk, 1971). In the lower portion of the planetary boundary layer, the

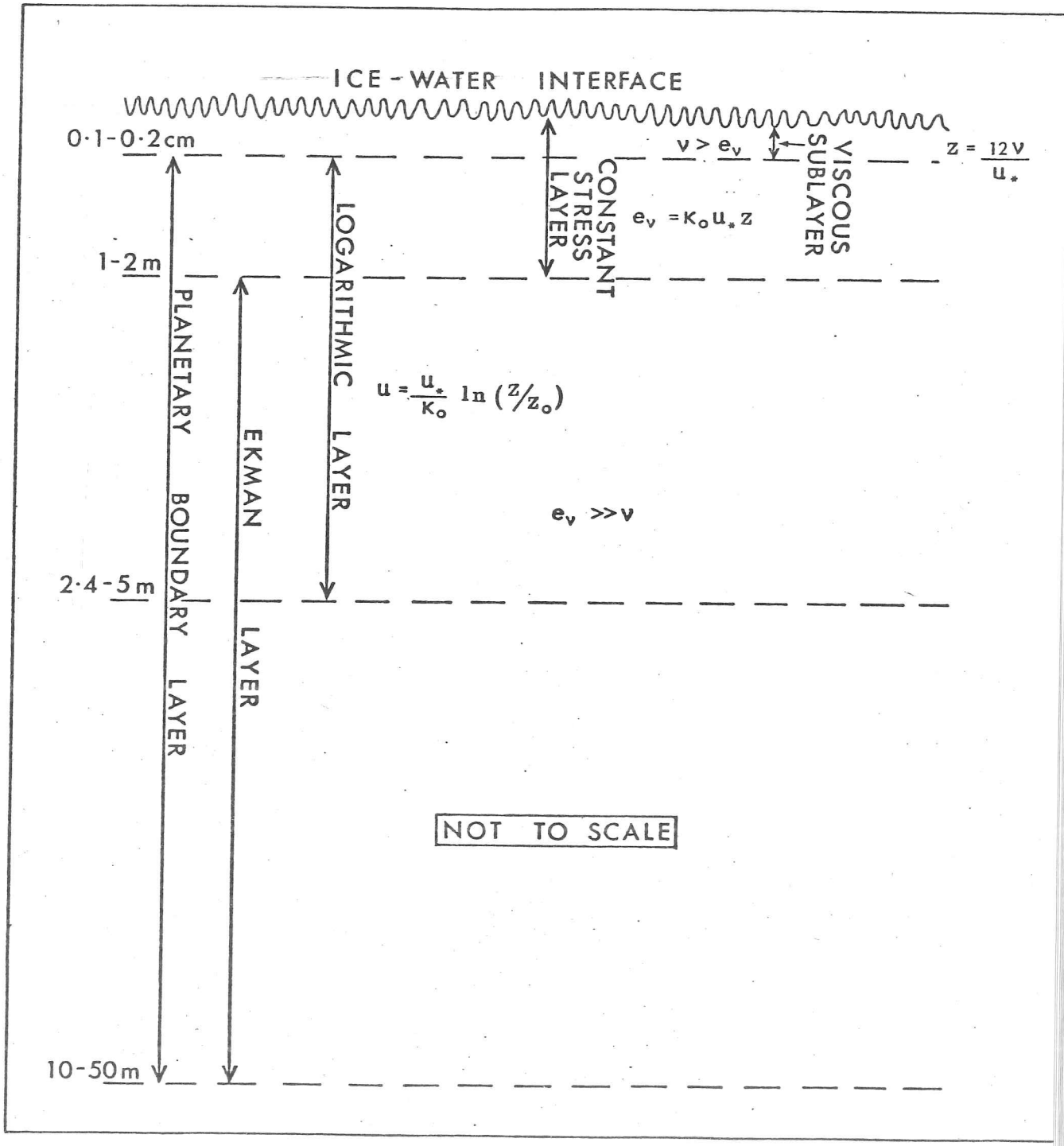

FIGURE 2.4 Simplified diagram of the fluid dynamical regimes under ice. Symbols defined in text.

effects of the earth's rotation are important and the current vectors rotate clockwise as the depth increases. This is called the Ekman layer. Above this, in the frictional boundary layer close to the interface, the effects of the Coriolis force are negligible and turbulence is generated by shear at the boundary (see for example Smith, 1971). Within this layer the horizontal shear stress, σ, varies slowly with depth and an eddy viscosity, e_ν, can be defined which depends only on the distance, z, from the interface and on the friction velocity, u_*, (Wimbush and Munk, 1971). Thus, within the constant stress region

$$e_\nu = \kappa_o u_* z \quad , \qquad [2.1]$$

where κ_o is von Karman's constant. It can be shown that this implies (Wimbush and Munk, 1971),

$$u = \frac{u_*}{\kappa_o} \ln\left(\frac{z}{z_o}\right) \quad , \qquad [2.2]$$

where

$$u_* = \left(\frac{\sigma^*}{\rho_1}\right)^{\frac{1}{2}} \quad . \qquad [2.3]$$

σ^* is the shear stress close to the interface and ρ_1 is the density of sea water. The constant of integration, z_o, is related to the roughness of the boundary (Turner, 1973). Values of z_o under sea ice range from 0.5 and 2.0cm (see for example Ling and Untersteiner, 1974). In practice, the region where the mean velocities conform to the logarithmic law is frequently found to extend beyond the constant stress region (Wimbush and Munk, 1971). Under sea ice Hunkins (1972) and Belyakov (1974) have both found reasonable fit to equation [2.2] to a depth of 5m whereupon there is a change in slope in the plot of the log of depth versus the velocity indicating a change in eddy viscosity. M^{c}Phee and Smith (1975) have assumed that a log profile is valid to produce values for u_* under Arctic sea ice. These results are in agreement with friction velocities obtained from other methods. Typically u_* is about $1 cms^{-1}$ in the Arctic Ocean, far from the shore. However, we estimate it may be as low as $0.05 cms^{-1}$ in a slack flow under a smooth cover, which is more typical of sheltered nearshore environments.

Immediately adjacent to the interface there may be a viscous sublayer, δ_ν, where the effects of viscosity, ν, dominate those of turbulent mixing and

$$e_\nu << \nu \ .$$

This will not exist if the interface is sufficently rough that the roughness elements protrude through the viscous sublayer; that is if the roughness Reynolds number, Re^*, defined in terms of the height of the roughness elements, l, is greater than 5 (Wimbush and Munk, 1972), that is

$$Re^* = \frac{u_* l}{\nu} > 5 \qquad [2.4]$$

The Monin-Obukhov length is a scaling parameter for flows where buoyancy and shear are important (Turner, 1973). This is given by

$$L = -\frac{u_*^3}{\kappa_o B} \ ,$$

$$L>0 \Rightarrow \text{statically stable} \ ,$$

$$L<0 \Rightarrow \text{statically unstable} \ ,$$

where B is the buoyancy flux which is caused, in our case, by rejection of salt during freezing. Thus for sea ice growth this expression is (McPhee and Smith, 1975)

$$L = \frac{u_*^3 10^3}{\kappa_o g V(C_\infty - C_{li})} \frac{\rho_l}{\rho_s} \ , \qquad [2.5]$$

where $(C_\infty - C_{li})$ is the difference in concentration between the bulk of the fluid and that immediately adjacent to the interface, ρ_l / ρ_s is the ratio of the brine to ice density, g is the acceleration due to gravity and V is the growth velocity. The importance of this length scale is that it represents the depth at which Reynolds stress terms and buoyancy flux terms are of the same magnitude. At depths much less than $|L|$ turbulent energy is maintained by the Reynolds stress and at depths greater than $|L|$ buoyancy effects are dominant and there is a region of irregular plumes and cells

(Phillips, 1977).

2.2.3 Natural convection under sea ice

In an attempt to explain apparent supercooling at depth (section 1.2), Coachman (1966) considered free convection induced by freezing at the surface of leads. He estimated the descent velocities of the cool, saline brine under the fast-forming lead ice and the slower, compensating upward movement under the thick ice. Following these ideas, Lewis and Walker (1970) interpreted their measurement of positive temperature excursions 22m below the ice-water interface, as the upwelling of warm water. They also identified the descent of a cold plume to 30m.

However close to the interface there must be some mechanism by which dense rejected brine is carried from the boundary. This problem has been addressed theoretically by Foster (1968; 1972) who extended a model he had previously developed for a fluid layer cooled from above (Foster, 1965).

In calm field conditions, positive temperature excursions of the order of $0.05^{\circ}C$ have been observed by Lake and Lewis (1970). These have a duration of greater than 20 minutes and were present as the thermistors were engulfed in the skeletal layer of the growing ice sheet. Lake and Lewis suggest that the fluctuations are a manifestation of natural convection at the interface which implies that similar temperature variations might be observed in the water underlying the ice. However, Lake and Lewis were unable to find such features but did note the infrequent passage of blobs of warmer water. Occasionally a thin layer of warmer water was found close to the ice-water interface. They suggest that any downward motion is centred around the brine drainage channels, with dense water moving towards these locations in thin layers immediately below the ice (see figure 2.5). In an area where light advection currents were measured, Lake and Lewis (1972) noted temperature fluctuations of higher frequency.

We shall describe the results of the field experience and laboratory experiments on free convection in the following summary;

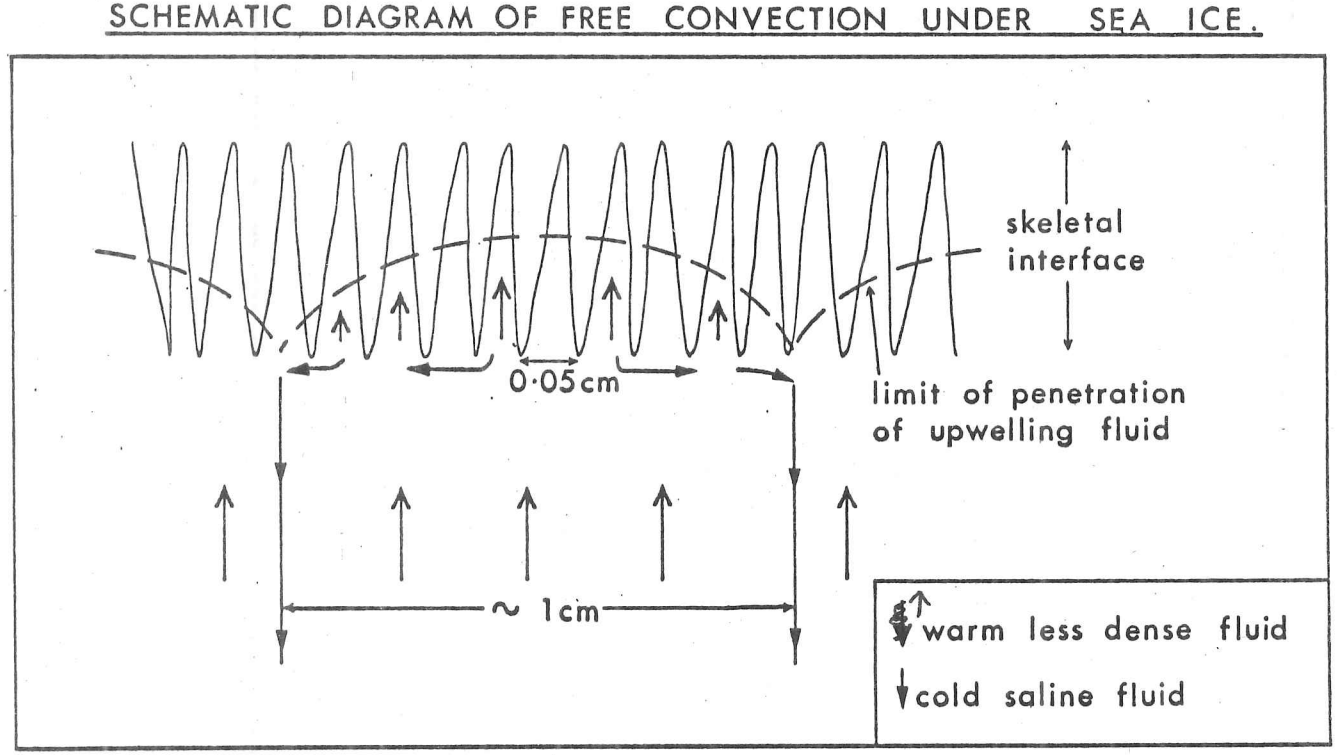

FIGURE 2.5 Picture of the buoyancy-driven flow very close to the interface. This removes salt from the ice-water boundary.

(i) As we have just seen, convection is not restricted to the water below the ice but penetrates within the skeletal layer. Neidrauer and Martin (1979) injected dye under growing ice in their experiments and observed the development of cusp-shaped patterns (see figure 2.5). They attribute these to broad regions of upward movement of fluid separated by narrow downflow regions. They were able to show that temperature fluctuations were associated with the fluid motion.

(ii) The dense brine descends in streamers, randomly distributed over the ice surface, (Foster, 1969; Farhadieh and Tankin, 1972; Wakatsuchi, 1977; Niedrauer and Martin, 1979) to a depth limited by the dimensions of the experimental apparatus. In the field, these streamers would descend until diffusion made them incoherent (approximately 10cm) or until they impinged upon a density gradient.

(iii) Foster (1968; 1972) points out that if $Ra_c > 10^7$ and $Sc > 100$ [2] then the convection should be intermittant; that is, the boundary layer will reach its critical Ra_c, overturn and destroy the stratification, whereupon the motion ceases and a build up of solute begins again at the ice-water interface. As the eddy diffusivity for solute transport , e_c, of the fluid increases, the tendency to exhibit the impulsive motion decreases. This intermittancy has been noted experimentally at high growth rates (10^{-4}cms^{-1}) (Wakatsuchi, 1977). Wakatsuchi observed that a salinity boundary layer was formed from which streamers sporadically descended in groups. However, Farhadieh and Tankin (1975) were unable to find this type of boundary layer under ice that was also solidifying rapidly (10^{-3}cms^{-1}). Their results were in better agreement with those of Wakatsuchi at lower growth rates (9×10^{-5}cms^{-1}) where brine originated in the ice and descended from the brine drainage channels.

(iv) Convective cell sizes have been measured in the laboratory to be

---

[2] The solute Rayleigh number, Ra_c, and the Schmidt number, Sc, are defined below, where β is the coefficient of haline expansion, D is the solute diffusivity and ΔC is the concentration difference across the fluid layer,z.

$$Ra_c = \frac{g\beta\Delta C z^3}{\nu D} \quad , \qquad S_c = \frac{\nu}{D} \quad .$$

1cm (Niedrauer and Martin, 1979)

0.2-0.3cm (Foster, 1969)

These measurements are in agreement with the predictions of Foster (1968; 1972) who obtains spacings of 0.2cm, if transport of solute is by molecular diffusion. These experiments may be critisised for imposing unrealistic boundary conditions, which may influence the convective cell size. However, Foster shows both experimentally (Foster, 1969) and theoretically (Foster, 1968 ;1972) that the boundary conditions have little effect on the motion.

(v)Foster's (Foster, 1968; 1972) theoretical studies suggest a hierarchy of convective cells, each determined by the magnitudes of the coefficients of transport of the solute. For example for rapid freezing ($1 cm hr^{-1}$) and molecular diffusion his model predicts that within 20 sec convective cells moving with a maximum vertical velocity of $0.01 cm s^{-1}$ and separated by 0.2cm will have developed. This will generate turbulent mixing with a solute eddy diffusivity, e_c, determined by the spacing and velocity of these cells Thus a second convective instability with a cell spacing of 20cm and velocity of $0.9 cm s^{-1}$ will be present. The time to the onset of this latter instability is 2 mins. This explains the difference in the experimentally measured values of spacing since Foster's observations were made only minutes after freezing whereas Neidrauer and Martin studied a well-developed ice sheet.

(vi) Wakatsuchi (1977) found empirically that the velocity, u_z, of a descending streamer was related to its width, w, by

$$\frac{u_z}{w} = 3.83\ s^{-1}$$

(vii) The salinity of the streamers is 2 to 6‰ greater than the surrounding sea water (Farhadieh and Tankin, 1975; Wakatsuchi, 1977).

It is very important to note that much of the experimental work, except that of Niedrauer and Martin, has dealt with very thin ice sheets, unnaturally high temperature gradients and very rapid ice solidification rates. The experimental observations will thus describe much more vigorous convection than would be expected under a thick ice sheet. Therefore, it is

not surprising that, despite concerted efforts, Lewis and Walker (1970) were unable ~~despite concerted efforts,~~ to find evidence of convective streamers in the field. In the absence of advection currents, the picture they give is one of extremely, slow laminar motion.

2.2.4 Forced flow at the ice-water interface

In regions in the vicinity of leads and polynyas, jets have been observed at the interface, flowing parallel to the ice-water boundary. This effect is most important in the deformed, offshore pack ice, although they are not associated with the relative motion of the pack and the ocean. It appears that these jets lie within 50cm of the interface and can have speeds of between 3 and 12 cms^{-1} when the ice is in motion (Smith, 1974) and, in calm conditions, they may reach $5cms^{-1}$ (Hunkins, 1972). They can persist for several days and maintain the same direction, pointing towards areas of open water. Hunkins (1972) has found that they are isothermal and thus suggested that they are related to the salinity structure, proposing three mechanisms for their generation. Subsequent data (Hunkins and Fliegel, 1974; Smith, 1974a) however, supports the hypothesis that boundary currents are associated with convection driven by brine rejection at the surface of leads.

Horizontal density gradients at the ice edge may also cause surface jets but, in this case, the driving mechanism is not convective. These are expected to run parallel to the boundary between the ice and the open water (M^{c}Phee, 1980).

We now direct our attention to the oceanography of the waters closer to shore. Data for nearshore regions in the winter are extremely sparse, and the measurements that Weeks and Gow made as an adjunct to the studies on c-axis alignment, are one of the few sources of information. Undoubtedly the most relevant and interesting current observations with regard to the alignment of crystal c-axes are those of Matthews (1981a,b). He recorded currents from November to February, approximately 1 and 3m above the sea

floor [3] in the Arctic island lagoons. A number of detailed studies of preferred c-axis orientations have been made in this area (Weeks and Gow, 1978,1980; Kovacs and Morey, 1978). The distinctive feature of these records is that the flow is accurately and invariably outwards from the shore and that the mean monthly speed dropped from 1.4cms^{-1} to below the threshold, as the winter progressed. From these measurements Matthews (1981a) was able to compute the compensating shoreward current which must exist just under the ice. Surface drifters confirm the existence of this shoreward current at least between the months of May and July (Matthews, 1981b). Matthews believes these currents are tidal and surge-pumped. These observations are not entirely consistent with the much sparser current observations of Weeks and Gow (1978,1980) and Kovacs and Morey (1978) which displayed a longshore component at a number of sites.Both sets of results agree that the magnitude of the current is small ($\sim$2cms^{-1}). The latter measurements were made in March and April which may account for the discrepancy.

In conclusion, from the sparse data available, it appears that currents under coastal fast ice in winter are light [4] and variable and that, in enclosed, shallow regions, the flow may be unidirectional and of very low intensity turbulence (Matthews, personal communication). Further out beyond the shelf break, the surface boundary layer will be more turbulent and lead driven convection can cause large and persistent currents just under the ice.

It is worth mentioning the effect that turbulent flow has on the ice interface in rivers. Turbulent heat transfer from the flux of relatively warm water causes ripples to develop with the crests running perpendicular to the current vector (Ashton, 1979). The wavelength of these is of the order of 30cm but increases as the water velocity decreases (Ashton and Kennedy, 1970). More recently Gilpin et al (1980) have shown that this phenomenon is not restricted to melting layers and that ripples may also

---

[3] The ice-water interface was approximately 2m above the upper current meter at the beginning of the record and approximately 1m above towards the end.

[4] Lake and Lewis (1972) measured speeds of 0.5 to 1cms^{-1}, 20cm from the interface.

be observed under growing ice in certain conditions. Whether these might exist under sea ice is a matter for speculation.

2.3 The effect of crystal alignment on sea ice properties

The importance of the effect of this ordered crystal array on the thermal, mechanical, electromagnetic and other properties of sea ice is well illustrated by the distinct anisotropy in impulse radar return over distances of the order of tens of kilometers. This was first reported by Campbell and Orange (1974b), who have surveyed young ice from a refrozen lead as well as multiyear ice. It was observed that when the E-field of a linearly polarised antenna is perpendicular to the mean crystal c-axis direction there is an almost total loss of signal from the reflecting horizon below the ice surface. [5] Kovacs and Morey (1978; 1979) have studied this anisotropy in more detail and find the following;

(i) that the frequency dispersion as well as the magnitude of the return are functions of the antenna azimuthal position;

(ii) that although the reflection from below the ice surface is highly anisotropic, the surface reflection is only weakly so;

Our own determinations of the polarising nature of aligned sea ice were in agreement with concurrent studies of Kovacs and Morey. Figure 2.2 and 2.3 show the preferred fabrics at our field site with respect to the antenna E-field orientation for minimum signal return (MIN) from the reflecting horizon. Once again the c-axes are grouped about the normal to this direction. A theoretical explanation for the anisotropy in return is given by Golden and Ackley (1980). In addition, a ground wave travels directly between the antennas through the surface layers. The propagation time of this wave is therefore sensitive to the surface dielectric constant.

---

[5] There is evidence to suggest that this horizon is not the macroscopic ice-water interface as might originally have been expected, for example Campbell and Orange (1974a).

We carried out a wide angle reflection and refraction (WARR) experiment at the site in figure 2.2. [6] This has the advantage over direct sounding techniques that it gives both ice depth and dielectric constant without having to measure either of these independently. The procedures used are given in Rossiter et al (in preparation) and the results are summarised in Table 2.2. The WARR estimate of ice thickness was in good agreement

TABLE 2.2

Antenna Orientation	Bulk Dielectric Constant
MAX orientation ground wave	3.4 ± 0.6
MIN orientation ground wave	3.6 ± 0.2
MAX orientation reflected wave	3.7 ± 0.3

with ice thickness determined by drilling (119cm compared with 120cm) which gives credence to our determination of dielectric constant. As expected, no orientation dependence was found at the ice surface. The strength of the reflected signal was reduced to a level which made it impossible to determine the dielectric constant in the MIN orientation.

In addition to being anisotropic to frequencies in the MHz range, Kohnen (1975) has found small and probably real differences in the D.C. resistivity of sea ice when soundings were made perpendicular to each other.

Crystal orientation also has a large effect on the compressive strength of sea ice (Peyton, 1966). Thus Vittoratos (1979) points out that the c-axis alignment he has observed around artificial ice islands will be of importance in determining how ice fails around an offshore structure. Martin (1979) has mentioned that the volume of oil entrained within ordered sea ice is greater than in sea ice with c-axes randomly distributed in the horizontal plane.

---

[6] The principle behind the WARR tecnique is described in Annan and Davis (1976).

3. LABORATORY EXPERIMENTS

3.1 Design of apparatus

The aim of the experiments described in this chapter is to discover which of the mechanisms listed in Table 2.1 is controlling the preferred orientation of c-axes in sea ice. Our prime concern is to study the effect of fluid flow on the texture and, for structural studies of this type, NaCl solution may be substituted for sea water. Weeks and Cox (1974) have summarised some of the techniques used in previous laboratory investigations of the physical and mechanical properties of sea ice but there have been no published accounts of laboratory simulation of the alignment of crystal c-axes. [1]

One obvious way to produce a flow under a growing sheet of sea ice is to use a rotating tank with the ice cover supported rigidly above. This principle is frequently used by crystal growers (Czochralski growth) to ensure stirring in the melt and to damp natural convection (Cole, 1971). However the mutual interaction of interface shape, natural convection at the solidifying front and the rotating fluid can produce instabilities (Greenspan, 1968) which disturb the circulation. Such disturbances have been noted in Czochralski growth; for example Bardsley et al (1968) show that the initial cell formation at the centre of a gallium-doped germanium crystal produces local turbulence which propagates radially outwards, controlling the cell structure and imposing a spiral pattern on the crystal interface. To avoid such complications and to ensure that the interaction of forced flow and natural convection is similar to that in nature, we have designed our apparatus to give a unidirectional current at the ice-water interface.

---

[1] A. Kovacs (personal communication) has reported an alignment between the crystal c-axes and the current in a circular tank but this work has not been published.

The direction and quantity of heat flow is extremely important in any experiment where we wish to reproduce the growth of columnar grains. The removal of too much sensible heat produces underwater ice, as in the experiments of Wakatsuchi (1974), or causes frazil to appear in the flowing water mass (Martin, 1981). Conversely if too much heat remains in the system the thermal gradient in the fluid at the interface becomes large enough to suppress cellular growth (see equation [1.4]) which is crucial for the interaction of the current and the c-axes and, in extreme cases, can inhibit ice growth. In addition if large quantities of heat are present in a system there is an increased possibility of lateral heat flow which is known to produce a preferred orientation of c-axes. Over and above these requirements, ice growth must be prevented in any moving parts of the apparatus.

The most successful version of our apparatus is shown schematically in figure 3.1 and in the photograph of figure 3.2. Tank B, the test section, is made of glass reinforced polyester (Osmaglass). It is 122cm X 61cm X 61cm in size and is set inside a 183cm X 122cm X 76cm steel tank (tank A). A copper funnel connects one end of tank B to a centrifugal pump which draws the NaCl solution through the lower portion of the test section. From here it is discharged, via a valve controlling the volume rate of flow, into tank C which is raised above the level of the rest of the apparatus. Two sets of pipes leave tank C. The lower ones return the fluid to tank A while the upper set are generally above the water level and are intended to prevent tank C from overflowing should the lower pipes become blocked by ice. The valve is therefore used to adjust the water level in tank C to a position between the pipe inlets. If this is too low the possibility of the lower pipes freezing shut is greatly increased and air is drawn in with the fluid causing large air bubbles to form in and under the sea ice slab.

Tank C has two purposes; firstly it allows a suitable amount of the 300-600W of heat introduced by the pump to be dissipated, effectively distancing the pump from the test section. Secondly turbulence and splashing in tank A are minimised by injecting the returning fluid below the water level. Laminar flow is produced in the test section by two layers of waxed paper honeycomb.

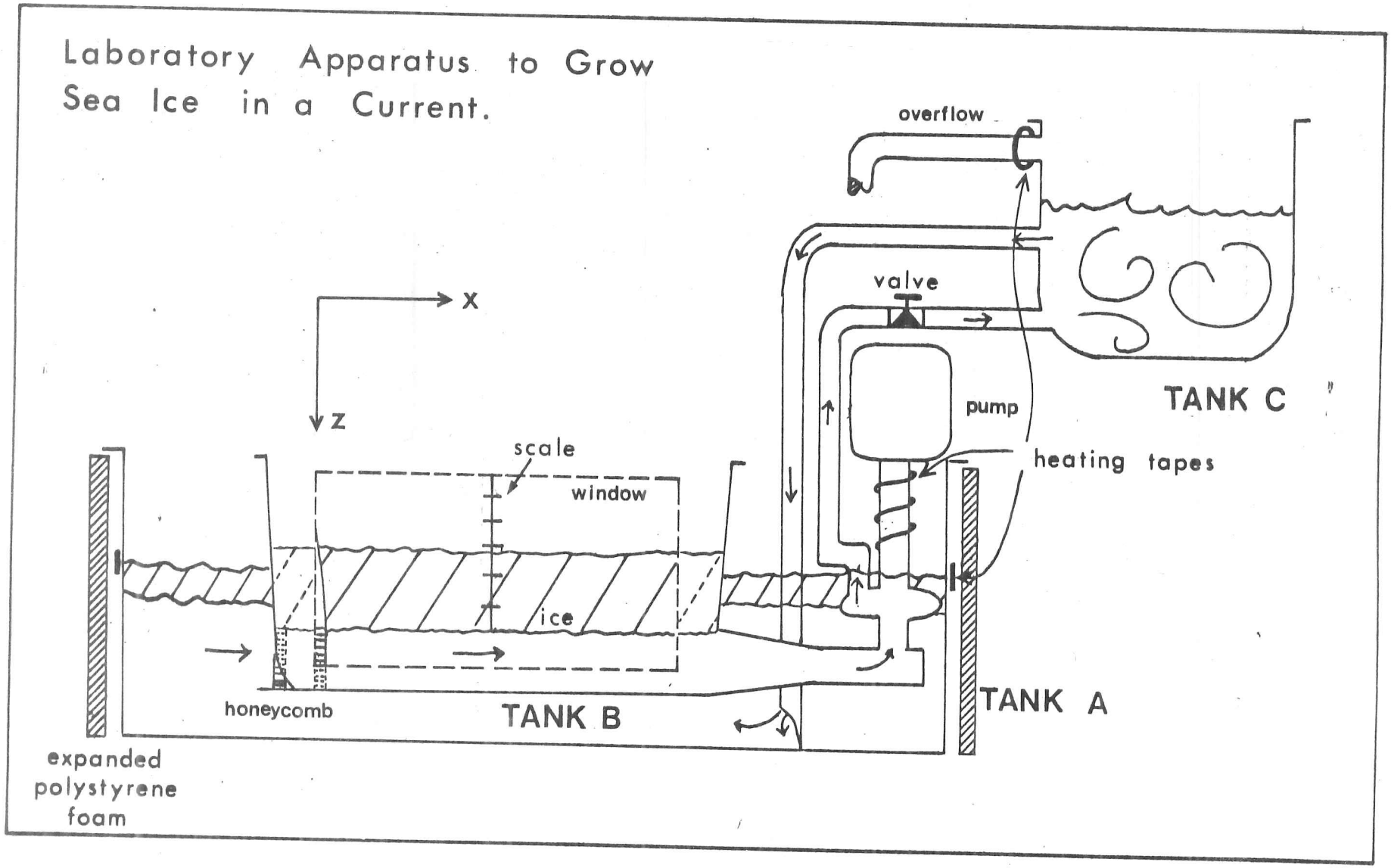
Laboratory Apparatus to Grow Sea Ice in a Current.
overflow
valve
x
z
pump
TANK C
heating tapes
scale
window
ice
honeycomb
TANK B
TANK A
expanded polystyrene foam

FIGURE 3.1

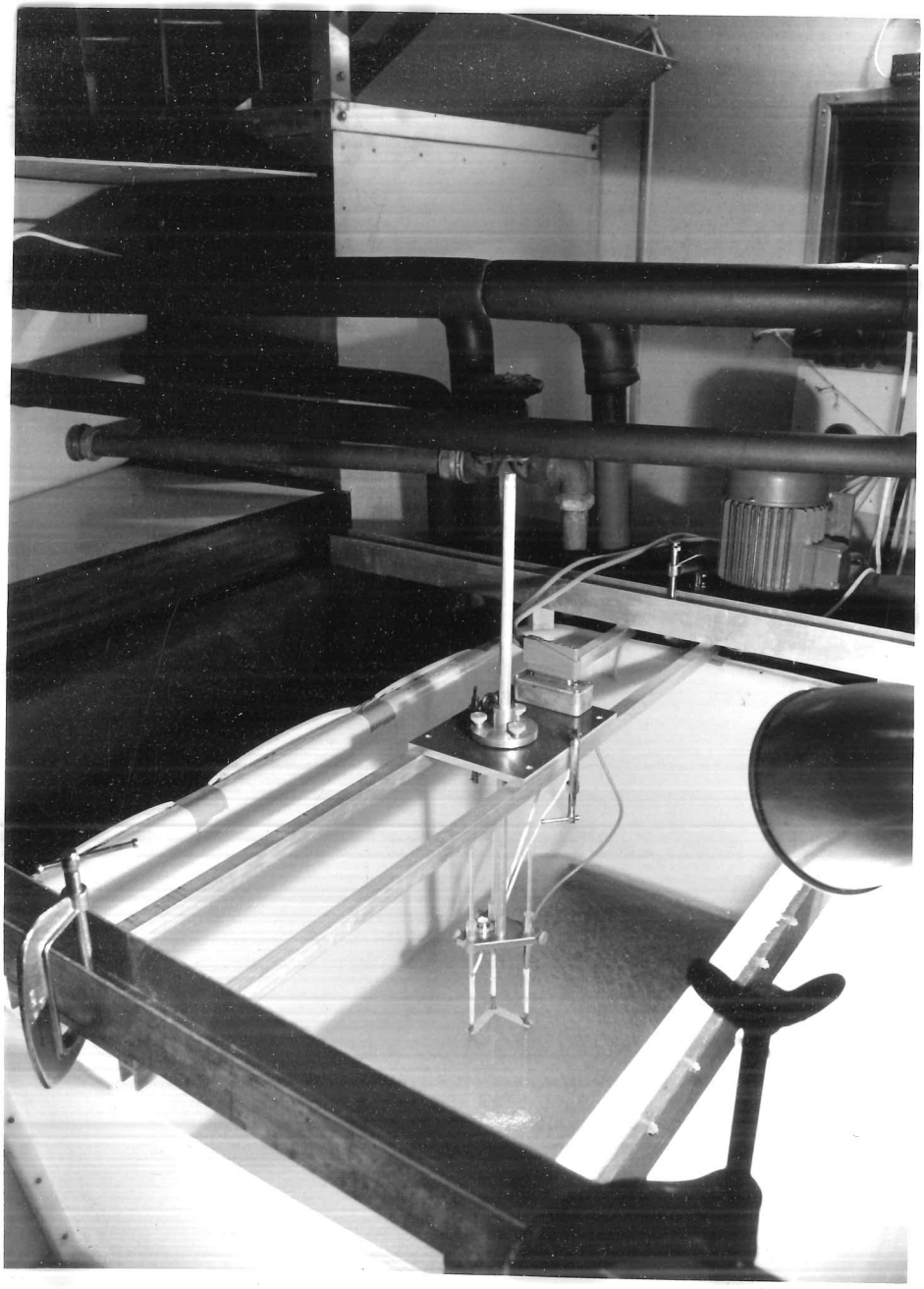

FIGURE 3.2 Photograph showing the initial ice skim on tank B (centre of photograph). The pump, valve and pipes are in the background. Tank C is on the top left of the photograph. Thermistor probes used during Run 8 are shown in position in tank B, which is just over 100cm long. The current flows towards the pump.

A rule of thumb for avoiding secondary eddies in channel or pipe flow is that the width should be approximately six times the height (R. Britter, personal communication). In the present case the width to height ratio is four so that we have taken the precaution of choosing a test tank with curved edges at the base which also assists in the reduction of secondary flow. It was not possible to produce a well-developed velocity profile in our test tank since we would have required an inlet section 10 times longer than the cold room (Schlichting, 1968). Thus, although it has not been possible to model the boundary layer found under sea ice in nature, we have chosen current speeds (between 2 and 4cms^{-1}) similar to those measured under Arctic sea ice in locations where c-axis alignment was observed (Weeks and Gow, 1979; Kovacs and Morey, 1978).

To maintain a constant current under the ice of the test section, the depth of the water layer beneath the ice is kept constant. This is achieved by adding brine to lift the thickening slab of ice upwards. The addition of brine with a concentration lower than that in the experiment also makes it possible to avoid the rise in concentration that accompanies the rejection of brine on freezing in a closed system. However this higher freezing point solution, even when cooled to the stage where ice crystals form on the surface, inevitably produces a thermal disturbance to the system. We were therefore always careful to add much less than 10% of the total volume of brine in the apparatus, during the time taken for the fluid to circulate the system once. The level at which the ice-water interface is to be held to maintain the constant volume (subsequently called the reference level) and a scale for measuring ice thickness are inscribed on a 1.2cm thick perspex window which covers one side of the test section. A periscope was constructed from a plastic drainage inspection pipe to observe the freezing process.

To simulate freezing in the ocean, our model sea ice should believe that it is surrounded by an infinite sea ice sheet. Heat loss through the sides of tank A is therefore reduced by heating tapes and by 2cm thick expanded polystyrene foam. When the pump is operating it is not necessary to use these tapes since the heat from the pump and the turbulence in the outer tank cause the ice to be thinner than in the test section. Thus although, in principle, the ice cover on the outer tank should provide the

ideal thermal boundary condition at the edges of the test section, in practice it is important to further insulate all sides of the inner tank, except the window, with 2cm of expanded polystyrene foam and Karrimat insulation. All pipes are covered with Armaflex insulation and heating tapes are placed around the overflow inlets. Despite the quantities of heat produced by the pump, the "overspill" hole on the shaft could only be kept open with heating tapes. If this is allowed to freeze over, brine is drawn into the pump motor.

Corrosion is a problem in experiments with cold salty water. Where possible plastic or paper has been used but where the machining qualities of a metal are required copper was selected. The pump shaft is gunmetal. Coating the steel tank with chlorinated rubber paint was completely unsuccessful. Epoxy based paint proved tougher but we were still faced with two holes after as many experiments. Finally the tank was lined with a tailored butyl rubber insert which is ideal for this sort of experiment.

Experiments performed on this apparatus took between 4 and 14 days to complete and since they differed in detail we shall describe each individually. A separate cold room was set up for the analysis of samples which would generally entail a further 1 to 3 months of work. This analysis was similar for each experiment and we shall describe the procedures in the next section.

3.2 Sample analysis

Analysis and storage of samples must take place at temperatures low enough to avoid structural change in the NaCl ice. Gow (1980) reports that no recrystallisation was observed in cores from the Antarctic ice cap which were stored for a number of years at -35°C. However this was not the case for samples stored at -10°C to -18°C. The problem is even greater for the NaCl-water system than for these land ice cores since there is 21°C difference between the~~ir respective~~ of NaCl ice and the freezing point of pure ice. eutectic point~~s~~. To keep below the eutectic point, -25°C was chosen as a reasonable temperature at which to work and store the artificial sea ice. We checked for recrystallisation and grain growth in samples which had been stored at this temperature for

several months and found no evidence of any changes.

The ice was dealt with in the following six stages;

1. The right-handed coordinate system which we use is shown in figure 3.1 and 3.3. The sheet of sea ice was cut into managable blocks and the edge at the largest value of x (i.e. the downstream edge in forced flow experiments) was marked with dye. The block was then placed in a labeled polythene bag, the code for positions being given in figure 3.3(a) to (d). Run 7 does not fit the general pattern used in the other experiments because cold room breakdown made it necessary to perform the analysis of these samples more rapidly.

2. At least one block was chosen to give ice "salinity". This was cut up into 1 or 2cm chunks which were melted within 24 hours of the completion of the experiment and measured either with a salinity-temperature bridge or with a conductivity measuring set. The conductivity meter had been calibrated with Copenhagen water and we found good agreement with standard tables. To obtain NaCl concentration from conductivity we therefore used standard tables (Wolf et al, 1978). When using the salinometer, the salinity reading was converted to conductivity and hence to concentration of NaCl using tables. This procedure was checked by measuring a selection of samples with both the conductivity meter and the salinity bridge and again agreement with tables and between meters was good.

3. The ice thickness at the four edges and on the four faces of each block were recorded along with the horizontal dimensions at the top and bottom. These were used to construct a contour map of the ice thickness at the end of the experiment, assuming the upper ice surface was flat (figure 3.3).

4. At selected locations, vertical sections approximately 1cm thick were photographed against a black background to record features such as brine drainage channels.

5. The ice thickness contour map and knowledge of the heat and fluid flow were used to choose the locations at which thin sections were made. A Leitz base sledge microtome was modified to handle large samples

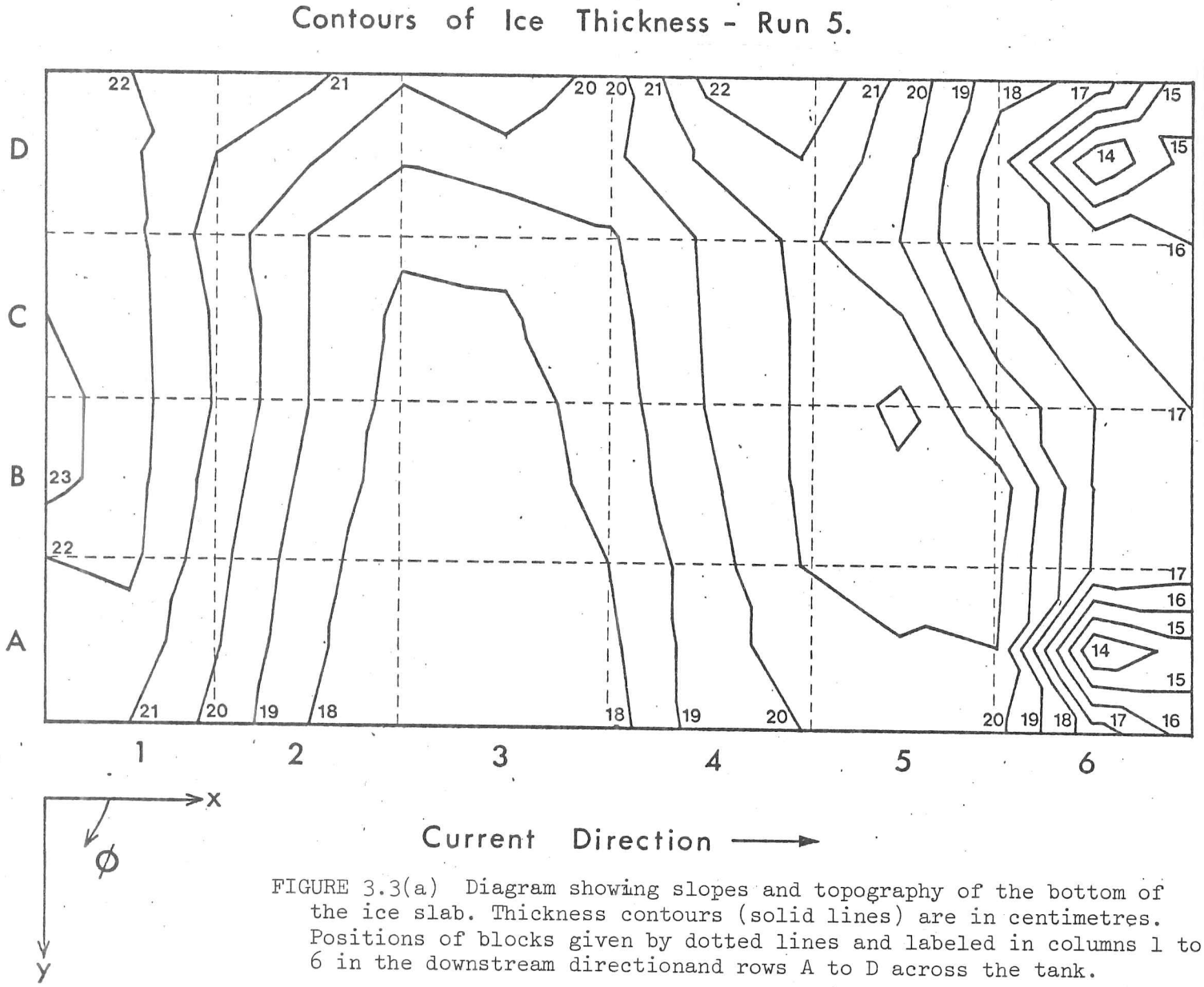

FIGURE 3.3(a) Diagram showing slopes and topography of the bottom of the ice slab. Thickness contours (solid lines) are in centimetres. Positions of blocks given by dotted lines and labeled in columns 1 to 6 in the downstream directionand rows A to D across the tank.

Contours of Ice Thickness - Run 6.

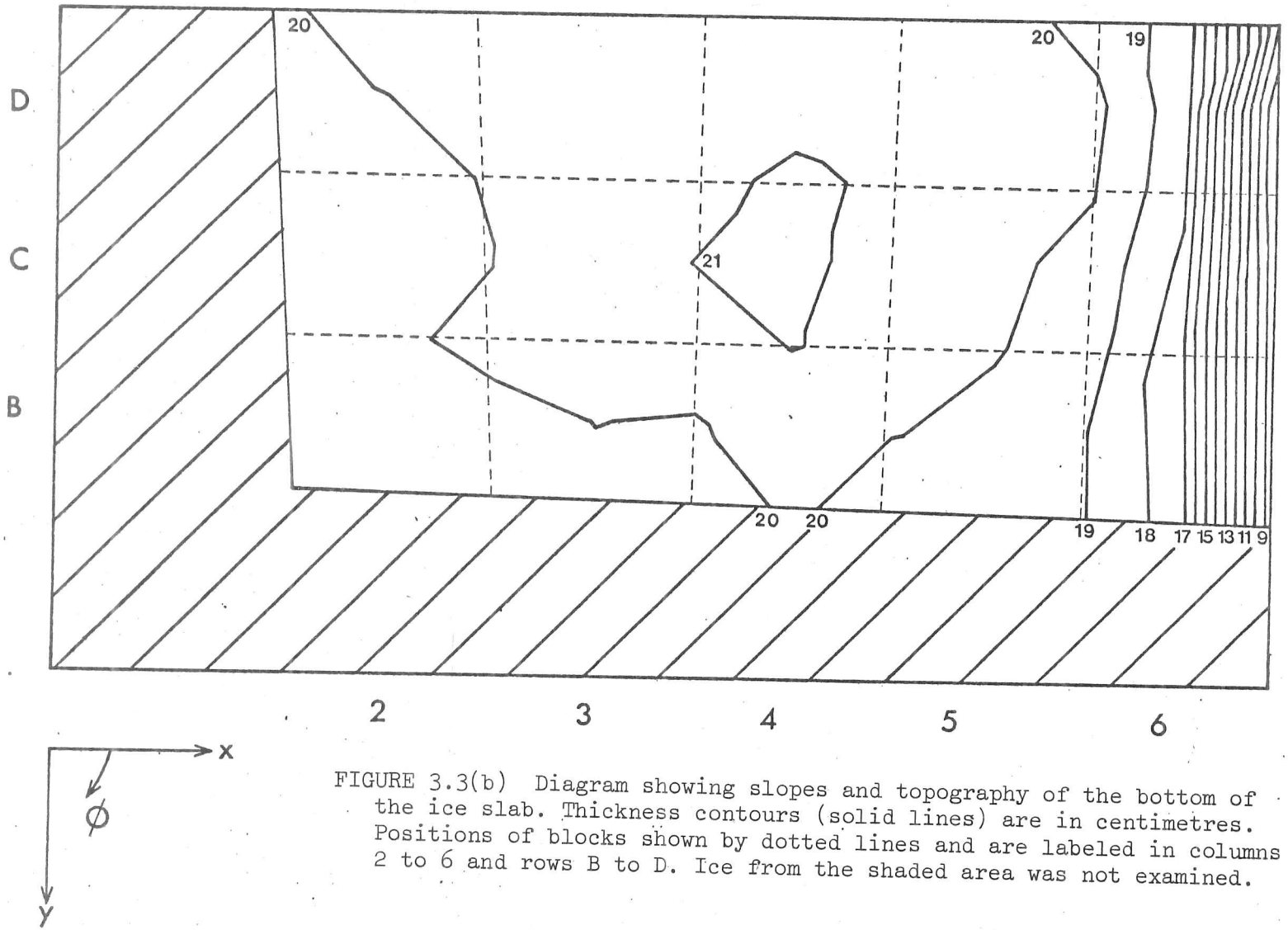

FIGURE 3.3(b) Diagram showing slopes and topography of the bottom of the ice slab. Thickness contours (solid lines) are in centimetres. Positions of blocks shown by dotted lines and are labeled in columns 2 to 6 and rows B to D. Ice from the shaded area was not examined.

Position of Blocks, Thin Section and Ice Thickness Contours
Run 7.

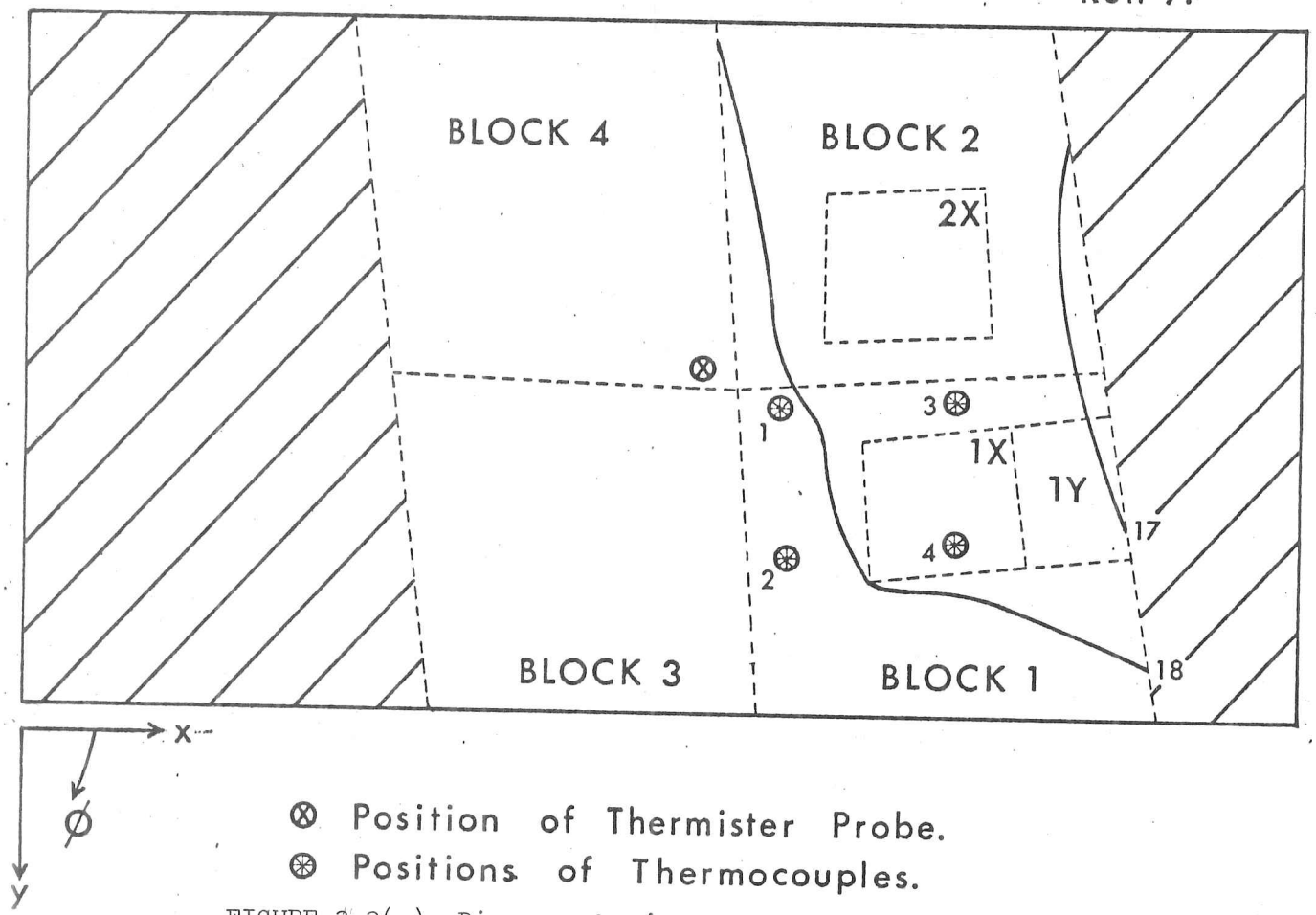

FIGURE 3.3(c) Diagram showing the slopes and topography of the bottom of the ice slab with thickness contours in centimetres. Thin sections were taken at positions 1X and 2X (marked by dotted lines) and salinity was measured at 1Y. The large Blocks 1 to 4 are also marked by dotted lines. Ice from the shaded area was not examined.

Contours of Ice Thickness - Run 8

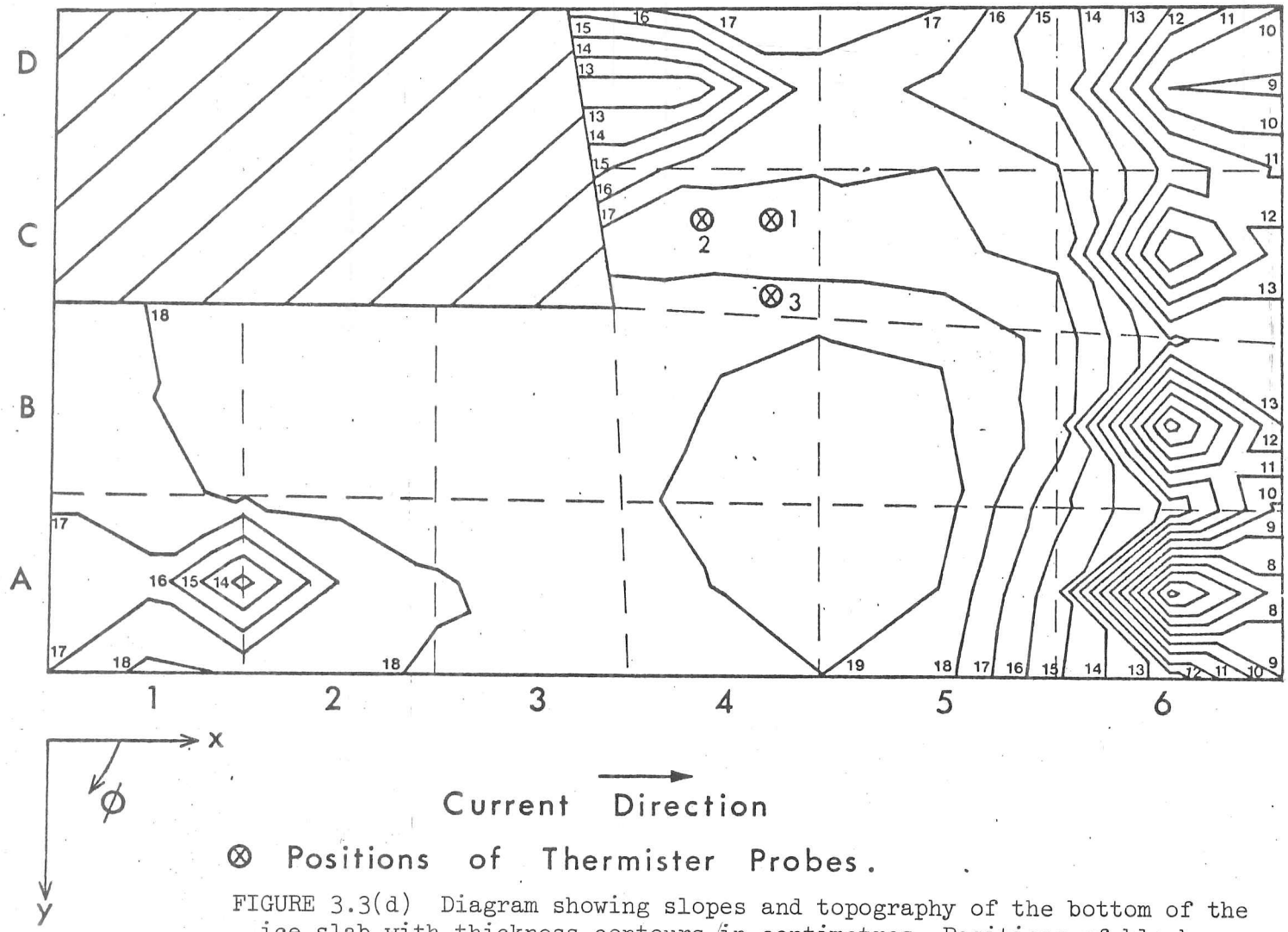

FIGURE 3.3(d) Diagram showing slopes and topography of the bottom of the ice slab with thickness contours in centimetres. Positions of blocks given by dotted lines and labeled in columns 1 to 6 and rows A to D. Ice from the shaded area was not examined.

(10.5cm X 10.5cm) and to work at -25°C. Thin sections were prepared following the procedures in Langway (1958). Spherulitic growth, similar to that described in Knight (1962b, 1967), frequently took place at the ice-glass bond. It was most troublesome if the spherulites formed slowly so that it was important to reduce the section to its final thickness of 0.05cm as rapidly as possible. For this reason the microtome knife was always kept well stropped.

6. The c-axis measurements were made on a universal stage which has been specially designed to deal with the large grain sizes found in ice. Dr. R. Ramseier of SURSAT, Canada kindly supplied drawings for the construction of this stage. A standard technique for finding the c-axis of a grain of ice has been described in Langway (1958). However methods of collecting a sample of measurements from a population vary and we shall describe the procedure that we followed.

3.2.1 Sampling of c-axis measurements

The conditions during freezing allow the location, depth and orientation of a thin section to be chosen. However such subjectivity is undesirable when making c-axis measurements. We wish to know the areal proportion of c-axes in a particular range of directions. Thus, unlike many other sampling problems, we wish the large grains to be more frequently sampled than the smaller ones. The thin section is therefore regarded as a continuous distribution of c-axis directions rather than a group of grains of finite dimensions. From this we draw a stratified, random sample (Chayes, 1956) which is an unbiased representation of the total population. This was carried out by placing a 1cm X 1cm grid over the thin section and selecting a coordinate pair within each of these squares using random number tables. This method is efficient, avoids clustering and does not require any definition of grain size.

3.3 Preliminary runs

Four experiments were performed before we were satisfied that freezing took place in a realistic manner. We mention these briefly because they illustrate some of the problems we encountered. The first attempt, after ten weeks of ice growth, resulted in the ice melting at -30°C. On analysis the solution was found to contain large amounts of paint polymers, some salts of iron and aluminium and, by comparison, a mere trace of NaCl! After extensive modification to our apparatus, the second run was considerably more successful and has been described in Langhorne (1980). Over 30cm of ice was grown in 17 days but analysis showed that most of the accumulated ice thickness was due to consolidated frazil. Figure 3.4 shows the small grain size and the high air bubble density obtained from this run . Despite this, we were encouraged to find a very weak downstream alignment (figure 3.5, see section 3.8.1 for an explanation of the fabric diagram) superimposed on the c-axis vertical distribution of the frazil ice. Run 3 was similarly hampered by the formation of frazil ice and, although we overcame this problem during Run 4, this experiment reached an abortive conclusion when the "overspill hole" on the pump shaft froze shut, drawing brine into the pump motor.

3.4 Detailed description of experiments

In this remainder of the chapter we describe four successful experiments, two of which were performed in brackish water and two in saline solution. It has been suggested that a crucial test of the ideas of Weeks and Gow (1978) lies in the texture of fresh water ice grown in a current. That is, the planar interface of pure ice has no means of interacting anisotropically with the current and the strength of the alignment cannot increase in these circumstances. However there are other physical properties whose directional dependence change as we move from the pure to the saline material and these may be responsible for the preferred orientation of c-axes. For example, the thermal conductivity of pure ice is virtually isotropic but it is well known that the laminate structure of sea ice causes this property to be anisotropic. Thus, the observation of zero rate of change in the strength of alignment is a

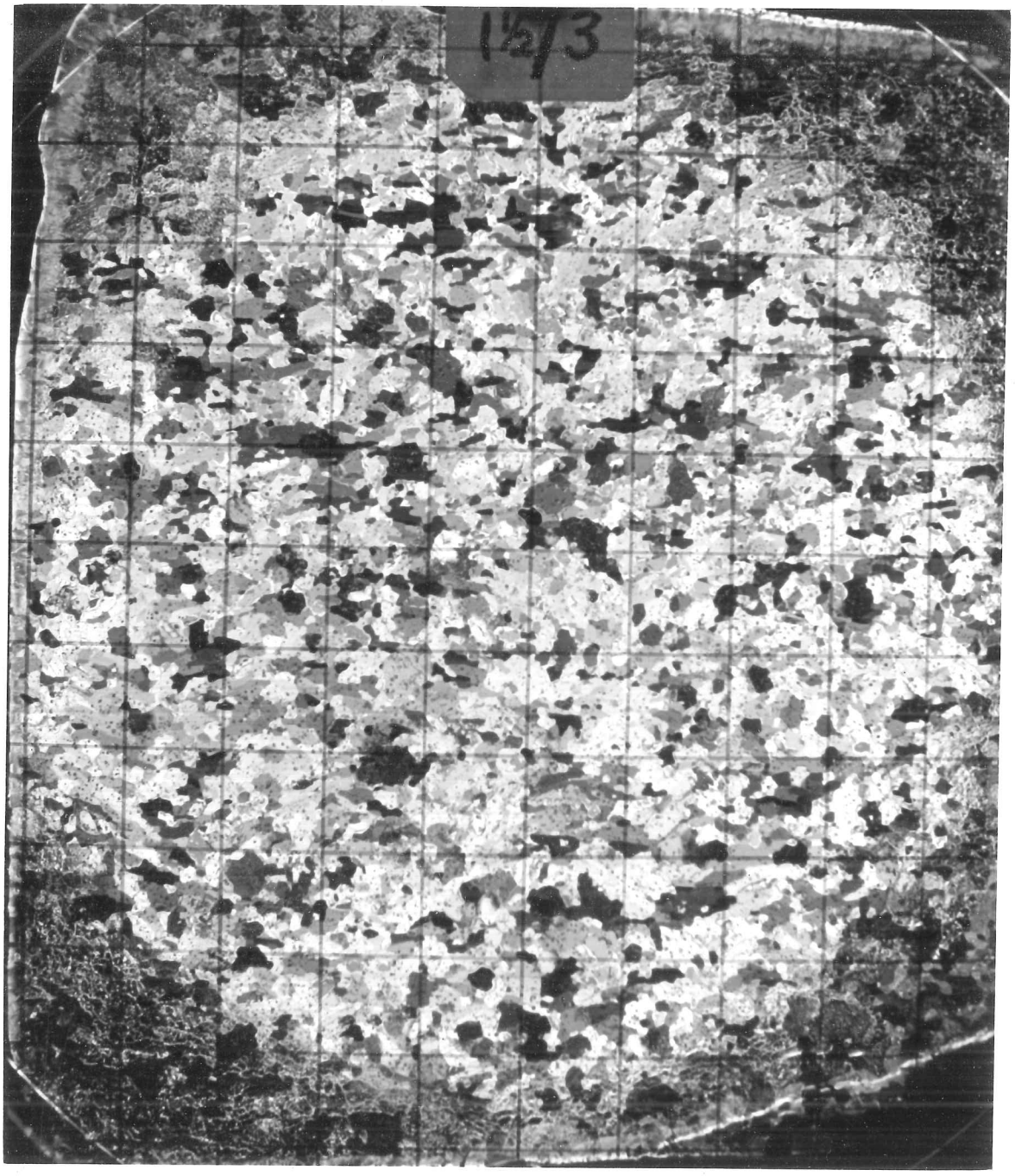

FIGURE 3.4 Horizontal thin section from 30cm below the ice surface in Run 2. Note the small grain size and the high air bubble density. Section covered by a 1cm grid. The current flowed from the top to the bottom of the photograph.

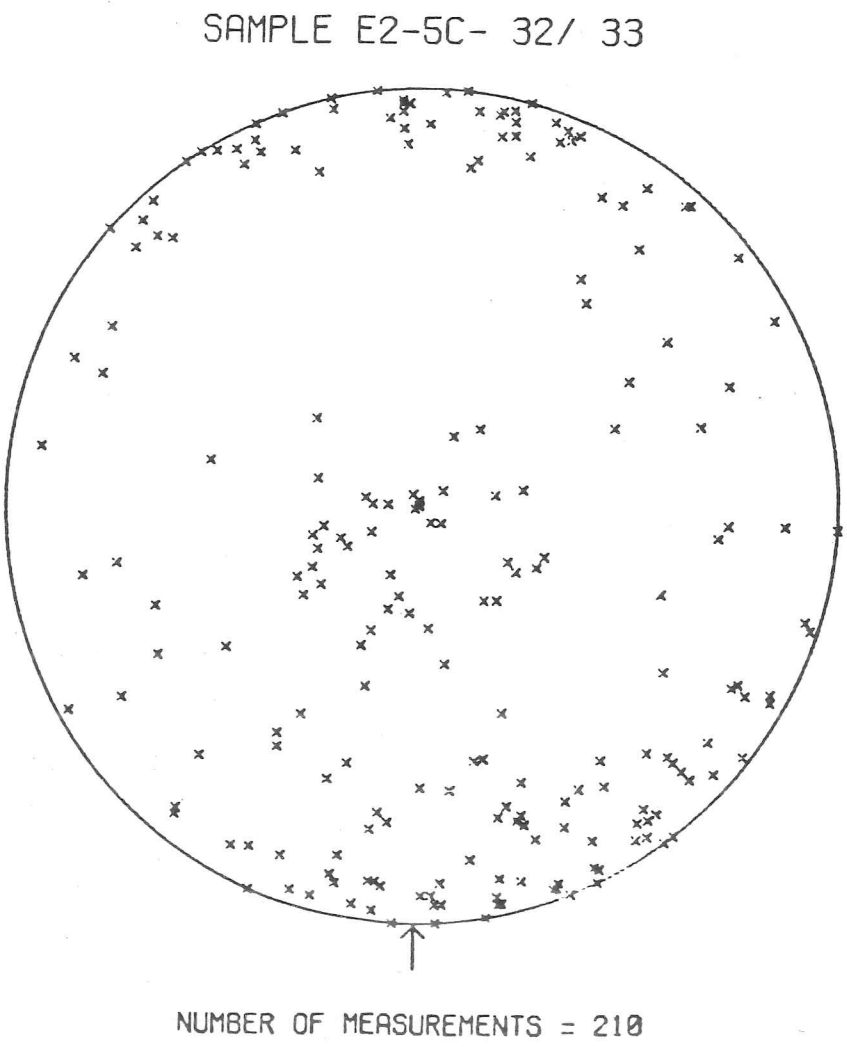

FIGURE 3.5 Equal-area projection of the c-axis measurements, 30cm from the upper ice surface during Run 2. Arrow is approximately the current direction in the experiment.

necessary, but not a sufficient, condition for the proof of the control of the current on the orientation of the c-axes. The stability of the water mass also varies with salinity and, rather than perform experiments in pure water, we shall compare saline ice grown from a brine which is thermally stable (brackish) with that from a thermally unstable solution (saline). Comparison of experiments with and without forced flow is obviously essential.

3.4.1 RUN 5 - Brackish - Forced Flow ($u_\infty = 3.4 cms^{-1}$)

The aims of this experiment were;

(i) to find the effect of forced flow on ice growing in a solution which is thermally stable;

(ii) to perform the low concentration portion of the brackish-saline comparison.

Air temperature : $-20 \pm 3^{o}C$

Concentration : cooled brine was added during the experiment to maintain a constant current under the ice (see section 3.1) and this also kept the solution concentration between 17 and 19‰. At these concentrations the brine can be stably stratified since the temperature at which the solution has maximum density is above the freezing point. However, the rejection of brine on freezing will produce concentration-driven convection when the growth rate, and thus the solute Rayleigh number, are large. As the growth rate falls, the conditions may become suitable for the formation of salt-fingers as described in Turner (1973).

Flow : velocity profiles are given in section 3.7.1.

Growth velocity : figure 3.6 shows that the growth velocity tended towards zero after approximately 20cm of ice had grown.

Nucleation : the water level at the beginning of the experiment was set 8.5cm above the reference level. This ensured that the initial skim did not form on a disturbed surface and prevented the crystals of this fragile

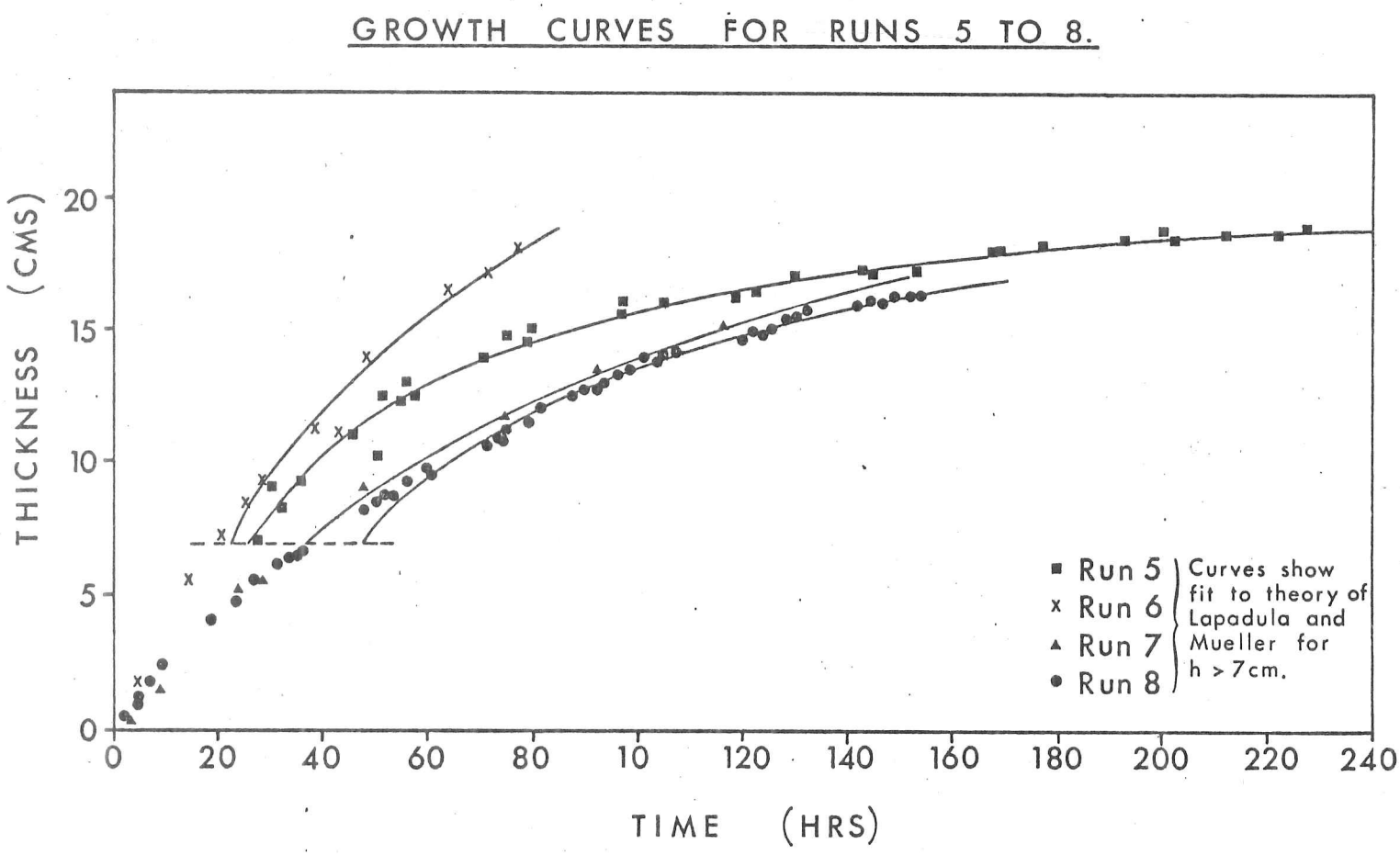

FIGURE 3.6 Diagram showing the increase in ice thickness during Runs 5 to 8. Symbols show the measurements for each experiment and the curves are the predictions of the theory of Lapadula and Mueller.

layer being herded downstream. Within 4 hours of the first appearance of ice there was a solid slab covering the test section.

Heat flow : after a solid cover had formed, three fans were placed over the inner tank to increase the turbulent heat transfer from this region. The heating tapes gave a total output of 400W.

Relative ice thicknesses : ice nucleation and growth was much more rapid on the test section than in the outer tank. For example, when the ice on tank B was 10cm thick it was only 1-2cm thick on tank A.

Structural observations : by the time the ice was 10cm thick the patchy appearance of a skeletal interface was not obvious and when the ice was finally removed there was no evidence of a cellular structure. Unfortunately the visibility under the ice was not good enough to give an direct measurement of the time at which this cellular to planar transition took place. We shall return to a discussion of this in section 4.3.2.

3.4.2 RUN 6 - Brackish - No Forced Flow

The purpose of this experiment was;

(i) for comparison with Run 5 but without forced flow.

Air temperature : $-20 \pm 3^{o}C$

Growth velocity : it can be seen from figure 3.6 that the growth rate has not been accurately matched to that in Run 5.

Concentration : the addition of cooled brine during the experiment was not necessary and the concentration was allowed to rise from 17‰ to 22‰

Heat flow : because the pump produces heat it is difficult to reproduce the thermal regime in corresponding experiments with and without forced flow. Ideally we would like to have fluid motion in the outer tank without flow in the test section. From the practical point of view this was not possible

and, as an alternative, the valve on the pump was closed while the motor was running so that heat was produced but there was no forced flow in the test section. However this prevented ice formation and we were forced to switch the pump off, leaving large thermal gradients in the fluid. Fans were again placed on the inner tank once the ice was solid and heating tapes gave the same output as during Run 5.

Nucleation : the unusual thermal conditions in the cooling down period caused the initial nucleation to differ from that observed in the other three experiments. Growth began in the outer tank and the ice remained thicker there during the first stages of the experiment. Despite this, the effect of the heating tapes was such that 28 hours after ice formation began in the test section, the areas around the edges of tank A and around the pump were still ice free.

Relative ice thicknesses : although ice growth began in tank A, the fans ensured that the ice in the test section rapidly took over this lead. This slab was relatively flat, except at the edge closest to the honeycomb where the interface shelved sharply upwards.

Flow : the possibility of some directional free convection exists but no direct observations were made.

Structural observations : a skeletal interface was noted throughout the experiment.

3.4.3 RUN 7 - Saline - No Forced Flow

The aims of this experiment were;

(i) to reduce lateral heat flow;
(ii) to measure the thermal gradients in the horizontal and vertical planes;
(iii) to observe natural convection carefully;
(iv) to look, very simply, for signs of horizontal stresses in the artificial sea ice sheet;

(v) to use a solution concentration high enough for the colder surface water to overturn with the warmer brine underneath;

(vi) for comparison with Run 8 but without forced flow.

Air temperature : $-15 \pm 3^{o}C$

Growth velocity : the air temperature during this experiment was higher than its forced flow counterpart and we see from figure 3.6 that this has successfully given very similar growth velocities in the two experiments.

Concentration : the initial concentration was sufficiently high for the solution density to be maximum at the freezing point. Thermally-induced mixing therefore produced uniform profiles of temperature and concentration before freezing began. A starting concentration of 29‰ was used and this rose to above 38‰ during the experiment because no compensating additions of brine were made.

Nucleation : the air temperature in the cold room was raised as the freezing point was approached and a careful record was kept of the initial ice formation and the resulting natural convection. In the test section a complete cover formed in approximately 2 hours. The air temperature was again dropped to $-15^{o}C$ when the ice in the inner tank was solid.

Flow : a description of the patterns of convection during ice formation is given in section 3.7.4.

Heat flow : the heating tapes were set to give a fraction of the output used in the previous two experiments and fans were not placed on the inner tank. Vertical temperature gradients were measured, throughout the experiment, with a thermistor probe and thermocouples were used to find temperature differences in three directions in a horizontal plane, 5cm below the ice surface. These measurements are described in section 3.5.1 and in appendix 1.

Relative ice thicknesses : as a result of the reduction in lateral heat flow, the ice thickness in the inner and outer tanks was fairly uniform.

Stress : because there were no additions of brine during this experiment, the ice froze firmly to the sides of the tanks A and B causing pressure to build up in the fluid below. This was relieved by the percolation of brine to the ice surface. Although this is not a good model of conditions in the field, it is difficult to imagine how the application of a hydrostatic pressure could influence the orientation of grains in the horizontal plane. There was no indication of the existence of horizontal stresses in the bubble-packing material which lined the walls of the test section during this experiment. These stresses would have produced an increase in air pressure within the bubbles. In a similar experimental arrangement, Knight (1966) also found no evidence of horizontal stresses.

3.4.4 RUN 8 - Saline - Forced Flow ($u_\infty = 2.9 cms^{-1}$)

The aims of this final experiment were as follows;

(i) to find the effect of forced flow on ice growing in a solution where the temperature of maximum density is the freezing point;
(ii) to reduce lateral heat flow; (iii) to measure horizontal and vertical temperature gradients when the pump is running;
(iv) to perform the high concentration portion of the brackish-saline comparison.

Air temperature : $-20 \pm 3^{o}C$

Growth velocity : the velocity was again approaching zero when the experiment was terminated indicating the limits that the pump imposes on the growth of ice.

Nucleation : the formation of the initial skim followed the same pattern as observed in Run 5. In the test section, the downstream corners and a strip approximately 15cm from the honeycombs were the final positions to become ice-covered. The latter location is influenced by the edge at the channel entrance. Current observations confirmed that flow was intermittent and variable in these two regions. It took two hours for the cover on the inner tank to become complete and, as in Runs 5 and 7, ice

formation on the outer tank lagged behind that on the test section. The initial water line was 5cm above the reference level.

Flow : a description of the velocity profile is given in section 3.7.2.

Relative ice thickness : the pattern observed during nucleation is maintained throughout the experiment and is due to the effects of fluid flow. The ice remained thinner in the outer tank than in the test section. This was most apparent under the support which rigidly fixed the periscope in front of the window. In previous experiments the periscope had been inserted into the outer tank when we wished to take a reading of ice thickness. However this disturbed the system, causing flooding on the ice surface, which we avoided in this run.

Heat flow : only the heating tape which prevented freezing around the pump "overspill hole" was used and ice growth in the test section was not enhanced with the fans. Before freezing began three thermistor probes were rigidly mounted in the inner tank, to measure horizontal and vertical temperature gradients (described in appendix 1 and section 3.5.2).

Concentration : the addition of cooled brine to maintain a constant current speed, also meant there was little increase in the concentration of the solution during the experiment (30‰ to 32‰). Because of the reduced lateral heat flow compared with Run 5, the ice was not freely floating and had to be lifted each time brine was added. A level was used to check that the ice surface was always returned to the horizontal in its new position.

A summary of the most important features of the four experiments is given in table 3.1.

TABLE 3.1

Measurement	BRACKISH		SALINE	
	Run 5 Forced flow	Run 6 Natural convection	Run 7 Natural convection	Run 8 Forced flow
Fluid motion	$u_\infty = 3.4 cms^{-1}$	no observations	light & variable	$u_\infty = 2.9 cms^{-1}$
Concentration	17-19‰	17-22‰	>29‰	30-32‰
Air temperature	-20°C	-20°C	-15°C	-20°C
Horizontal temperature gradients	0.1^a °Ccm^{-1}	0.05^a °Ccm^{-1}	0.02^a °Ccm^{-1} 0.02^b °Ccm^{-1}	0.07^a °Ccm^{-1} 0.10^b °Ccm^{-1}

a - deduced
b - measured

3.5 Temperature measurements

We have attempted, particularly in the saline experiments, to reduce the horizontal temperature gradients. However our apparatus is small and we can only be partially successful in doing this. It is important, therefore, that we know the magnitude and direction of this temperature gradient which may be the driving force for c-axis alignment.

We have measured the vertical temperature gradient in addition to the horizontal gradient. In pure ice, the vertical temperature gradient is always given, to a good approximation, by the temperature difference between the top and bottom surfaces, divided by the thickness of the ice. This is not necessarily the case in sea ice because it solidifies over the range of temperatures between the freezing point and the eutectic point. Thus if a sea ice sheet is thickening, latent heat is continously being released as brine pockets shrink and the vertical temperature gradient becomes a function of depth in the ice. Since the thermal properties of sea ice are functions of temperature and salinity which vary through the sea ice sheet, it is no simple matter to calculate the temperature-depth curve.

It is considerably simpler to measure the vertical thermal gradient than the horizontal temperature gradient and since the former is not strongly dependent on x and y, we may use it in the following way to obtain horizontal temperature gradients at all locations in our ice slab.

Close to the ice-water interface, we assume that the isotherms in the solid are approximately parallel to the boundary giving

$$\underline{H}_s = G_{si}\underline{s} \qquad [3.1]$$

where $\underline{H}_s$, the horizontal temperature gradient, and $\underline{s}$, the slope of the interface, are both vectors lying in the horizontal plane. G_{si} is the magnitude of the vertical temperature gradient in the solid at the interface. Thus, at all locations where there are c-axis measurements, the magnitude and direction of the slope of the interface can be measured to within 40% from figure 3.3 and from photographs of thick sections. Measurements of the vertical temperature gradient are given in appendix 1 and, using these in equation [3.1], we derive horizontal temperature gradients which compare favourably with measurements at two locations in sections 3.5.1 and 3.5.2.

In the course of the brackish experiments, only the vertical temperature gradient in the liquid was measured and this is used in the section 4.4 in relation to the stability of the ice-water interface. In appendix 1 we describe calculations of the horizontal temperature gradient during Run 5.

3.5.1 Horizontal Temperature Gradients - Run 7

During this run, vertical temperature gradients in the ice were measured with a thermistor probe while a grid of four thermocouples determined the horizontal temperature gradient at one location. The configuration and positions of these are shown in figure 3.3(c). We describe the details of the construction of these probes and the measurements of temperature and vertical temperature gradient in appendix 1.

Thermocouples were placed 5cm below the ice surface when the ice was 1.5cm thick and horizontal temperature gradients were measured between 1 and 2, 1 and 3, and 1 and 4 (see figure 3.3(c)). The magnitude and direction of the resultant horizontal temperature gradient and the uncertainty in this quantity are shown in figure 3.7. The measurement error on the chart recorder ($\pm 2\mu V$) and any calibration differences thermocouples are included in this uncertainty.

Because of the vertical temperature gradient (see figure A1.4), apparent temperature differences will arise from the inaccuracy in placing the junctions at exactly the same depth beneath the ice surface. This produces a systematic error in the measurement of the horizontal temperature gradient of the order of $\pm 0.005^{o}Ccm^{-1}$ in magnitude and $\pm 10^{o}$ in direction. The data of figure 3.7 appear to have a cyclic component in magnitude and direction which may also result from this positioning uncertainty. The periodic temperature at the surface (see figure A1.3) will be damped by an amount depending on its distance from the ice surface and the temperature difference between two such "out of phase" thermocouple junctions will then be cyclic. Thus, figure 3.7 shows the upper limit of the horizontal temperature gradient, at the location of the thermocouples, averaged over an area of $100cm^{2}$.

The ratio of the vertical to horizontal temperature gradients at any time is of the order of 20:1. Lewis (1967) estimates this ratio is 25:1 in 180cm thick sea ice and we are satisfied with our approximation to the field situation.

We are now in a position to check the accuracy of equation [3.1]. As we shall presently see, a sample of c-axis measurements was made on ice which formed between 110 and 130 hours. Using the results for the vertical temperature gradient at this time (figure A1.4), equation [3.1] gives

$$0.020^{o}cm^{-1} \qquad 160^{o}$$

The horizontal temperature gradient has been measured up until 100 hours only, when the magnitude and direction were

$$0.017 \pm 0.008^{o}Ccm^{-1} \qquad 149 \pm 15^{o}$$

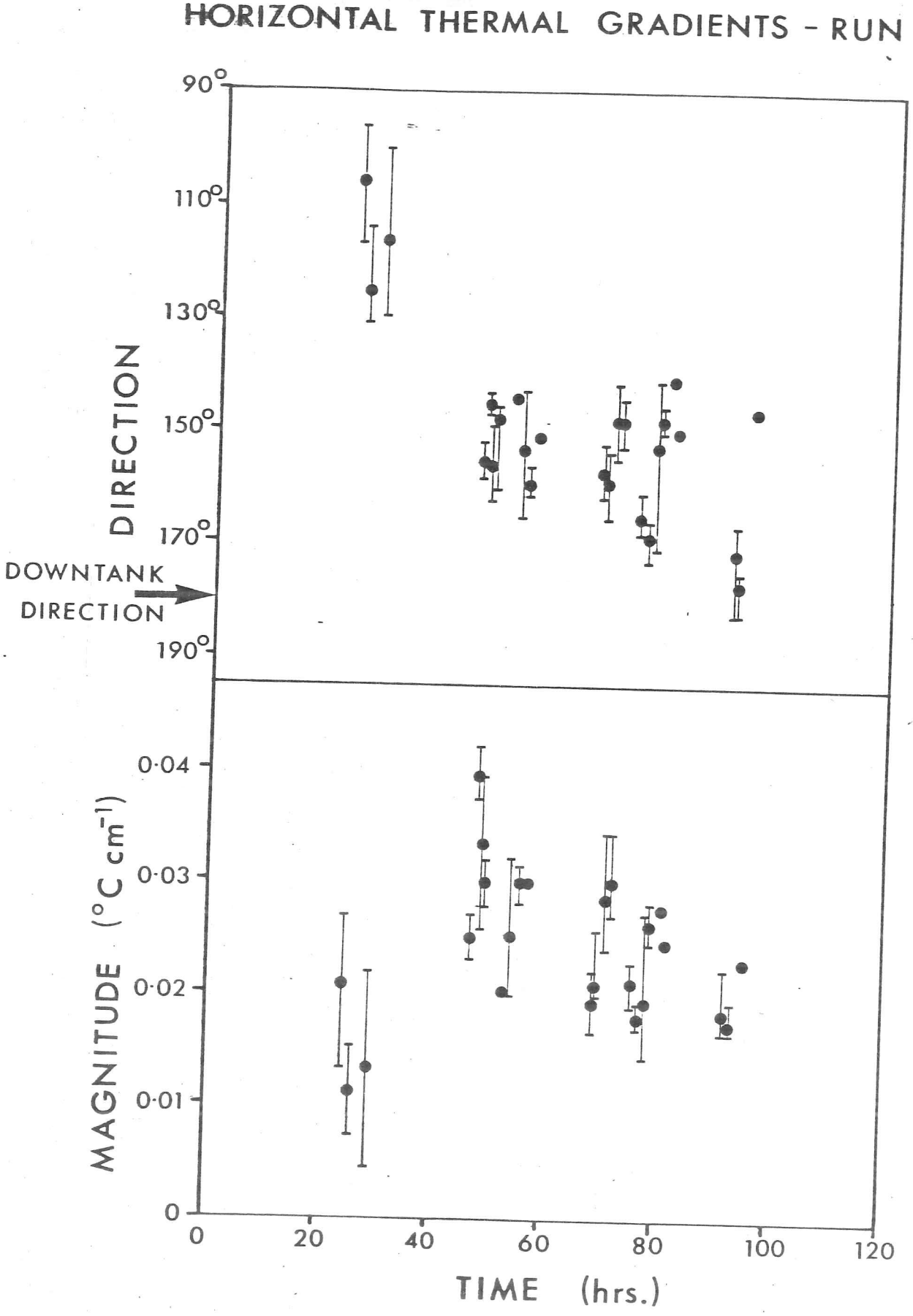

FIGURE 3.7 Horizontal temperature gradients measured by an array of thermocouples shown in figure 3.3(c). The direction is referenced to the coordinate system in figure 3.3 and the results are plotted so that the long axis of the tank is the origin of direction.

Thus, in this case, calculated and measured horizontal temperature gradients agree within 20%.

3.5.2 Horizontal Temperature Gradients – Run 8

From the discussion in the previous subsection it is obvious that it is very important to position the temperature sensors accurately in a plane parallel to the upper ice surface. In other words, gravity should be normal to the plane containing the sensors. The probe support designed for this purpose is described in appendix 1, along with the measurements of temperature and vertical temperature gradient performed during this experiment.

Figure 3.2 and figure 3.3(d) show the configuration of the probes, 1 and 2 being approximately 5cm apart in the downstream direction while 1 and 3 have a similar spacing in the cross-tank direction. Thus two components of the horizontal temperature gradient were measured at depths of 8, 10 and 12cm below the ice surface. Each error in temperature must be combined with the error due to the displacement of the thermistors in a vertical temperature gradient of $0.60^{\circ}Ccm^{-1}$. In comparison with this the 2% error in horizontal spacing of the thermistors may be ignored. The resultant horizontal temperature gradient and the corresponding errors in magnitude and direction have been found graphically and are shown in figure 3.8.

Comparison of figure 3.7 with 3.8 shows that the horizontal temperature gradients during the forced flow experiment were almost three times as large as those in the corresponding natural convection experiment. In addition, the ratio of vertical to horizontal temperature gradients has decreased to between 8:1 and 10:1. This is undoubtedly due to the heat from the pump. Figure 3.8 shows that within error, the direction of the horizontal temperature gradient is constant with time and independent of the depth at which it is measured. The same is not true of the magnitude. In all three cases this increases sharply as the interface approaches the thermistors then drops to a mean value which slowly decreases with time. This implies there is a narrow region at the interface where the vertical temperature gradient is different from the mean value. We shall discuss

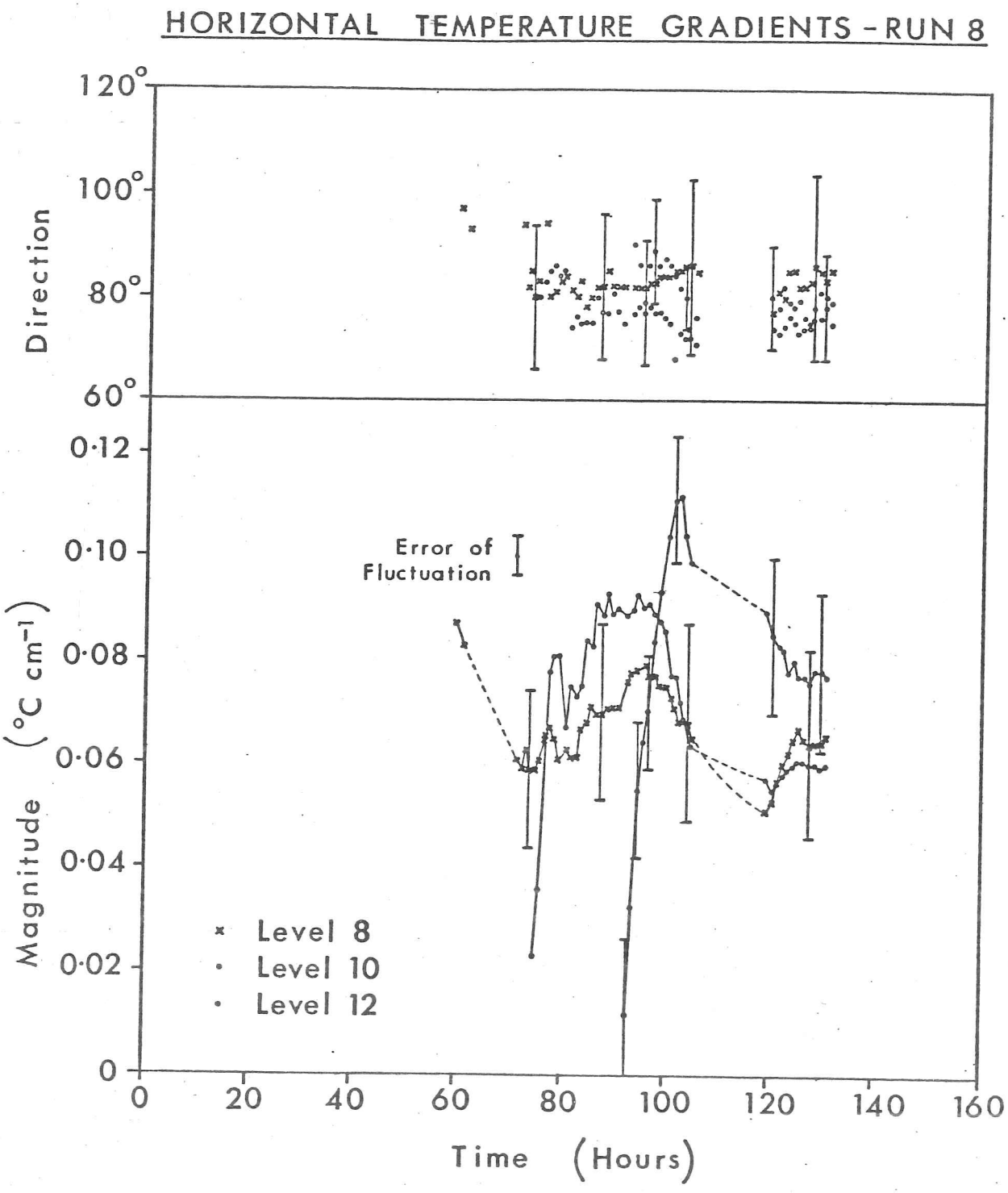

FIGURE 3.8 Measured horizontal temperature gradients at 3 levels during Run 8. The direction is given according to the coordinate system in figure 3.3 so that the gradients are approximately perpendicular to the current direction.

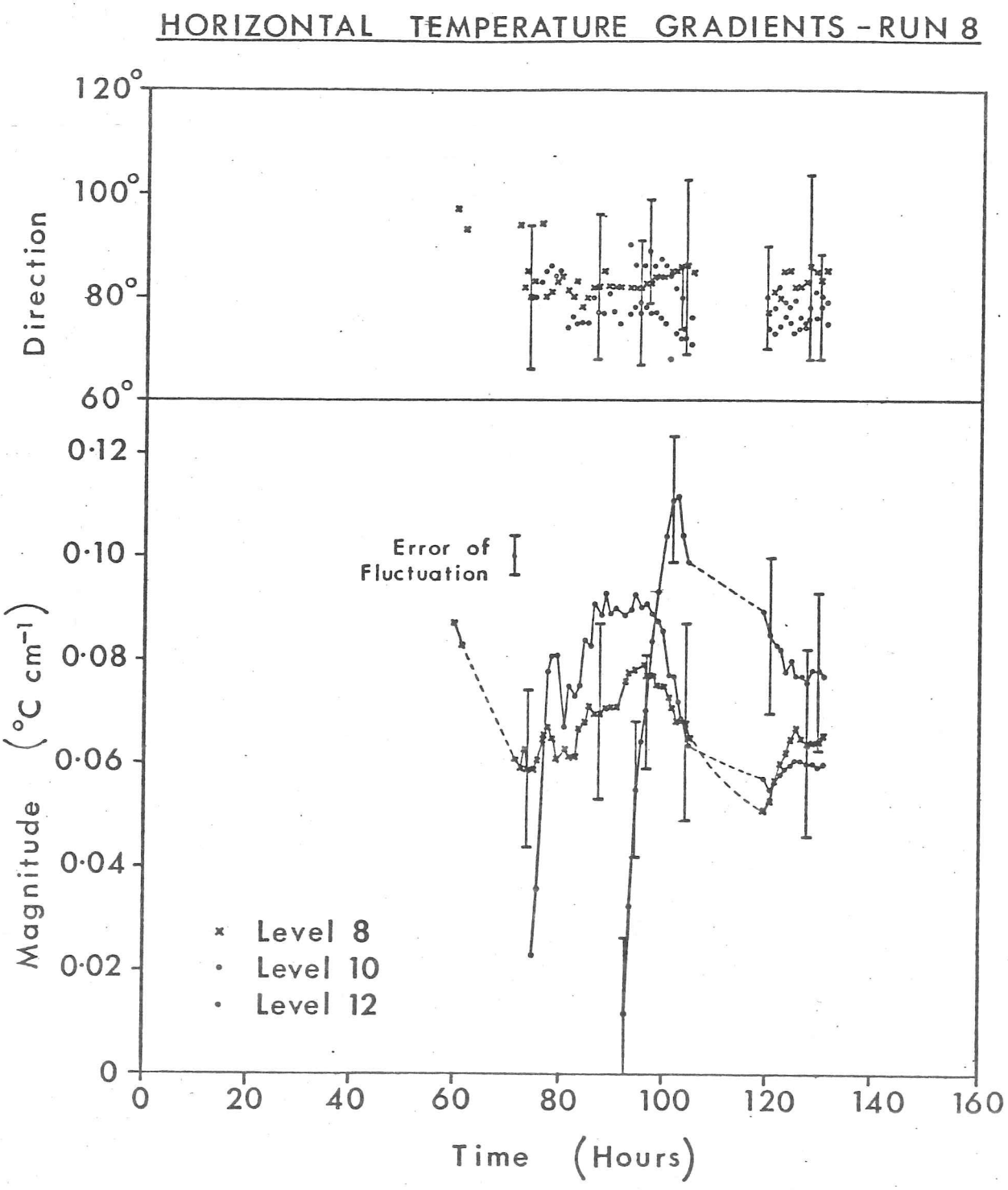

FIGURE 3.8 Measured horizontal temperature gradients at 3 levels during Run 8. The direction is given according to the coordinate system in figure 3.3 so that the gradients are approximately perpendicular to the current direction.

this further in section 3.5.3.

C-axis measurements were made at the location of the thermistor array, at a depth of 15cm which corresponds to a time of freezing of 115 hours (see figure 3.6). The horizontal temperature gradient, 12cm below the ice surface, at this time was

$$0.092 \pm 0.015^{o}Ccm^{-1} \qquad 80 \pm 10^{o}$$

which is again within 20% of the prediction of equation [3.1] of

$$0.108^{o}Ccm^{-1} \qquad 90^{o}$$

The vertical temperature gradient was taken from figure A1.6.

3.5.3 High Frequency Temperature Fluctuations - Run 8

The rectangular portion in figure A1.5(a) is expanded in figure 3.9 to show the range of the temperature fluctuations and the cooling rates at the ice-water interface. The amplitude of the fluctuations is typically $0.05^{o}C$ but may be as large as $0.1^{o}C$. The frequency is greater than 0.2Hz which was the maximum sampling frequency that we could obtain. We have already described previous observations of temperature fluctuations under growing sea ice in section 2.2.3, however these were sampled at much lower frequencies than the present measurements.

Temperature fluctuations during the solidification of metals (Cole and Bolling, 1966, 1967; Cole, 1967, 1971; Flemings, 1974) and semiconductors (Hurle et al, 1974) have received a good deal of attention. It has been conclusively shown that convection in the melt is responsible for these and that they increase in magnitude and frequency as the flow is increased (Cole, 1971). It is important to note that their occurrence does not necessarily imply turbulence in the melt (Cole, 1971) and they can be associated with slow, cellular and regular oscillatory motions of the fluid. Measurements of the critical Rayleigh number for the onset of oscillations have been made (Hurle et al, 1974) but the rectangular geometry and the low Prandtl number of molten metals prevents direct application to the present solidification problem. The experiments of

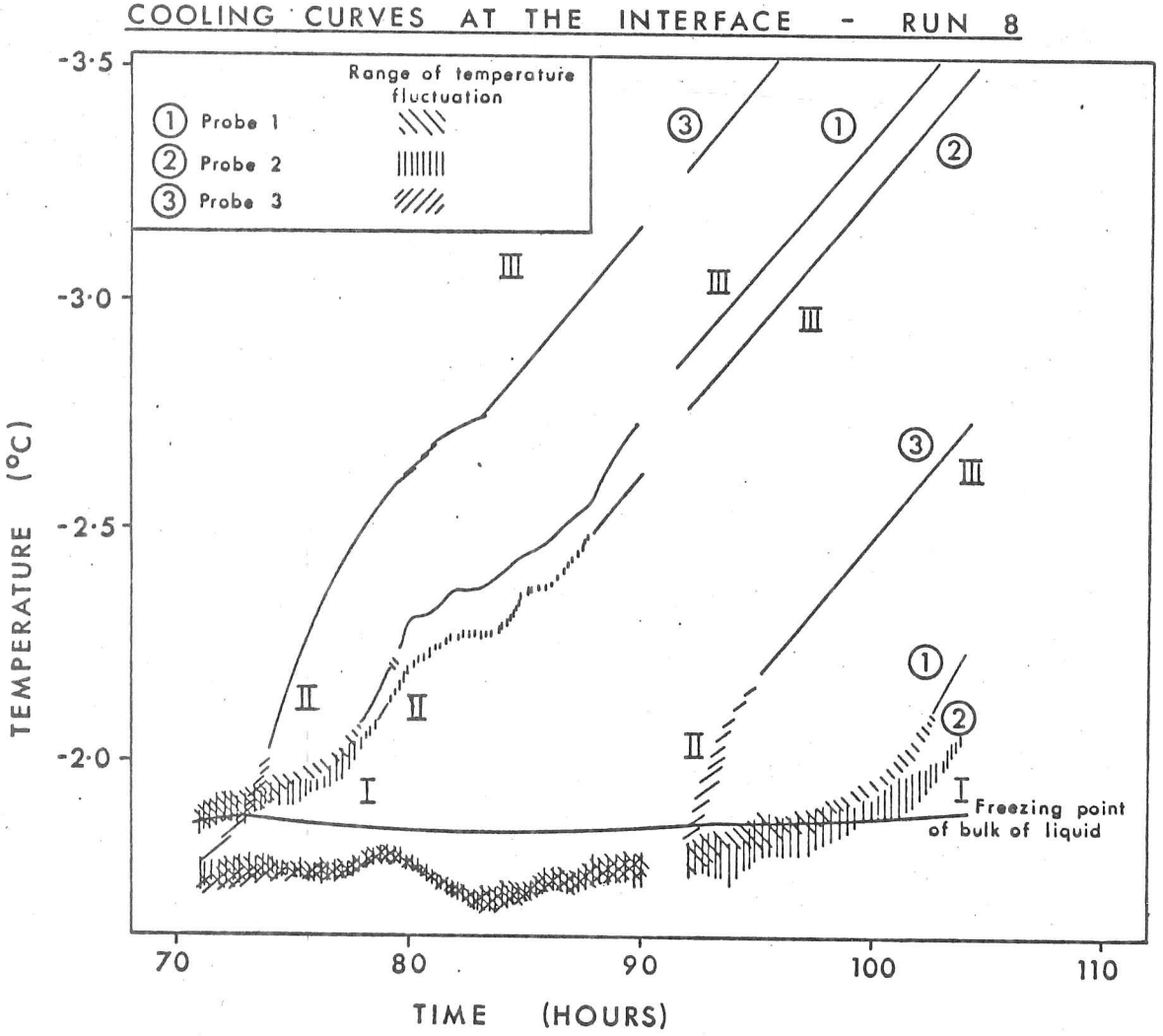

FIGURE 3.9 Expanded diagram of the rectangular area in figure A1.5. Hatched regions show range of high frequency fluctuations in temperature. Regions I, II and III are explained in the text and in figure 3.10. Note that temperature increases downwards in this figure.

Gilpin et al (1978) give more insight to our case. They observed temperature fluctuations associated with the formation of vortices in laminar flow over a heated flat plate under conditions of thermal instability. We shall discuss the effects of these vortices further in section 3.7.2.

Cole (1967) has measured temperature profiles in a convecting melt close to the solidifying front of a tin alloy. He found that there was a laminar region with a large temperature gradient and small temperature fluctations immediately adjacent to the interface. This was bounded by a buffer and finally a turbulent region where the oscillations in temperature were greater and where the thermal gradient was smaller. He also showed that the application of a forced flow increased the ratio of the temperature gradients in the laminar and turbulent portions of the boundary layer. Referring once again to figure 3.9 we compare Cole's findings with our own, assuming that the temperature regime is stationary and that we may interpret the cooling curves as the effective movement of the thermistors through successive temperature gradients; that is (Lewis, 1967)

$$\frac{\partial T}{\partial x} = v^{-1} \frac{\partial T}{\partial t} \quad . \qquad [3.2]$$

Figure 3.10 is a schematic interpretation of the results of 3.9. We have crudely catagorised the results on the basis of cooling rate or alternatively vertical temperature gradient. The properties of each of the regions are as follows;

Region I

This region is characterised by a small temperature gradient and large fluctuations in temperature which increase as the interface is approached. From direct observation we are certain that this region is below the macroscopic ice-water interface and since the freezing point in the bulk of the fluid exceeds the temperature in part of this zone, we may conclude that both temperature and salinity gradients exist in the liquid. Heat transport is by conduction and convection. This region is analogous to

SCHEMATIC INTERPRETATION OF COOLING CURVES - RUN 8

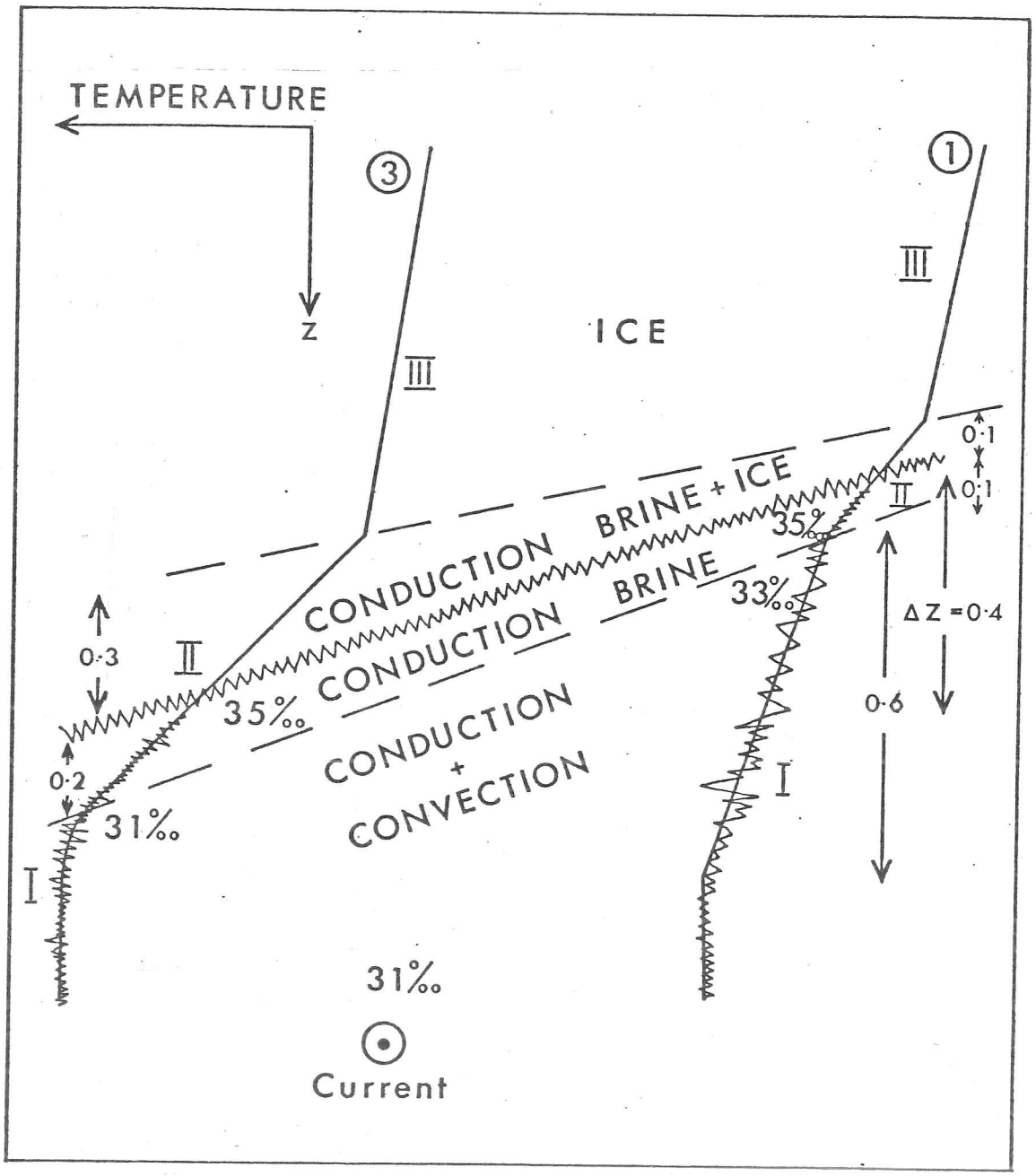

FIGURE 3.10 Schematic interpretation of the results shown in figure 3.9. Region I is in the liquid, Region II is "solid"plus liquid and Region III is "solid". See text for further discussion. Δz is the difference in ice thickness between probes ① and ③. Probes ① and ② are assumed to be coincident (see figure 3.3(d)). Distances in diagram are in centimetres and the current is perpendicular to the plane of the page. The position of the ice-water interface is estimated and shown by a jagged line.

Cole's buffer region since there is no zone of well-developed turbulence in this experiment.

Region II

A sharp increase in the vertical temperature gradient now takes place with temperature gradients typically of $1.3^{o}Ccm^{-1}$. Any brine in this layer exceeds the bulk salinity by 6‰ and the concentration gradient, close to the interface, may be as large as 20 to 24‰cm^{-1}.

The steep temperature gradient indicates that this is a region of thermal conduction and that there is brine present. Calculation of the thermal conductivity yields a value between that of saline ice and brine. In addition the existence of rapid temperature fluctuations in a portion of this zone suggests that some of Region II is below the interface since fluid motion cannot penetrate too far into the intercellular grooves without buoyancy forces becoming dominated by viscous forces. Unfortunately we were unable to determine the position of the interface to sufficient accuracy during the experiment to mark it on figure 3.10 and we have therefore taken its most likely position as the level at which temperature fluctuations cease. This region corresponds to Cole's laminar zone.

Region III

This region is within the solid and the values of temperature gradient from equation [3.2] agree with measured vertical temperature gradients to within 15% which is satisfactory. Figure 3.9 shows that even in this zone there are disturbances from the mean temperature gradients. This has previously been attributed to the passage of brine through the ice (Lake and Lewis, 1970).

3.6 Growth curves

We have already seen the growth curves for Runs 5 to 8 in figure 3.6. Many equations describing ice growth exist in the literature (see Stehle, 1965 for a summary of some of these) but the most appropriate for our experiments is the formulation of Lapadula and Mueller (1966). This considers solidification on a flat plate in an infinite fluid at an initially uniform temperature. Heat is transferred to the solid from the liquid by convection and, in our particular case, we assume that this is uniform in space and constant in time. The treatment assumes that;

(i) all the physical parameters are constant,

(ii) there is a flat and definite interface between the solid and the liquid,

(iii) the temperature of the cold surface is uniform and constant,

(iv) conduction of heat in the solid is one-dimensional.

Lapadula and Mueller (1966) have used Biot's method to solve the problem and although their solution is approximate, the numerical solution of Beauboeuf and Chapman (1967) shows that, for the thermal properties of sea ice (i.e. $\eta \sim 0.10$), there is negligible difference between the two results.

Rewriting Lapadula and Mueller's treatment for the special case of a constant heat flux gives the following non-dimensional expression,

$$\frac{\kappa_s}{f(\eta)} \frac{t}{\ell^2} = - \{ \frac{h}{\ell} + \ln(1 - \frac{h}{\ell}) \} \qquad [3.3]$$

where

$$\ell = \frac{k_s \Delta T}{q} , \quad \eta = \frac{K_s \Delta T}{\kappa_s L} ,$$

and

$$f(\eta) = \frac{2\eta^2 + 10\eta + 15}{5\eta(\eta+3)} .$$

In the above

$$\Delta T = T_{li} - T_{surf} ,$$

where

h = ice thickness

T_{li} = temperature of the liquid at the interface

T_{surf} = temperature at the ice surface

q = convective heat input from the liquid

κ_s = bulk thermal diffusivity in the solid

L = latent heat per unit volume

K_s = bulk thermal conductivity in the solid

All quantities are time averages.

It is well known that the thermal constants for sea ice are a function of salinity and temperature which vary through the sea ice sheet and with time. Thus, to apply the above model, we must assume that we can define spatial and temporal averages of temperature, $\tilde{T}$, and concentration, $\tilde{C}$, and that the appropriate thermal constants in equation [3.3] are the values at these means. That is $K_s = K_s(\tilde{T},\tilde{C})$, $\kappa_s = \kappa_s(\tilde{T},\tilde{C})$ and $L = L(\tilde{C})$.

The average concentration in each experiment is estimated from the profiles in figure 3.11 and the latent heat is then found from the calculations of Schwerdtfeger (1963).

In appendix A1.3.3 we have seen that the temperature in the air just above the ice surface may be significantly different from the temperature just beneath the surface. Consequently we have used the temperature found by extrapolating the vertical temperature gradient to zero depth (see figures A1.3 and A1.5) in equation [3.3]. Where this was not available, in Runs 5 and 6, we have subtracted an "interface resistance" of approximately $4^{o}C$ from the air temperature just above the ice surface. The temperature at the ice-water interface, T_{li}, has been measured in all experiments. The arithmetic mean of the temperature at the air-ice and ice-water boundaries was used as the bulk temperature, $\tilde{T}$, of the ice.

In appendix A1.3.5 we found a value for the thermal diffusivity for Run 8 which we now use in our calculations for both Runs 7 and 8 since $\tilde{T}$ and $\tilde{C}$ were similar in these two experiments. The thermal diffusivity for Runs 5 and 6 was estimated by multipying Schwerdtfeger's prediction by the factor which related his results to ours in Run 8. Since the model is not

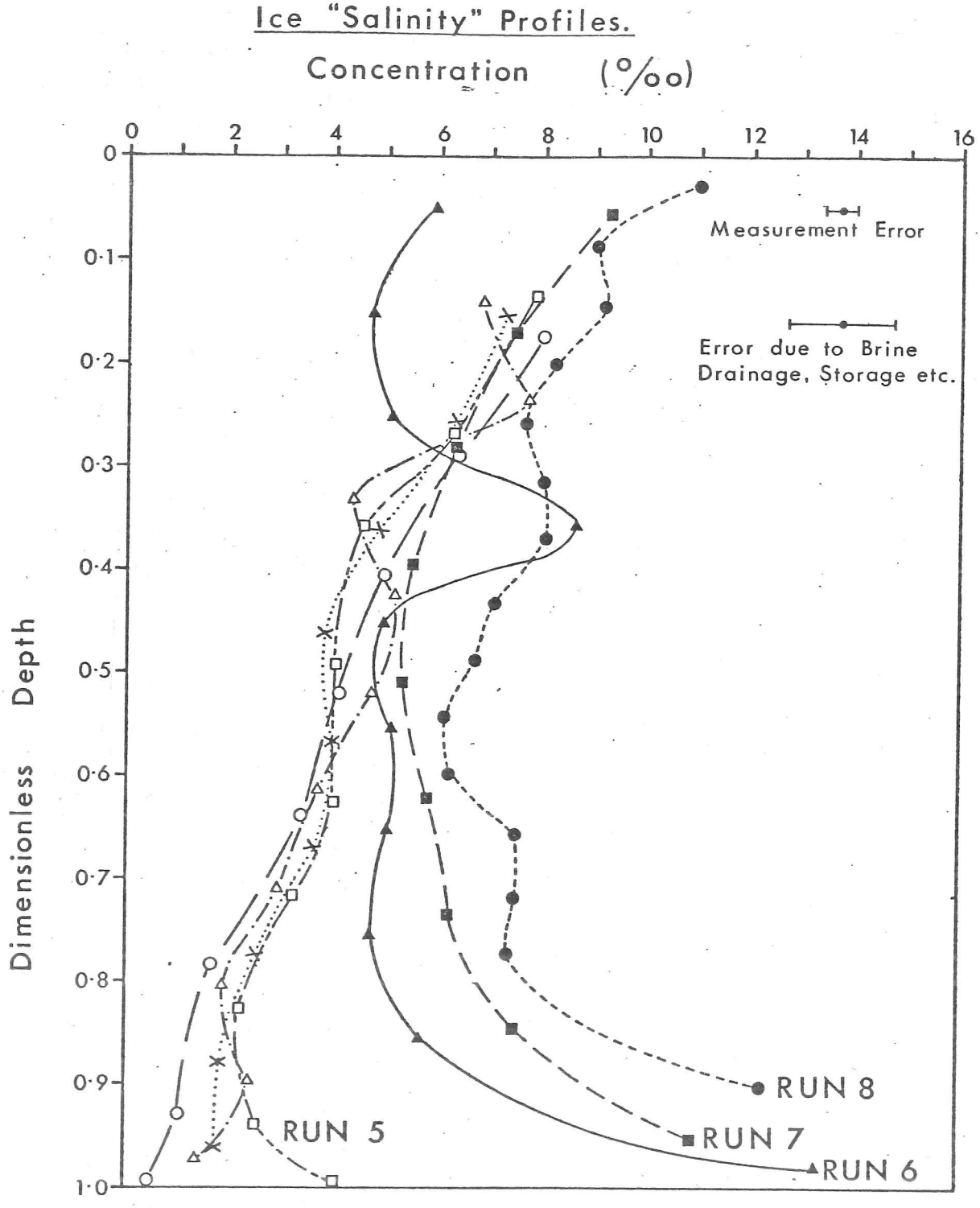

FIGURE 3.11 Profiles of concentration of NaCl in the artificial sea ice. This has been measured at four locations in Run 5.

sensitively dependent on the value of κ_s, [2] we do not feel this is a serious approximation.

The values taken for all the above parameters for the four experiments are given in the upper portion of Table 3.2.

TABLE 3.2

Parameter	Run 5	Run 6	Run 7	Run 8
$\tilde{C}$ (‰)	4	5	7	8
T_{surf} (^oC)	-13	-12	-8	-10.5
T_{li} (^oC)	-1.1	-1.3	-2.3	-1.9
$\tilde{T}$ (^oC)	-7.2	-6.7	-5.2	-6.2
L (Jcm^{-3})	272.6	263.7	246.2	237.4
κ_s (cm^2s^{-1})	$12x10^{-3}$	$12x10^{-3}$	$9x10^{-3}$	$9x10^{-3}$
ℓ (cm)	20	60	40	22
t_{start} (hrs)	25	20	35	40
h_{start} (cm)	7	7	7	7
N	33	9	4	33
$\kappa_s/f(\eta)$ (cm^2s^{-1})	3.65	3.25	1.59	2.56
r^2	0.990	0.980	0.998	0.994
K_s ($Jcm^{-1}{}^oC^{-1}s^{-1}$)	$2.3x10^{-2}$	$2.3x10^{-2}$	$1.9x10^{-2}$	$2.0x10^{-2}$
q ($Jcm^{-2}s^{-1}$)	$1.4x10^{-2}$	$4.0x10^{-3}$	$2.7x10^{-3}$	$7.9x10^{-3}$

From equation [3.3] we can see that ℓ is the thickness at which the heat extracted at the ice surface is balanced by the convective heat input at the ice-water interface. In other words, the ice thickness tends to ℓ asymptotically. For Runs 5 and 8, ℓ can be found to $\pm$3cm (see figure 3.6), to $\pm$20cm for Run 7 but is no more than a crude estimate for Run 6.

Because the thermal properties of the sea ice sheet are dependent on the growth rate, the region where the growth velocity is changing most

---

[2] For example, 90% change in κ_s gives only 10% change in the derived vertical temperature gradient in the ice.

rapidly cannot be expected to conform to these bulk estimates. Consequently we have used data where the ice thickness is greater than 7cm to obtain our fit to equation [3.3]. Figure 3.6 shows these fitted curves and our experimental results. Table 3.2 gives the values of ℓ used for plotting t/ℓ^2 versus $-[h/\ell+\ln(1-h/\ell)]$ and the resulting $\kappa_s/f(\eta)$ for each experiment. K_s and q are then obtained from η and ℓ. The values of K_s are consistent with previous measurements of the thermal conductivity of sea ice at similar temperatures and salinities as shown in Table 3.3 indicating that this theory is an appropriate description of ice growth in our experiments. The derived, convective heat fluxes have expected relative magnitudes. That is,

$$q_{\text{Run 5}} > q_{\text{Run 8}} > q_{\text{Run 6}} > q_{\text{Run 7}}$$

TABLE 3.3

Thermal conductivity $Jcm^{-1}{}^{o}C^{-1}s^{-1}$	Run 5 $\tilde{T}=-7.2^{o}C$ $\tilde{C}=4‰$	Run 6 $\tilde{T}=-6.7^{o}C$ $\tilde{C}=5‰$	Run 7 $\tilde{T}=-5.2^{o}C$ $\tilde{C}=7‰$	Run 8 $\tilde{T}=-6.2^{o}C$ $\tilde{C}=8‰$
Present	2.3×10^{-2}	2.3×10^{-2}	1.9×10^{-2}	2.0×10^{-2}
Lewis (1967)	2.3×10^{-2}	2.3×10^{-2}	2.3×10^{-2}	2.3×10^{-2}
Schwerdtfeger (1963)	2.1×10^{-2}	2.1×10^{-2}	2.1×10^{-2}	2.0×10^{-2}
Anderson (1960)	2.2×10^{-2}	2.2×10^{-2}	2.1×10^{-2}	2.1×10^{-2}

One of the most important parameters in solidification problems is the velocity of growth. This can be obtained by differentiating equation [3.3] giving

$$V = \frac{\kappa_s}{f(\eta)h}\left(1 - \frac{h}{\ell}\right) . \qquad [3.4]$$

Substitution of the empirically determined values of $\kappa_s/f(\eta)$ gives the growth velocity as a function of the ice thickness (figure 3.12). From this we can immediately obtain the growth velocity for a thin section at a

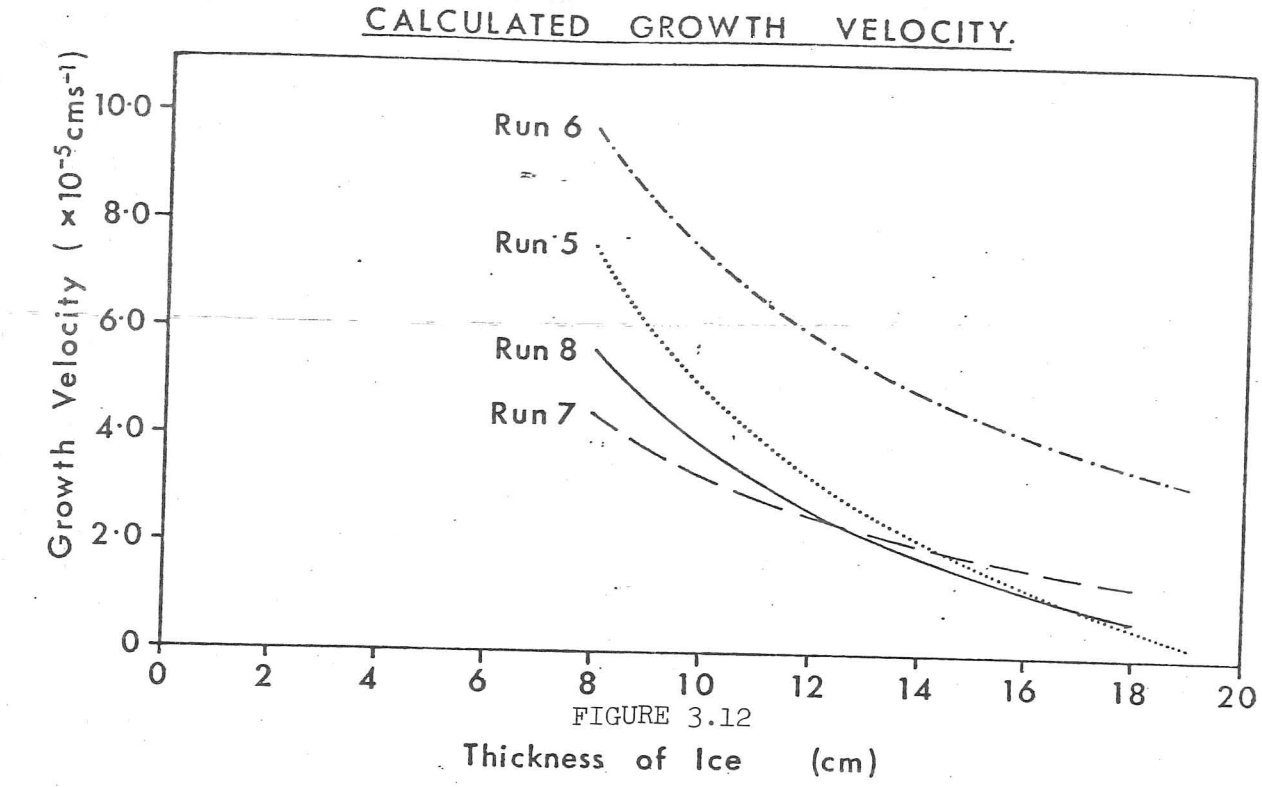

FIGURE 3.12

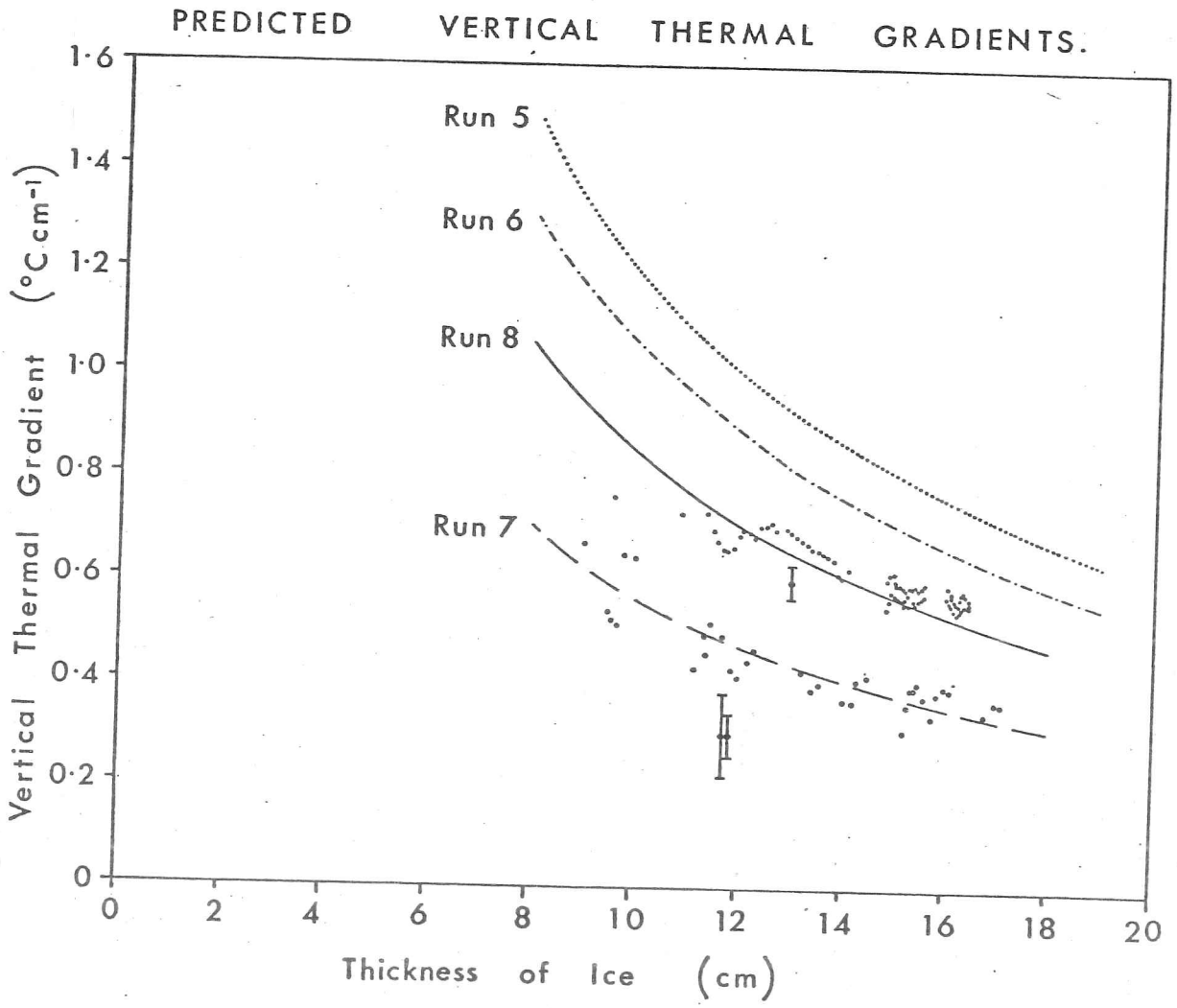

FIGURE 3.13

Solidification velocity (figure 3.12) and vertical temperature gradients (figure 3.13) calculated from the theory of Lapadula and Mueller. These are displayed as a function of thickness so that the value may be found directly from the thin section depth. Measured values of temperature gradient also given.

given depth. It is obvious from figure 3.12 that Run 6 has a significantly higher growth rate than the other three experiments.

As a further check on the validity of this theory, we can use the boundary condition at the interface,

$$K_s G_{si} = LV + q \qquad [3.5]$$

to obtain a value of the vertical thermal gradient in the solid, G_{si}. In using equation [3.5], we are assuming that the vertical temperature gradient is independent of z although this is not implicit in the theory of Lapadula and Mueller. Likewise the thermal conductivity is regarded as constant in z which is probably true within 20% (Lewis, 1967). Figure 3.13 shows the calculated vertical thermal gradients and the agreement between predicted and measured values for Runs 7 and 8 is good. In the absence of measured temperature gradients in Runs 5 and 6, these curves may be used in conjunction with equation [3.1] to estimate the horizontal temperature gradient to within 40-50%. A large portion of this latter uncertainty is due to inaccuracies in the determination of the slope of the ice-water interface.

The approximations that have been made in the foregoing analysis force us to conclude that none of the parameters which are a result of the fit of our data to the theory of Lapadula and Mueller (1966) have been determined to better than 25%. However we are well satisfied with the self-consistency of the results and with their agreement with data from other sources.

3.7 Fluid motion and interface shape

3.7.1 Run 5 (Forced flow - Brackish)

Measurements of fluid speed were made with a Nixon Instrumentation miniature vane current meter. These were not performed during the c-axis orientation experiments to avoid interfering with the developing grain

structure. Therefore at the completion of each run, a thin cover of ice was allowed to form over fluid flowing with the valve setting unchanged. Profiles of fluid speed were then measured in the z-direction under this "simulated" skim of ice and dye was injected just below the ice-water interface to trace the direction of flow. Although there was a slight unsteadiness of motion the current was laminar.

Figure 3.14 shows the measurements made at four locations under the "simulated" ice skim for the valve setting used in Run 5. Non-saline, rather than brackish water, was used and although neither of these will be thermally unstable, salt-driven convection will have taken place at the ice-water interface during Run 5. This was not present when the flow was measured and these profiles (figure 3.14) are therefore a gauge of the fluid dynamical characteristics of our flume.

The measurements in figure 3.14 have a spread of about $1 cms^{-1}$. This spread must be partially due to the varying channel depths under the ice because of the changes in ice thickness, particularly in the x-z plane (figure 3.3(a)). The shape of the interface during the "simulation" is very similar to that at various times during Run 5 as shown in figure 3.15. The vertical scale in this figure is exaggerated by a factor of 5.

There is an apparent maximum in speed just below the ice which we attribute to the fact that the ice is sloping downwards in the downstream direction. The fluid is thus flowing in a slowly converging "pipe" of cross-section shown in figure 3.14. We display the data tilted by half the slope of the ice-water interface so that the "pipe" is converging symmetrically on the upper and lower boundaries (see figure 3.16).

The curve in figure 3.16 is taken from measurements by Nikuradse (Schlichting, 1968) in the inlet portion of a circular pipe in the presence of laminar flow. We have substituted the half depth of the fluid, R, as the "pipe" radius, in this case, since we are only concerned with fluid motion in the x-z plane. The speed was constant, within error, in the y-direction. $\bar{u}$ is the magnitude of the rectangular velocity distribution at the entrance and we have chosen this to be compatible with

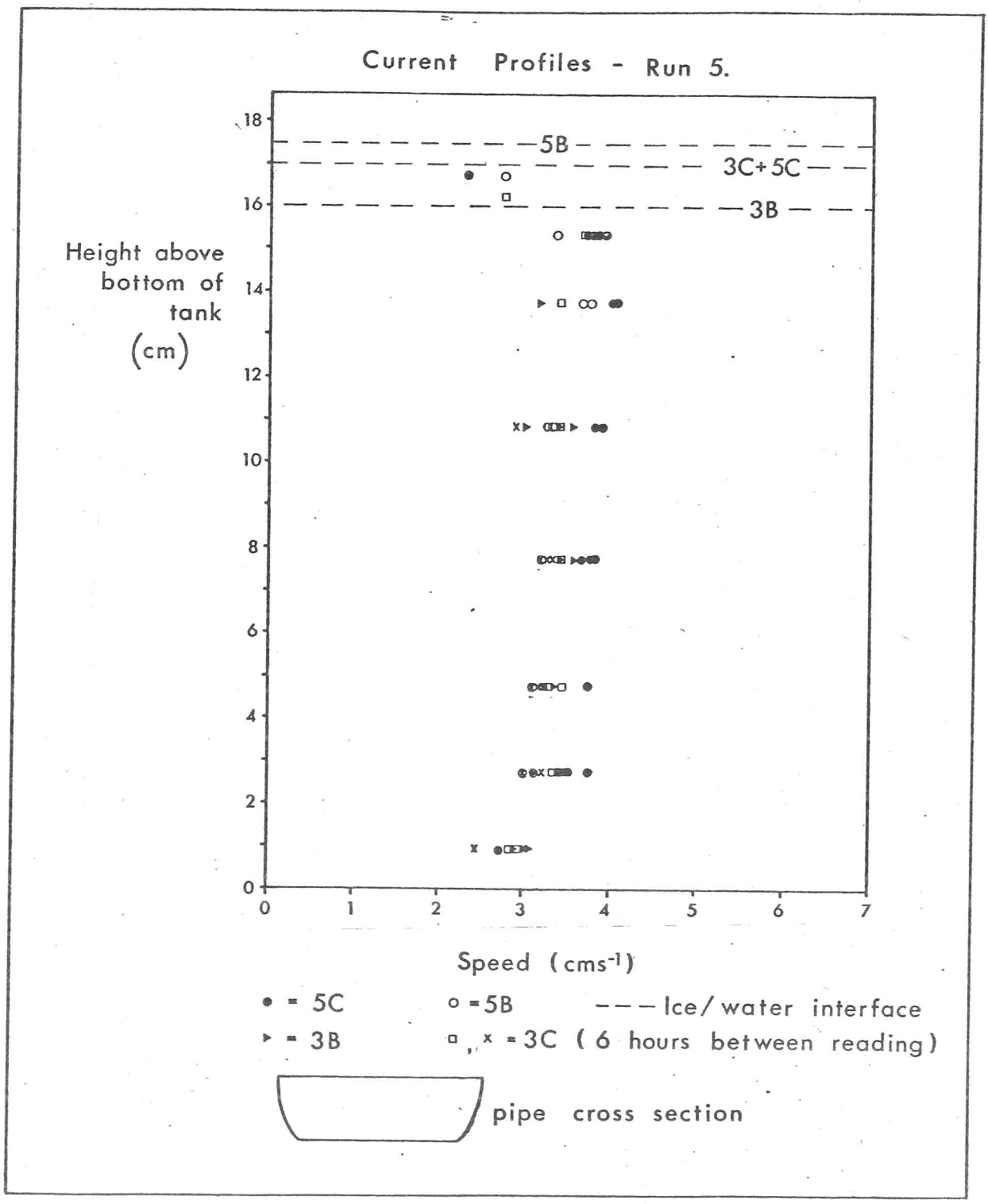

FIGURE 3.14 Current speeds at four locations during Run 5. The positions of the interface at the time the profiles were being measured is given by dotted lines.

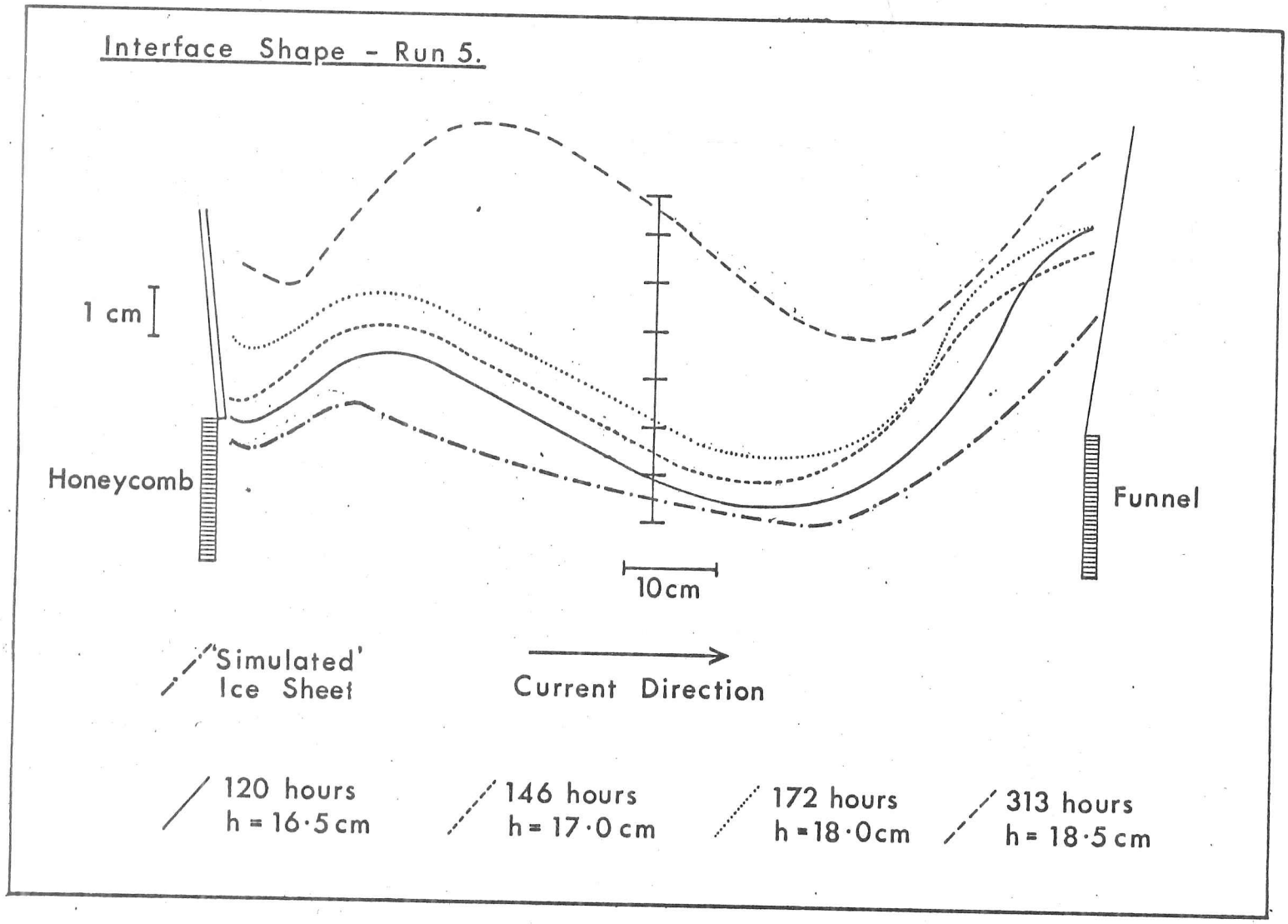

FIGURE 3.15 Diagram showing the shapes of the interface along the centreline of tank B at various times during Run 5. Note the similarity in shape between these and that of the "simulated" ice sea ice sheet. The vertical scale is exaggerated with respect to the horizontal.

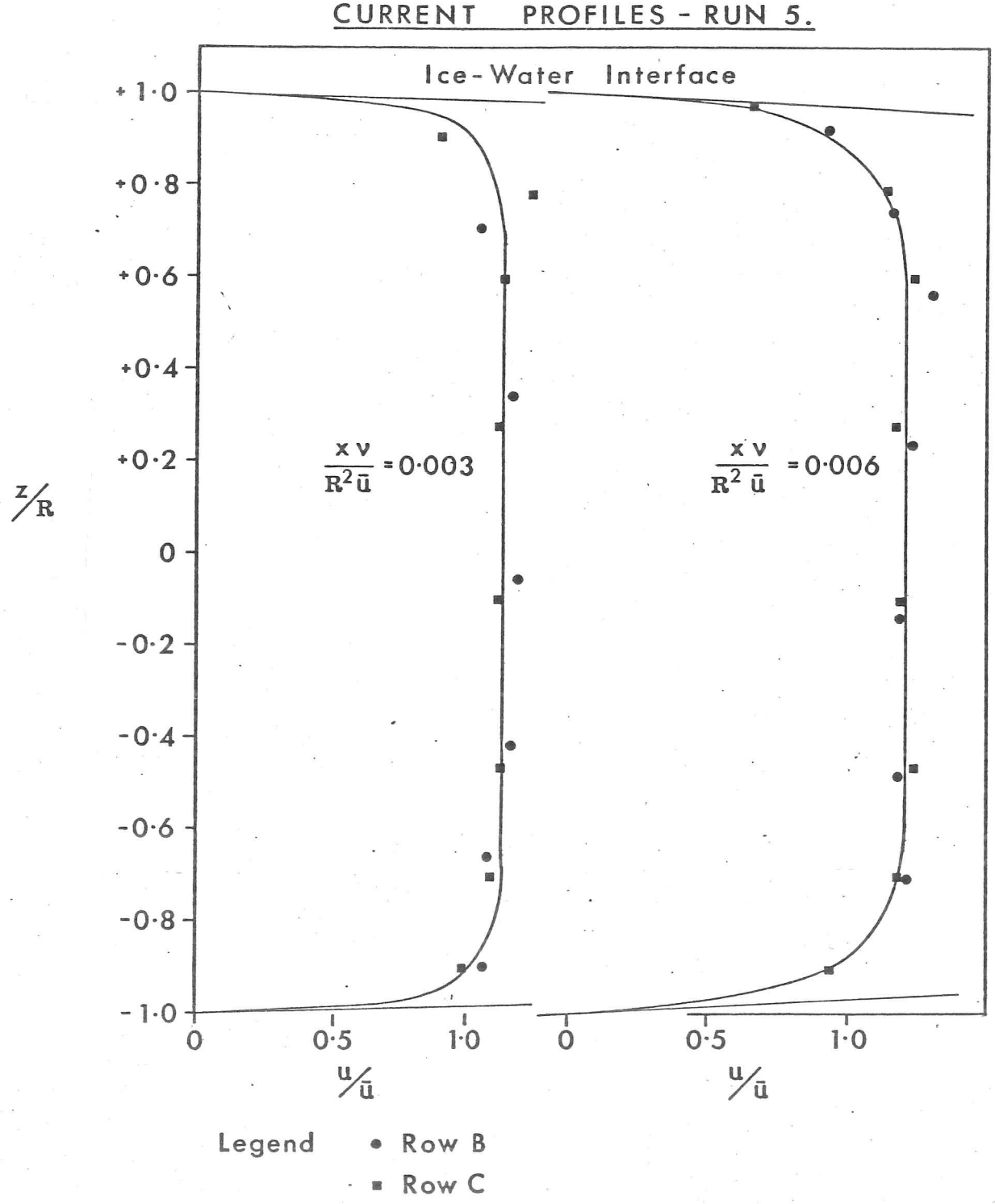

FIGURE 3.16 Non-dimensional current profiles for Run 5. The curves are measurements by Nikuradse. Note the tilt on the upper and lower bounds of the pipe due to the slope of the interface. See text for details.

the speed measured at the centre of the tank. The numbers used to non-dimensionalise our data are given below, where ν is the fluid viscosity.

	x	R	$\bar{u}$	$\frac{x\nu}{R^2\bar{u}}$
3B	35.8	8.0	2.9	0.003
3C	35.8	8.5	2.9	0.003
5B	66.6	8.8	2.7	0.006
5C	66.6	8.5	3.1	0.006

We are not only satisfied that our data fall quite closely on the curves of Nikuradse but also that the values of $\bar{u}$, which we have used to acheive this fit, agree with each other to within 10%. We estimate the accuracy of the current measurements is $\pm$8%.

It might be argued that our data should be consistent with the distribution of velocities in a laminar boundary layer on a flat plate with zero pressure gradient in the outer flow; that is Blasius flow. However, although our boundary layers are of the correct thickness, the measured speeds do not fall on the Blasius boundary layer profile. We believe that the lack of agreement is due to the acceleration of the external flow and its associated pressure drop and to the shape of the leading edge. Both of these disturb the development of the boundary layer from the shape predicted by Blasius (Schlichting, 1968).

Hirata et al (1979a) have theoretically and experimentally examined the formation of an ice layer on a flat plate in laminar flow. Although this problem is similar to the present, conditions at the leading edge and pressure effects in the external flow make it unprofitable to attempt to fit their theory for ice thickness as a function of downstream coordinate x.

The effect of the edge, at the entrance of the flume, on the formation of initial skim has already been noted in section 3.4.4. Figure 3.15 shows that the ice remains thinner close to the honeycombs indicating that the

heat and solute transfer Nusselt numbers [3] are increased by mixing in this region. This higher level of mixing was confirmed by dye. The Nusselt numbers then decrease downstream as the laminar boundary layer becomes thicker and, as a result, the ice profile slopes downwards. This is fortunate since the flow in this portion of the test tank is then converging and the possibility of boundary layer separation is decreased. Ice samples taken from this region will have solidified in well-defined conditions of fluid motion. The steep shelving of the interface at downstream corners is also due to vigorous mixing.

3.7.2 Run 8 (Forced flow - Saline)

Flow was measured in fluid of approximately the concentration used in the c-axis orientation experiment and is thus characteristic of the early stages of freezing in Run 8. Because the profiles in Run 5 were not sensitively dependent on y and because their x dependence could be calculated, we have measured the speed at one location only, in this case.

The slope of the interface in the downstream direction in Run 8 is gentler than in Run 5 and no correction for flow convergence is necessary. Figure 3.17 shows the data and Nikuradse's curve for

x	R	$\bar{u}$	$\frac{x\nu}{R^2\bar{u}}$
40.0	8.1	2.4	0.005

However, the fit of the data with the previous measurements is only satisfactory at the bottom of the tank. Close to the ice-water interface, from $z/R = +0.5$ to $z/R = +1.0$ our measurements do not fall on the curve. A similar distortion of the velocity profiles and corresponding increase in thickness of the boundary layer have been observed by Hirata et al (1979b) in the transition between laminar and turbulent flow over an ice surface. Re^x, associated with this transition, is typically 1×10^5. Re^x for the location of the profile in figure 3.17 is 6×10^3 which is significantly

---

[3] The Nusselt number is the ratio of actual heat transfer to the heat transferred by conduction alone.

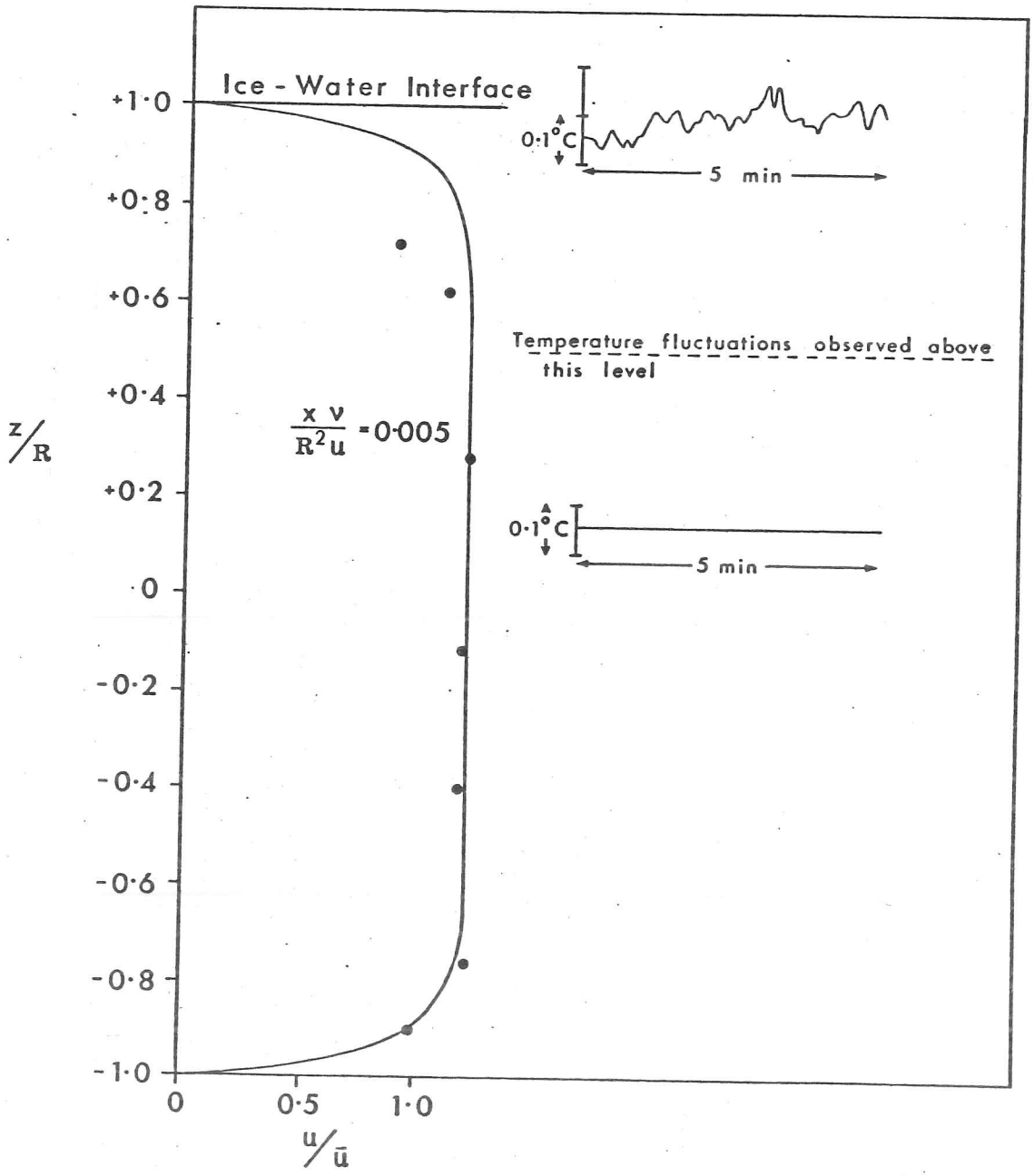

FIGURE 3.17 Non-dimensional current profiles for Run 8. Examples of the high frequency temperature fluctuations are plotted at the measured values of z/R. The curve is from the measurements of Nikuradse.

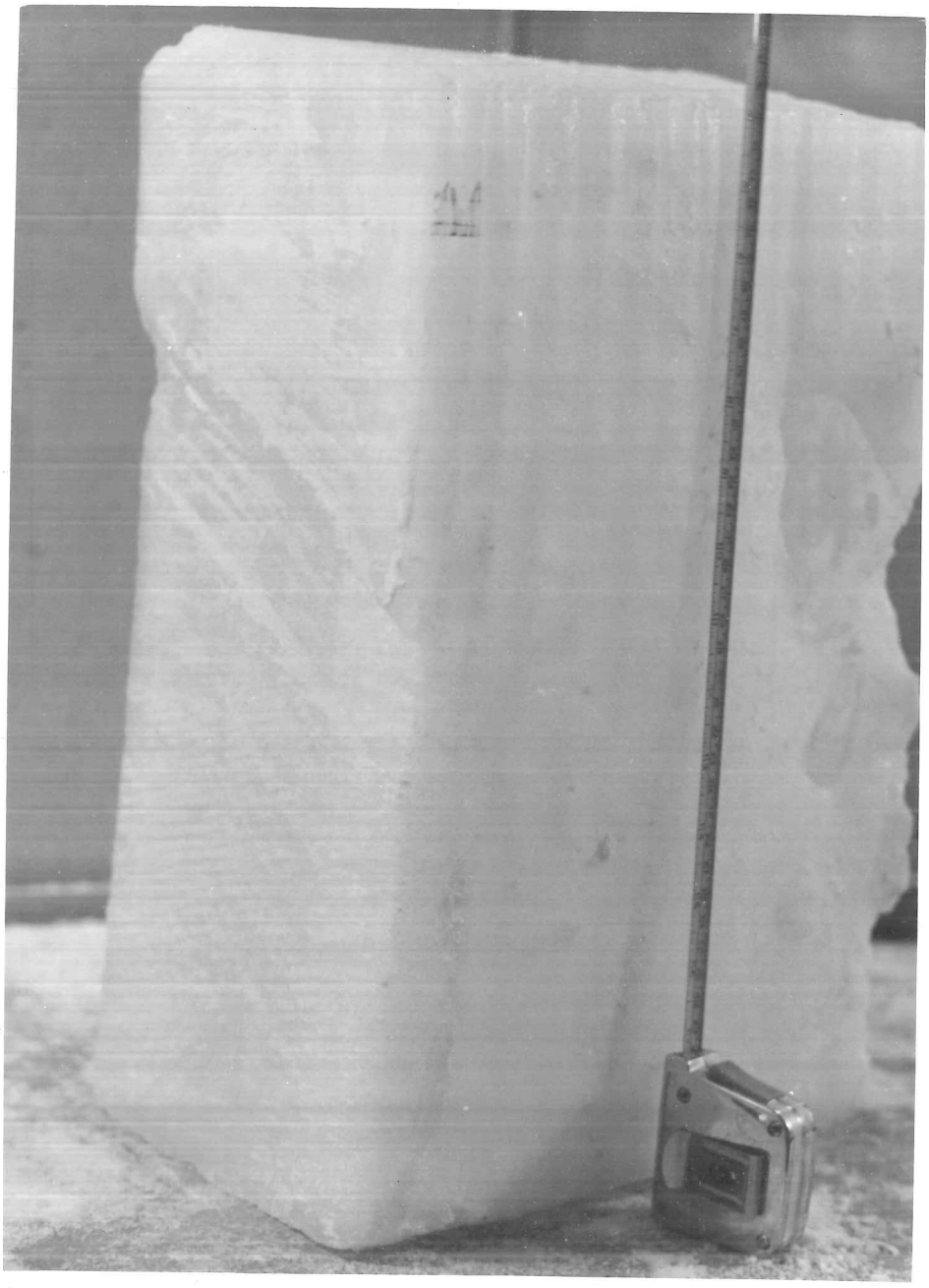

FIGURE 3.18 Photograph of the bottom of the ice slab at the entrance of tank B (leading edge to top of photograph) after the completion of Run 8. Note the ridges in the ice running parallel to the current (downwards in the photograph) for approximately 30cm from the leading edge.

less than the critical value determined previously. The explanation for this discrepancy lies in the temperature fluctuations just below the ice-water interface which are also shown in figure 3.17. The fluid layer, close to the interface, where these fluctuations are observed is roughly coincident with the region where there are deviations from the expected velocities. Confirmation that this buoyancy-driven convection is moving the laminar to turbulent transition upstream is given in the following paragraphs.

In figure 3.18 a series of evenly spaced ridges are observed parallel to the current direction, running from the leading edge to a position about 30cm downstream. [4] These ressemble features reported by Hirata et al (1979a) for the upward freezing of pure ice in a warm laminar flow. They suggest that these grooves are the result of longitudinal vortices produced by thermal instability in the thick boundary layer. However, in their experiment the circulation was too weak for measurements of these grooves to be made to test this hypothesis.

In the absence of ice, similar vortices have been studied theoretically (Wu and Cheng, 1976) and experimentally (Gilpin et al, 1978) and they are first stage of a laminar to turbulent transition. Wu and Cheng (1976) predict that the Grashof, $Gr^{x'}$, [5] and Reynolds number, $Re^{x'}$, based on the downstream coordinate, x', at which these rolls are first observed, are correlated by

$$Gr^{x'} = A(Re^{x'})^{\frac{3}{2}} \qquad [3.6]$$

This relationship was confirmed by Gilpin et al (1978) who also found that empirical and theoretical values of A were in agreement.

The theory has been developed for thermal instabilities but can be applied to haline convection if we replace the Prandtl number, Pr, by the

---

[4] These were also noted during ice growth in Run 5 when they continued for 70cm from the leading edge. This is virtually the whole length of the tank.

[5] The Grashof number is a ratio of buoyancy to viscous forces

Schmidt number, Sc, and $Gr^{x'}$ by $Gr_c^{x'}$. Wu and Cheng have calculated that $Gr^{x'}$ (or $Gr_c^{x'}$) decreases as Pr (or Sc) increases and as $Re^{x'}$ decreases (see equation [3.6]). Thus for the large Sc and small fluid velocities in our experiment the onset of longitudinal vortices will take place very close to the leading edge. For $Sc \sim 5 \times 10^3$, which is the value in our experiments, Wu and Cheng predict a critical Grashof number of

$$Gr_c^X \sim 2$$

where $Gr_c^X = \frac{g\beta\Delta C X^3}{\nu^2}$ and $X = (\frac{ux'}{\nu})^{\frac{1}{2}}$

which for the values in Run 8 predicts

$$x' \sim 0.5cm$$

In the above, g is the acceleration due to gravity, β is the coefficient of haline expansion and ΔC is the concentration difference across X driving the instability. Using this x' in equation [3.6] predicts a value of $A \sim 2$ which is very close to Wu and Cheng's calculated value for a Pr (or Sc) of the order of 10^3. Thus the first stages of a laminar to turbulent transition occur only 0.5cm from the leading edge of the slab of ice in Run 8.

Although Gilpin also found surprisingly good agreement between measured and calculated vortex wavelengths, we have not been able to duplicate this consistency. We expect the pattern of washing of the interface to yield one vortex wavelength equivalent to the spacing between ridge crests of figure 3.18. However this latter dimension is of the order of 0.8cm while the predicted wavelength for x' = 0.5cm is 0.06cm. Because this prediction is very similar to the intercellular spacing, it is not surprising that we are unable to detect any regularity on this scale. We postulate instead that a hierarchy of cells may exist as suggested by Foster (1968, 1972) and described in section 2.2.4, each determined by a different diffusivity. Thus, for the observed ridge wavelength, an eddy diffusivity of $e_c = 1.4 \times 10^{-2} cm s^{-1}$ is required(Wu and Cheng, 1976). Assuming "Reynolds analogy", that the eddy diffusivities for momentum and solute are equal (Turner, 1973), and using Prandtl's mixing length hypothesis (Schlichting, 1968)

$$e_c = \Lambda^2 \left(\frac{du}{dz}\right)_{z\sim 0} , \qquad [3.7]$$

Λ = observed ridge wavelength

we find a reasonable value for the velocity gradient close to the interface, that is

$$\frac{du}{dz} = 4s^{-1} .$$

We have seen that these ridges develop in thick laminar boundary layers with slow fluid velocities in conditions of thermal or haline instability. We might therefore expect them to be observed under growing sea ice. Their existence may explain the parallel rivulets at the ice-water interface, observed after an oil spill (NORCOR, 1975). These run parallel to the current and have a characteristic wavelength of 25cm.

3.7.3 Summary of forced flow

Flow in our tank is laminar, provided there is no thermal or haline instability. In the presence of free convection at the upper boundary, the formation of longitudinal vortices is predicted at $Re^x \sim 60$, and this is confirmed in our experiments by the presence of ridges in the ice very close to the leading edge. These are associated with laminar flow and mark the first stage of the laminar to turbulent transition. Despite the higher currents in Run 5, this regime persists for almost the entire length of the tank. On the other hand in Run 8, flow close to the ice-water boundary leaves this quasi-laminar region approximately 30cm from the leading edge when $Re^x \sim 5 \times 10^3$. This early transition is undoubtedly due to the larger value of Gr^x_c in the saline experiment compared with its brackish equivalent.

3.7.4 Free convection – Runs 6 and 7

We have already described previous observations of free convection under growing sea ice in section 2.2.4. In our experiments, the purpose of visualising the flow was to find out if the geometry of the tank would force the buoyancy-driven convection into a regular and directional

pattern. This, of course, is undesirable.

Dye was injected under the ice several times during Run 7 and, at all times, the motion was observed to be laminar. In the early stages of ice growth the flow, close to the ice-water interface, was variable in speed (from $\sim 0.04 cms^{-1}$ to $\sim 0.1 cms^{-1}$) and direction. However, at the bottom of the tank it consistently moved in the -ve x direction while a compensating flow in the +ve direction was noted above this.

By the time the ice was 5cm thick, all motion at the interface was vertically downwards with typical speeds of 0.1 to $0.2 cms^{-1}$. The horizontal component of flow, which did not appear until the dye was 2cm below the ice-water boundary, was neither constant in space nor time and was of the order of $0.03 cms^{-1}$. There may have been layers of fluid moving in the +ve x direction which interleaved with layers travelling in the opposite direction, but visibility was not good enough to determine this conclusively. When the ice thickness had reached 13cm the water was almost still.

No direct observations of free convection were made during Run 6 . However any slight preference for motion in the x direction, as observed above, will be greatly magnified because of the large temperature and salinity differences between the fluid in tank A and the fluid in the test section. These are the result of the rather peculiar thermal regime (section 3.4.2) during the cooling down period and the resulting, substantially different rates of ice growth in the inner and outer tanks. The interchange will therefore be between the fluid in tank A and tank B through the honeycomb. Any noticeable effect from this hypothetical motion should thus decrease in the +ve x direction.

The slope of the interface was substantially smaller in the experiments without forced flow (figures 3.3(b) and (c)) and is controlled by heat loss through the walls of the test section.

3.7.5 Interface slope

We have seen that fluid flow, when present in our experiments, is largely responsible for the shape of the interface. Variations in the thickness of a sea ice cover in nature are generally attributed to irregularities in snow cover and slopes between 1:8 (Kovacs, 1979) and 1:30 (Lewis, 1967) have been reported. Typical values for experiments with forced flow are 1:5 and for those without such flow are 1:14, which compare reasonably with the field measurements.

It is important to point out the distinction between interface slope and a tilt of the interface. Since the slope is related by equation [3.1] to the horizontal temperature gradient and since there is an anisotropy in thermal conductivity, then the preferred grains are those with their c-axis perpendicular to the direction of maximum slope. Alternatively, if the slab of sea ice is physically tilted, for example by a compressive pressure field in nature or by lifting it upwards in our experiment, only the c-axes which lie in the axis of tilt remain in the horizontal plane (see section 2.1). The c-axes lying along this axis are thus favoured. In both cases the resulting distribution is the same but the origin of alignment is quite different. Fortunately, from observations made in Run 8, we feel that there is negligible tilting of the ice-water interface during our experiments.

3.8 Structural features and c-axis measurements

3.8.1 C-axis statistics

The Lambert equal-area projection has been chosen to display our data since the density of plotted points on the projection correctly represents their density in space. Accordingly grains with their c-axis perpendicular to the plane of the diagram will be plotted at the centre of the circle while those in the plane of the projection lie on the perimeter. The resulting figure is frequently referred to as a fabric diagram. A program

has been written by the author to plot these data from the universal stage measurements and this is described in Langhorne et al (1980). We have followed Kamb (1959b) and Budd (1972) in presenting scatter diagrams rather than the conventional contour diagrams so the data may be interpreted by the reader.

To summarise the distribution of c-axes we use the moment of inertia method described fully in Mardia (1962) and which we shall outline in this section. We imagine that a sphere surrounds the c-axis distribution and that each point where an axis cuts this sphere is assigned unit mass. The principle axes, and their corresponding moments of inertia, are found for the resulting distribution of mass. Thus data which are tightly grouped around a particular principal axis will yield a small value of the moment of inertia. In practice it is more convenient to find

$$\tau_j = 1 - \frac{I_j}{N} \quad , \qquad [3.8]$$

where I_j, $j = 1,3$, are the moments of inertia and N is the total number of measurements. τ_j are the normalised eigenvalues, corresponding to the eigenvectors $\underline{t}_j$, of $\underline{T}$ which is the normalised matrix of the sums and products of the direction cosines. From the properties of eigenvalues and eigenvectors we also have that

$$\tau_1 + \tau_2 + \tau_3 = 1 \quad , \qquad [3.9]$$

and thus that

$$0 < \tau_j < 1 \quad . \qquad [3.10]$$

A value of τ_j close to 1 therefore indicates that the data are well grouped about the direction $\underline{t}_j$ and conversely for small τ_j. By convention, the magnitudes of the normalised eigenvalues are such that

$$\tau_1 < \tau_2 < \tau_3 \quad , \qquad [3.11]$$

and their relative values therefore describe the distribution. The two cases which occur most frequently in our data are

$$\tau_3 > \tau_2 \sim \tau_1 \Rightarrow \text{unimodal}$$

$$\tau_3 \sim \tau_2 > \tau_1 \Rightarrow \text{symmetric girdle} \qquad [3.12]$$

If we assume that the Bingham distribution is a suitable description of our data, [6] it is shown that (Mardia, 1962) the eigenvector $\underline{t}_3$, corresponding to the largest eigenvalue, τ_3, is the maximum likelihood estimate of the mean direction.

The moment of inertia method is ideal for our purposes. Firstly, it does not distinguish between directional and axial data and is thus suited to our data, which spans only a hemisphere. Secondly it gives us measure of the grouping about a particular direction which is precisely what we wish to know in these experiments.

It is difficult to quantify the strength of a fabric (Hooke and Hudleston, 1980) and there is no standard technique for dealing with this problem. We require a single number to give a measure of "groupedness" around the mean direction and we must, therefore, reject some of the information in the normalised eigenvectors. The fact that the c-axes invariably lie close to the horizontal plane (that is τ_1 close to 0) is well known and since our principle aim is to distinguish between unimodal and symmetric girdle distributions (see equation [3.12]), we consider only the magnitudes of τ_3 and τ_2. In addition, from equation [3.9] we see that the normalised eigenvectors are not independent and although the absolute values of τ_3 and τ_2 will depend on the magnitude of τ_1, the ratio of τ_3 to τ_2 will not. We refer to the latter as the concentration parameter and use it as our measure of fabric strength. It is simply a measure of the grouping of the data about the mean axis as compared with the concentration around a direction normal to this mean. Again the calculation of the normalised eigenvectors from the universal stage measurements has been programmed in Fortran.

---

[6] The Bingham distribution is the most general description of spherical data, particular cases including symmetric girdle, unimodal and uniform distributions.

3.8.2 Introduction to texture measurements

In the following sections of this chapter we describe the textures resulting from each experiment. These descriptions are accompanied by equal-area projection diagrams of the c-axis measurements, referenced to the +ve x direction, which for the forced flow experiments, is also approximately the direction of the current.

In the fabric diagrams and the photographs, thin sections are named in the following way;

E5 - 5B - 13/14
Experiment number | Location in tank | Depth of sample

The slash indicates that the sample lay between the depths, given in centimeters below the ice surface. Because the slab of ice was uneven, the same depth at different locations may correspond to different times of solidification, and hence to different growth parameters (for example growth velocity, vertical temperature gradient). The actual thin section depths are therefore corrected to the thickness shown in the growth curve (figure 3.6) and these corrected depths are used whenever there is comparison between a number of locations in one experiment (for example, in the concentration parameter versus depth diagrams of figure 3.23).

3.8.3 Texture for Run 5 (Brackish - Forced Flow)

Figure 3.19 shows a typical vertical thin section from this experiment. C-axis horizontal grains nucleate at the surface and columnar growth has proceeds from there, the c-axis remaining close to the horizontal plane for most of the subsequent growth. Previous observations of an initial skim formed of c-axis horizontal grains (Bennington, 1963b, 1968) took place in calm conditions with rapid cooling. We suggest that the essential similarity between these observations and our experiment is that, just prior to freezing, marginal supercooling can take place in a thin layer on the surface, encouraging the fast-growing direction to point downwards. In this experiment the stability of the brackish water allows this supercooling to take place.

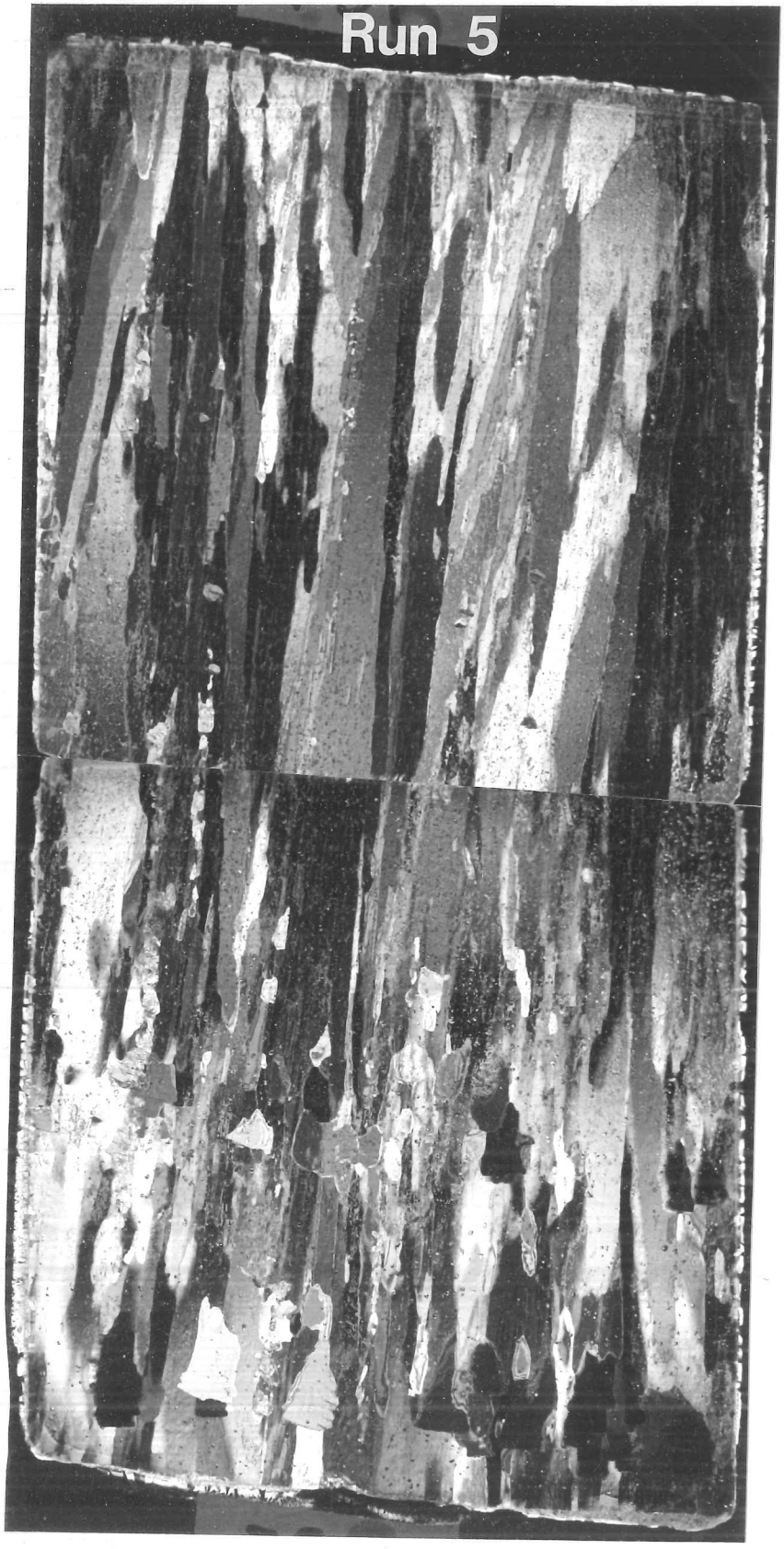

FIGURE 3.19 Vertical thin section from the upper ice surface to the bottom of the ice, showing the columnar growth during this experiment.

Close to the ice surface (figure 3.20(a)) the appearance of the grains is very similar to real sea ice. Platelets are delineated by brine pockets and the c-axes are distributed randomly in the horizontal plane (figure 3.21(i)). However this likeness decreases as we go deeper in the ice (figure 3.20(b)) for, although the ratio of grain length to width increases, the grain size does not increase by as much as expected. In addition the platelets are not so well delinated as those at higher levels. However figure 3.21(n) shows that 20cm of ice growth have resulted in a noticeable grouping about the current direction.

The resemblance between our artificial ice and sea ice almost vanishes if we look at thin sections from Row 2 (see figure 3.3(a)), which is the region where there is most mixing. The upper section (figure 3.22(a)) is not unlike that from other locations in the tank (for example figure 3.20(b)), but despite an ice thickness of 10cm, the c-axes are almost randomly distributed in the horizontal plane (figure 3.21(a)). However with a further 6cm of growth, the features of the ice change drastically (figure 3.22(b)) and the grains become circular and the c-axes lie around the vertical direction (figure 3.21(b)). We can also see the initial signs of this transition in the lower portions of the vertical thin section (figure 3.19) where the triangular shaped grains have a vertical c-axis. According to Shumskii (1964), the transition from horizontally to vertically oriented c-axes is caused by the disappearance of constitutional supercooling at the interface (section 1.3). The cellular to planar transition is also driven by the loss of supercooling and we shall discuss the conditions for this in section 4.3.2.

Figure 3.23(a) shows that as the ice thickens the maximum liklihood estimate of the mean direction of the distribution of c-axes, $\underline{t}_3$, tends towards the x direction which, in this case, is also approximately the current direction. Figure 3.24 shows still better correspondence between the measured current and the mean c-axis at the base of the ice, the average difference between the two angles being 7^{o}.

Figure 3.23(a) also shows that the concentration parameter, which initially increases with depth, becomes constant from about 12cm onwards.

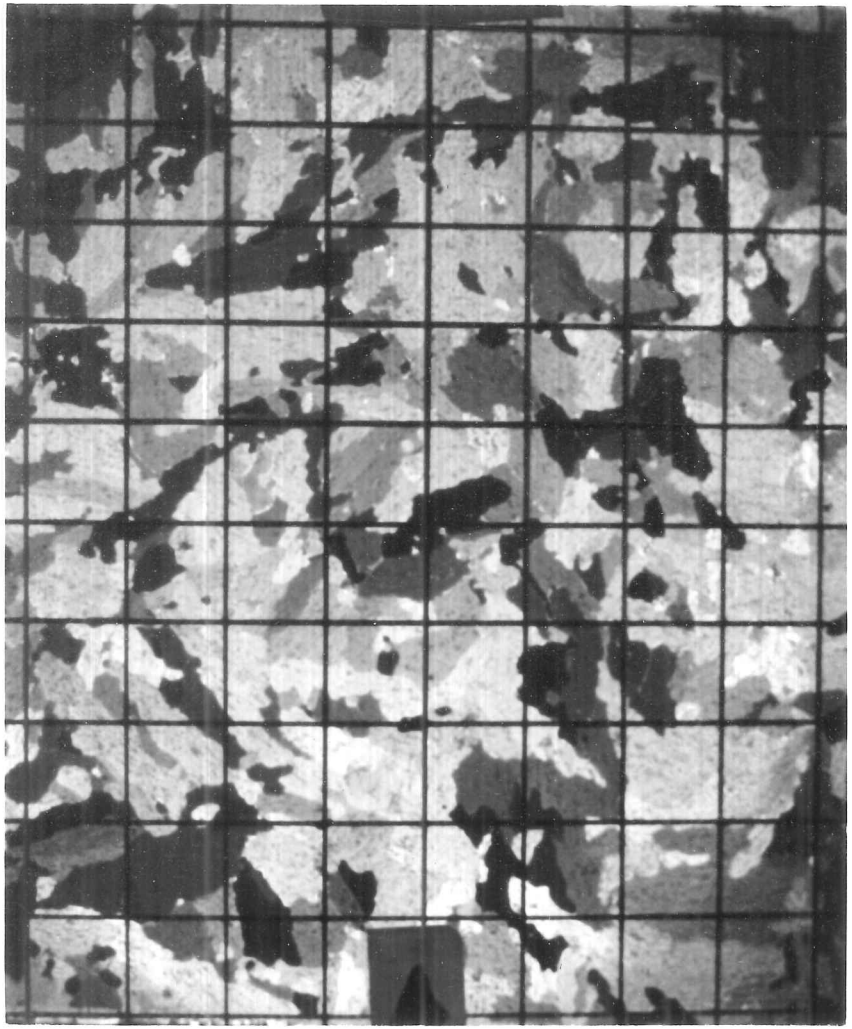

FIGURE 3.20 (a) Horizontal thin section taken 2cm from the upper ice surface in Run 5 (brackish-forced flow). Current flowing from top to bottom of photograph. Grid 1cm square.

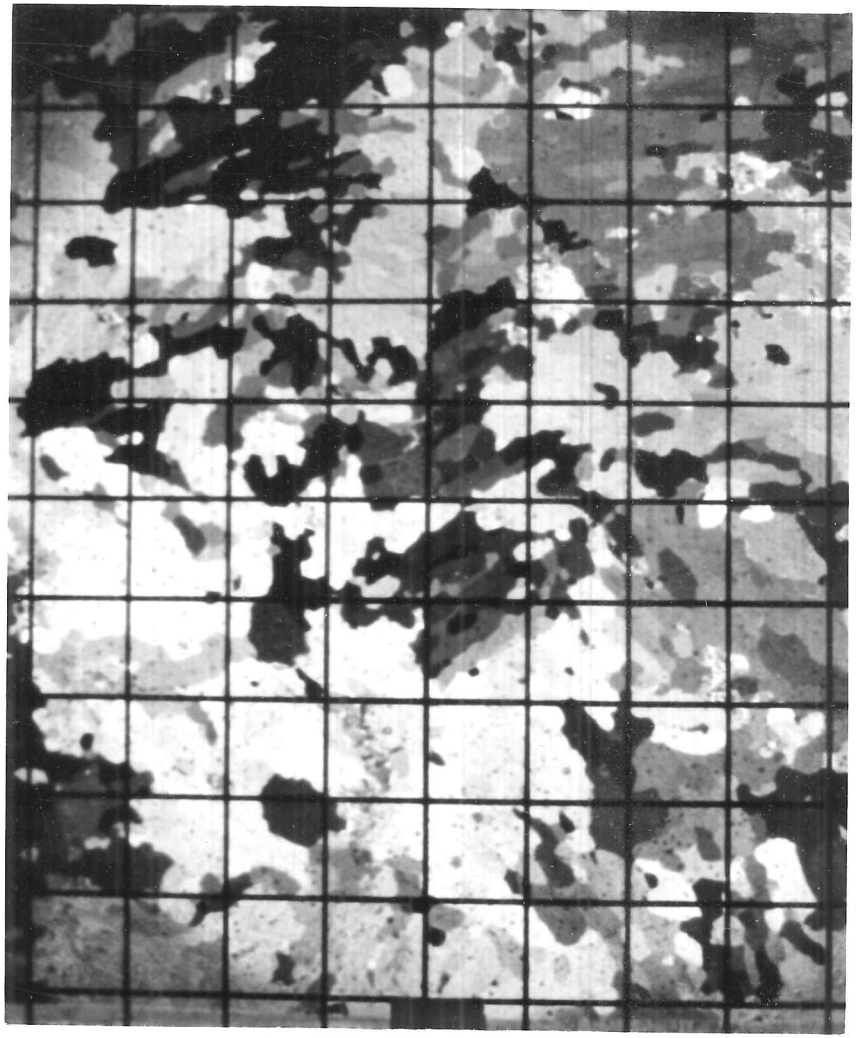

FIGURE 3.20 (b) Horizontal thin section taken 21cm below the upper ice surface. Same position and scale as (a).

FIGURE 3.21
Equal-area projection diagrams for Run 5. Approximate current direction is shown by arrow. 64 measurements made in each case.

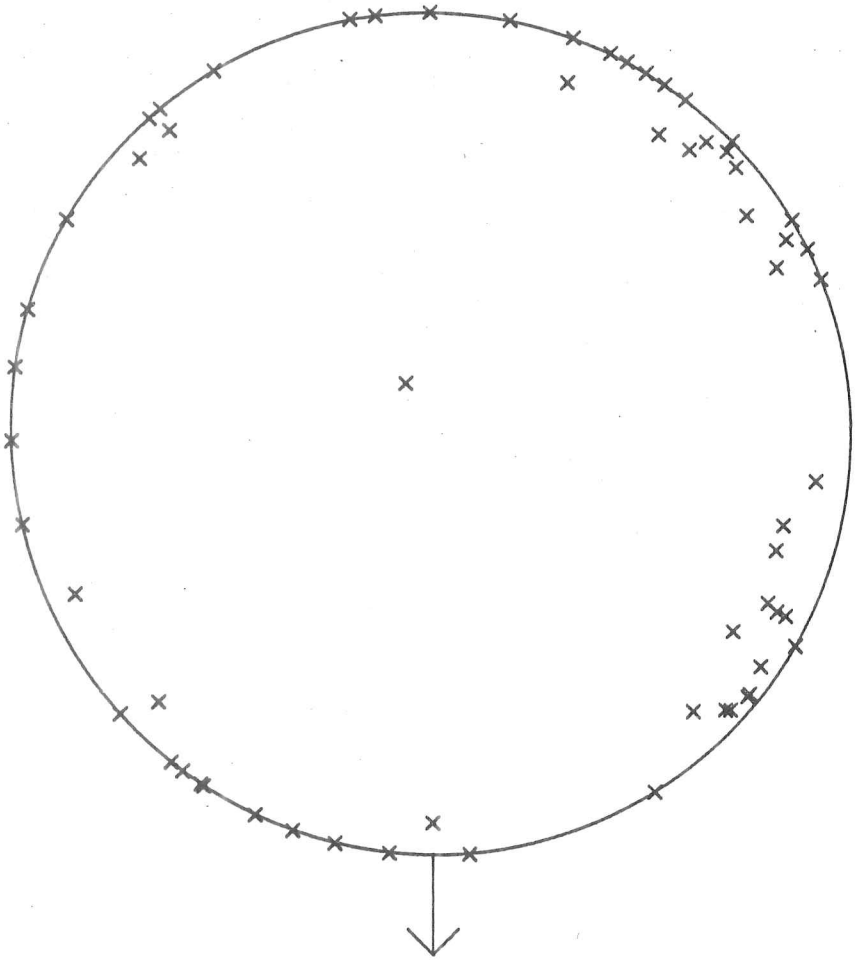

SAMPLE E5-2B-10/11

FIGURE 3.21(a)

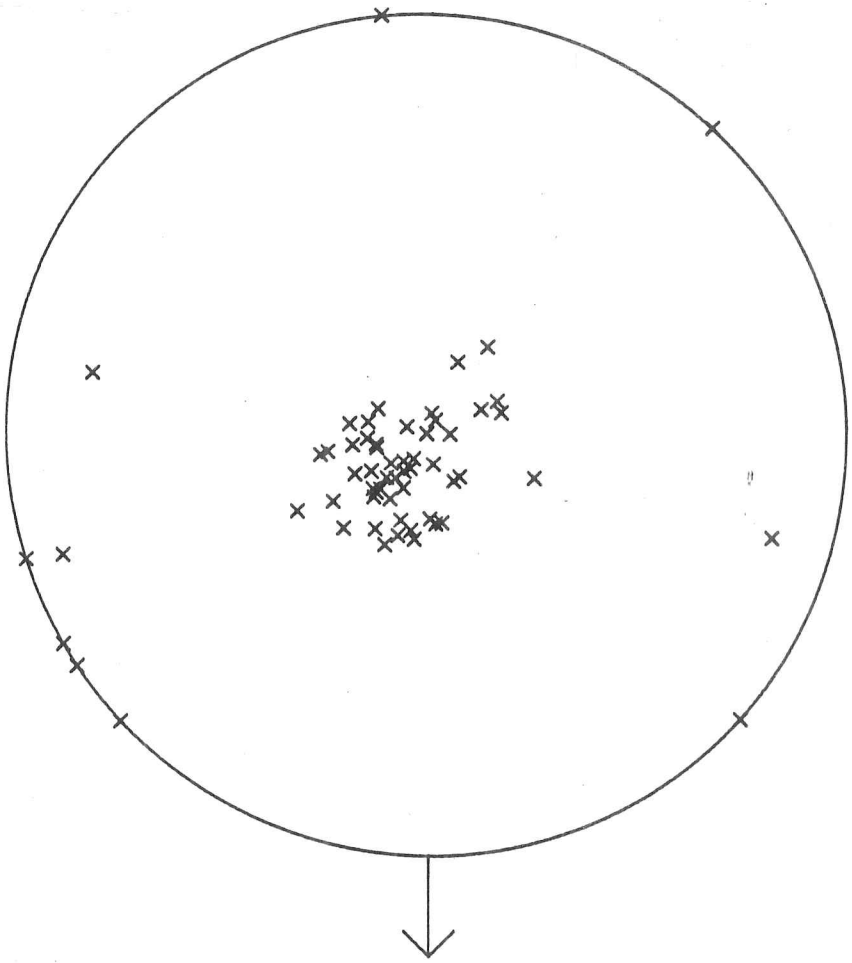

SAMPLE E5-2B-16/17

FIGURE 3.21(b)

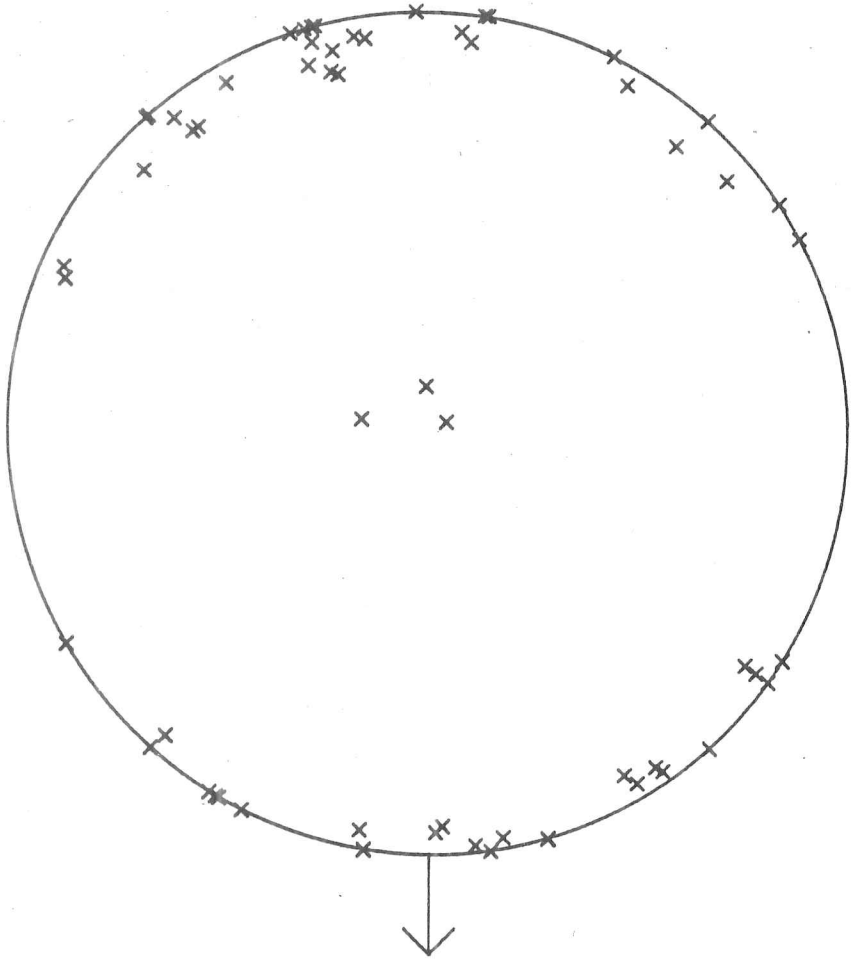

SAMPLE E5-3B-12/13

FIGURE 3.21(c)

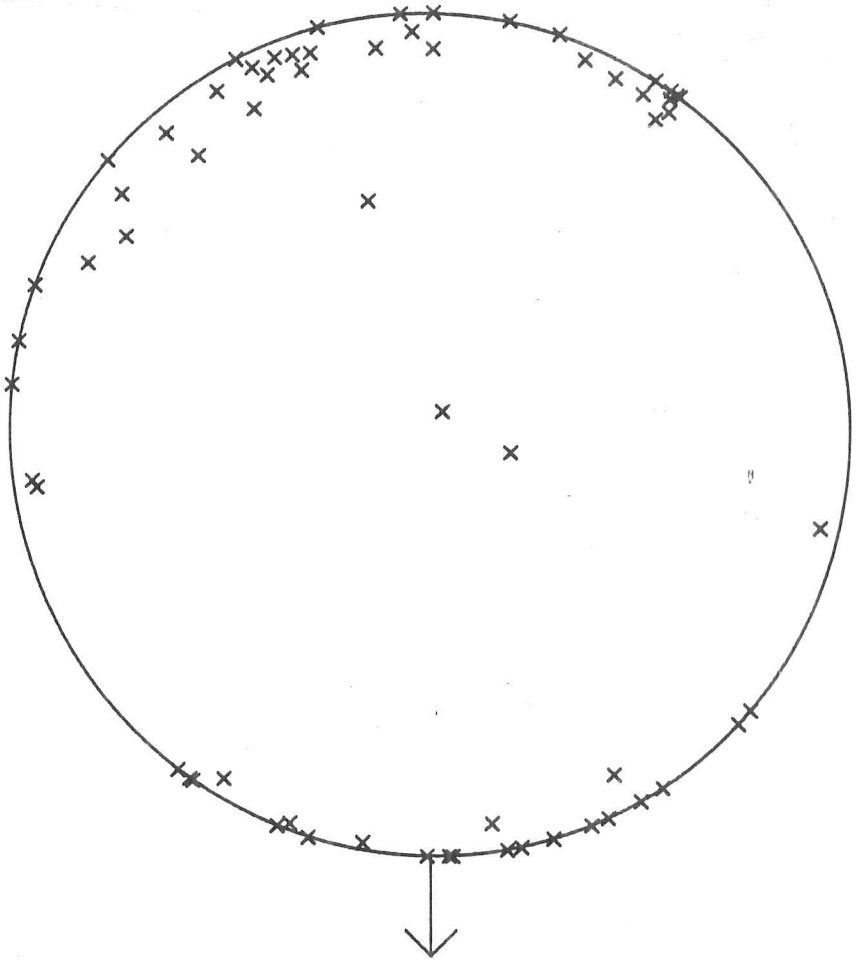

SAMPLE E5-3C-12/13

FIGURE 3.21(d)

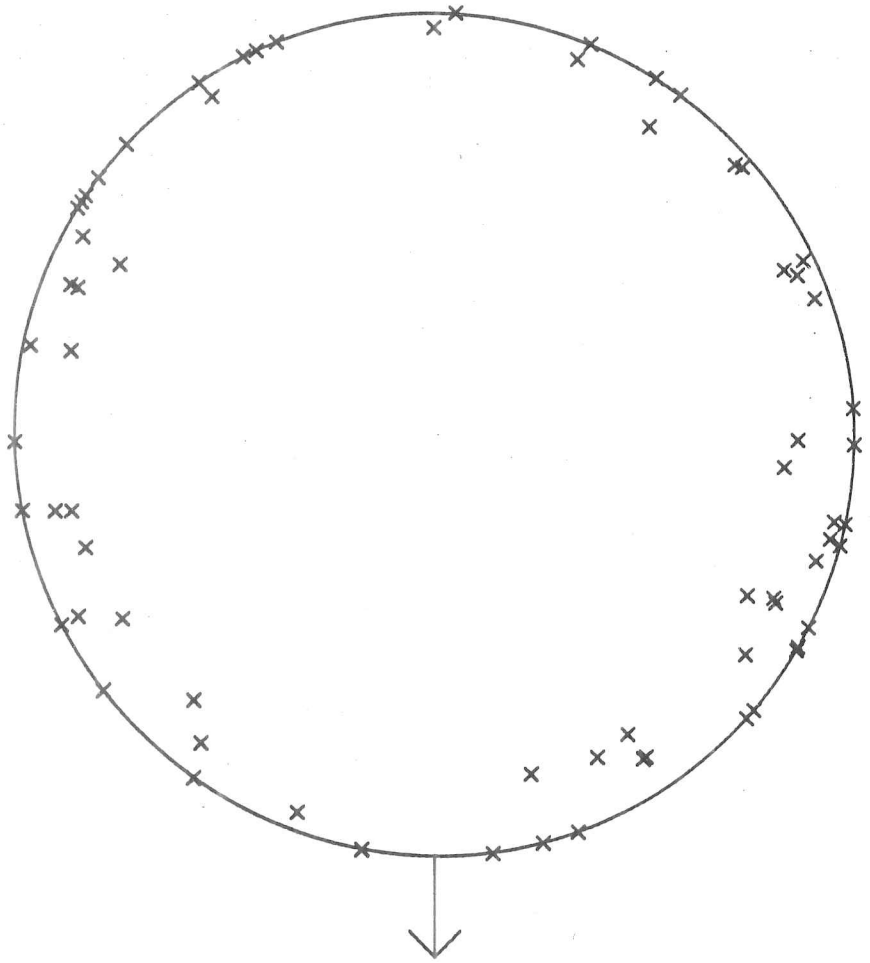

SAMPLE E5-4B- 5/ 6

FIGURE 3.21(e)

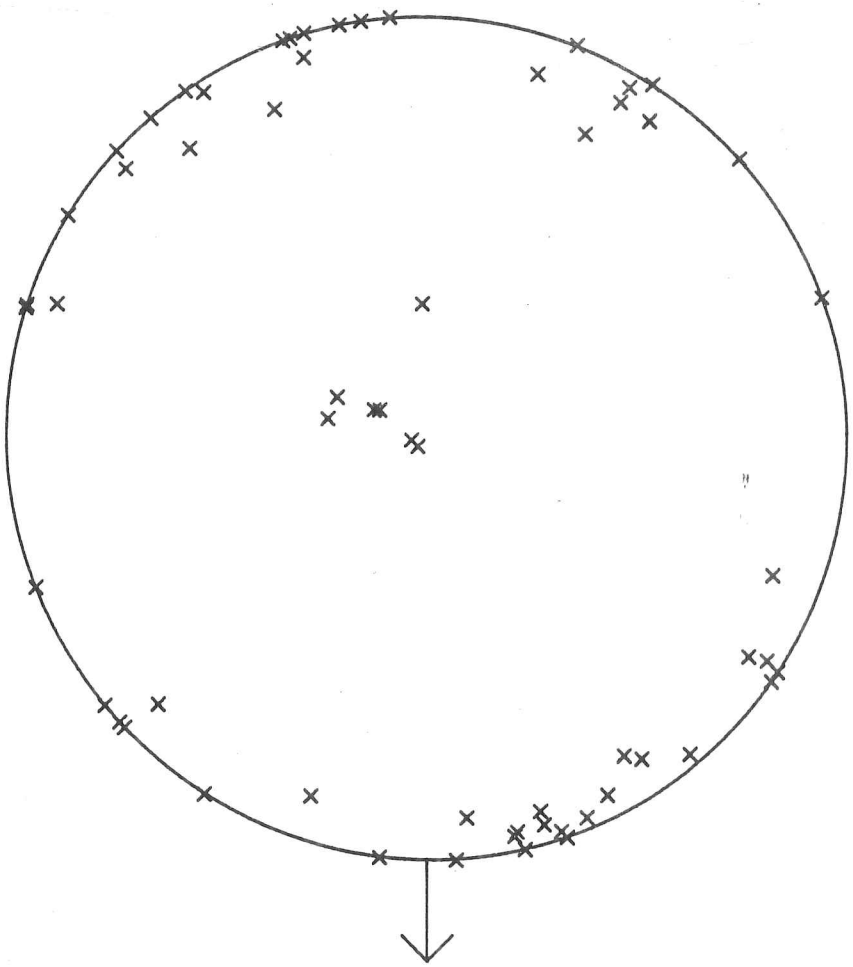

SAMPLE E5-4B-17/18

FIGURE 3.21(f)

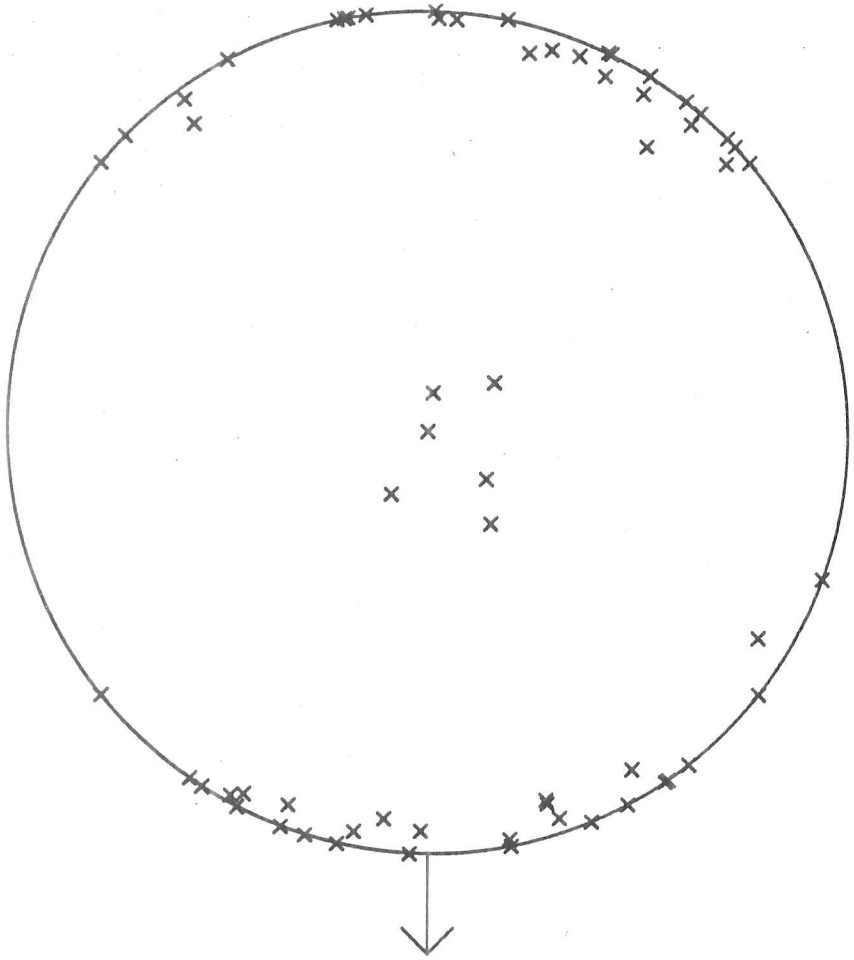

SAMPLE E5-4C-17/18

FIGURE 3.21(g)

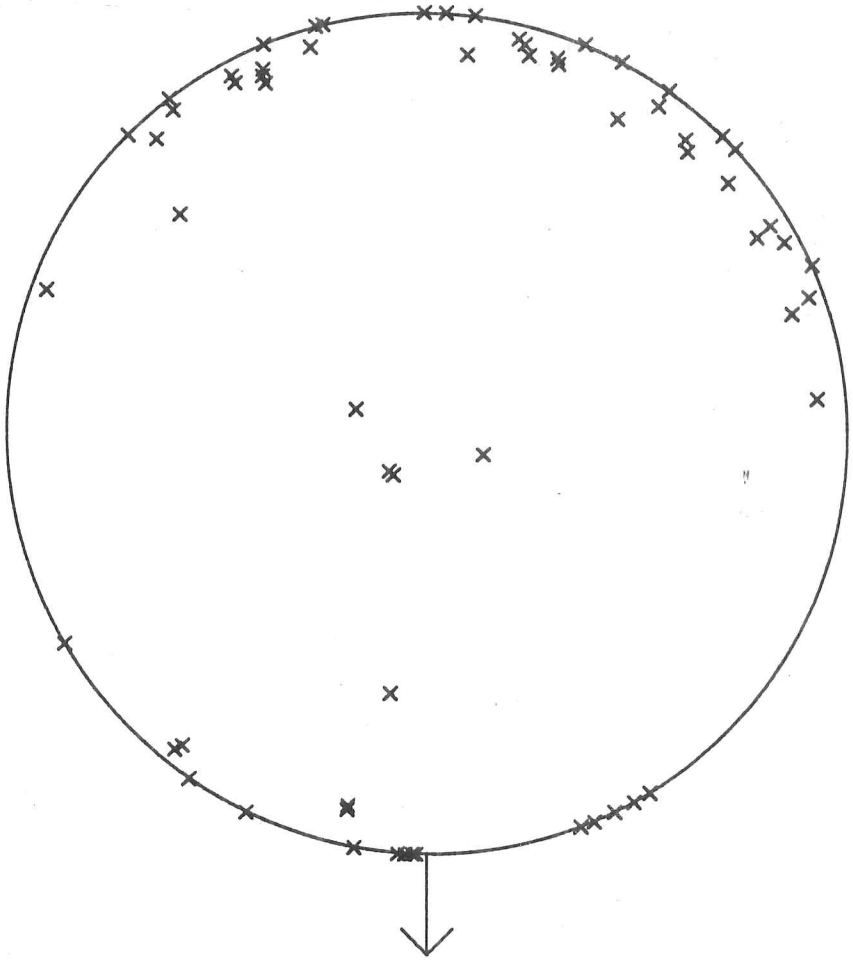

SAMPLE E5-5C-17/18

FIGURE 3.21(h)

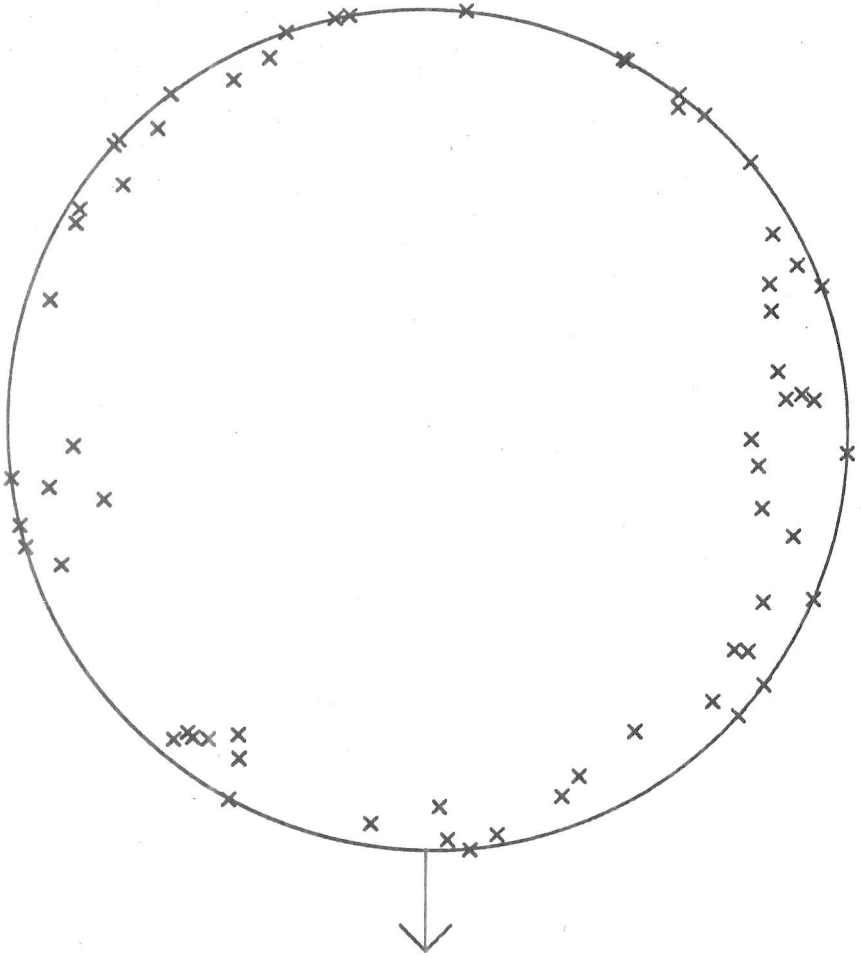

SAMPLE E5-5B- 1/ 2

FIGURE 3.21(i)

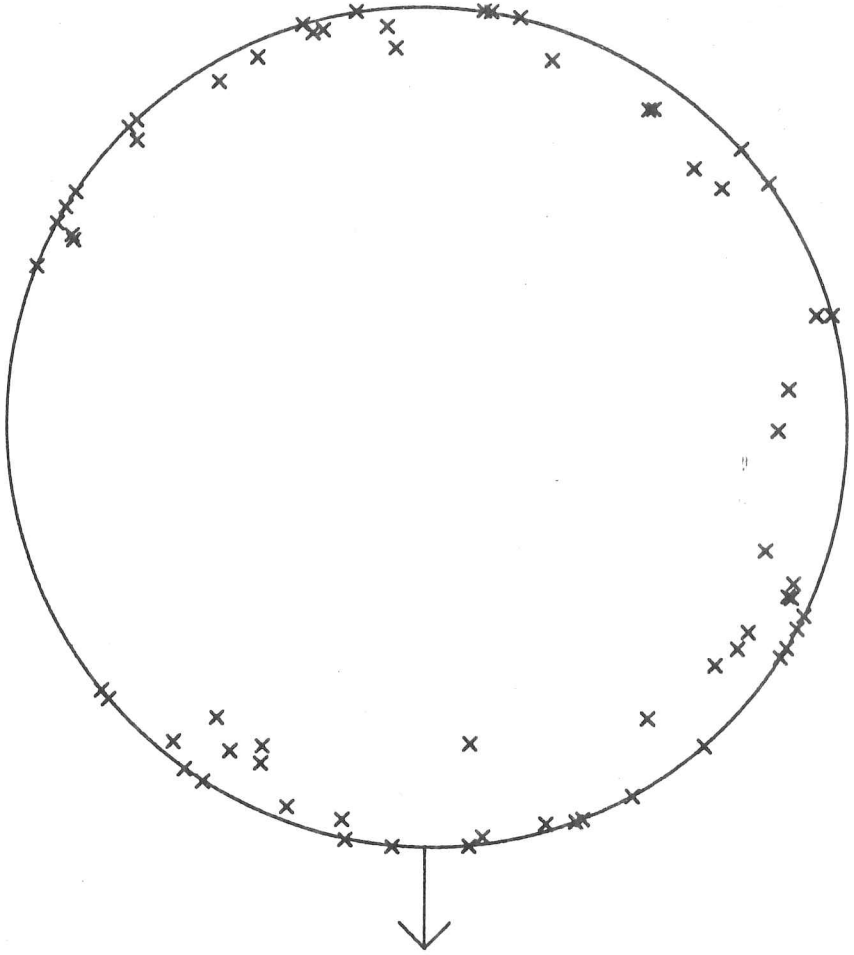

SAMPLE E5-5B- 5/ 6

FIGURE 3.21(j)

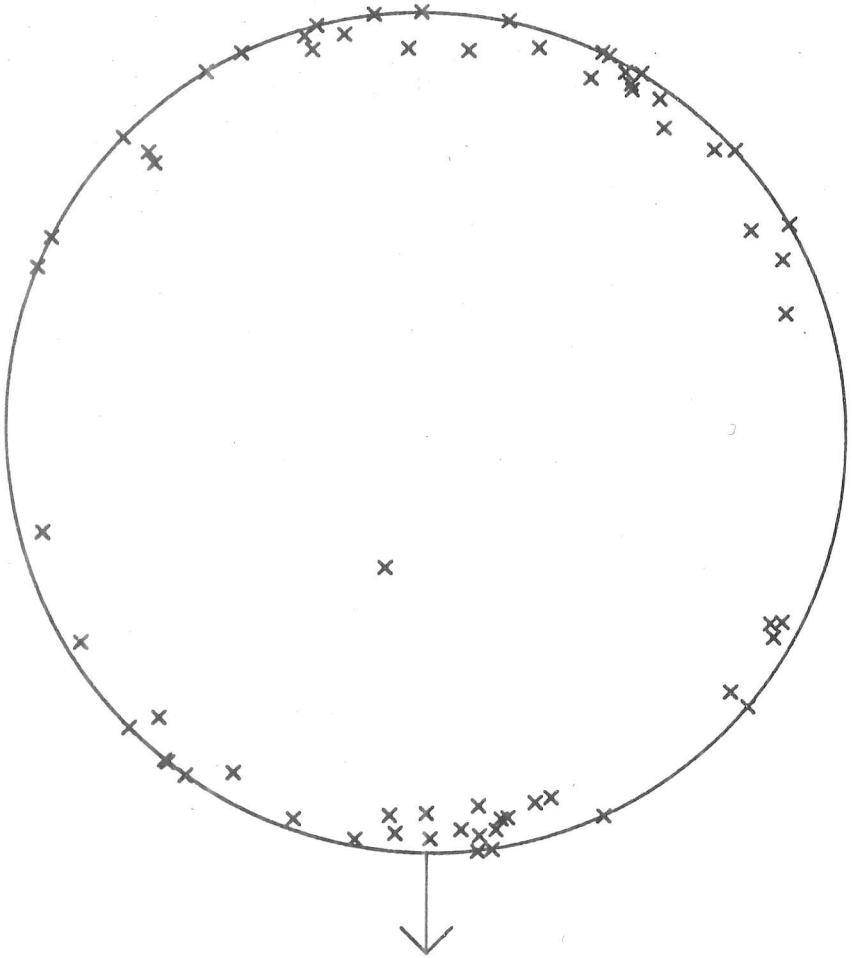

SAMPLE E5-5B-10/11

FIGURE 3.21(k)

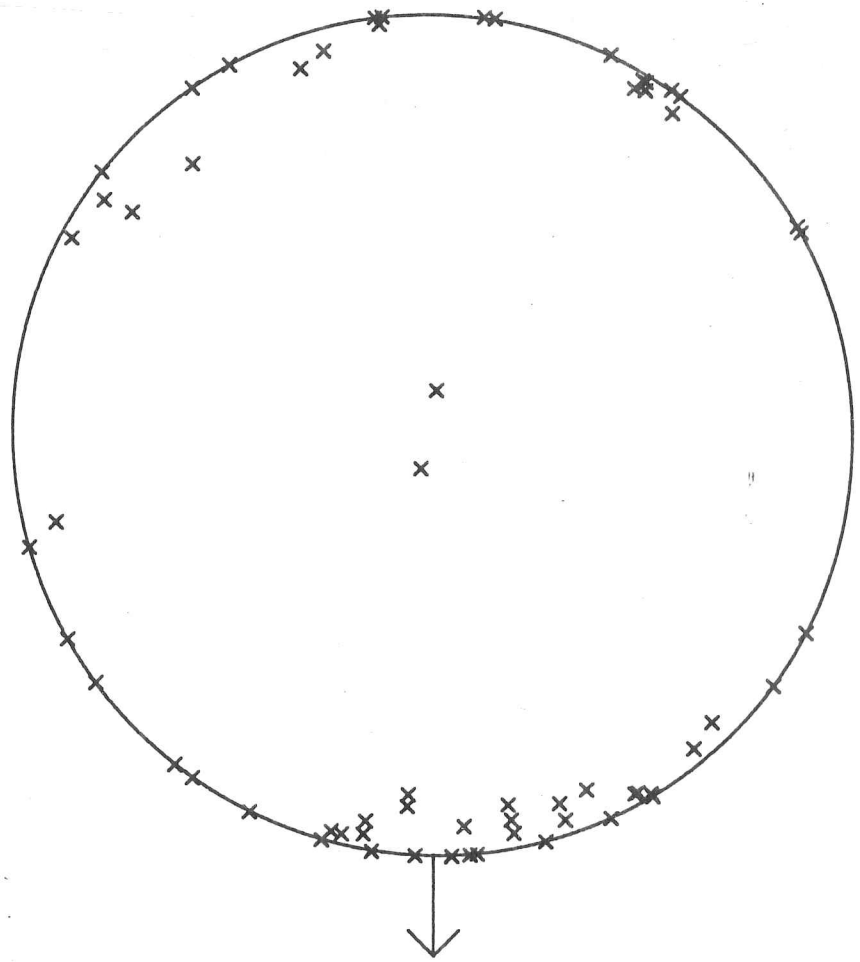

SAMPLE E5-5B-13/14

FIGURE 3.21(l)

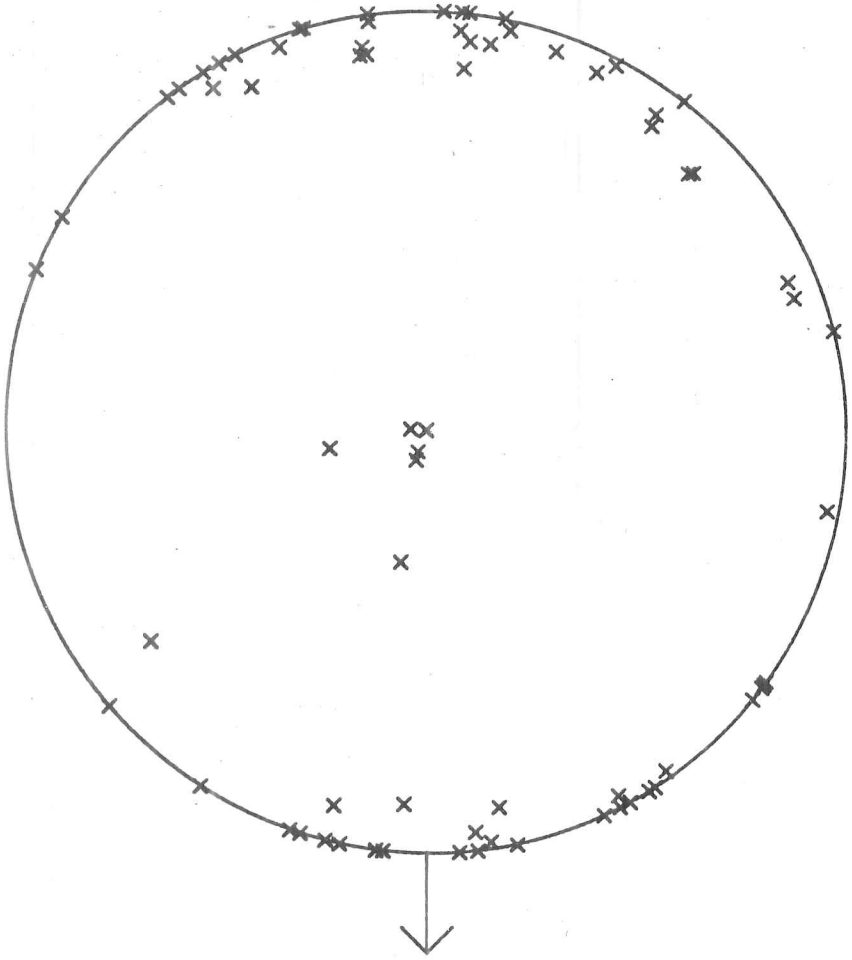

SAMPLE E5-5B-17/18

FIGURE 3.21(m)

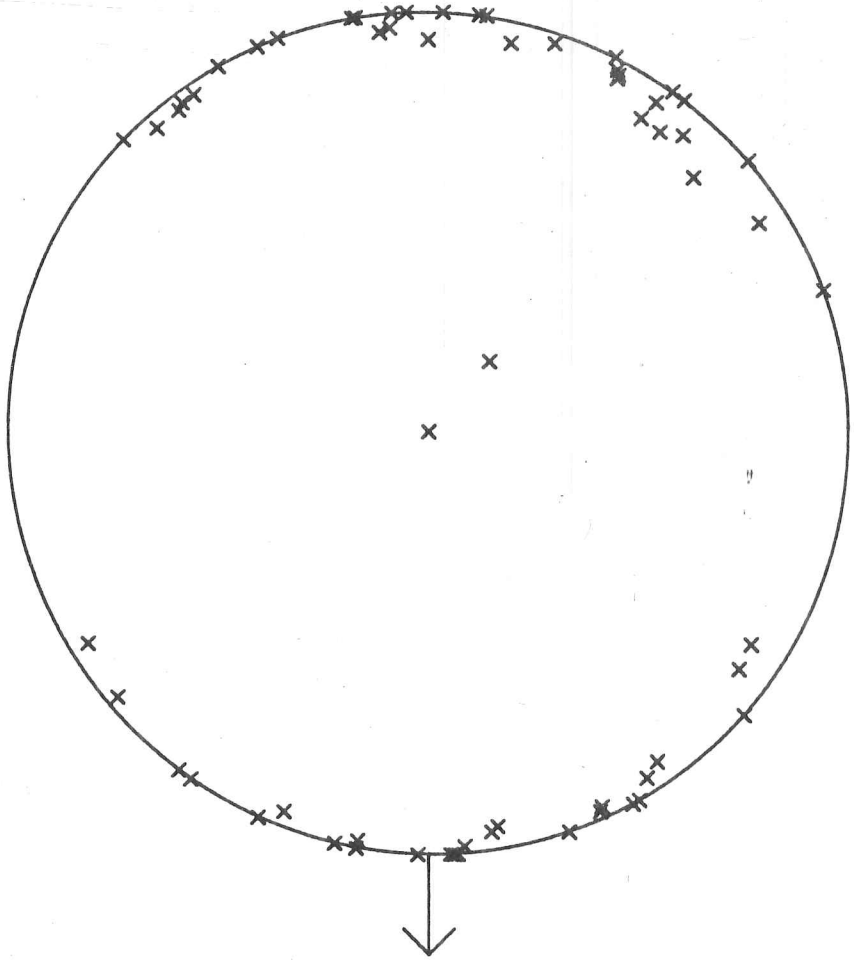

SAMPLE E5-5B-20/21

FIGURE 3.21(n)

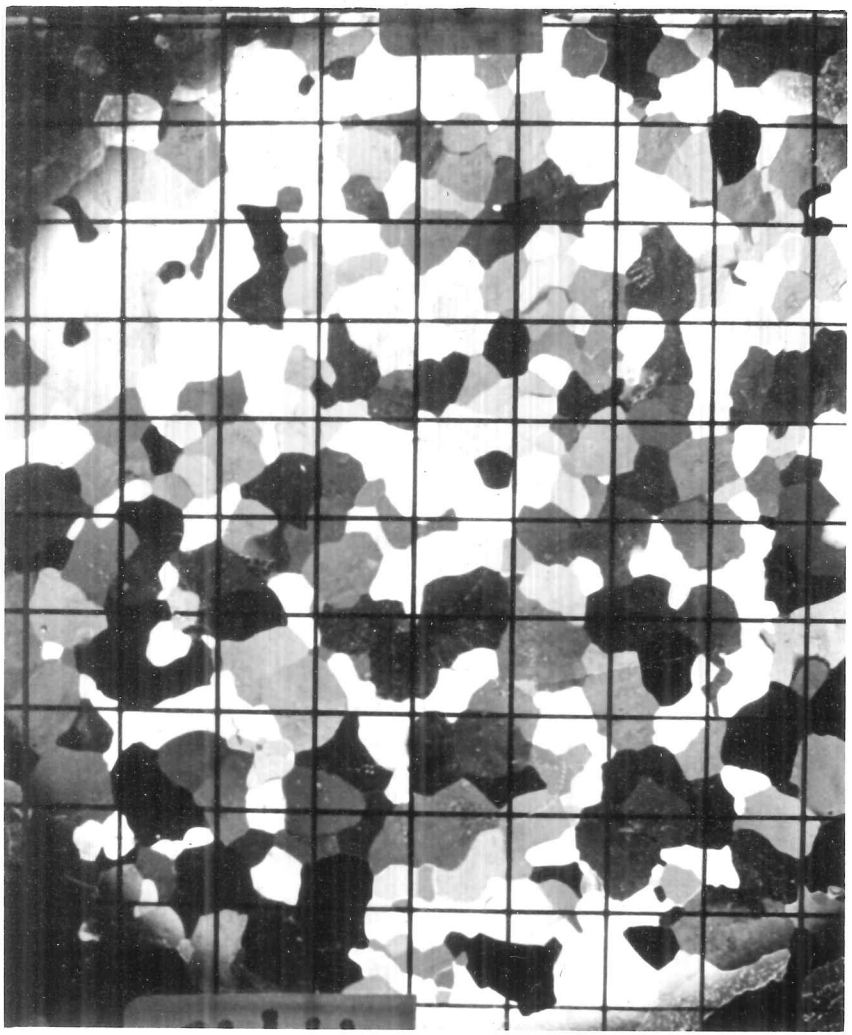

FIGURE 3.22 (b) Horizontal section from same location as (a) but taken 6cm below (a). Note the change in the appearence of the grains

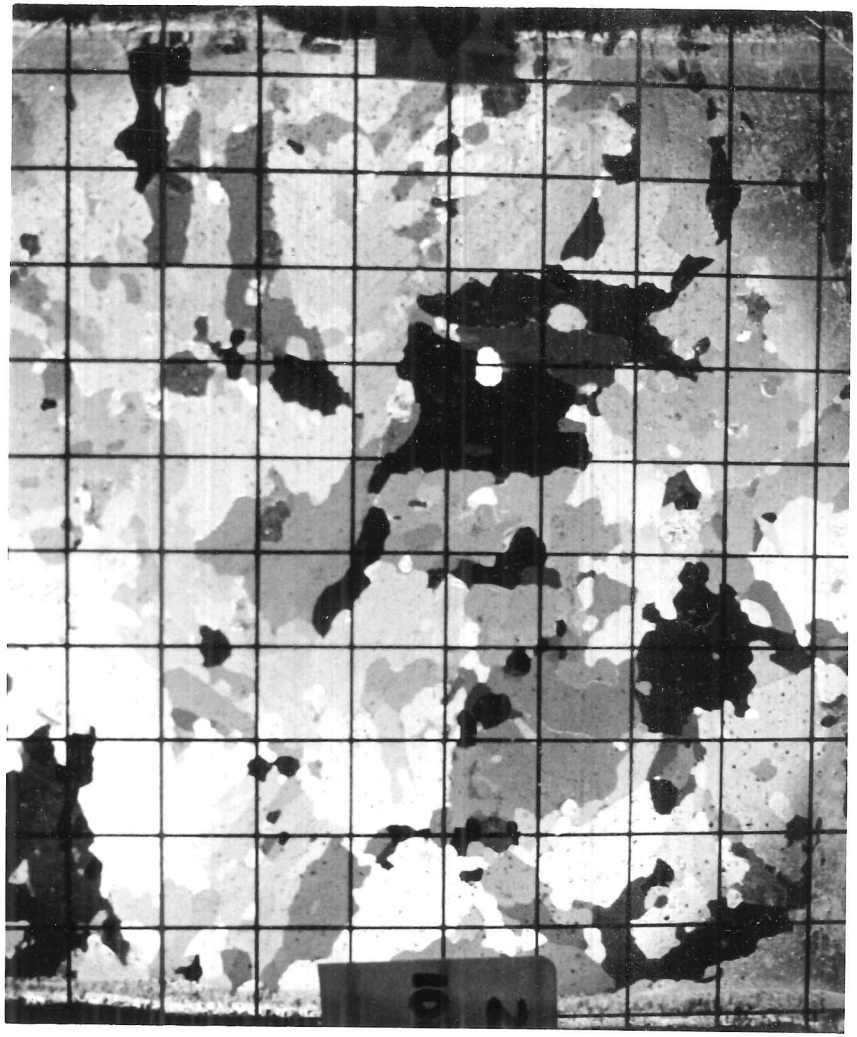

FIGURE 3.22 (a) Horizontal thin section from 10cm beneath the ice surface in Run 5 (brackish-forced flow). Section located only 15cm from the entrance to tank B and flow therefore unsteady. 1cm square grid.

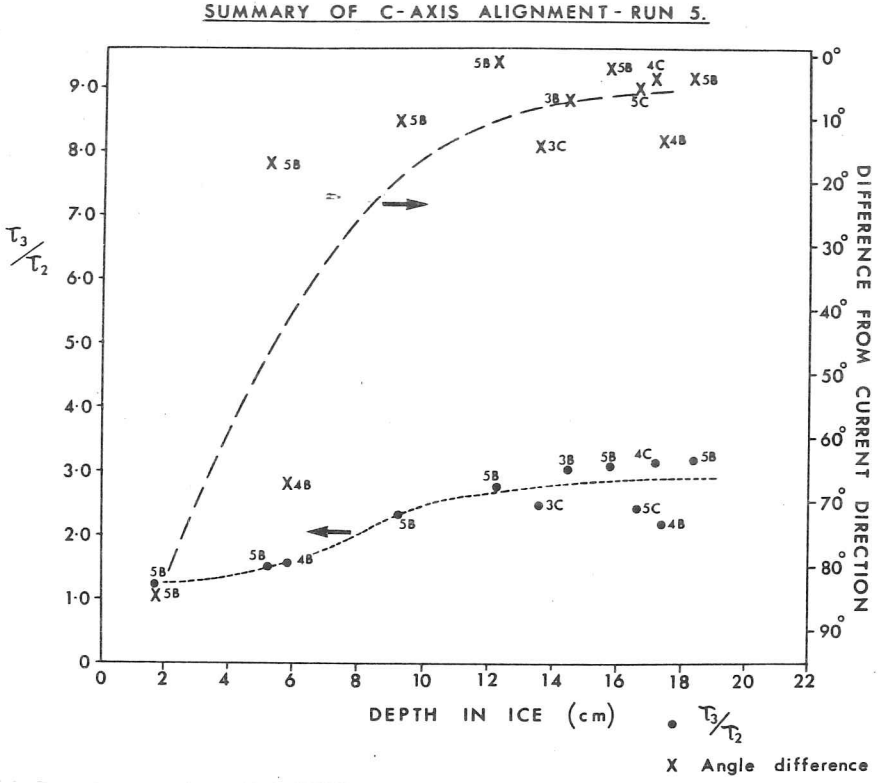

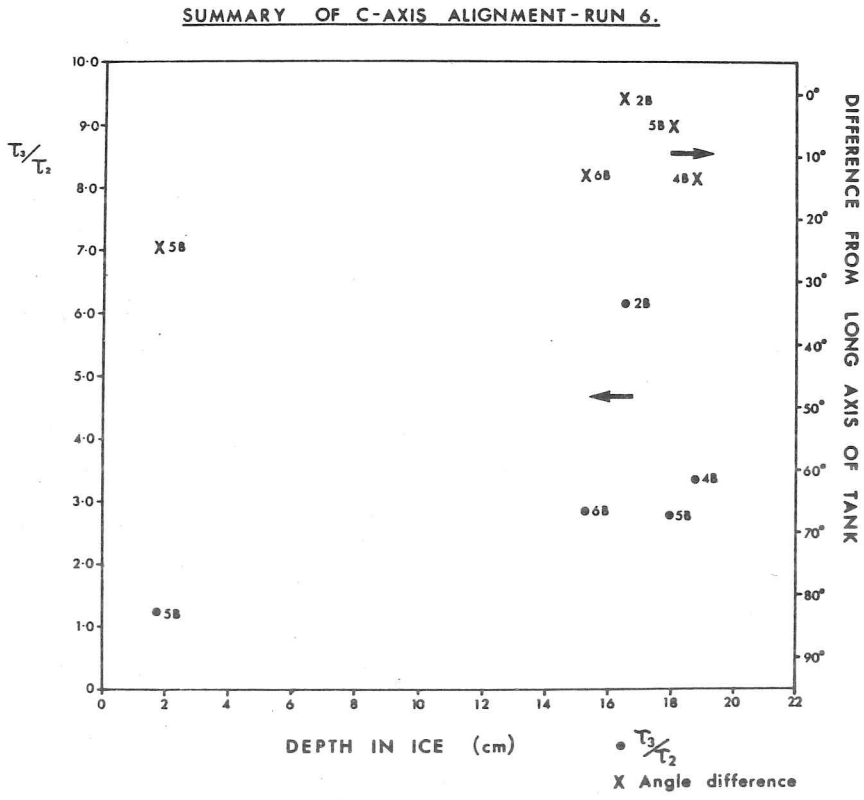

FIGURES 3.23(a) and (b) Diagrams of the concentration parameter (shown by dots) as a function of depth in the ice for the brackish experiments. The difference between the mean c-axis direction and the current or x-direction is also given (shown by crosses). Dotted lines indicate trends in data.

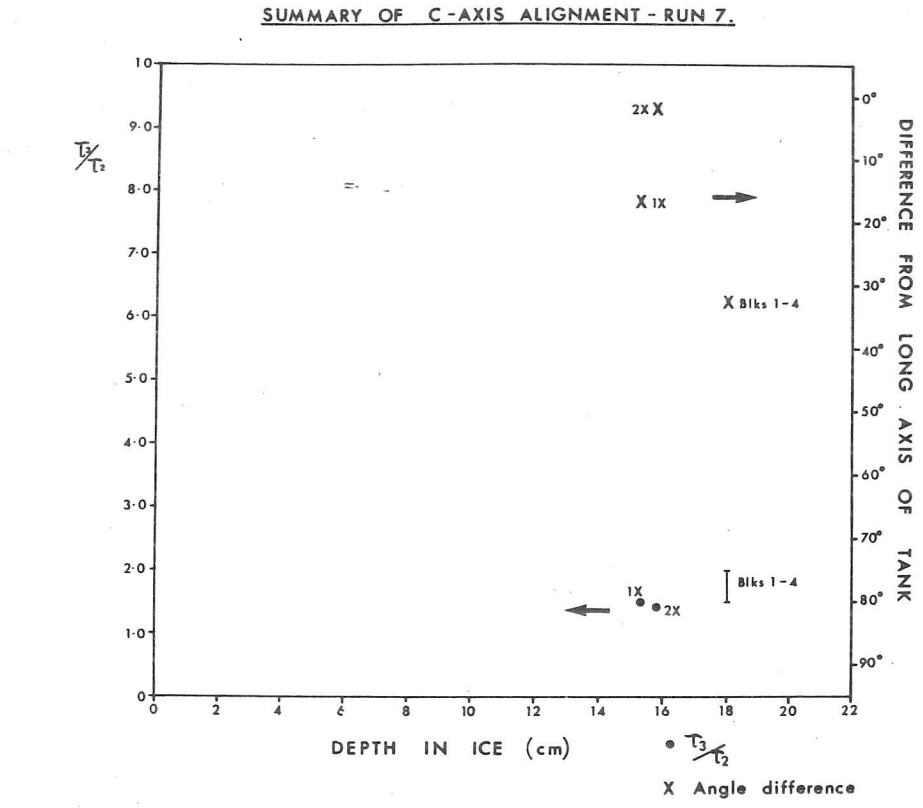

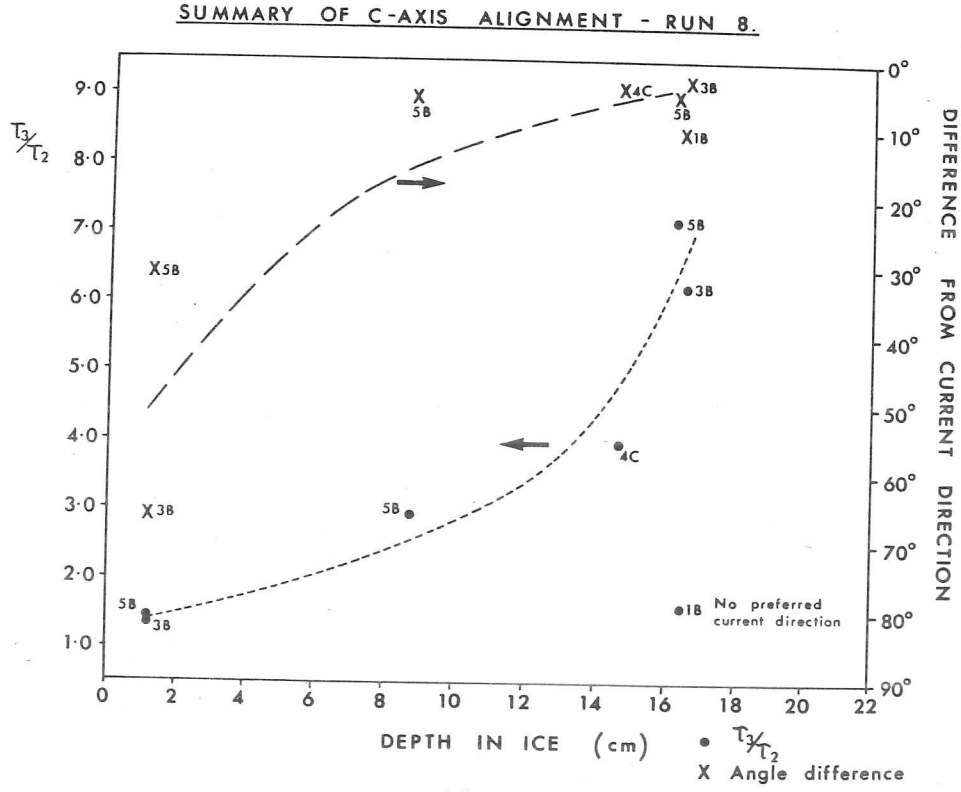

FIGURES 3.23 (c) and (d) As caption for previous page but displaying data for saline experiments.

Current and c-axis directions - Run 5.

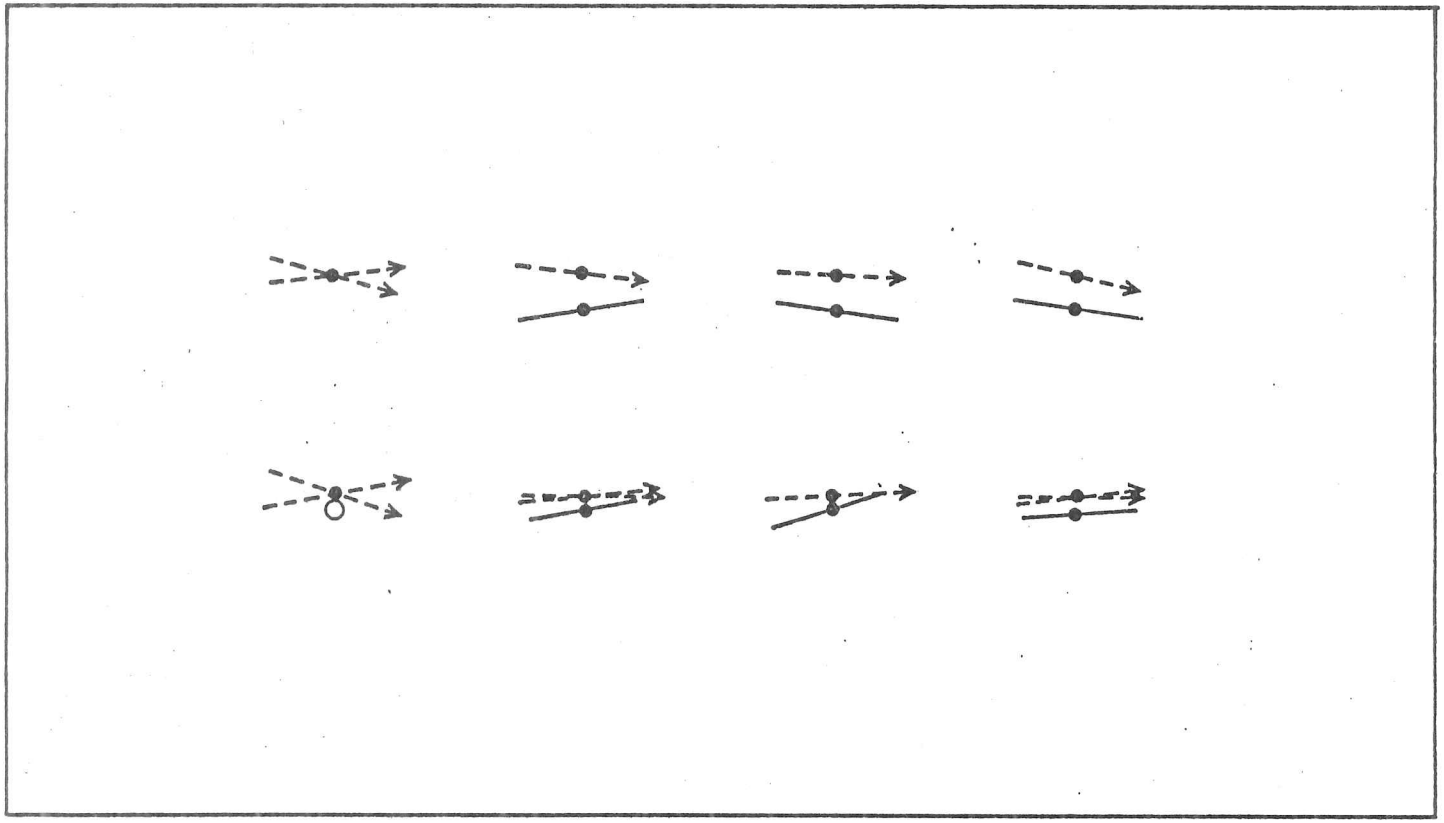

----→ The current direction from the simulated ice sheet.

—— The measured mean c-axis direction.

FIGURE 3.24
Mean c-axis measured at the base of the ice.

This depth is approximately the position of the cellular to planar transition which can be determined, quite independently of any texture studies, from the salinity profiles in figure 3.11. The profile for Run 5 diverges from those for the other experiments at a dimensionless depth of 0.55, that is approximately 11cm (see footnote of section 4.3.2 for further discussion of transition point). This adds further weight to the argument that the current is controlling the orientation since, at this point, the flow can no longer interact anisotropically with the salinity boundary layer

On the other hand, if the preferred orientation is controlled by heat flow, the mean c-axis of the grains will be normal to the horizontal temperature gradient, which we find from equation [3.1]. However, figure 3.25(a) shows there is no systematic relationship between the c-axis direction predicted from horizontal temperature gradients and the mean c-axis. Likewise the concentration parameter and the magnitude of the horizontal temperature gradient are unrelated (see figure 3.25(b)).

3.8.4 Texture for Run 6 (Brackish - No Forced Flow)

Run 5, with its low brine concentration, displayed some features which were atypical of sea ice. Although the same brine concentration was used in this experiment, the grains that developed are very similar to those found in nature. Columnar growth extends through the ice cover (figure 3.26), the c-axes being horizontally oriented at all levels (for example figures 3.27(c) and (d)). The platelets and the grains coarsen from the surface (figure 3.28(a)) to the bottom (figure 3.28(b)) and the grains elongate perpendicular to the c-axis. The characteristic, small angle differences between platelets are also present.

Figure 3.23(b) and 3.27(a),(b),(d) and (e) show that once again the preferred c-axis orientation is in the x direction and that this alignment was generally stronger than that found in Run 5. However the depth-dependence of the concentration parameter and the angular difference from the x direction is virtually non-existent. In addition, figures 3.25(a) and (b) show that the alignment is not due to heat flow in

FIGURE 3.25(a)
Diagram of the measured mean c-axis direction versus the directions predicted from the horizontal temperature gradients which were calculated from equation [3.1]. If there was significant correlation between these, the data would lie on straight line of slope 1 (shown in bold). Measured and calculated quantites can differ by up to 90° and the shaded region is thus prohibited.

FIGURE 3.25(b)
Diagram of concentration parameter versus the calculated horizontal temperature gradients. Note that the two measured gradients are plotted, with errors, and the corresponding calculated gradients are just within this error.

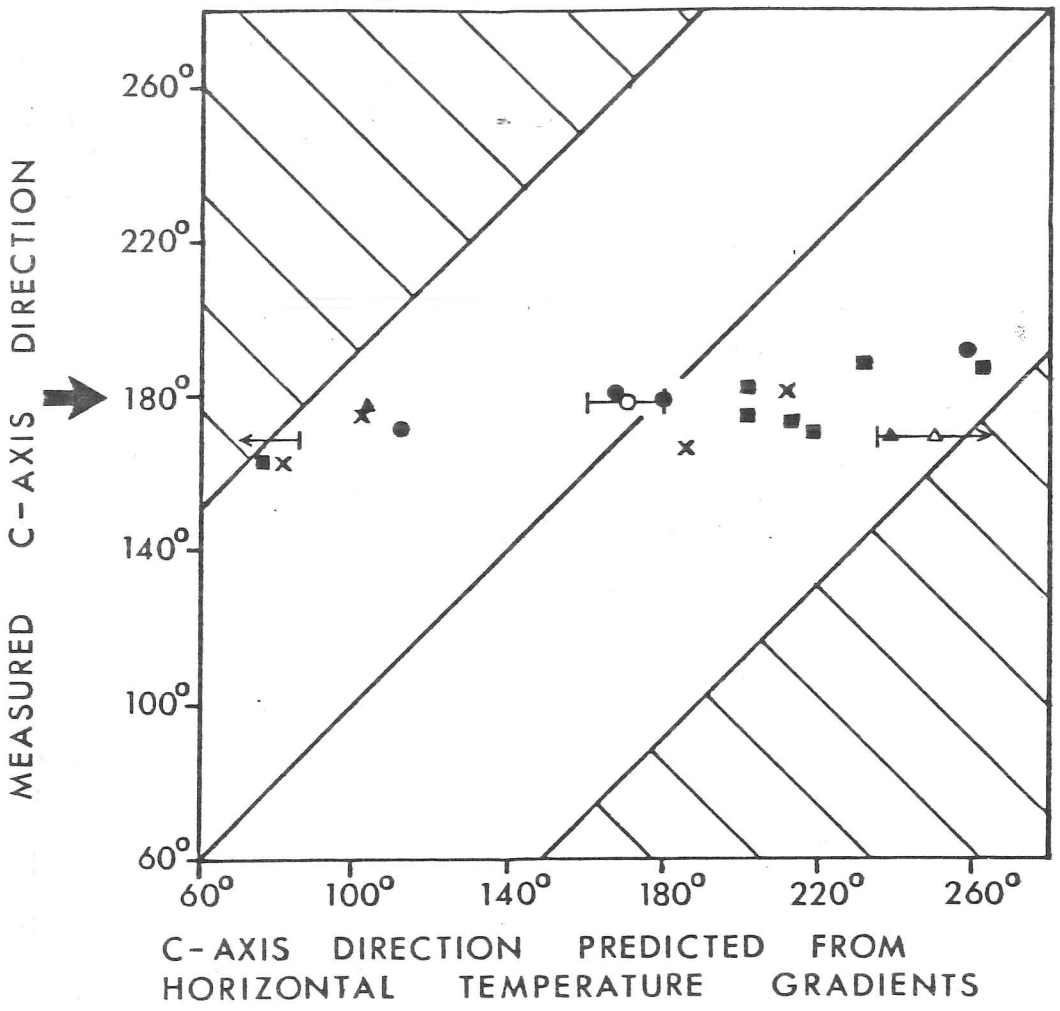

FIGURE 3.25(a)

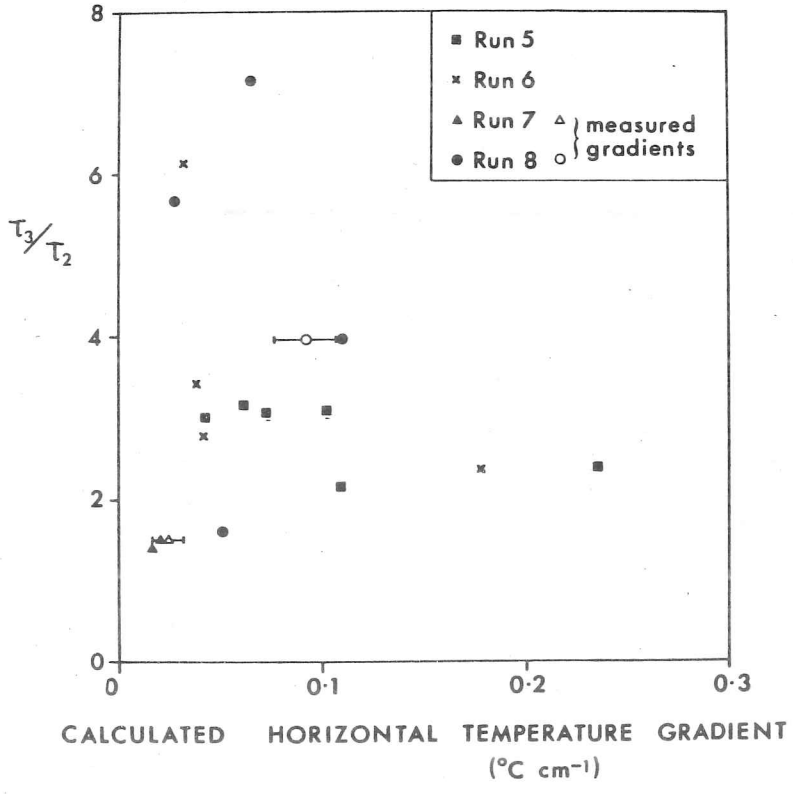

FIGURE 3.25(b)

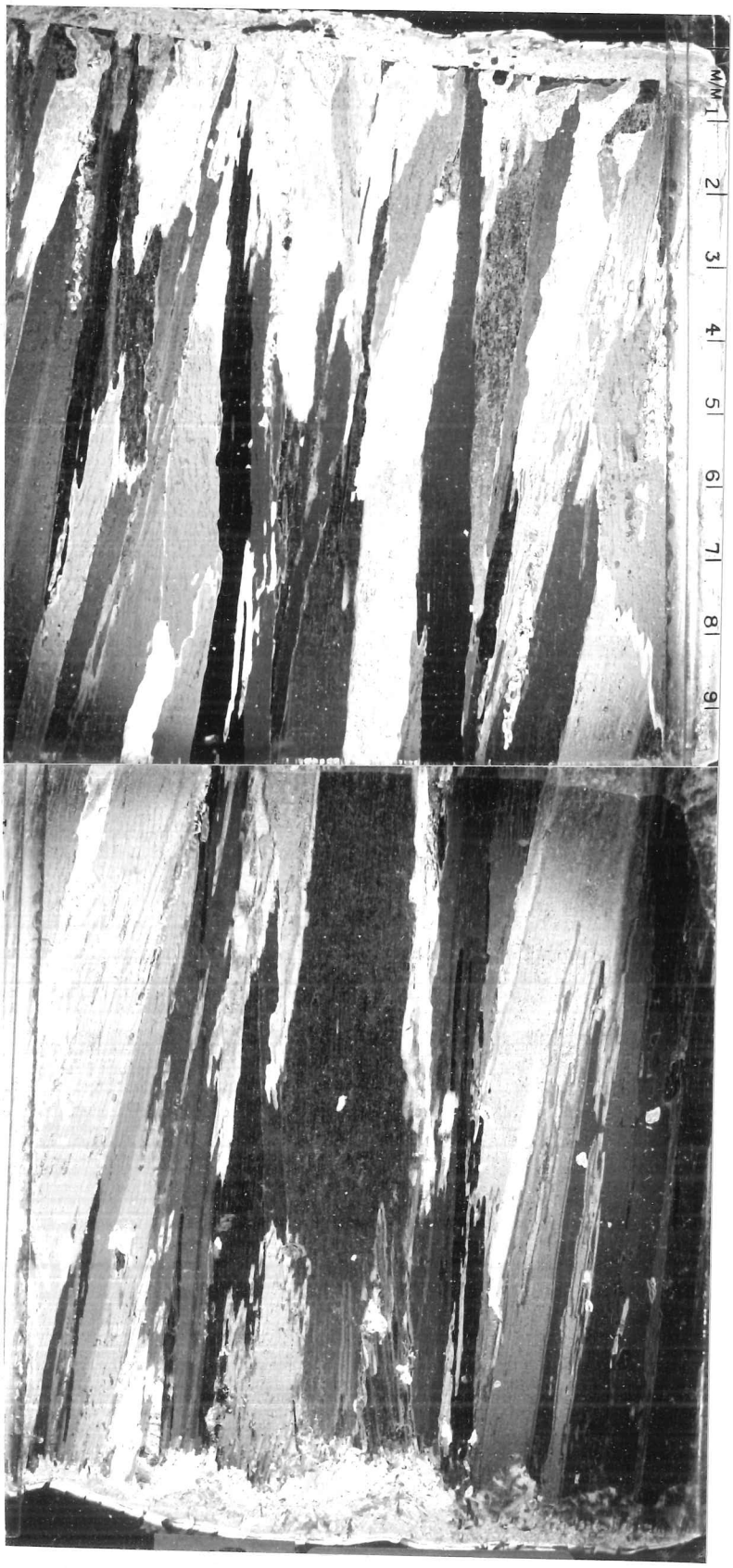

FIGURE 3.26 Vertical thin section from upper ice surface to the base of the ice for Run 6. Columner growth extends throughout the ice thickness.

FIGURE 3.27
Equal-area projection diagrams for Run 6. The long axis of the tank is shown by an arrow in these figures. 64 measurements were made in each case.

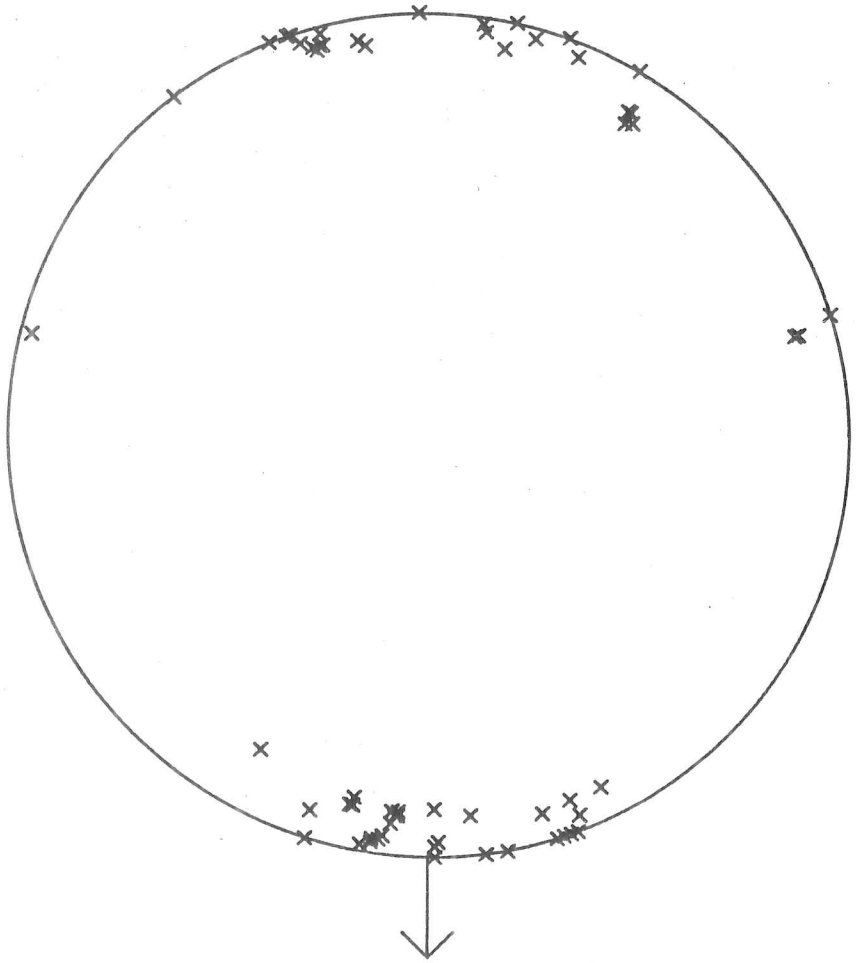

SAMPLE E6-2B-16/17

FIGURE 3.27 (a)

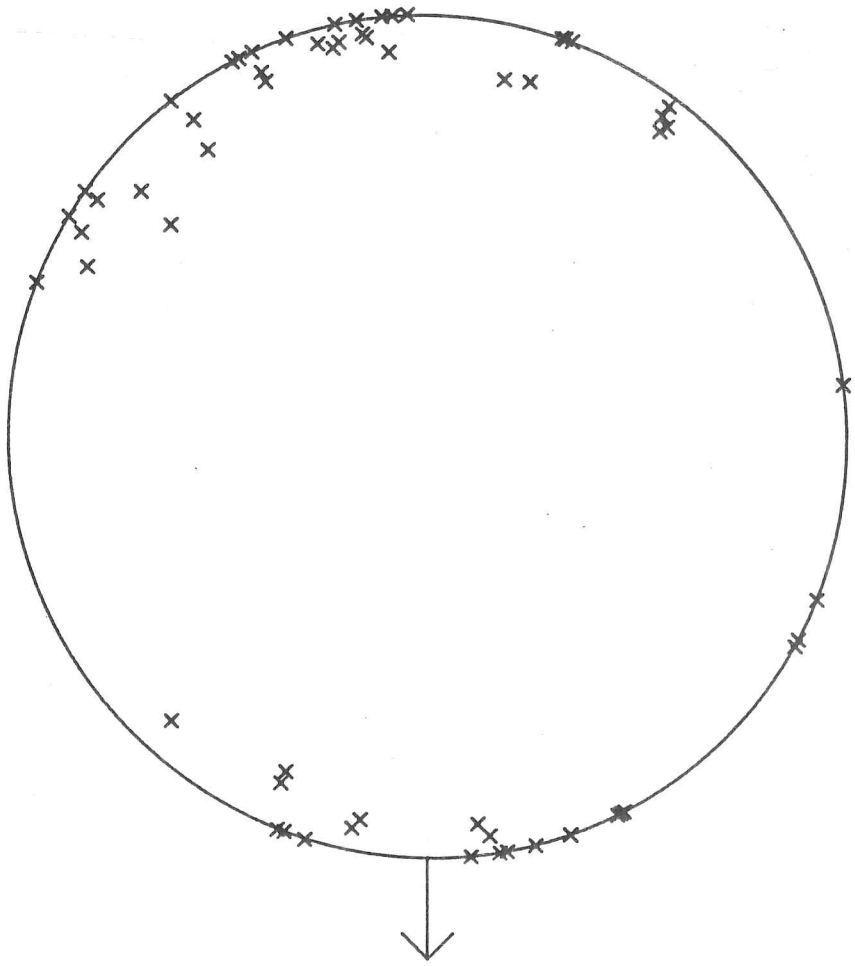

SAMPLE E6-4B-18/19

FIGURE 3.27 (b)

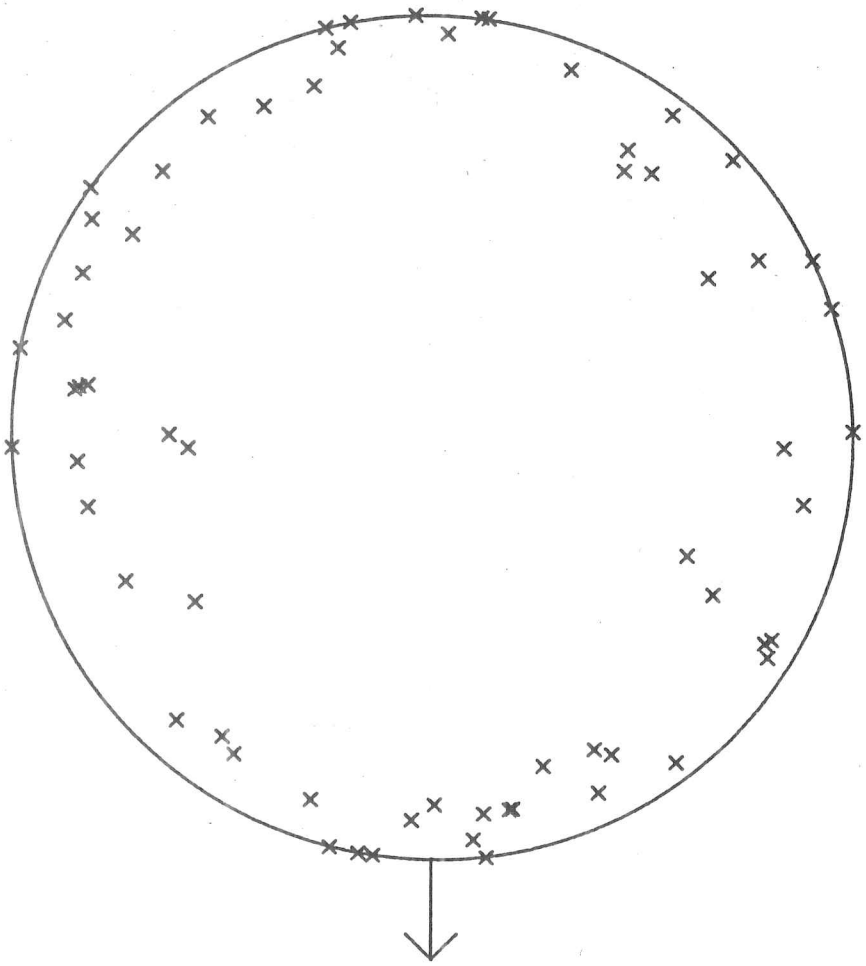

SAMPLE E6-5B- 1/ 2

FIGURE 3.27 (c)

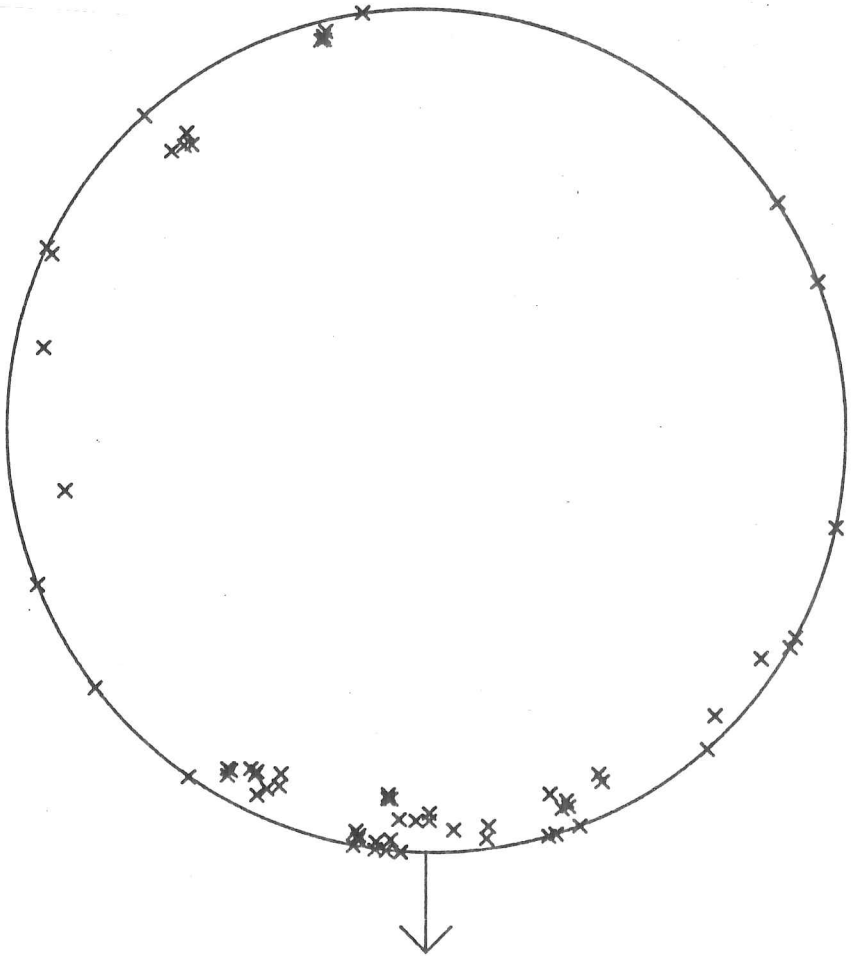

SAMPLE E6-5B-17/18

FIGURE 3.27 (d)

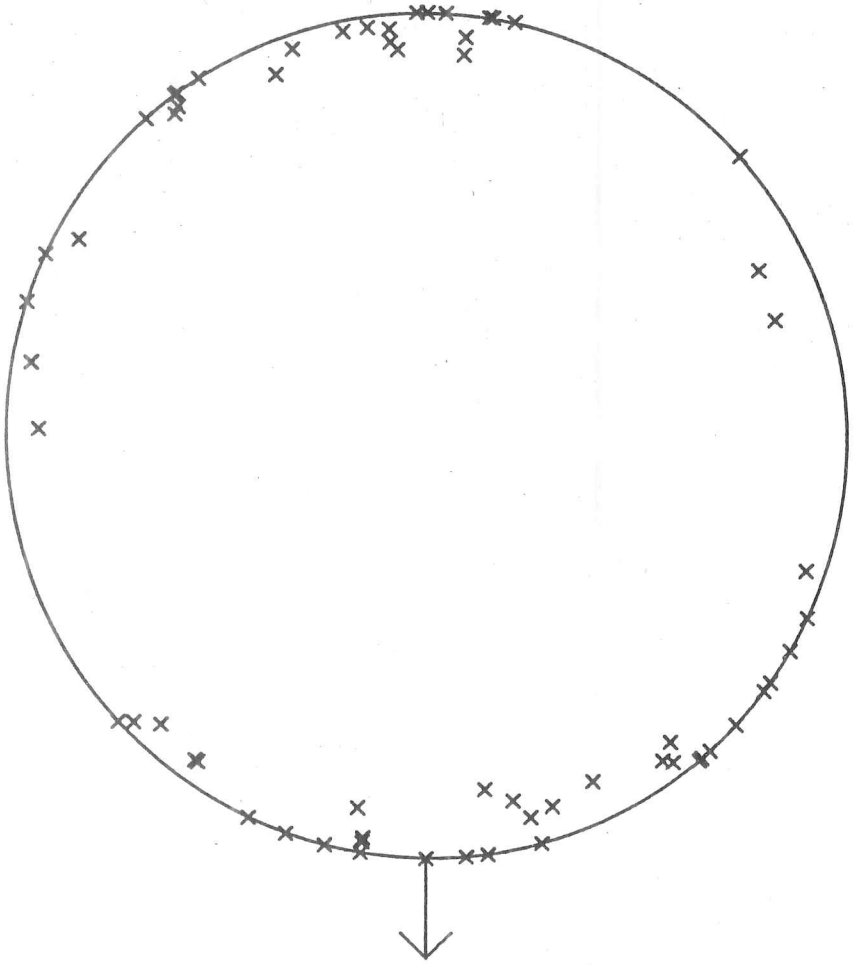

SAMPLE E6-6B-16/17

FIGURE 3.27 (e)

FIGURE 3.28 (b) Horizontal thin section from 18cm below the ice surface at the same location as (a). Scale is the same as in (a).

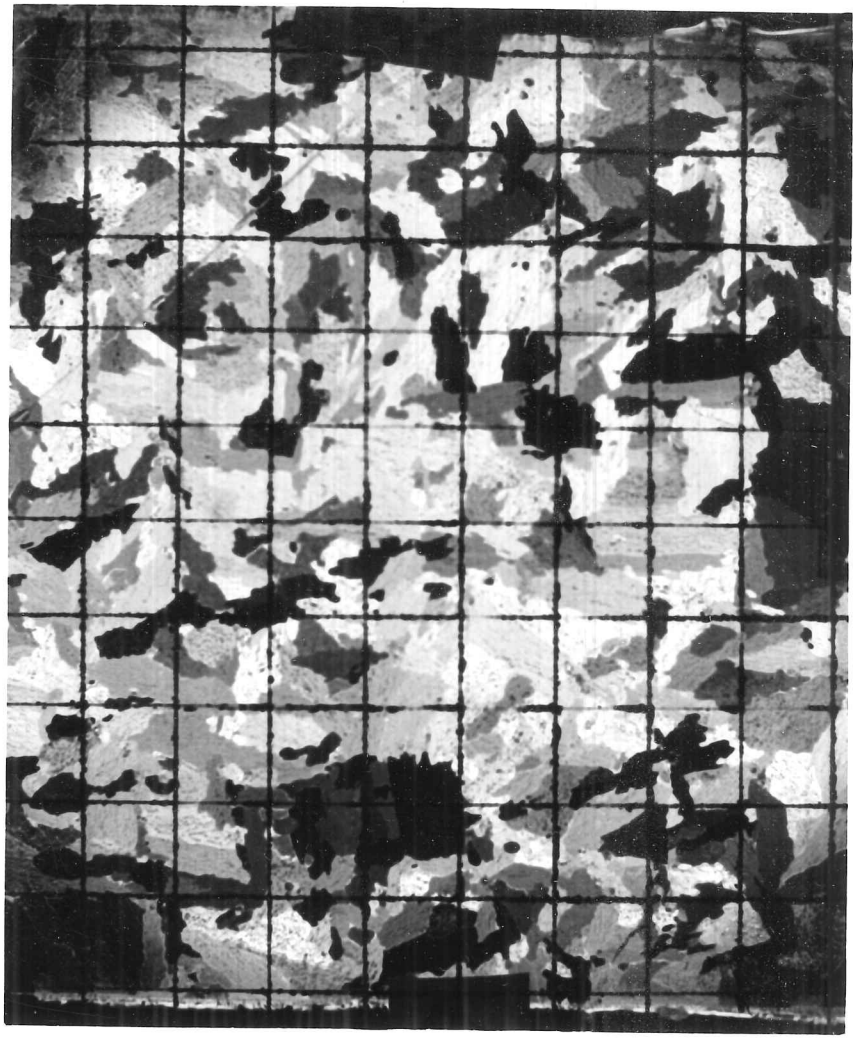

FIGURE 3.28 (a) Horizontal thin section from 2cm below the ice surface in Run 6 (brackish-no forced flow). Covered by a 1cm square grid.

the horizontal plane.

However, if the concentration parameter is plotted as a function of the downtank coordinate x, as in figure 3.29, some order evolves. Thus it appears that the closer a sample lies to the entrance of the tank the better aligned it is. From the discussion in section 3.7.4, we have reason to believe that the natural convection during this experiment followed a similar pattern and we hypothesise that this is responsible for the c-axis orientation.

3.8.5 Texture for Run 7 (Saline – No Forced Flow)

Due to emergency cold room maintenance, it was necessary to collect texture information using a different procedure from the other experiments. Oil-soluble dye was brushed on to the skeletal ice-water interface and the bottoms of blocks 1 to 4 (see figure 3.3(c) for the locations of these) were photographed. [7] Platelet orientations were measured from these photographs since the c-axis is perpendicular to the elongated direction of the platelet. However, only the component in the horizontal plane is obtained. A total of 473 measurements were made on blocks 1 to 4 using the sampling scheme described in section 3.2.1. In order to compare these results with data from the other experiments, a method similar to that of Kamb (1959b) was used. Data were placed in bins of dimensions $\Delta\phi = 30^{\circ}$ and $\Delta\theta = 60^{\circ}$, centred on the horizontal component of the mean c-axis direction (see figure 3.30). We chose the surface samples E5-5B- 1/ 2 and E6-5B- 1/ 2 as our reference and from these we calculated the standard deviation about the mean of the number of c-axes which fall in each bin. We then compared a range of values of the concentration parameter with fabric strengths described in terms of multiples of this standard deviation. This led us to the conclusion that the collective results of blocks 1 to 4 were typical of concentration parameters between 1.5 and 2.0. This has been plotted on figure 3.23(c). We were fortunate to supplement these measurements with two samples of c-axes measurements made in the conventional manner when the cold room was

---

[7] This method was communicated to me by Dr. S. Martin of the University of Washington, Seattle.

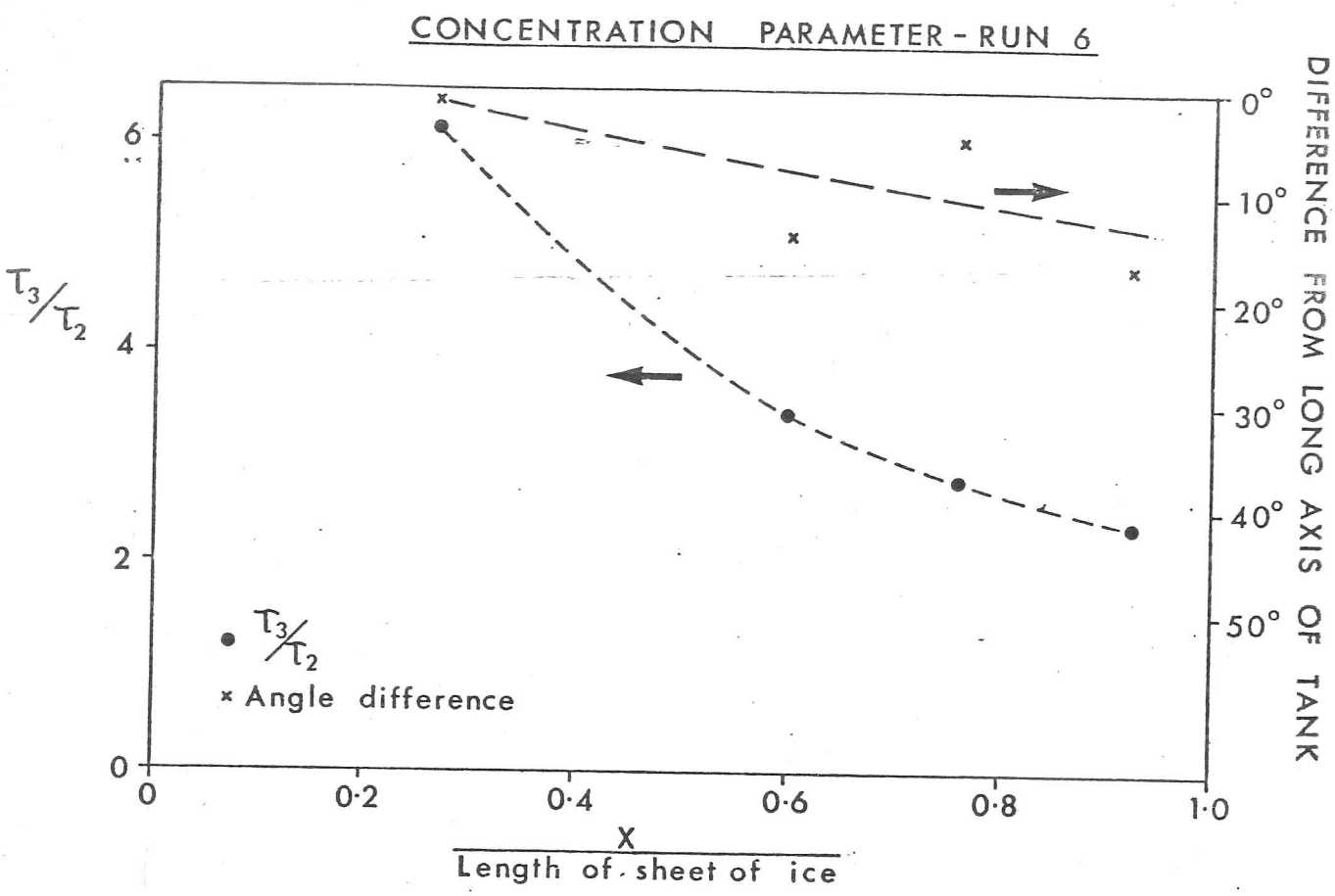

FIGURE 3.29 Diagram of the concentration parameter as a function of the dimensionless distance from the honeycombs. Dotted line indicates the trend in the data.

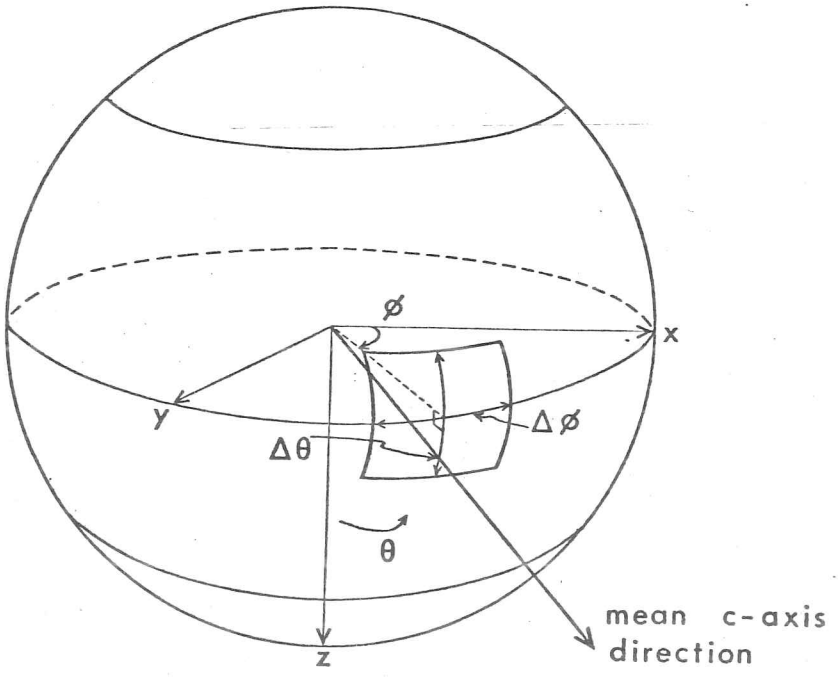

FIGURE 3.30 Diagram of the angular bins used for grouping c-axis data.

restored to working order.

The features of the ice in this experiment were similar to those in Run 6, but with a coarser platelet spacing and a larger grain size (figure 3.31) which are both characteristic of the lower growth velocity. The major structural difference from Run 6, is the c-axis vertical layer at the ice surface. Increased mixing, due to thermal instability in this experiment, prevented the formation of a cool, surface layer and the grains therefore expand most easily in the plane of the surface. Columnar growth with the c-axis horizontal proceeds from approximately 1cm below the surface.

However figure 3.32(a) and (b) show that the texture which developed at depth was quite different from that in Run 6. At depths of 15cm below the surface the c-axes still essentially form a symmetric girdle distribution. It follows that the concentration parameter (figure 3.23(c)) will be low compared with the other experiments.

It should be noted that the values of horizontal temperature gradient were low during this experiment. However this cannot explain the lack of alignment since in figure 3.25($\frac{b}{a}$) we see that highest concentration parameters occur at similar values.

3.8.6 Texture for Run 8 (Saline – Forced Flow)

One of the most distinctive features of this experiment is shown in figure 3.33(a). The grains consistently grow in a direction opposing the flow, regardless of the slope of the interface. This upstream deflection, although previously unreported for sea ice, has been noted in the dendritic growth of pure ice in supercooled, flowing water by Miksch (1969). It is also well known in the metals literature (Cole, 1971; Flemings, 1974) and is characteristic of dendritic solidification in the presence of a flowing melt; indeed empirical equations derived for the solidification of steels (Takahashi et al, 1979; Takahashi, 1981) have been used to derive the velocity of the melt from the angle of deflection of the grains.

FIGURE 3.31 Horizontal thin section from Run 7 (saline-no forced flow) taken 15cm below the ice surface. Note the well-defined platelets. 1.5xreal size.

FIGURE 3.32
Equal-area projection diagrams for Run 7. The long axis of the tank is shown by an arrow in these figures. 64 measurements were made in each case.

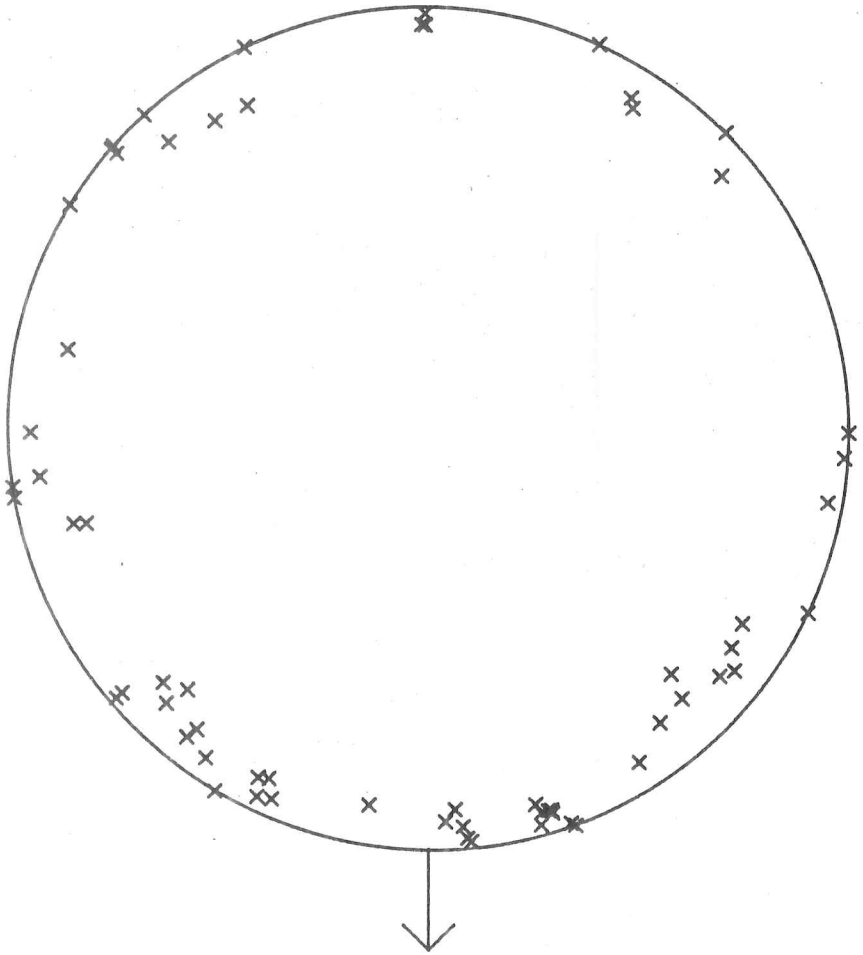

SAMPLE E7-1X-15/16

FIGURE 3.32 (a)

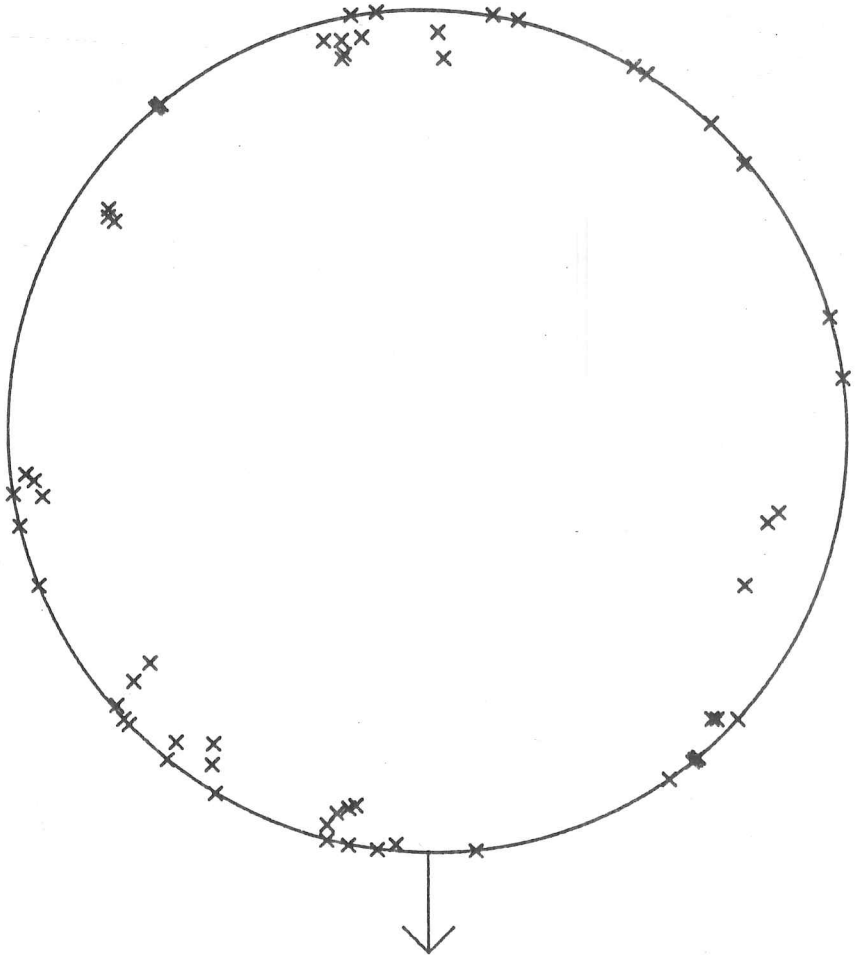

SAMPLE E7-2X-15/16

FIGURE 3.32 (b)

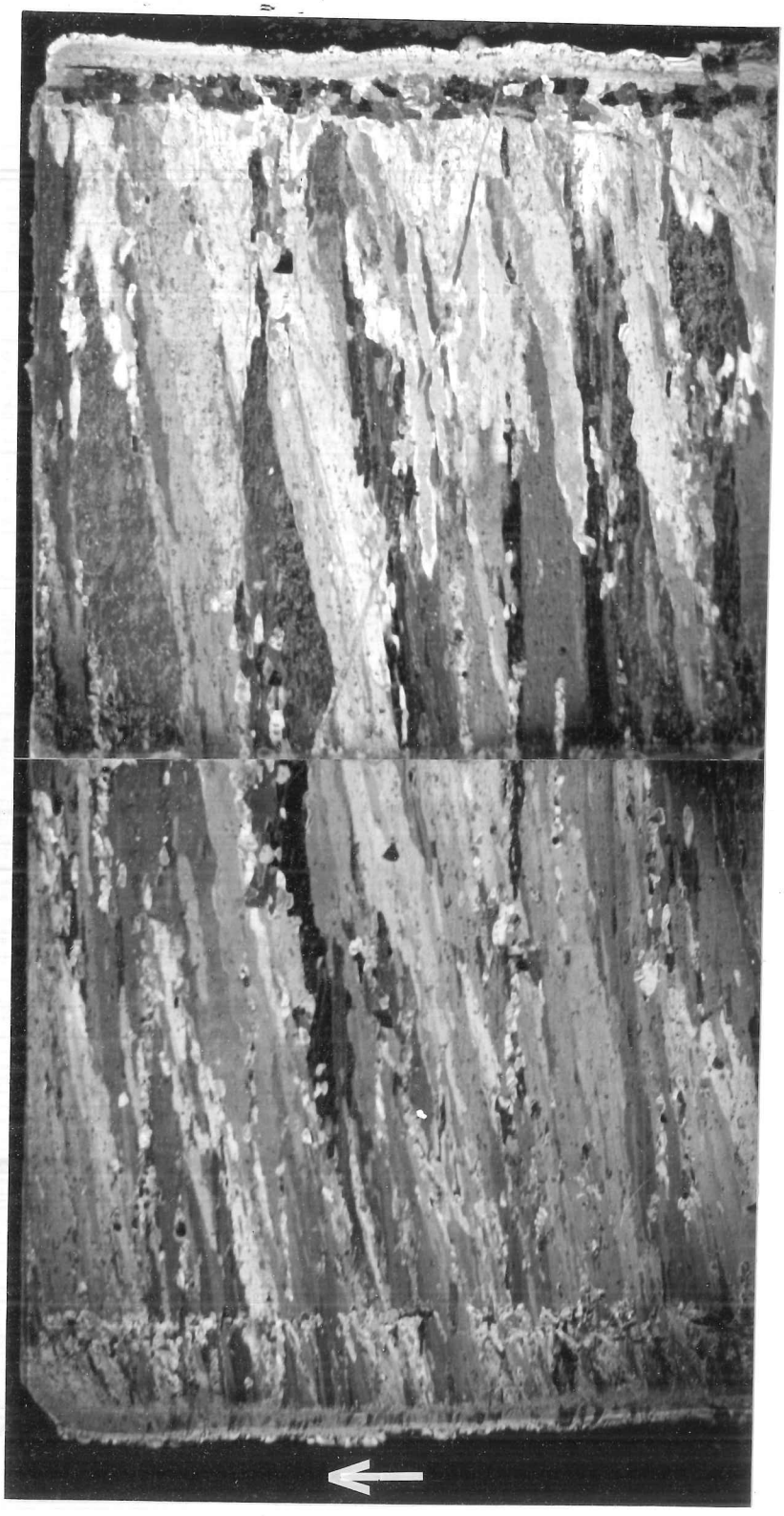

FIGURE 3.33 (a) Vertical thin section in the x-plane from Run 8. Columner growth extends from the ice surface to the base and there is also an upstream deflection of the grains into the current (shown by an arrow). Note the 0.7cm thick c-axis vertical layer at the upper ice surface.

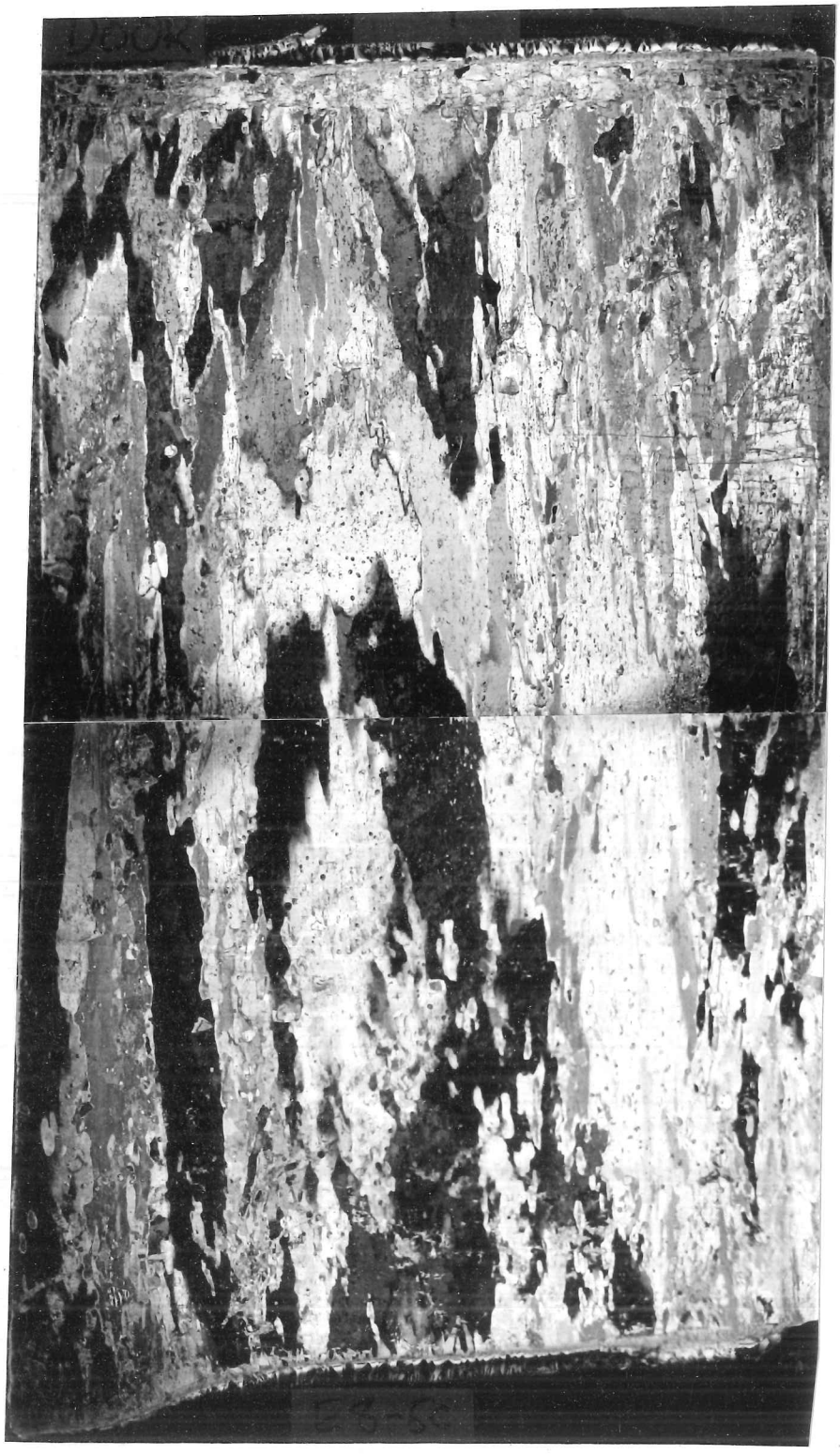

FIGURE 3.33 (b) Vertical thin section in the y-plane from Run 8, so that the current was normal to the plane of this section. Note the difference in appearence of the grain boundaries as compared with 3.33(a).

Figures 3.34(c),(d),(f) and (g) show that the observed tilt is not just a motion of the grain boundaries in the upstream direction. The grouping of the points about the downstream pole indicates that the c-axes maintain their orientation normal to the columnar axis. We shall return to a more detailed discussion of this grain deflection in the section 4.6.

Figure 3.33(a) shows that, in common with Run 7, there is a 0.7cm thick, c-axis vertical layer at the ice surface. This layer appears to thicken to approximately 1cm in the downstream direction which may be due either to the heat flux from the water decreasing as x increases or to herding of the freely floating crystals by the current. Inspection of the grains just below this zone and of figures 3.34(b) and (e) indicates that grains which tilted into the flow have nucleated about 1cm from the surface. Many of these grains have too high an angle of deflection to continue growing downwards and are subsequently squeezed out.

The structural characteristics of the surface samples is typical of sea ice (figure 3.35(a)). The grains develop through the ice (figures 3.35(b) and (c)) in such a way that, although the appearance of the thin sections is becoming more chaotic with depth, the c-axes (figure 3.23(d)) are rapidly becoming more aligned. The chaotic appearance is due to the large numbers of small angle differences between the platelets comprising a grain. Comparison of figure 3.35(c) with 3.31, which is its counterpart from Run 7, illustrates that the platelet spacing is considerably smaller in the present case.

The distinctive appearance of the almost straight grain boundaries of figure 3.33(a) is lost if the vertical thin section is made in the y-plane. This is illustrated in figure 3.33(b) where these diffuse boundaries immediately indicate that the c-axes are preferentially normal to the plane of this section; that is they are grouped in the x direction. At locations where universal stage measurements were not made, we have used this to confirm there were no deviations from the general pattern of c-axis alignment.

Figures 3.34(c),(d),(f) and (g) show that the observed tilt is not just a motion of the grain boundaries in the upstream direction. The grouping of the points about the downstream pole indicates that the c-axes maintain their orientation normal to the columnar axis. We shall return to a more detailed discussion of this grain deflection in the section 4.6.

Figure 3.33(a) shows that, in common with Run 7, there is a 0.7cm thick, c-axis vertical layer at the ice surface. This layer appears to thicken to approximately 1cm in the downstream direction which may be due either to the heat flux from the water decreasing as x increases or to herding of the freely floating crystals by the current. Inspection of the grains just below this zone and of figures 3.34(b) and (e) indicates that grains which tilted into the flow have nucleated about 1cm from the surface. Many of these grains have too high an angle of deflection to continue growing downwards and are subsequently squeezed out.

The structural characteristics of the surface samples is typical of sea ice (figure 3.35(a)). The grains develop through the ice (figures 3.35(b) and (c)) in such a way that, although the appearance of the thin sections is becoming more chaotic with depth, the c-axes (figure 3.23(d)) are rapidly becoming more aligned. The chaotic appearance is due to the large numbers of small angle differences between the platelets comprising a grain. Comparison of figure 3.35(c) with 3.31, which is its counterpart from Run 7, illustrates that the platelet spacing is considerably smaller in the present case.

The distinctive appearance of the almost straight grain boundaries of figure 3.33(a) is lost if the vertical thin section is made in the y-plane. This is illustrated in figure 3.33(b) where these diffuse boundaries immediately indicate that the c-axes are preferentially normal to the plane of this section; that is they are grouped in the x direction. At locations where universal stage measurements were not made, we have used this to confirm there were no deviations from the general pattern of c-axis alignment.

FIGURE 3.34
Equal-area projection diagrams for Run 8. The approximate current direction is marked with an arrow in these figures. 64 measurements were made in each case.

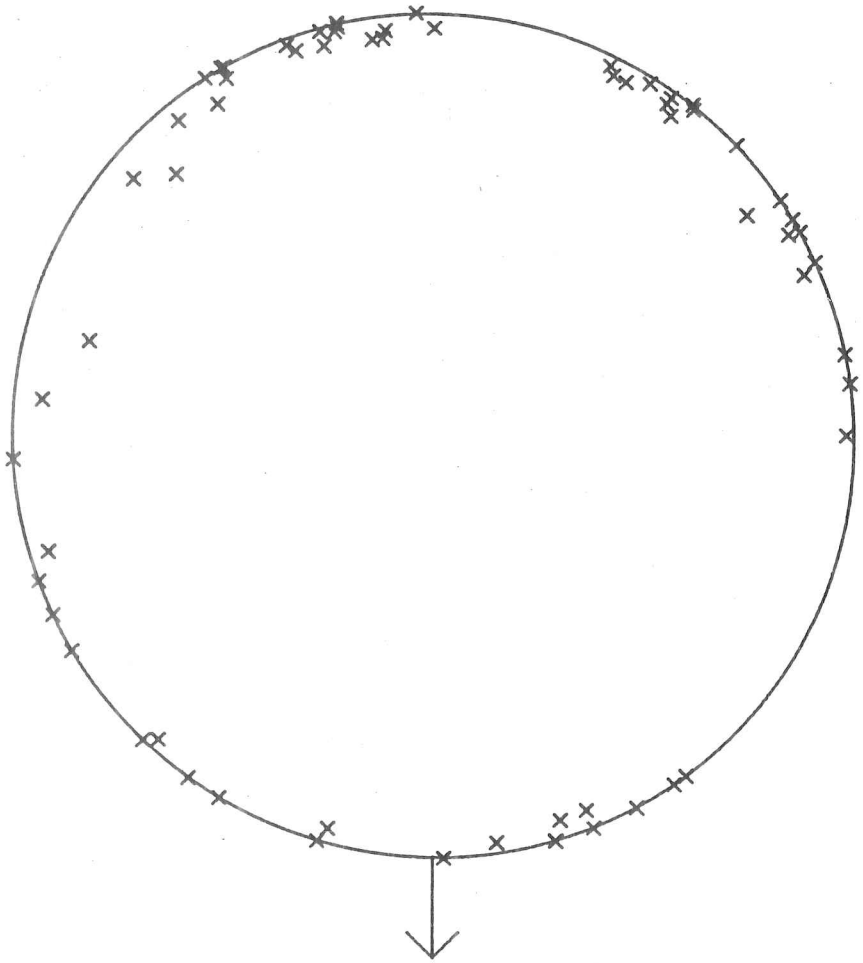

SAMPLE E8-1B-16/17

FIGURE 3.34 (a)

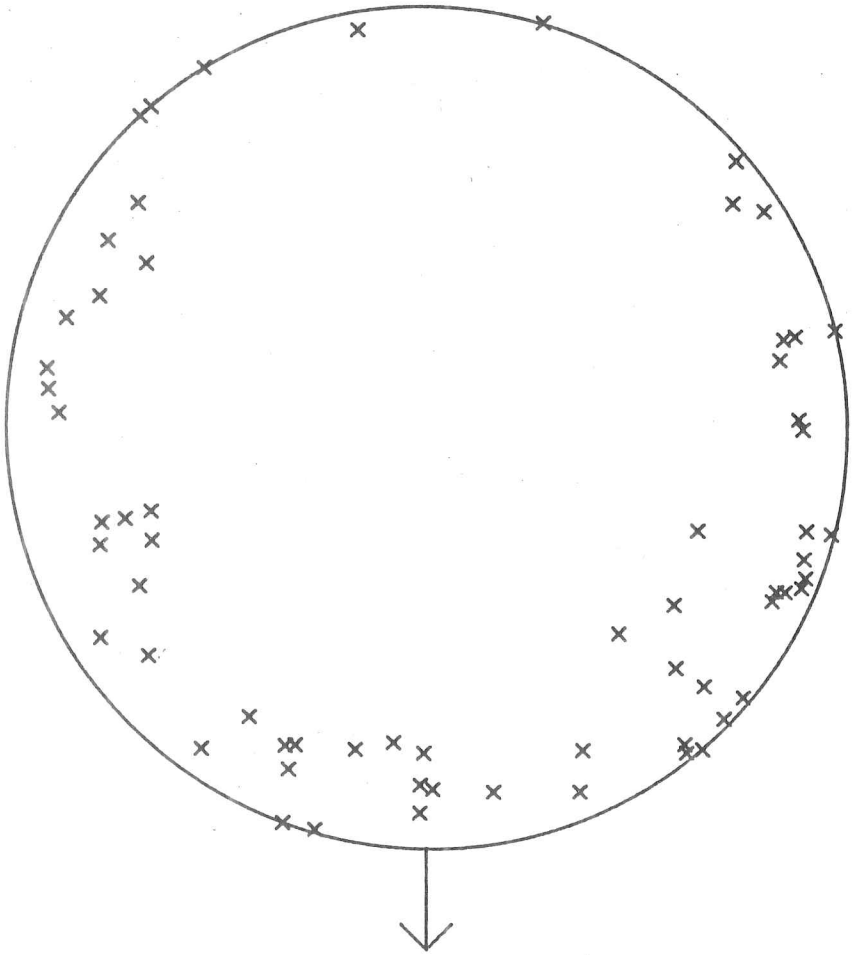

SAMPLE E8-3B- 1/ 2

FIGURE 3.34 (b)

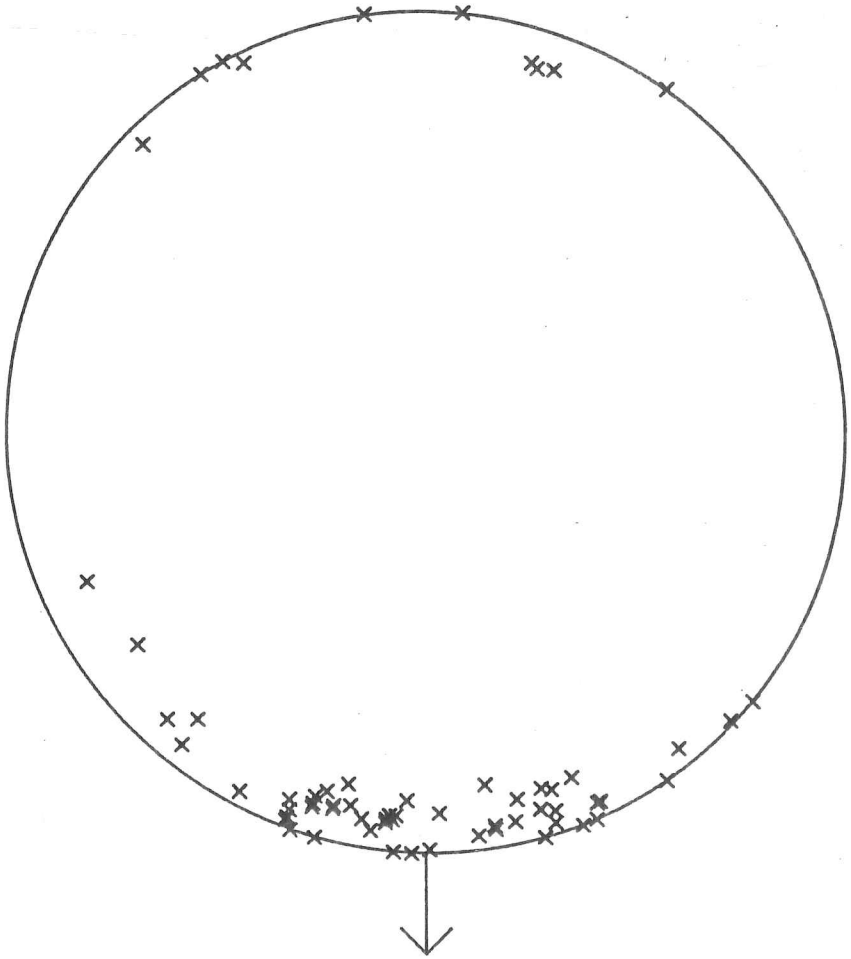

SAMPLE E8-3B-17/18

FIGURE 3.34 (c)

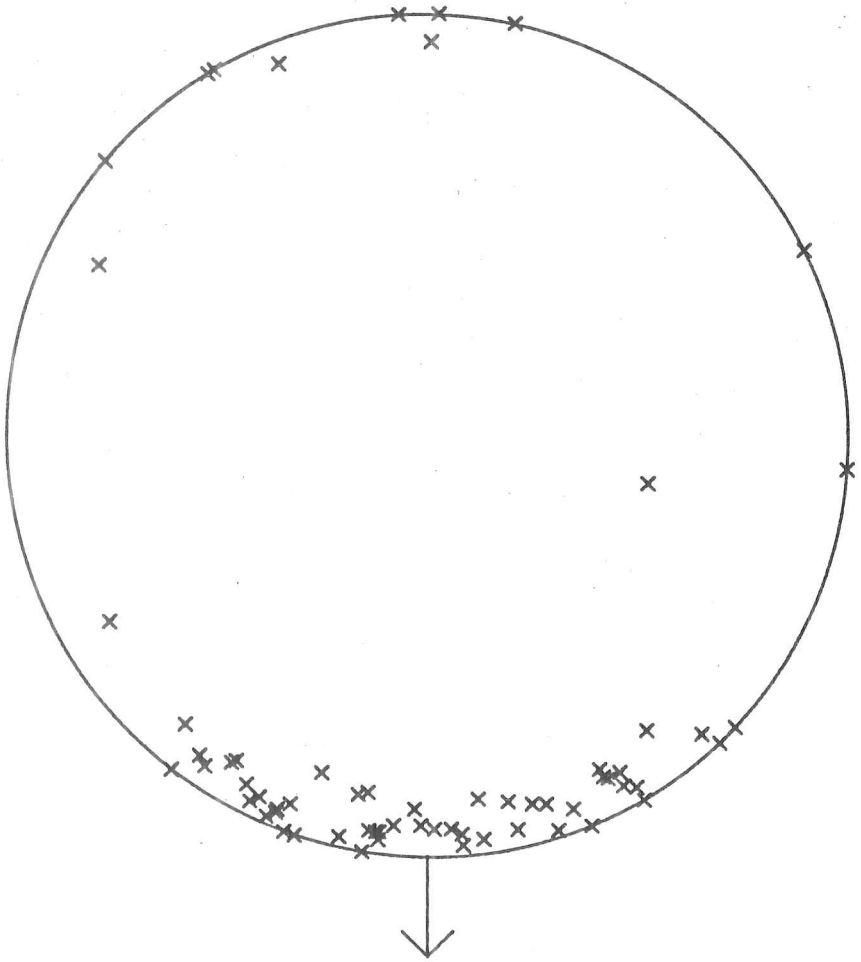

SAMPLE E8-4C-14/15

FIGURE 3.34 (d)

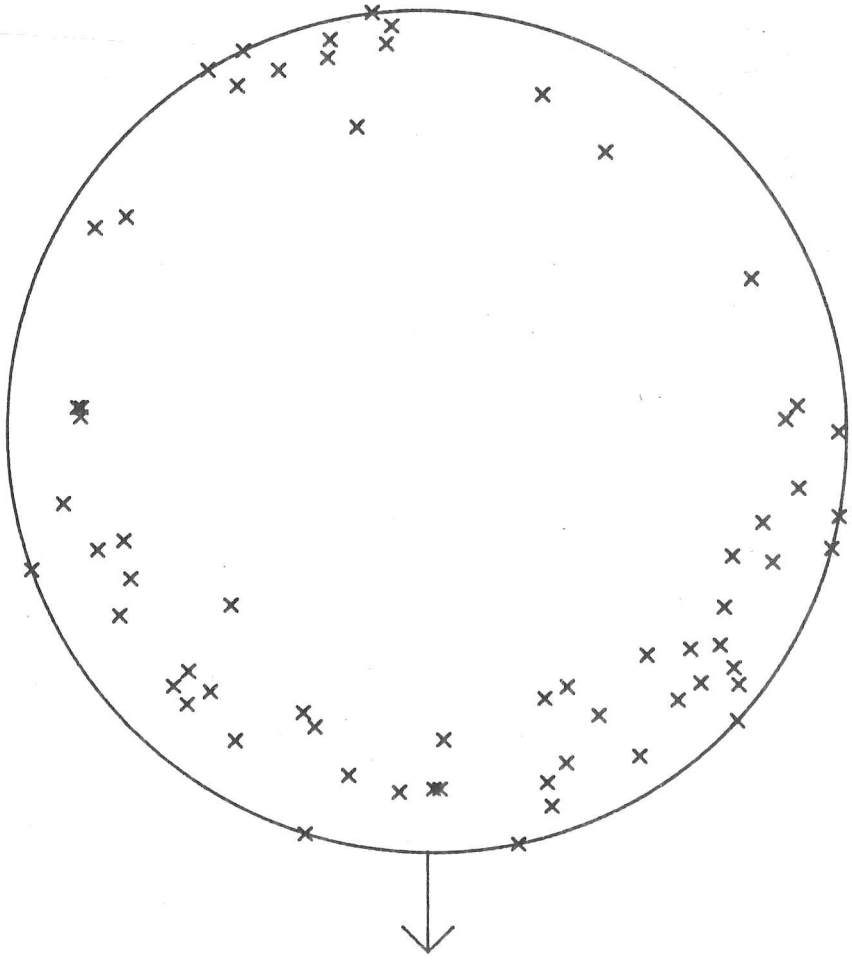

SAMPLE E8-5B- 1/ 2

FIGURE 3.34 (e)

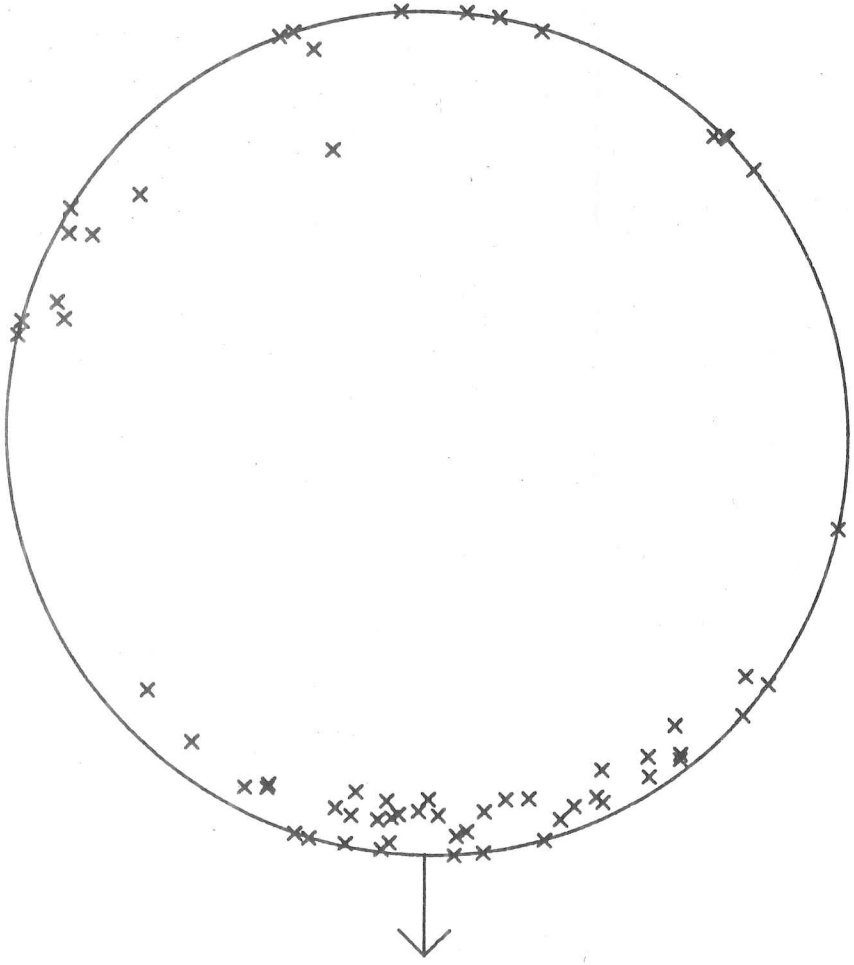

SAMPLE E8-5B- 9/10

FIGURE 3.34 (f)

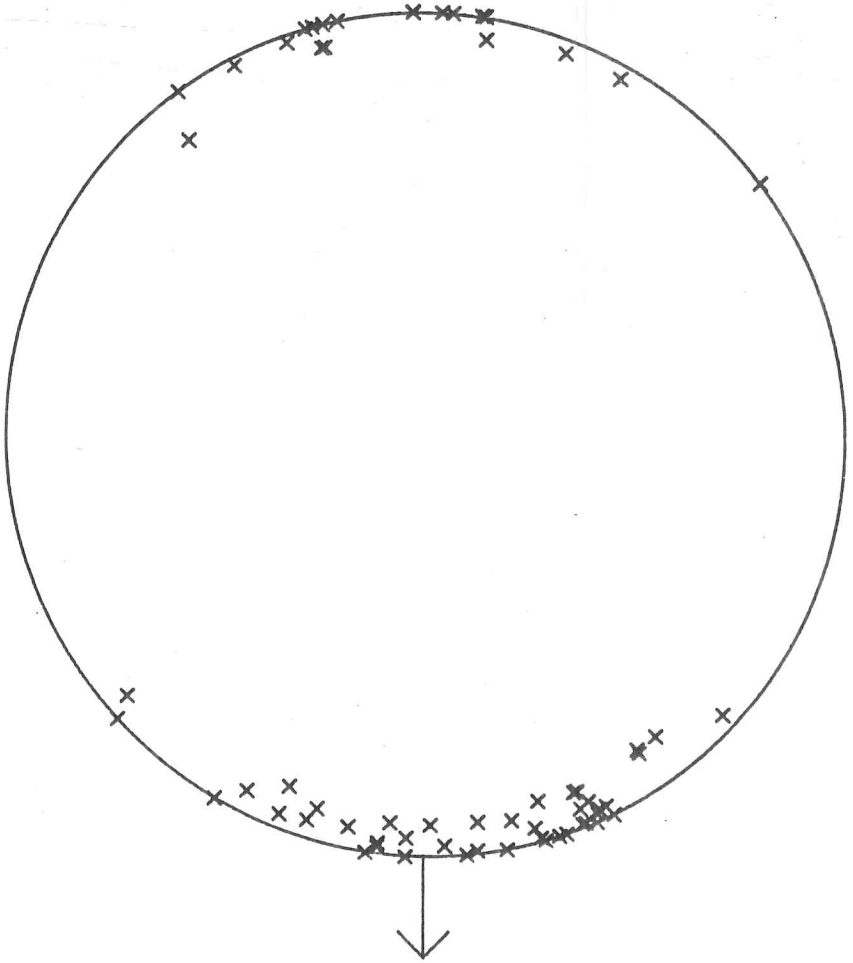

SAMPLE E8-5B-16/17

FIGURE 3.34 (g)

FIGURE 3.35 (a) Horizontal thin section from Run 8 (saline-forced flow) taken 1cm below the ice surface. 1.3xreal size. Current direction from top to bottom of photograph.

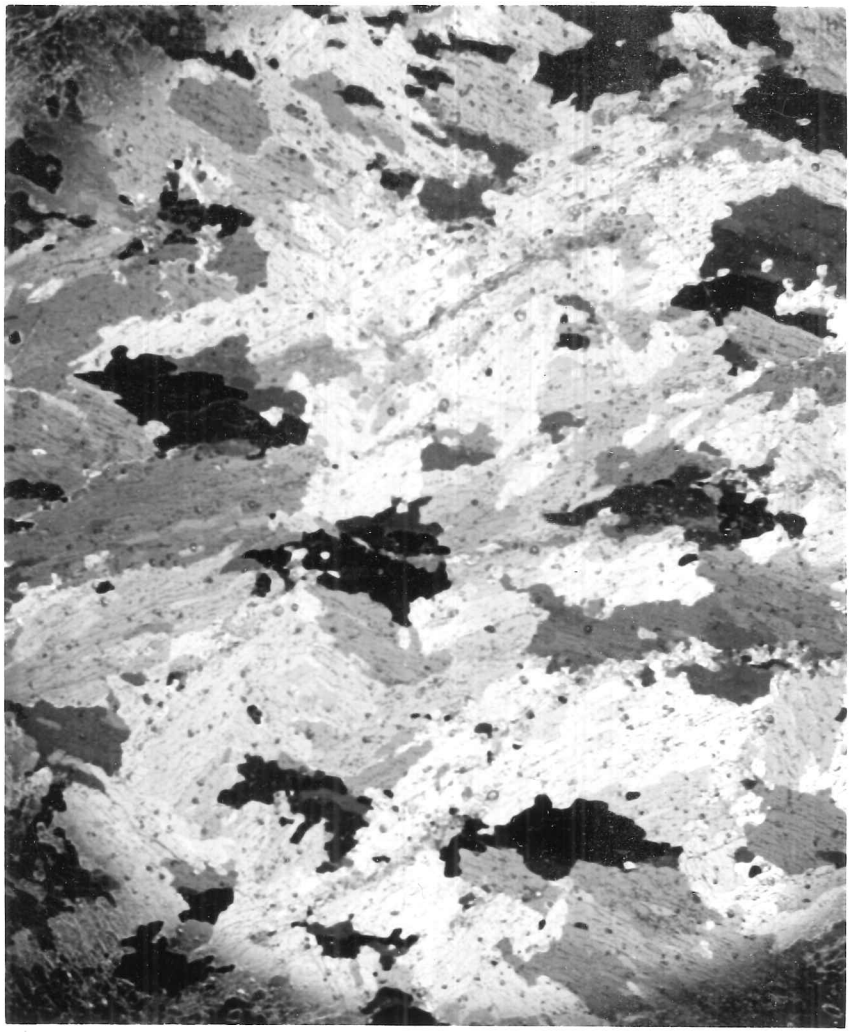

FIGURE 3.35 (b) Horizontal thin section from same location as (a) but taken 9cm beneath the ice surface. 1.3xreal size.

FIGURE 3.35 (c) Horizontal thin section taken 17cm below the ice surface at the same location as (a). Current direction from top to bottom of photograph. Note finer platelet spacing than figure 3.31. 1.5xreal size.

Figure 3.23(d) shows a systematic and rapid increase in the concentration parameter with depth, the axis of alignment being the current direction. The anomalous data point, 1B, was purposefully taken from the leading edge where there was no well-defined direction of flow. It's randomness therefore further supports the interaction between currents and grain orientation. In distinct contrast, figure 3.25(a) and (b) show that there is no correspondence between horizontal temperature gradient and the mean c-axis direction.

3.9 Summary of laboratory experiments

In the present chapter we have described four laboratory experiments to determine the mechanism controlling the alignment of crystal c-axes during the growth of NaCl ice. The apparatus was designed to differentiate between the two most likely mechanisms; lateral heat flow and the fluid motion at the ice-water interface, although we also implicitly test the effects of the earth's magnetic field, horizontally oriented stresses, tilting of the sea ice sheet, and the alignment in the initial skim. Corresponding experiments with and without a current were performed in brackish ($\sim$20‰) and saline ($\sim$30‰) solutions. In the absence of ice growth, flow in the apparatus was laminar but buoyancy-driven convection at the growing ice interface produced a distortion of the velocity profiles, enhancing the laminar to turbulent transition. C-axis distributions were measured optically at a number of locations in each of the experiments. The most important results of these experiments were;

(i) where there was fluid motion the c-axes aligned in the direction of the current and, provided conditions remained constant, the strength of this alignment increased rapidly,

(ii) where direct observation has confirmed there was negligible fluid motion ($<0.1 cms^{-1}$), there was a significant reduction in alignment,

(iii) in the brackish experiment with flow, where a cellular to planar transition occurred. This tests the hypothesis that currents orient the

c-axes since, at the transition point, the rate of increase of the strength of the alignment should tend to zero. This was observed.

(iv) no systematic relationship was found between the horizontal temperature gradient and the mean c-axis of the distribution.

We shall elaborate on many of the features noted during the experiments in the next chapter.

4. INTERPRETATION OF EXPERIMENT

4.1 Introduction

Our experimental results indicate that, in the absence of horizontal stresses and substantial tilting of a slab of sea ice, there is no correlation between the magnitude or direction of the horizontal temperature gradient and the mean c-axis direction. Fluid motion, however, appears to have a profound effect not only on the alignment of crystal c-axes but also on a number of other structural properties of the solidified material. Although there are no reports of unidirectional flow producing a preferred orientation of c-axes in materials other than sea ice, the importance of the motion of the melt in determining grain structure and solute segregation has been recognised (see for example the review by Beeley, 1979). Because there are a number of similarities between the solidification of metals and aqueous solutions many of these studies have been carried out using high concentration brines (for example Cole and Bolling, 1967).

The trapping of liquid droplets and their subsequent migration along a temperature gradient are common to sea ice (see sections 1.6.1 and 1.9.2), metal alloys, some organics (Allen and Hunt, 1979) and doped semiconductors (Bardsley et al, 1980). Likewise chains of small, randomly oriented grains, similar to the spindules which Lake and Lewis (1970) describe as the remnants of brine drainage channels (see section 1.9.2), are also observed in metals where they are termed "freckles" (Giamei and Kear, 1970). They are also attributed to concentration-driven convection and their behaviour (Copley et al, 1970; Kaempffer and Weinberg, 1971) resembles that described for brine drainage channels (section 1.9.2). Indeed, according to the "freckle potential" derived by Copley and others (Copley et al, 1970), sea ice provides the ideal conditions for drainage channel production; that is low temperature gradient and growth velocity,

coupled with low thermal and solute diffusivities in the liquid.

However the limitations of comparisons between materials must be kept clearly in mind. Differences in solidification geometry and Prandtl number, for example, will alter patterns of convection and the relative thicknesses of thermal and viscous boundary layers. [1]

These material-specific characteristics are not restricted to bulk properties. The cells on the interface of a metal alloy are generally rounded and dendritic side-branching often takes place (e.g. Morris and Winegard, 1969). The cells follow the isotherms, which contrasts with the crystallographically-controlled, faceted cells formed by some semiconductors and organics (e.g. Bardsley et al, 1968). An indication of whether a surface has the potential to form facets is given by Jackson's α factor (Woodruff, 1973) which is the product of a material-dependent term [2] and a factor related to the crystallographic face where solidification is taking place. The significance of this factor is that if $\alpha < 2$ the cells on the interface are of the rounded metallic type while facet formation is predicted for $\alpha > 2$.

At present, all that is known of the cell shape in sea ice is that they are elongated perpendicular to the c-axis. We may deduce some further information from α but, unfortunately, the value of material-dependent term of α equals 2.62 for water (Woodruff, 1973) which suggests that ice can and does exhibit both types of behaviour. For growth on the basal plane, that is parallel to the c-axis, $\alpha > 2$, suggesting that the platelets in sea ice are bounded by faceting planes. This is observed in germanium which has a similar value of entropy of melting per mole (that is 3.15). However $\alpha < 2$ for growth perpendicular to the c-axis. and the tips of the cells in sea ice should be rounded.

---

[1] The Prandtl number of metals is of the order of 1, while in our case Pr = 14. In addition, sea ice grains grow downwards into an infinite melt which is quite different from the closed geometry used in the horizontal solidification of metals.

[2] This essentially is the entropy of melting per mole divided by the gas constant.

4.2 The effect of flow of the melt on the properties of a material

The influence of flow has been investigated in metal alloys by the suppression (Cole and Bolling, 1965; 1966; 1967) or enhancement (Cole and Bolling, 1967; 1968) of natural convection. The general results from these studies are that a reduction in the level of motion in the melt favours columnar growth and coarsens the structure. Our experiments are consistent with this observation (compare figure 3.35(c) with 3.31 for forced flow and no forced flow respectively). In metals and high concentration aqueous solutions free convection can be sufficiently strong to shear or melt off the tips of the dendrites (Tiller and O'Hara, 1968). However, at the low solute concentrations and fluid velocities used in our experiments, extensive dendritic shearing does not take place, although there is an increase in the degree of misalignment between platelets during forced flow experiments (see figure 3.35(c)). However, in the ocean, at locations where there are high salinities and fluid velocities, there is no reason why dendritic shearing should not take place and this may be the origin of some of the frazil ice layering in a dynamic sea ice cover.

Dendritic shearing is commonly observed on a very localised scale in sea ice in the vicinity of brine drainage channels (section 1.9.2) where the brine streamers cause remelting and mechanical fracture of the fragile skeletal layer. These channels of solute-rich fluid can also nucleate a mushy layer (M^{c}Donald and Hunt, 1969) which could explain the mushy ice observed under columnar ice in the very shallow lagoons around the Arctic islands (Matthews, personal communication).

4.2.1 The effective segregation coefficent with a flowing melt

In section 1.6.2, solute redistribution during the cellular growth of sea ice from a convecting melt is described, with some success, by equation [1.8]. However since this was formulated for solidification with a planar interface with no fluid motion, we must deduce that the consistency with experimental data was fortunate. In addition, more recent studies on aluminium alloys (Takahashi et al, 1972) has shown that there is no correlation between the δ_c of equation [1.7] and the thickness of the viscous sublayer. Alternatively Takahashi and his collegues (Takahashi

et al, 1972; 1976) find that the effective segregation coefficient, k_{eff}, in the presence of fluid motion, is a function of the fluid velocity, u, and is given by

$$k_{eff} = 1-(1-k_e)(1-S^*)\frac{A\lambda}{h_m}\frac{u}{V} \quad , \qquad [4.1]$$

where k_e is the equilibrium segregation coefficient, V is the growth velocity, A is an experimental constant, h_m is the thickness of the region where the solid fraction is less than 1, λ is the platelet spacing and S^* is the fraction solid at the location where the liquid is trapped by the solid. The values of A and S^* are unknown for sea ice although they have been determined for other materials. The thickness of the skeletal layer may be equated with h_m. The applicability of this equation to solute segregation in sea ice awaits experimental verification.

4.3 Stability of the ice-water interface in the presence of fluid motion

4.3.1 Introduction

In section 3.8.3 we described the transition [3] from a cellular to planar interface which took place during the brackish experiment with forced flow. No such transition was observed during the corresponding experiment without forced flow and it appears that the water motion stabilises the interface morphology. This effect has previously been observed in aqueous solutions (Weeks and Lofgren, 1967; Szekely and Jassal, 1978) and is expected because of the interaction of flow with the temperature and solute gradients ahead of the interface (Cole, 1967 and section 3.5.3). Indeed, this alone may cause the difference in interface response in our experiments.

---

[3] It is important to note that the planar to cellular transition is reversible (Morris and Winegard, 1969) and that theories derived for the onset of instability also apply to the cellular to planar transition.

The onset and magnitude of constitutional supercooling in a stirred melt has been formulated theoretically by Hurle (1961) and has received experimental verification for germanium alloys (Bardsley et al, 1961). Bardsley, and independently Hunt and collegues (Hunt et al, 1968), have established that the critical gradient of constitutional supercooling is small or zero at the transition from a planar to cellular interface. Hurle (1969) and Coriell and others (1976) have extended the morphological stability theory of Mullins and Sekerka to the case where the fluid motion imposes a finite boundary layer on the conditions in the melt. This predicts that for a given material with a fixed growth velocity, and interfacial gradients of temperature and concentration, stirring enhances the planar to cellular transition. Under the same conditions, the stability theory of Delves (1968; 1971; 1974) arrives at the contradictory prediction that, for a material such as ice, the interface is strongly stabilised by stirring. This discrepancy may be solely due to the differences in the model of the fluid boundary layer; Coriell has assumed there is a diffusive zone close to the interface and complete mixing outside this, while Delves has used a parabolic velocity profile.

An interaction has also been found between the convection cells due to hydrodynamic instability, and the cells due to morphological instability of the interface (Hamalainen, 1967). Coriell and others (1980) have tackled this immensely complex problem numerically.

4.3.2 Comparison of experiment with theory of Delves

We compare the predictions of Delves with the cellular to planar transition in Run 5, since his model of the boundary layer in the fluid close to the interface is similar to that in the experiment. Delves (1971) has formulated approximations for ice, each of which is applicable in one of four different wavelength regions. The bounds of these zones are determined by the mechanisms transporting momentum, heat and solute, and are thus dependent on the thickness of the Blasius boundary layer which is itself a function of the distance downstream, x, from the entrance of the test section. Figure 4.1 shows these zones of approximation and the dominant transport mechanisms in each of the regions for the fluid velocity, $u_\infty = 3.4 cms^{-1}$, used during Run 5. Platelet spacings have been

REGIONS OF APPROXIMATIONS FOR STABILITY CONDITIONS.

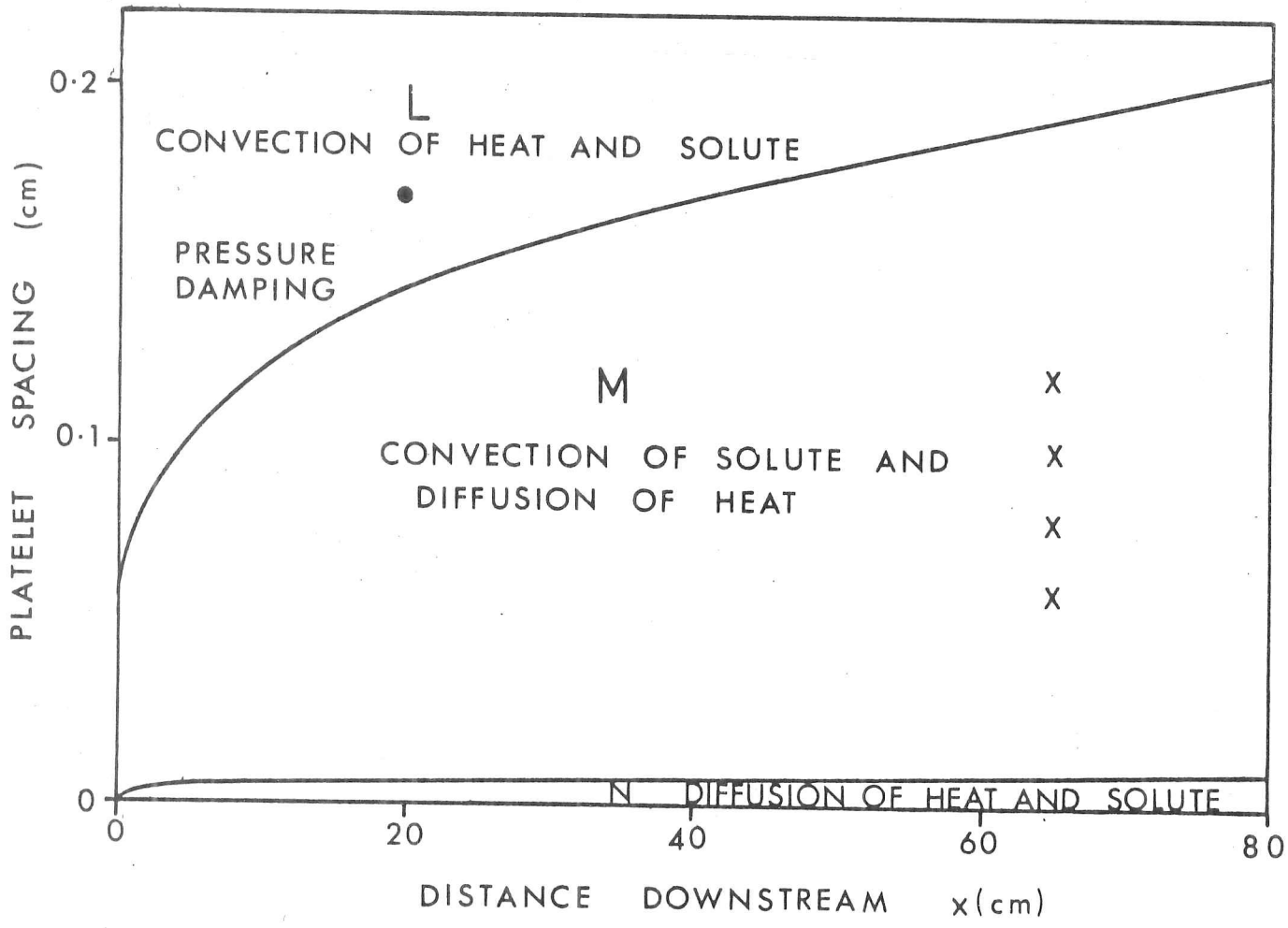

FIGURE 4.1

The onset and magnitude of constitutional supercooling in a stirred melt has been formulated theoretically by Hurle (1961) and has received experimental verification for germanium alloys (Bardsley et al, 1961). Bardsley, and independently Hunt and collegues (Hunt et al, 1968), have established that the critical gradient of constitutional supercooling is small or zero at the transition from a planar to cellular interface. Hurle (1969) and Coriell and others (1976) have extended the morphological stability theory of Mullins and Sekerka to the case where the fluid motion imposes a finite boundary layer on the conditions in the melt. This predicts that for a given material with a fixed growth velocity, and interfacial gradients of temperature and concentration, stirring enhances the planar to cellular transition. Under the same conditions, the stability theory of Delves (1968; 1971; 1974) arrives at the contradictory prediction that, for a material such as ice, the interface is strongly stabilised by stirring. This discrepancy may be solely due to the differences in the model of the fluid boundary layer; Coriell has assumed there is a diffusive zone close to the interface and complete mixing outside this, while Delves has used a parabolic velocity profile.

An interaction has also been found between the convection cells due to hydrodynamic instability, and the cells due to morphological instability of the interface (Hamalainen, 1967). Coriell and others (1980) have tackled this immensely complex problem numerically.

4.3.2 Comparison of experiment with theory of Delves

We compare the predictions of Delves with the cellular to planar transition in Run 5, since his model of the boundary layer in the fluid close to the interface is similar to that in the experiment. Delves (1971) has formulated approximations for ice, each of which is applicable in one of four different wavelength regions. The bounds of these zones are determined by the mechanisms transporting momentum, heat and solute, and are thus dependent on the thickness of the Blasius boundary layer which is itself a function of the distance downstream, x, from the entrance of the test section. Figure 4.1 shows these zones of approximation and the dominant transport mechanisms in each of the regions for the fluid velocity, $u_\infty = 3.4 cms^{-1}$, used during Run 5. Platelet spacings have been

REGIONS OF APPROXIMATIONS FOR STABILITY CONDITIONS.

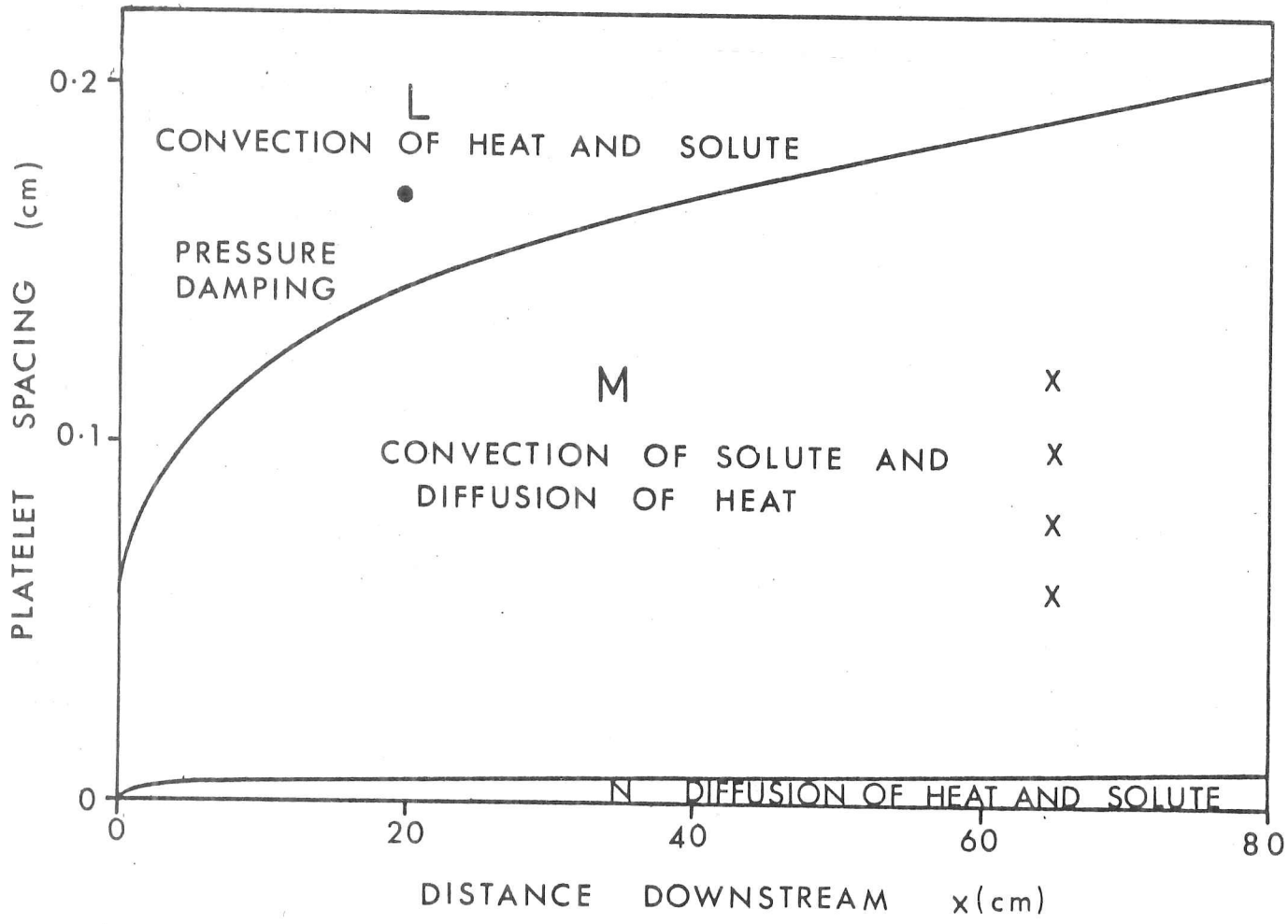

FIGURE 4.1

estimated to within ±30% at various depths in the ice at two locations and we find that stability is generally determined by the convection of solute and the diffusion of heat (Region M in the terminology of Delves).

Delves (1971) gives a lengthy expression for the stability criterion in Region M which, for the H_2O-NaCl system of the salinity and fluid velocity in our experiment, varies with temperature gradient in the liquid and solid, growth velocity, platelet spacing and distance from the leading edge. The vertical temperature gradient in the fluid was measured towards the end of the experiment and is assumed constant. The vertical temperature gradient in the solid and the growth velocity are related through equation [3.5] and the curve separating regions of stability and instability is therefore a function of λ and V at a given distance x.

Figure 4.2 shows these curves at various x along with the growth velocity at which transition [4] occurs in the experiment. At x = 65cm the general trend of the platelet spacings as a function of growth velocity is also given. In horizontal section there was a gradual change from the fine platelet spacings of the elongated cellular structure (see figure 3.20(a)) to coarser, irregular features (figure 3.20(b)). The width of the latter features has been measured as the "platelet spacing" in the NO CELLS region.

Theory and experiment qualitatively agree that the growth velocity at which transition takes place decreases with distance from the leading edge. We have already discussed the increased mixing in the region of x = 20cm which will cause the observed transition to occur at a higher V than predicted by theory. In addition, at x = 65cm, the value of V at the point where the observed platelet spacing curve crosses the stability

---

[4] James (1966) has described the sequence of events in a cellular to planar transition, from a well-developed cellular structure to the final disappearence of the undulations on the interface. In our experiments, the change in the slope of the salinity profile and in the rate of increase of c-axis alignment will respond to the start of this deterioration. The transition point defined in this way is given in section 3.8.3. However the theory of Delves predicts the disappearence of the undulations which is the final stage in the deterioration and we must redefine the transition point. In this case, it is taken as the maximum depth at which macrosegregation is observed in thick section photographs.

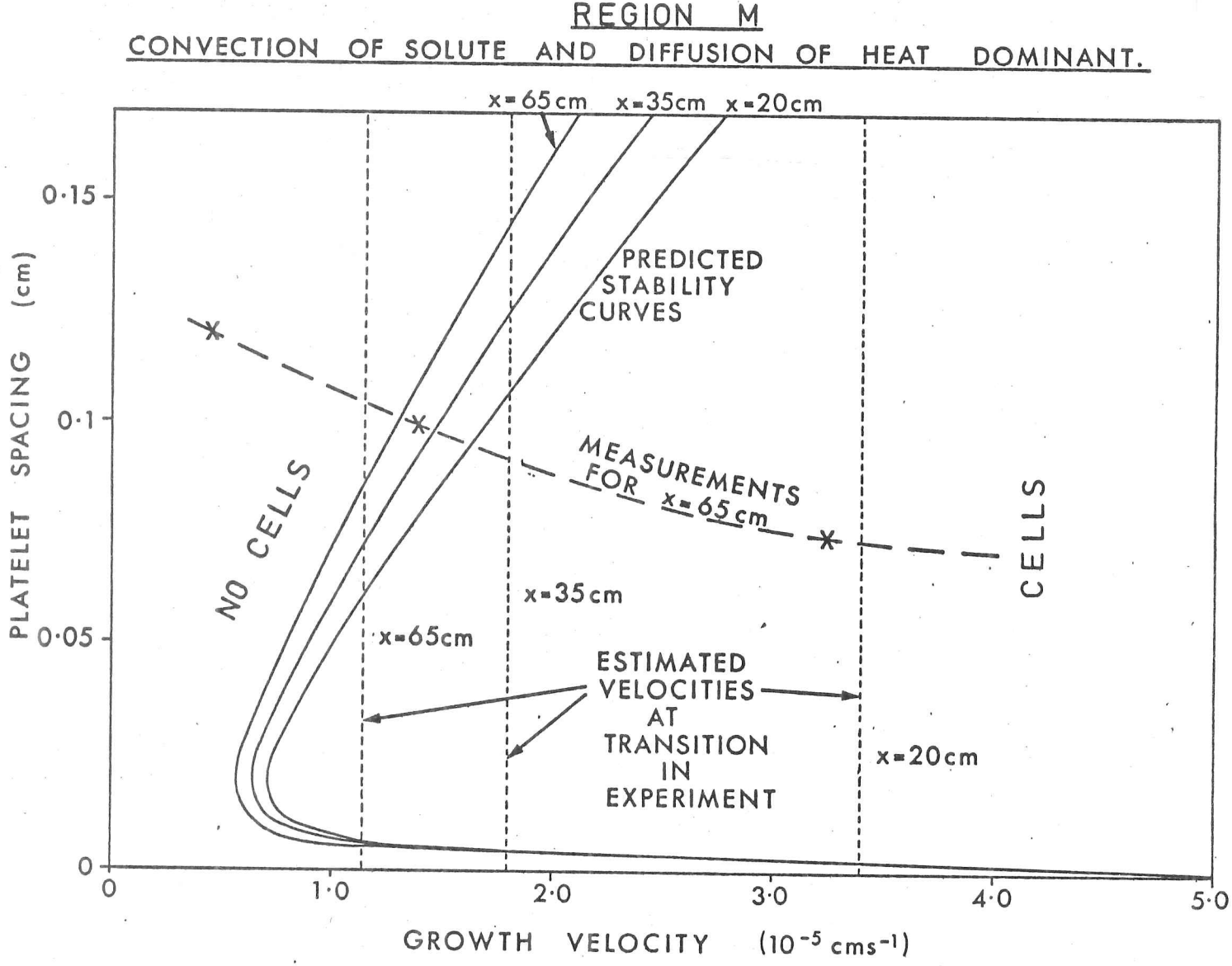

FIGURE 4.2 Comparison of data from our experiment (shown by dotted lines) with the theory of Delves (shown by solid lines) for 3 values of downstream coordinate x.

curve is the predicted critical growth velocity. This is surprisingly close to the experimentally determined value of V. We may conclude that the theory of Delves is a reasonable description of stability in the presence of the hydrodynamic boundary layer in our experiment.

Finally, Delves (1974) points out that the stabilising influence of the current acts only on these perturbations with their wave vector in the direction of the current, that is with the c-axis in the direction of the current. An anisotropy in response at the onset of cellular growth has been noticed by Bardsley (Bardsley et al, 1968) who found the wavelengths of the 2D cells were smaller when the wave vector and current were aligned.

4.4 Modification of cell spacing by flow

Two theories predicting cell spacing in a purely diffusive regime (Bolling and Tiller, 1960; Rohatgi and Adams, 1967) have been applied to NaCl ice (section 1.8). The lack of satisfactory agreement was attributed to the effects of convection (Lofgren and Weeks, 1969) but more recent derivations have not improved on this omission (Donaghey and Tiller, 1968; Hunt, 1979). There have been no decisive experiments to choose between these theories of platelet spacing.

Morphological stability theory can be used to calculate platelet spacing of the wavelength, λ, of the most rapidly growing perturbation is computed (Sekerka, 1968). Thus the stability theories of section 4.3.1 can be extended to provide an expression for the wavelength in the presence of a stirred melt. Assuming that the most rapidly growing λ is that which first becomes unstable, Coriell and others (1976) give the following approximate expression for the cell spacing in a stirred melt

$$\lambda = 2\pi \{(\frac{k_e}{4T_e \Gamma D}).(\frac{K_s G_{si} + K_l G_{li}}{K_s + K_l}).V\}^{-1/3} \quad , \qquad [4.2]$$

where T_e is the equilibrium freezing point, K_s and K_l are the thermal conductivities of the solid and the liquid, G_{si} and G_{li} are the vertical temperature gradients in the solid and liquid, D is the solute diffusivity and Γ is called the capillarity constant and is related to the ice-water

surface energy. We have fitted this equation to the data of Lofgren and Weeks (1969) and although a least squares fit yields V to the power of -1/3.14, the weighted mean of the temperature gradients in the solid and the liquid is found to be two orders of magnitude greater than the value that would be expected for Lofgren and Weeks experiment. Numerical solutions for the growth of a single dendrite in a flow (Cantor and Vogel, 1977) predict a reduction in cell or dendrite tip radius but it is important to realise that although this particular feature may be characteristic of an array of cells, a single dendrite is not a good approximation to a cellular interface. Experimentally, Takahashi (1981) observes that the dendrite spacing in steel decreases with increasing flow in the melt but he does not take into account the other parameters which are known to influence this spacing.

Our saline experiments also display an apparent decrease in cell spacing with an increase in fluid motion (compare figure 3.31 from the no forced flow experiment with figure 3.35(c) from the corresponding forced flow experiment) However, we must extract the dependence on other growth parameters before we can comment on this effect. We therefore use equation [1.13] which predicts

$$\lambda^2 G_{1i} V = 8D\Delta T(max) = 8mD\Delta C(max) \qquad [4.3]$$

where m is the slope of the liquidus. For metals, it is accepted that the undercooling in the intercellular grooves, ΔT, is very small and that the cell spacing adjusts to maintain this criterion (Flemings, 1974). For a constant concentration and no mixing, this supercooling is constant and the left hand side of equation [4.3] is constant. Expressions of the form of equation [4.3] have been successfully used to correlate cell spacing data in metals (Flemings, 1974).

The vertical temperature gradient in the liquid at the interface, G_{1i}, has been measured for Run 8 (forced flow experiment) but not for Run 7 (no forced flow). However, close to the interface in the region where the conduction of heat dominates convection

$$q=K_1 G_{1i} \qquad [4.4]$$

Using the convective heat flux from the liquid to the solid, q, from Table 3.2 we find that

$$G_{li}(\text{Run 7}) \sim 0.5^{o}\text{Ccm}^{-1} \text{ calculated}$$

$$G_{li}(\text{Run 8}) \sim 1.4^{o}\text{Ccm}^{-1} \text{ calculated}$$

$$G_{li}(\text{Run 8}) \sim 1.3^{o}\text{Ccm}^{-1} \text{ measured}$$

There is reasonable agreement between calculated and measured G_{li} for Run 8. We have measured platelet spacings for two thin sections and the corresponding growth velocities from figure 3.6 are

Run 7 $\lambda = 0.049\text{cm}$ standard deviation = 0.005cm

$V = 1.8\text{x}10^{-5}\text{cms}^{-1}$

Run 8 $\lambda = 0.034\text{cm}$ standard deviation = 0.003cm

$V = 1.2\text{x}10^{-5}\text{cms}^{-1}$

Inserting the data for Run 8 in equation [4.3] gives

$$m\Delta C = \Delta T \sim 6\text{x}10^{-4}{}^{o}\text{C}.$$

and thus $\Delta C \sim 11\text{x}10^{-3}$‰. If we postulate that mixing does not influence the constitutional supercooling or the solute diffusivity between the cells, then the left hand side of equation [4.3] for Run 8 equals that for Run 7. This is true within the standard deviation of the measured platelet spacing. Thus, in our experiment, the fluid motion either does not influence cell spacing, or it modifies the solute gradient, G_{li}/m, in the liquid close to the interface. That is, increased fluid motion lowers the concentration at the lower boundary, while the concentration deep in the intercellular groove is unaffected by the flow.

An interesting observation of the dependence of cell size and shape on fluid motion has been reported by Bardsley and others (Bardsley et al, 1968) for a germanium alloy immediately after the establishment of a cellular interface. They noticed that the cellular wavelength for a flow normal to the elongated direction of the 2-dimensional cells was approximately four times smaller than the values with fluid motion parallel to the elongation. According to the present model this suggests that mixing around the interface was greater when the current vector was

normal to the long axis of the cells, which is intuitively reasonable.

4.5 Flow around the cells

It is believed that the interaction of the fluid motion with the solute transport from the interface is responsible for the enhancement in the growth velocity of grains with the c-axis parallel to the current. However it is important to note that that, although the limiting boundary process is the rate of solute diffusion over the diffusive boundary layer, the process controlling the overall growth rate of the ice is the conduction of heat in the solid. This has been demonstrated in section 3.6 where a heat conduction model was fitted to our data with reasonable success. We are thus seeking a second-order disturbance in the growth velocity.

In the subsequent discussion we restrict ourselves to a qualitative rather than a quantitive description of the fluid dynamics, aiming to indicate the possible flow and solute transport regimes. Where possible we roughly assign numbers to the range of validity of each of these. We ignore buoyancy effects, which is justified if the ratio of the distance below the ice-water interface to the Monin-Obukhov length (see equation [2.5]) is less than 0.03 (Turner, 1973); that is, if the growth velocity is of the order of 10^{-5}cms^{-1}, then the friction velocity, u_*, must be greater than 0.07cms^{-1}.

Flow in the ocean is generally turbulent and the interaction of the flow with the roughness at the interface is described by the roughness Reynolds number, (see equation [2.4]). To use equation [2.4] we must know the depth of penetration of the flow between the cells. In metal alloys, this washing depth is only a small portion of the total thickness of the solid-liquid zone (Stewart and Weinberg, 1972; Takahashi et al, 1976), the fraction solid at the limit of penetration of flow being 12 to 22% (Stewart and Weinberg, 1972). Alternatively, Takahashi and others (Takahashi et al, 1972) have shown that the flow mixes to a depth approximately equal to the primary dendrite spacing, that is 0.7λ. Using the platelet spacing, λ, as the depth of penetration of fluid motion, figure 4.3 shows that for reasonable values of λ and u_*, the flow under a

normal to the long axis of the cells, which is intuitively reasonable.

4.5 Flow around the cells

It is believed that the interaction of the fluid motion with the solute transport from the interface is responsible for the enhancement in the growth velocity of grains with the c-axis parallel to the current. However it is important to note that that, although the limiting boundary process is the rate of solute diffusion over the diffusive boundary layer, the process controlling the overall growth rate of the ice is the conduction of heat in the solid. This has been demonstrated in section 3.6 where a heat conduction model was fitted to our data with reasonable success. We are thus seeking a second-order disturbance in the growth velocity.

In the subsequent discussion we restrict ourselves to a qualitative rather than a quantitive description of the fluid dynamics, aiming to indicate the possible flow and solute transport regimes. Where possible we roughly assign numbers to the range of validity of each of these. We ignore buoyancy effects, which is justified if the ratio of the distance below the ice-water interface to the Monin-Obukhov length (see equation [2.5]) is less than 0.03 (Turner, 1973); that is, if the growth velocity is of the order of 10^{-5}cms^{-1}, then the friction velocity, u_*, must be greater than 0.07cms^{-1}.

Flow in the ocean is generally turbulent and the interaction of the flow with the roughness at the interface is described by the roughness Reynolds number, (see equation [2.4]). To use equation [2.4] we must know the depth of penetration of the flow between the cells. In metal alloys, this washing depth is only a small portion of the total thickness of the solid-liquid zone (Stewart and Weinberg, 1972; Takahashi *et al*, 1976), the fraction solid at the limit of penetration of flow being 12 to 22% (Stewart and Weinberg, 1972). Alternatively, Takahashi and others (Takahashi *et al*, 1972) have shown that the flow mixes to a depth approximately equal to the primary dendrite spacing, that is 0.7λ. Using the platelet spacing, λ, as the depth of penetration of fluid motion, figure 4.3 shows that for reasonable values of λ and u_*, the flow under a

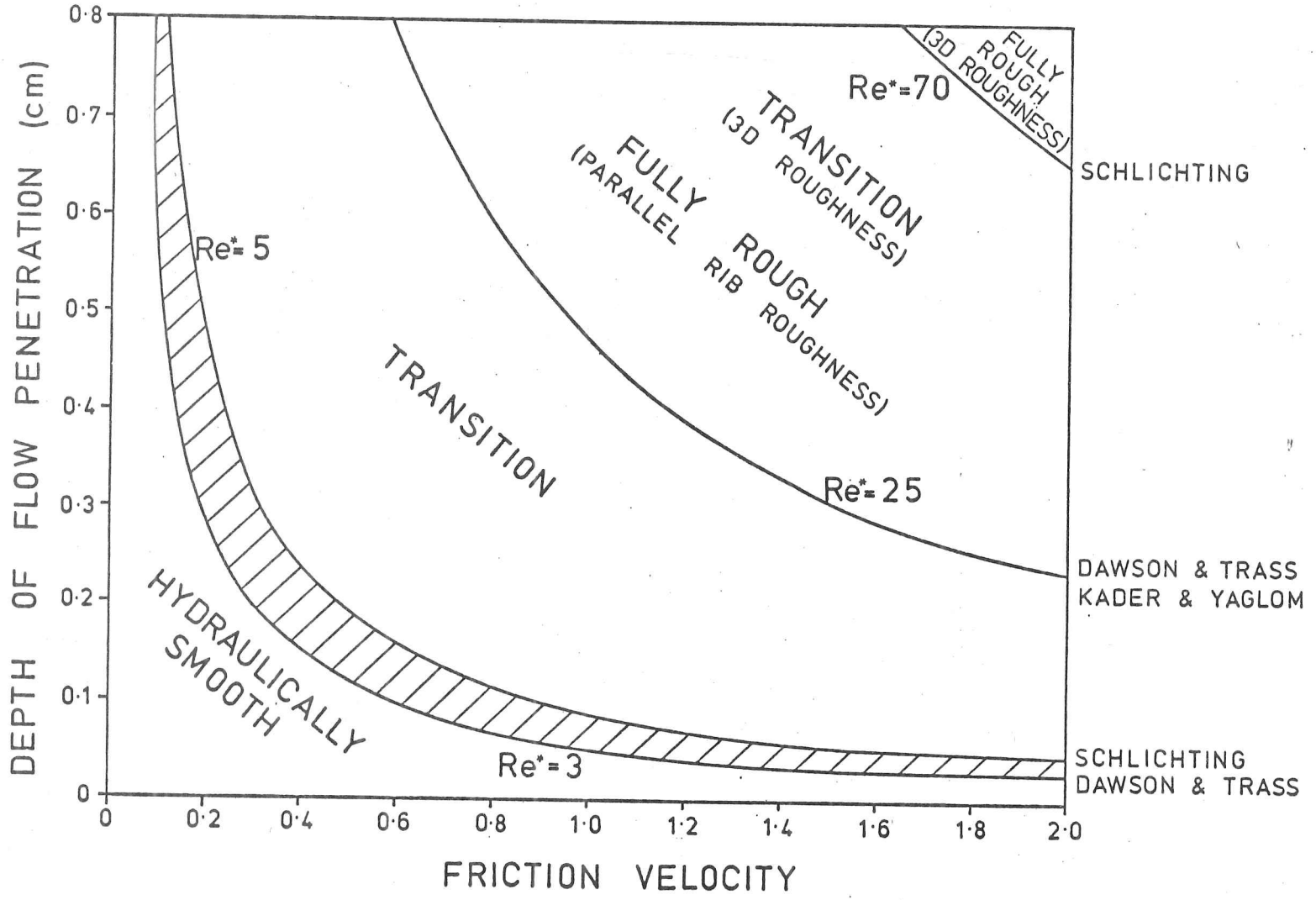

FIGURE 4.3 Diagram showing the flow regime at the skeletal ice-water interface as a function of the friction velocity and the washing depth between the cells.

flat sheet of sea ice generally lies in the hydraulically smooth regime and that the cellular interface is immersed in the viscous sublayer. As an approximation to the situation we have performed an experiment in a laminar flume.

4.5.1 Experiments in a laminar flume

The aim of this simple experiment was to visualise the flow around the cells in sea ice, using a plastic model of the interface (approximately 20x real size). Fluctuating velocity components were absent from this flume, which was kindly made available by Dr. Hunt, Department of Engineering, University of Cambridge. The fluid velocity at the tips was measured by timing the passage of dye over a number of cells.

In order to compare this experiment with data from other sources, we must find Re^*. The friction velocity is defined in equation [2.3], where for a laminar boundary layer

$$u_*^2 = \frac{\sigma^*}{\rho_1} = \left(\nu \frac{\partial u}{\partial z}\right)\Big|_{z \sim 0} \qquad [4.5]$$

σ^* is the fluid shearing stress at the wall, ρ_1 is the fluid density, and ν is the viscosity. Close to the boundary, a linear velocity profile is a good approximation and assuming that the depth of penetration of flow is some fraction, a_1, of the platelet spacing, λ, then at $z = a_1 \lambda$, $u = u_{tip}$ and

$$Re^* = \left(\frac{a_1 \lambda u_{tip}}{\nu}\right)^{\frac{1}{2}} . \qquad [4.6]$$

The general features of this flow visualisation experiment are;

(i) for $Re^* > 5$, eddies curled around the cells when the current was perpendicular to the cell ridges, but no eddies were observed with the flow and ridges aligned (see figure 4.4(a) and (b)),

(ii) the fluid was observed to decelerate on the upstream side of a cell, descend into the groove, and then return upwards on the downstream side (figure 4.4(c)),

(iii) as the roughness Reynolds number decreased below about 5, the eddies no longer penetrate the intercellular grooves and the fluid follows the streamlines which surmount the cells as shown in figure 4.5(a),

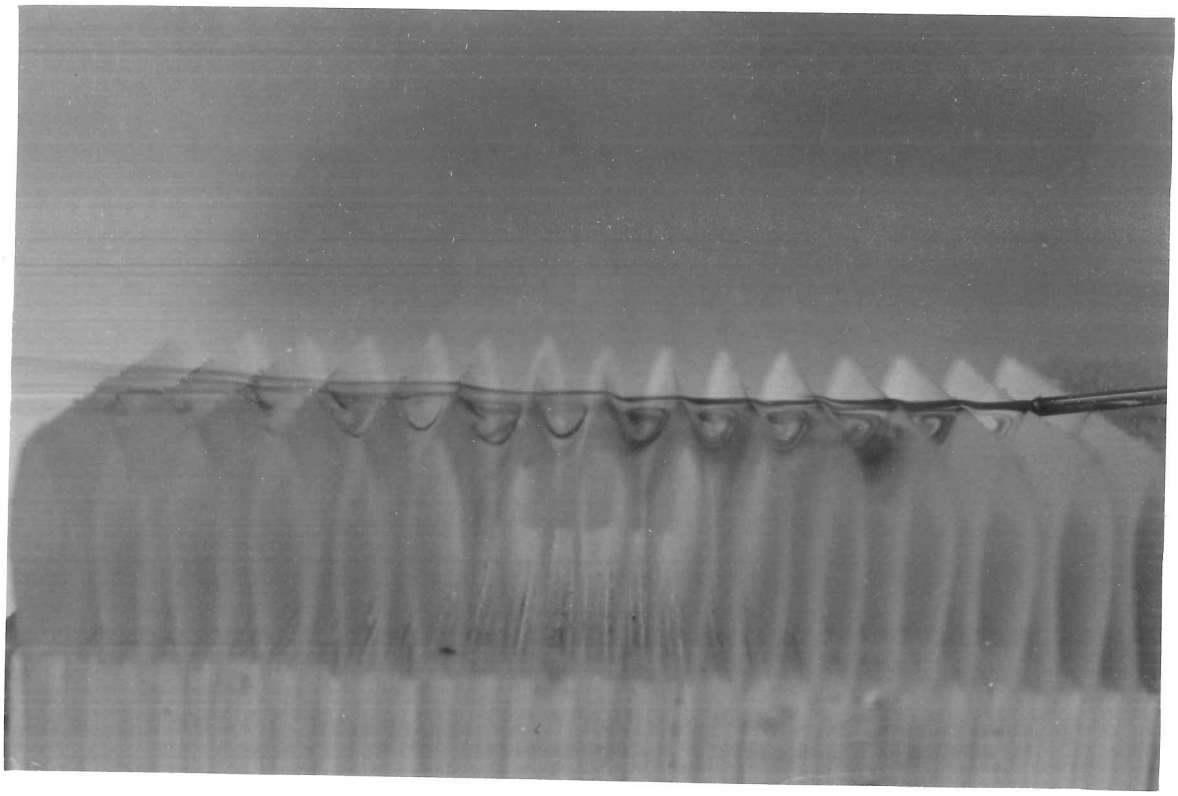

FIGURE 4.4 (a) Photograph showing eddies curling round the ice-water interface when the flow was perpendicular to the long axis of the cells. Roughness Reynolds number just greater than 5.

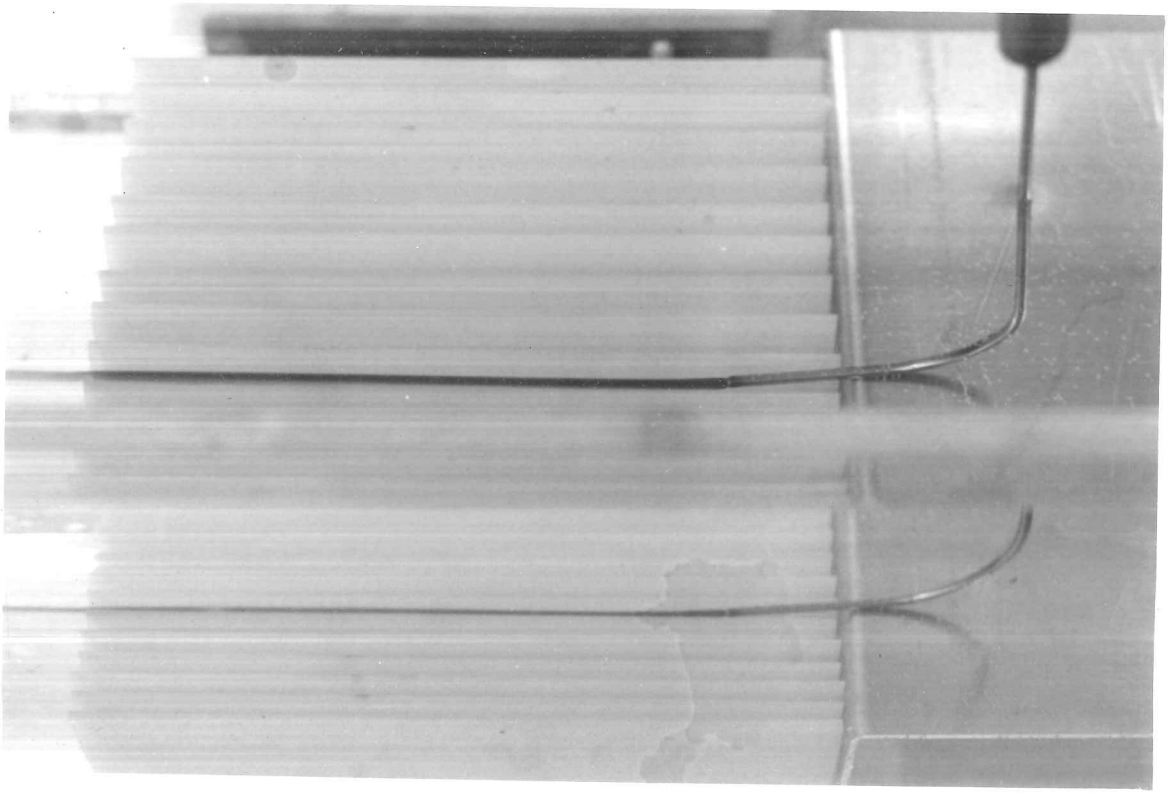

FIGURE 4.4 (b) Photograph showing the flow parallel to the long axis of the cells. Roughness Reynolds number just greater than 5.

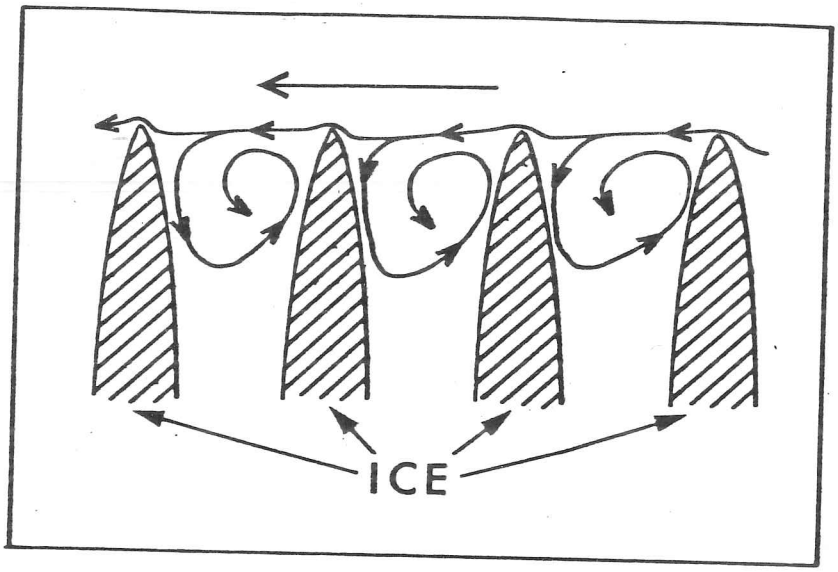

FIGURE 4.4 (c) Schematic diagram showing the flowlines of the eddies, traced by dye in figure 4.4(a). This has been constructed from observations in the flume.

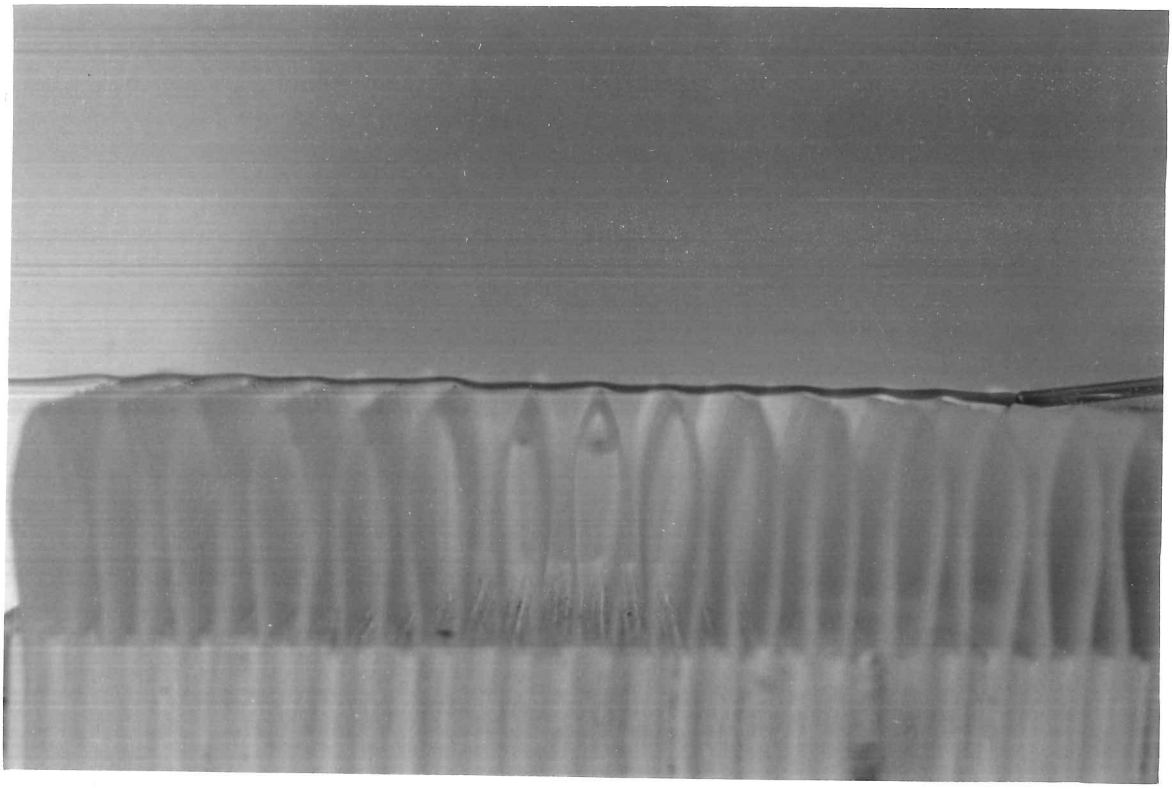

FIGURE 4.5 (a) Photograph showing flow perpendicular to the long axis of the cells over the model of the ice-water interface. Roughness Reynolds number just less than 5.

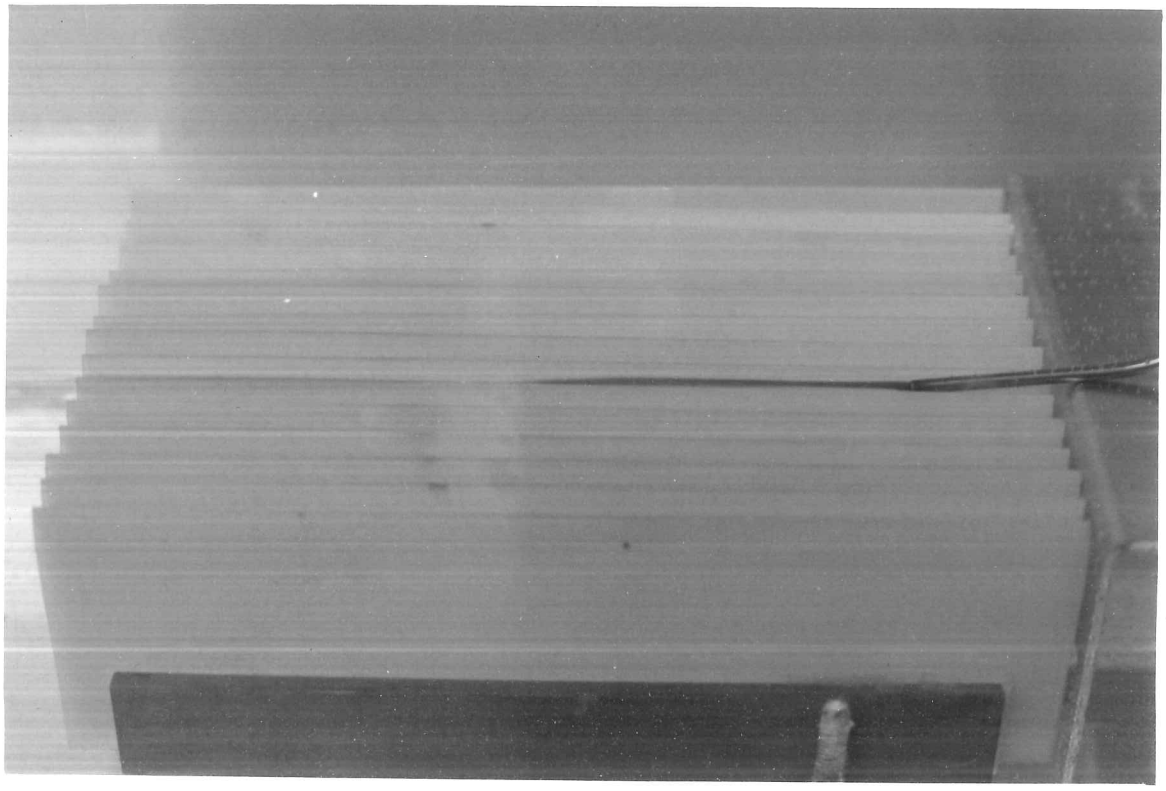

FIGURE 4.5 (b) Photograph showing flow parallel to the long axis of the cells at a Roughness Reynolds number just less than 5.

(iv) any small disturbance in the fluid greatly increased the potential for eddy formation,

(v) at the Reynolds numbers used in the experiment, the eddies do not mix the fluid well,

(vi) when eddies are formed the motion penetrates to a depth such that $a_1 \sim 0.6$.

From these experiments we may conclude that the flow in the intercellular regions in sea ice is generally not vigorous since, in the field, Re^* is almost always less than 5. Thus we must concentrate on the flow in the hydraulically smooth regime and regimes A, B, and C, discussed below, all lie in this region. We follow Yaglom and Kader (1974) in imagining that the eddy transport coefficients decrease rapidly towards the boundary, although we are not concerned with their dependence on z and u. Regimes A to D are defined by the relative magnitudes of these eddy coefficients, e_c and e_ν, and the corresponding molecular transport quantities, D and ν.

4.5.2 Regime A: Nusselt number $\sim$ 1 and no mixing

Figure 4.6(a) shows the relative magnitudes of the diffusive and viscous boundary layers, δ_ν and δ_c respectively, and the roughness. In this region the flow is so slow that the effects of solute diffusion are as important as convection. We estimate that this occurs when $Re^* < 0.01$. Of the four regimes shown in figure 4.6, this seems the least likely to produce a difference in the transport of solute and hence a difference in growth velocity, between the cell tips of grains with c-axes parallel and perpendicular to the current direction. We have, therefore, carried out a calculation to show that a small difference in concentration at the cell tip does, in fact, exist.

Assuming that diffusion in the x direction is negligible, the equation to be solved is

$$u_x \frac{\partial C}{\partial x} + (u_z - V)\frac{\partial C}{\partial z} = D\frac{\partial^2 C}{\partial z^2} \qquad [4.7]$$

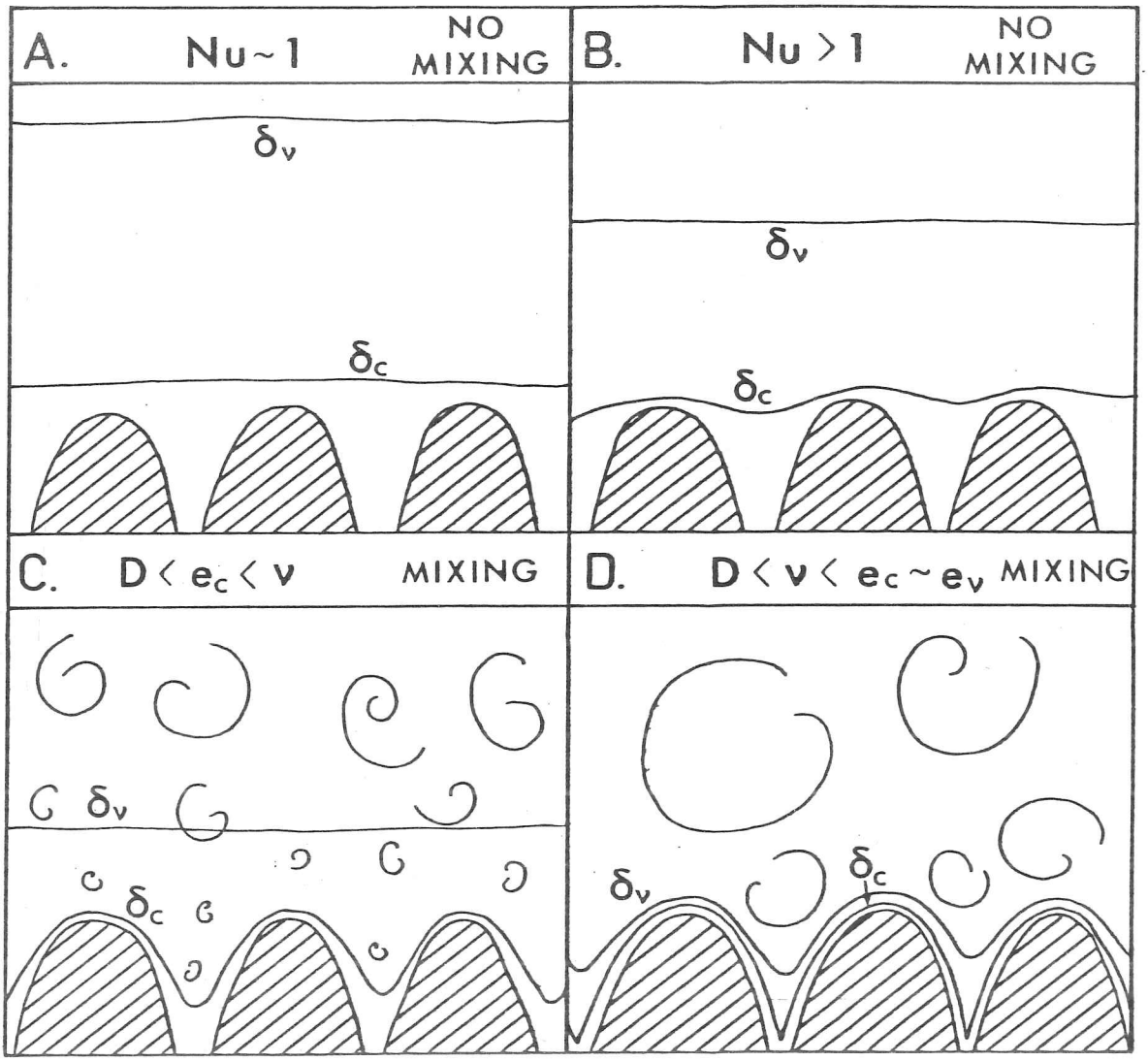

FIGURE 4.6 Schematic diagram of the relative thicknesses of the roughness, the viscous sublayer, δ_v, and the diffusive boundary layer, δ_c. The bounds of the layers are shown by solid lines and the roughness elements are shaded. Regimes A to D are discussed in the text.

For flow parallel to the c-axis, we approximate the boundary by a sinusoid and assume that the horizontal component of the fluid velocity follows this, that is

$$u_x = u_1(1 + \varepsilon_u e^{-pz} \cos \frac{2\pi x}{\lambda}) \quad , \qquad [4.8]$$

where ε_u is the amplitude of the perturbation in the flow and p is the rate of decay of the perturbation. u_1 is a function of z, but we are interested only in a small range and we ignore this dependence. From continuity the vertical component of the fluid velocity is

$$u_z = - u_1 \varepsilon_u \frac{2\pi}{p\lambda} e^{-pz} \sin \frac{2\pi x}{\lambda} \quad , \qquad [4.9]$$

and equation [4.7] becomes

$$u_1(1+\varepsilon_u e^{-pz} \cos \frac{2\pi x}{\lambda}) \frac{\partial C}{\partial x} - (u_1 \varepsilon_u \frac{2\pi}{p\lambda} e^{-pz} \sin \frac{2\pi x}{\lambda} + V) \frac{\partial C}{\partial z} = D \frac{\partial^2 C}{\partial z^2} \; . \qquad [4.10]$$

The equation for flow perpendicular to the c-axis is found by allowing $\varepsilon_u \to 0$ in [4.10] Assuming C is separable and is independent of x in the unperturbed case, then the solution of [4.10] is well-known (for example Flemings, 1974) and with appropriate boundary conditions is given by

$$C^{\perp} = C_\infty (1 + A \exp(-\frac{Vz}{D})) , \qquad [4.11]$$

where $A = k_{eff}(\frac{1}{k_e} - 1)$

and $C^{\perp}$ is the concentration for flow perpendicular to the c-axis and C_∞ is the concentration in the bulk of the fluid. Returning to flow parallel to the c-axis, C'' will respond to the perturbation in velocity and thus is written as

$$C'' = C_\infty(1+A\exp(-\frac{Vz}{D})).(1+\varepsilon_C \exp(-\frac{Vz}{D})\cos(\frac{2\pi x}{\lambda} + \chi)) \quad . \qquad [4.12]$$

This is substituted in [4.10] and terms to first order in the perturbed quantities are retained, giving the following expression for the phase difference, χ, between the velocity and concentration profiles.

$$\tan \chi = - \frac{V^2 \lambda \exp(-\frac{Vz}{D})}{\pi u_1 D \left(\frac{1}{A} + \exp(-\frac{Vz}{D}) \right)} \quad . \qquad [4.13]$$

1/A is of order 10^{-3}. Thus, close to the interface, we have

$$\tan \chi \sim - \frac{V^2 \lambda}{\pi u_1 D} \quad , \qquad [4.14a]$$

$$\cos \chi \sim \frac{V \epsilon_u}{Dp \epsilon_c} \left\{ \frac{(\frac{2\pi u_1}{\lambda})^2}{(\frac{2\pi u_1}{\lambda})^2 + (\frac{2V^2}{D})^2} \right\} \quad . \qquad [4.14b]$$

This predicts that χ is always negative; that is the concentration profile is displaced downstream from the velocity profile and hence, from the interface profile. This means that the concentration on the upstream side of the cell is slightly less than that on the downstream side, which is consistent with the observed tilting.

The growth velocity at the tip of a cell will increase as the tip concentration increases. Thus considering the difference in the concentration at the tip, x = 0, for grains with c-axis parallel and perpendicular to the velocity vector, we have

$$\Delta C_{tip} = C^{\perp}_{tip} - C^{''}_{tip} \quad . \qquad [4.15]$$

Since χ is almost always small, then from [4.14b]

$$\epsilon_c \sim \frac{V \epsilon_u}{Dp} \quad \text{and} \quad p \sim u_1^{\frac{1}{2}} \quad .$$

ϵ_u and u_1 have been estimated from figure 4.5(a) and thus for V = 3cmday^{-1}, λ = 0.05cm and C_∞= 30‰, ΔC_{tip} is of order 2×10^{-3}‰ or 2 parts per million.

Equation [4.14] implies that as $u_1 \to \infty$, $\chi \to 0^o$ and as $u_1 \to 0$, $\chi \to -90^o$ which may at first sight seem unrealistic. Physically, the equation we have solved is removing material from the tip region and "dumping" it, by diffusion, in the intercellular zone. Thus the longer it takes for the fluid to move to the centre of the groove, that is the slower the velocity, the more efficient is the "dumping" process. Of course this approach has completely ignored the important observation that an increase in fluid motion causes an increase in the solute transport and the dependence of

this increase on the c-axis direction. However, the calculation is valuable in that it indicates the order of magnitude of the concentration difference producing the c-axis alignment. This is approximately 1/5 of the depression in the concentration between the cells (see section 4.4).

4.5.3 Regime B: Nusselt number greater than 1 and no mixing

For $Re^* > 0.01$ but $D > e_c$ in the region of the cells, convection dominates diffusion and $Nu > 1$ (see figure 4.6(b)). For the case of the velocity normal to the c-axis (unperturbed), the solution equivalent to equation [4.11] would be the conventional concentration profile in a laminar boundary layer (see for example Kay and Nedderman, 1974). The upper limit of this regime is determined by the exact dependence on e_c on z and u which is unknown.

4.5.4 Regime C: $D < e_c < \nu$ and mixing

The eddies close to the interface are now of sufficient size that, although the cells are still within the viscous sublayer, δ_ν, (figure 4.6(c)) and $Re^* < 5$, the eddy transport coefficient for solute is greater than the solute diffusivity. From mixing length theory (see equation [3.7]) we expect $e_c \propto u_{tip} \propto u_\infty$, for flow parallel to the c-axis. If there is no mixing for grains with c-axis perpendicular to the current, then $\Delta C_{tip} \propto u_\infty$.

4.5.5 Regime D: $e_c \sim e_\nu > \nu > D$ and mixing

The flow is now sufficiently fast that it has entered the transition regime of figure 4.3, and the roughness elements protrude through the viscous sublayer (figure 4.6(c)). Both solute and momentum are removed from the interface under the control of the eddy transport coefficients. The eddies pictured in figure 4.4(a) are characteristic of this regime and are very similar to the motion induced between closely spaced rows of 2D hills (Hunt, 1980) or between the elements of repeated rib roughness with a pitch to height ratio of the order of 1 (Perry et al, 1969; Webb et al, 1971). This so called "d-type" roughness might more appropriately

be thought of as a smooth wall containing a pattern of narrow cavities. An interesting feature of this motion is that small fluctuations in the outer flow can cause large disturbances at the boundary and ejection of fluid at the roughness elements (Perry et al, 1969; Townsend, 1976).

Although "d-type" roughness is not easy to describe mathematically, expressions for the turbulent mass transfer Stanton numbers [5] for a smooth boundary (Kader and Yaglom, 1972), "k-type" (Kader and Yaglom, 1975) and sand (Yaglom and Kader, 1974) roughness have been derived. [6] Thus we arrive at the form of ΔC_{tip} in this regime by assuming it is proportional to the ratio of St^r (for sand roughness) to St^s (for a smooth wall). Approximating the lengthy expressions of Yaglom and Kader gives

$$\Delta C_{tip} \propto \frac{St^r}{St^s} \sim 3(a_1 \lambda u_*)^{-\frac{1}{2}} \quad . \qquad [4.16]$$

$St^r/St^s > 1$ and grains with the c-axis parallel to the flow are favoured but ΔC_{tip} again decreases with fluid velocity.

4.5.6 Relevant experiments in flow over roughness

The experiments of Dawson and Trass (1972) suggest that for high values of Sc, such as in sea ice growth, the value of Re^* at which the elements begin to influence the flow may be reduced. They have found St^r/St^s is perceptively greater than 1 for roughness Reynolds numbers below 1. Recently Gee and Webb (1980) have studied the effect of changing the angle between the current direction and the ridges of the roughness elements. St^r decreased monotonically from its maximum when the flow was perpendicular to the long axis of the ribs, to a minimum when the flow and ridges were at 30^o. Qualitatively this result is important since it is exactly the type of dependence we seek if flow is to orient grains in sea

---

[5] In this context, the Stanton number is the ratio of the actual mass transfer rate the ~~the~~ mass flow in an undisturbed stream moving at the same velocity.

[6] "k-type" roughness is repeated rib roughness with a large pitch to height ratio and sand roughness consists of randomly distributed, closely-spaced elements.

ice.

Thus, in conclusion, we estimate that for our experiments and for most situations in the field, regime B or C will describe the physical processes at the interface. The other regimes are not unobtainable however. Regime A may be the situation for slow, unidirectional natural convection. Experimental evidence suggests that the limit of regime D may be lowered by the high Sc, making this a more common occurrence under natural conditions.

4.6 Tilting of the grains

In section 3.8.6 we observed the upstream deflection of the columnar axis of the grains in the saline experiment with a flow. This preference occurred even when the interface sloped gently upwards in the current direction. This would normally force the columnar axis to slope in the downstream direction.

The tilting is well-known in the solidification of metal alloys (Cole, 1971; Flemings, 1974), where the dendrites respond rapidly to the flow. However there is a lack of agreement regarding the causal mechanism for tilting. For thermal dendrites, such as pure ice (Miksch, 1969), it must be due to the distortion of the direction of heat flow either in the bulk of the fluid, or by washing around the dendrites. The problem has been tackled by statistically correlating random heat fluctuations in the liquid with supercooling events in the solid-liquid region (Samoilovich, 1978), but the expression obtained is in terms of molecular quantities and is not readily usable.

Theoretical predictions imply that the effects of flow on constitutional dendrites is greater than for thermal dendrites (Cantor and Vogel, 1977). Thus the frequent observation of grain deflection in alloys is not surprising since, in addition to the modification to the thermal field, the flow will reduce the diffusion boundary layer on the upstream side of the dendrites (Flemings, 1974). An alternative suggestion

(Takahashi et al, 1976) considers the nucleation of new dendrites in the interdendritic region because of constitutional supercooling. When the flow is present, the potential nucleation site is displaced upstream of centre and the new grain is forced to grow into the current by the existing dendrites.

Empirical equations relate the deflection angle to the fluid and growth velocities for carbon steel (Takahashi et al, 1979; Takahashi, 1981).

In ice, Miksch (1969) has observed that the a- and c-axes do not respond to the flow and that the columnar axis is at an angle to the dendrite direction. At first sight this may seem inconsistent with our results. However, in a polycrystalline material, the surviving grains are those which have been favoured by the rules of geometric selection which, in this case, are those with the columnar and dendrite direction coinciding. Through this mechanism, flow in the melt has produced a deflection in the preferred texture of metal alloys (Abe and Togano, 1969, 1970) which is similar to the distortion of the horizontal fabrics in our experiment.

Finally, it is interesting to note that this tilting alone is capable of producing a preferred orientation. When the c-axis is parallel to the current in a grain with differently oriented neighbours, the lateral expansion on the upstream side is enhanced by a factor $V_a \sin\theta / V_c$ [7] above the expansion rate for the case of no flow. However, if the c-axis of a grain in the same location is perpendicular to the current vector, it will not "feel" the same advantage due to the flow, since growth in the current direction is controlled by V_a, irrespective of tilt. Where there is divergent growth between tilted and non-tilted grains, a supercooled region will appear and branching of the tilted grain is favoured over the vertical cell.

---

[7] V_a = growth velocity parallel to the a-axes, V_c = growth velocity parallel to the c-axis, θ = angle of grain deflection

Grain deflection has never been observed in the field.

4.7 An equation for alignment

4.7.1 Introduction

We have already observed in section 3.6 that, apart from the initial 5-10cm, the growth of sea ice is controlled by the conduction of heat through the solid. However, the transport of salt-enriched fluid from the interface produces a slight dependence of the accretion rate on the angle between the current direction and the mean c-axis direction. The full mathematical description of this second-order effect is extremely complex. It requires calculation of small differences in chemical potential between neighbouring grains which result from the distortion of the isoconcentration lines by the flow. In addition, the fluid motion and the interface and cell shape are mutually interacting. In the preceding sections we have decoupled the problem and have investigated the effect of flow on cell spacing (section 4.4) separately from the influence of the cells on the mixing in the fluid (section 4.5). We have shown that the transport of solute from the interface is enhanced when the flow is parallel to the c-axis. We must finally tackle the description of the rate of increase of c-axis alignment which results from this increase in solute transfer.

4.7.2 Formulation of the equation

We shall follow the work of the metallurgists on the kinetics of precipitation (Turnbull, 1953) and on the diffusion-controlled growth of phases (Fine, 1964)

We assume that all the crystal c-axes of a sample of sea ice lie within 30° of the horizontal plane. At a given time, we define f as the fractional area of interface which has the crystal c-axis lying within a bin of dimensions $\Delta\theta = 60^{\circ}$, $\Delta\phi = 60^{\circ}$ (see figure 3.30 for definitions of $\Delta\theta$ and $\Delta\phi$), centred on the horizontal plane and on the current direction

respectively. The rate of increase of this fraction will be controlled by the movement of grain boundaries and thus depends on the length of the perimeter of the growing grains. In order to arrive at a first approximation it is necessary to assume that the grains expand isotropically. This is not strictly correct since the rapid growth kinetics normal to the c-axis produces an increase in the grain length to breadth ratio with depth (see section 1.2). We also suppose that the grains are spherical and uniform in size, which is reasonable in the early stages of growth (figure 1.2(a)) but is a very crude approximation at later times (figure 1.2(b)). This can be partially dealt with by the introduction of a shape factor, although a severe departure from sphericity can change the form of the dependence between f and t (Fine, 1964). Using these assumptions we obtain

$$\frac{df}{dt} \propto (nf)^{\frac{1}{2}} \quad , \qquad [4.17]$$

where n is the number of growing grains per unit area of the interface. n is determined by nucleation and it is reasonable to assume that it does not vary drastically. We subsequently omit it from our expressions. Since there is a finite amount of material available for consumption by favoured grains, the rate of increase of alignment will decrease as f increases, and equation [4.17] becomes

$$\frac{df}{dt} \propto f^{\frac{1}{2}}(1-f), \qquad [4.18]$$

which we may write as

$$\frac{df}{f^{\frac{1}{2}}(1-f)} = \frac{dt}{R_f}. \qquad [4.19]$$

R_f can be thought of as a relaxation time for the alignment of crystal c-axes. From analogy with similar problems (Fine, 1964), we expect it to contain a shape factor and a diffusivity term describing the motion of the grain boundaries as a function of the solidification parameters. Integrating equation [4.19] gives

$$\ln\left(\frac{1+f^{\frac{1}{2}}}{(1-f)^{\frac{1}{2}}}\right) + A = \frac{t}{2R_f} \quad . \qquad [4.20]$$

At $t = t_o$, $f = f_o$ and equation [4.20] becomes

$$\ln\left(\frac{1+f^{\frac{1}{2}}}{(1-f)^{\frac{1}{2}}}\right) - \ln\left(\frac{1+f_o^{\frac{1}{2}}}{(1-f_o)^{\frac{1}{2}}}\right) = \frac{t-t_o}{2R_f} \quad . \qquad [4.21]$$

t_o is the time for nucleation to take place and f_o is the fraction of grains within 30^o of the current direction at $t = t_o$. In our experiments we have chosen the time origin as the time at which nucleation took place. We equate t_o to the time between complete ice cover and the development of a fabric with c-axes predominently in the horizontal plane. If the initial c-axis distribution is a symmetric girdle then $f_o = 0.33$.

Setting

$$F(f) = \frac{1+f^{\frac{1}{2}}}{(1-f)^{\frac{1}{2}}} \quad , \qquad [4.22]$$

we may rewrite equation [4.21] as

$$F(f) = F(f_o)\exp\left(\frac{t}{2R_f}\right) \qquad [4.23]$$

nucleation growth

Because of the nature of nucleation, there will be some scatter in the first term of this equation from location to location. However, the growth term will not be subject to this random spread, provided the factors determining R_f are constant with position and time.

4.7.3 Fit of alignment equation to data of saline experiments

Figure 4.7 shows the data from the saline experiments plotted according to equation [4.21] with F(f) given by [4.22]. Full lines are drawn through measurements from a single location, while the dashed lines are the least

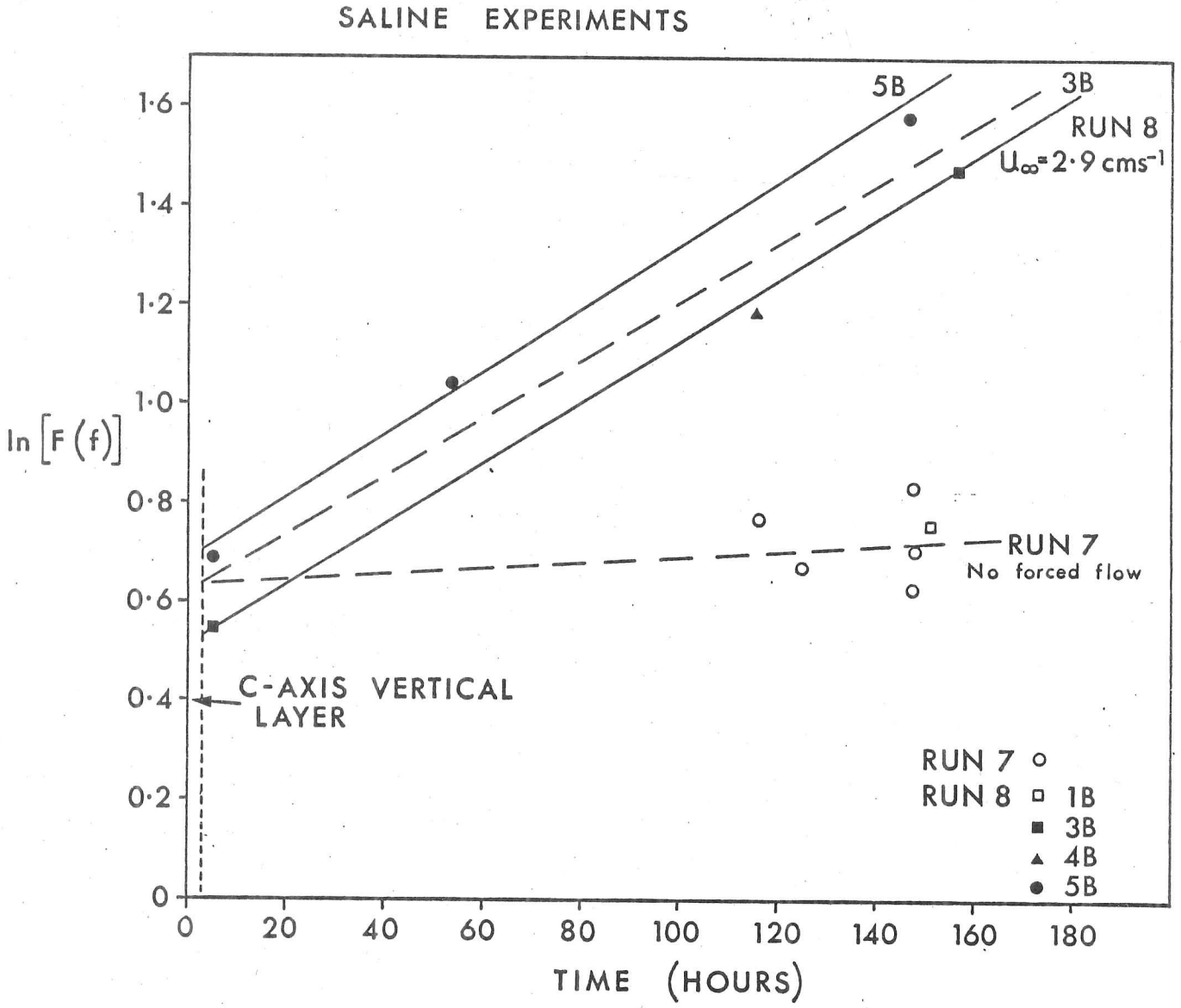

FIGURE 4.7 C-axis alignment data plotted according to equation [4.21] Slope gives the alignmment relaxation time and the value of f at the intercept with $t=t_o$ is the original strength of the fabric. In this figure t_o is shown by a dotted line indicating where c-axis horizontal grains began.

squares fit for all the data from a single experiment. [8] The alignment relaxation time, R_f, is related to the slope of these lines, while the initial ordering is derived from the intercept. The important features of figure 4.7 are outlined below.

(i) The data of Run 8 show a reasonable fit to a straight line (correlation coefficient = 0.94) and are therefore adequately described by equation [4.21].

(ii) As expected, the values of R_f for Run 8 are similar, for c-axis measurements from two separate locations, and for the least squares fit to all the data (see Table 4.1). However f_o, which is obtained from the value of ln[F(f)] at the intercept, is 0.23 and 0.37 for 3B and 5B respectively (figure 3.3(d) shows the positions of 3B and 5B). f_o is therefore spread about 0.33.

(iii) t_o for both the saline experiments has been marked on figure 4.7 by a dotted line. This is the time at which grains with horizontally oriented c-axes appeared under the 0.7cm thick c-axis vertical layer which formed initially. The values of f_o quoted above result from projection to t_o = 3 hours.

(iv) No surface sections were made for Run 7 and we therefore cannot test whether these data lie on a straight line. However we have seen that the initial stages of growth followed the same pattern for these experiments and we choose the same value of f_o (i.e.f_o=0.32) for the collective data of Runs 7 and 8. It is pleasing that this average is very close to the value for a symmetric girdle distribution.

(v) The data point for position 1B in Run 8 is anomalous in that it falls in the region of the data from Run 7. This can be explained by the lack of preferred current direction at the location of 1B, close to the entrance of the test section (see section 3.8.6). It is therefore naturally grouped with the data for no forced flow.

---

[8] To test the validity of equation [4.23] it would be useful to have sets of c-axis measurements throughout the thickness of the ice at various locations, and thus at various values of f_o. This would enable us to distinguish between the scatter in f_o and in R_f. However our experiments were designed to explore the relative effects of thermal gradients and fluid flow on the distribution of c-axes rather than to test equation [4.23].

	Comment	C_∞ (%)	u_∞ (cm/s)	R_f (hrs)	f_o	Correlation coeff. r^2	R_τ (hrs)	τ_{30}	r^2
Run 7	Insufficient data to estimate error in R_τ	35	0	700	0.32	-	1200^{+2000}_{-800}	0.56	-
TUKTOYAKTUK	Time derived from salinity profile	21	1	-	-	-	160^{+300}_{-50}	0.52	0.741
TUKTOYAKTUK	Time derived from tables of Thorndike et al	21	1	-	-	-	500^{+400}_{-100}	0.60	0.735
Run 8	Using all data	31	2.9	90	0.32	0.941	120^{+20}_{-10}	0.56	0.945
Run 8	Data from position 5B only	31	2.9	80	0.37	-	-	-	-
Run 8	Data from position 3B only	31	2.9	80	0.23	-	-	-	-
Run 5	Data before transition only	18	3.4	50	0.23	0.999	60^{+20}_{-15}	0.49	0.980
Run 5	All data after transition	18	Eff. zero	3600	-	-	-	-	-
Run 6	Correlation coefficient indicates no relationship	20	0	70	0.34	0.448	-	-	-

TABLE 4.1

(vi) The most striking feature of figure 4.7 is the significant difference in the slopes for Runs 7 and 8, and thus in the values of the alignment relaxation time, R_f. That is

$$R_f = 90\text{hours}, \qquad u_\infty = 2.9\text{cms}^{-1}$$
$$R_f = 700\text{hours}, \text{ No forced flow}$$

We may therefore hypothesise that the velocity of the fluid at the interface is important in determining the magnitude of R_f.

4.7.4 Fit of alignment equation to data of brackish experiments

We have plotted the data from the brackish experiments in the same way in figure 4.8 and we shall list its important features.

(i) The data of Run 6 do not lie on a straight line, confirming our statement that the results of this experiment cannot be described in the same way as the other three. Figure 3.29 has shown, in this case, that the alignment is a function of the distance from the entrance of the test section.

(ii) The effect of the cellular to planar transition in Run 5 is emphasised by displaying c-axis measurements in terms of F(f). The slope, and thus R_f, changes sharply at t = 45hours, which is also the transition point determined, quite independently, from the salinity profiles (figure 3.11 and the discussion of section 3.8.3).

(iii) t_o has been set equal to zero since grains with horizontally oriented c-axes are nucleated at the surface. f_o is slightly lower than the corresponding quantity in Run 8, indicating a very slight preference for the c-axes to lie perpendicular to the current direction.

(iv) R_f has been determined for the data of 5B before the transition giving

$$R_f = 50\text{hours}, \qquad u_\infty = 3.4\text{cms}^{-1}$$

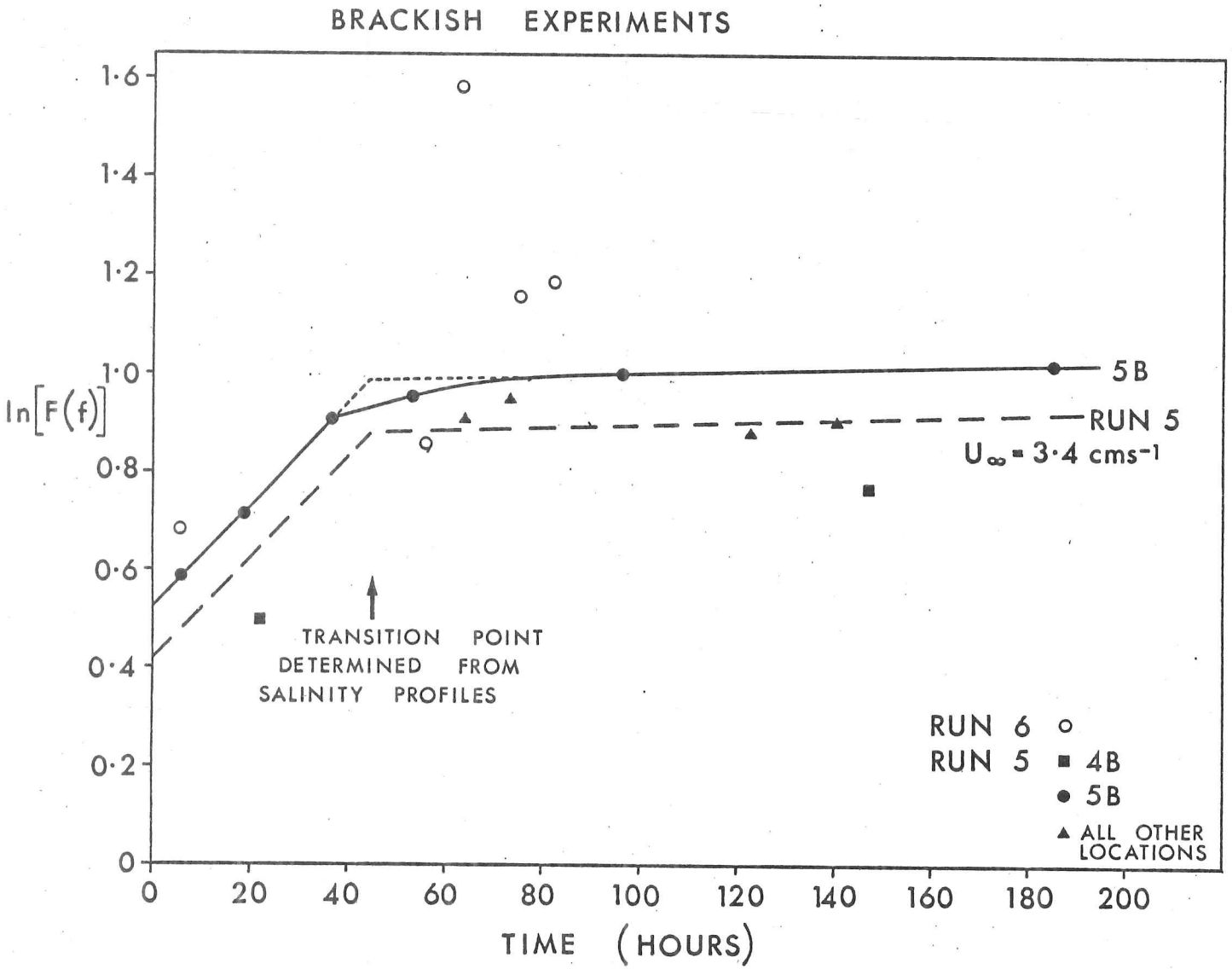

FIGURE 4.8 C-axis alignment data plotted according to equation [4.21] Slope gives the alignment relaxation time which changes abruptly at the cellular to planar transition. t_o=0 during the brackish experiments.

4.7.5 Fit of alignment equation to field measurements

We have shown that the limited data sets from our experiments are described by equation [4.21] yielding values of R_f which follow a consistent pattern. To supplement these data we turn to the field measurements which were made by the author in the Beaufort Sea near Tuktoyaktuk, and are described in Section 2.1

There are a number of quantities which we do not know for the field data. Firstly, we have no record of the increase in thickness with time. Secondly the current flowing under the ice, prior to the field study, is unknown and we have therefore, chosen to formulate the rate of alignment in terms of τ_3 (see section 3.8.1) rather than f. The disadvantages of this are that an alignment in any direction will give the same result, and that the physical significance of an increase in τ_3 is not so easily related to the movement of grain boundaries. To deal with the second of these complications we have calculated values of the alignment relaxation time in terms of τ_3, R_τ, for the laboratory experiments (figure 4.9 shows data of runs 7 and 8). $R_\tau \geqslant R_f$ (see table 4.1) because at small t, $F(\tau_3) > F(f)$. In other words the alignment around any axis is greater than the grouping around the current direction. At later times, when the preferred direction is established as the current direction $F(\tau_3) \sim F(f)$. A symmetric girdle distribution of c-axes is indicated by $\tau_{3o} = 0.5$.

In our field measurements, two methods have been used to convert the distance of a thin section from the upper ice surface to the time of ice formation at that depth. Ice growth in the ocean is governed by the thickness and distribution of snow cover, the convective heat transfer at the air-ice interface and, to a lesser extent, the balance of radiative fluxes. Equation [3.3] due to Lapadula and Mueller (1966) is therefore not suitable. A number of equations exist for the calculation of ice thickness (Stehle, 1965) and these generally reduce to the form

$$\Delta Tt \propto h^2 \qquad [4.24]$$

That is the accumulated degree days of freezing is proportional to the

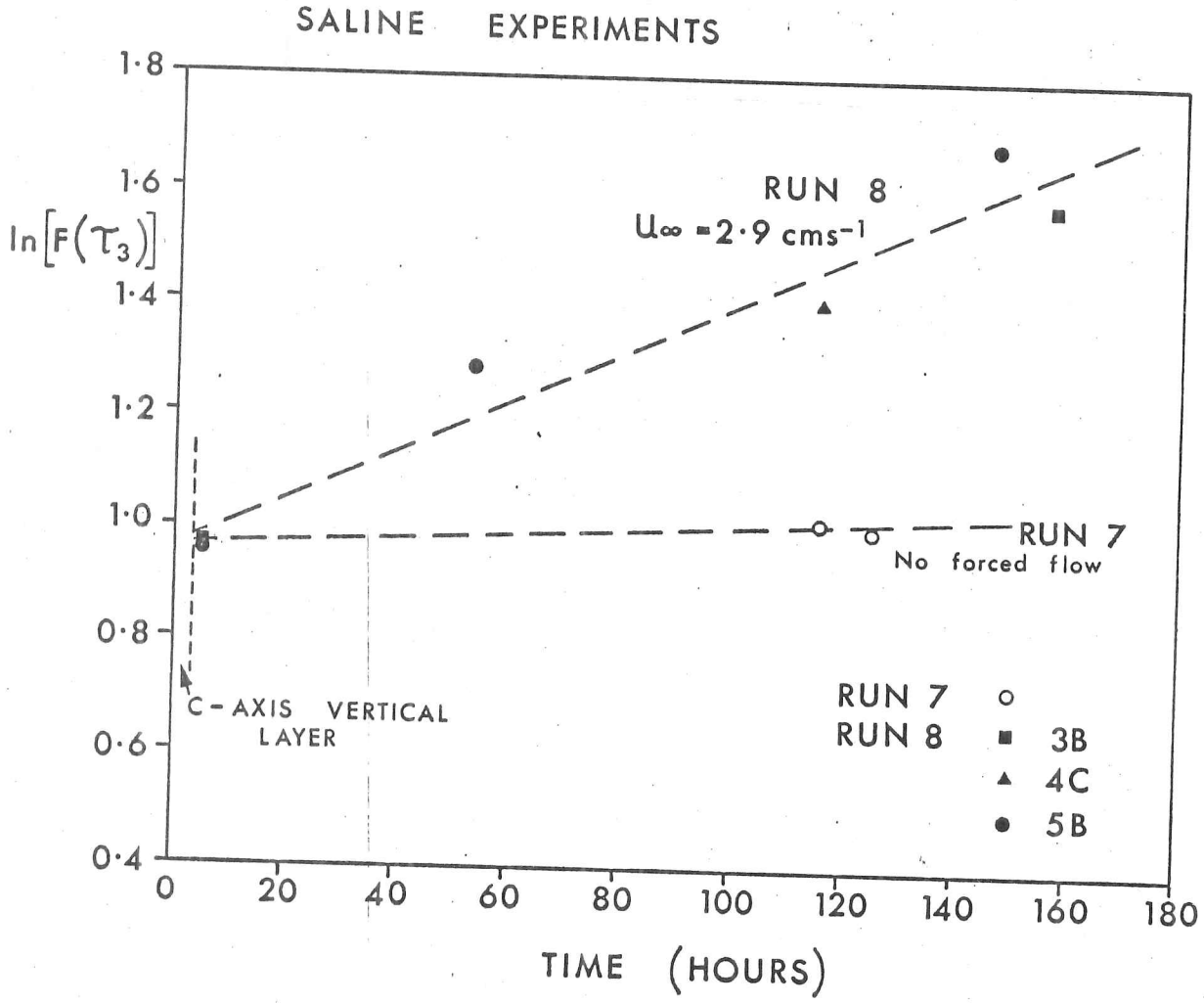

FIGURE 4.9 Data of figure 4.7 plotted in terms of τ_3 rather than f for comparison with field results.

square of the ice thickness. However, during the time of formation of the ice cover at our field site, ΔT cannot be approximated by a constant and we are unable to use a relationship of this type.

From climatological data, Thorndike and others (1975) have constructed a table of sea ice growth rates for the Arctic Ocean, as a function of the ice thickness and the time of year. We have used this table to project back in time from an ice thickness of 120cm, observed off Tuktoyaktuk in March. The measured growth velocity at this time was $1 \times 10^{-5} cms^{-1}$ which is close to the tabulated value of $9.4 \times 10^{-6} cms^{-1}$. $F(\tau_3)$ as a function of time derived in this way is given in figure 4.10. Only c-axis measurements within 75cm of the upper surface have been used because of the intrusion of a band of c-axis vertical grains disrupted growth at this depth (see figure 1.3). The resulting $R_\tau = 500^{+400}_{-100}$ hours is larger than values for Runs 5 and 8 because of the temporal variablity of current direction in the field, particularly due to tidal action. The lower fluid velocity may also be important. In addition, it is not surprising that there is a larger spread of results about the least squares fit ($r^2 = 0.74$). $\tau_{3o} \sim 0.6$ which is not significantly different from the expected value for a symmetric girdle distribution.

The second method of calculating the times of ice formation is believed to give better estimates of the relative growth velocities, but may not describe absolute times well. Nakawo and Sinha (1981) have shown that, after an initial rapid desalination, sea ice at a given level reaches a stable salinity (see section 1.9.2). This stable salinity is related to the growth velocity via equation [1.7] and Nakawo and Sinha have found values of δ_c/D and k_e for winter ice growth in the high Arctic. We have measured the growth velocity and salinity profiles for the sea ice off Tuktoyaktuk between the 14 and 25 March. It is therefore possible to find δ_c/D for our problem, assuming Nakawo and Sinha's value of $k_e = 0.12$. [9] Our value of $\delta_c/D = 1.6 \times 10^4 scm^{-1}$ compares reasonably with that of Nakawo and Sinha,

---

[9] In section 1.6.2, we described laboratory experiments which led to $k_e \sim 0.23$. This discrepancy is not surprising since these experiments were designed to measure brine entrapment before brine drainage took place.

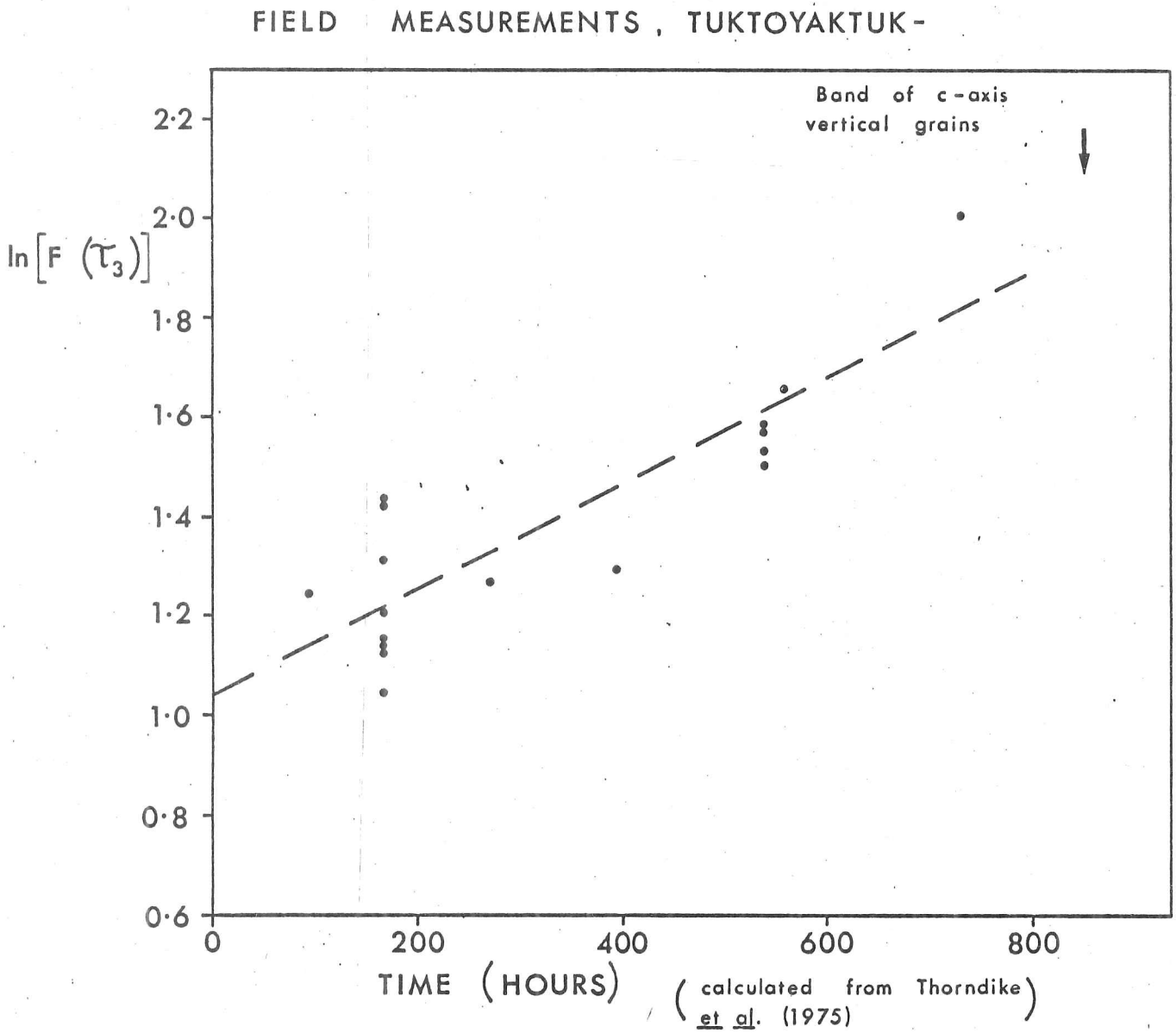

FIGURE 4.10 C-axis alignment data from the field plotted according to equation [4.21] . Times have been estimated from the tables of Thorndike et al.

$\delta_c/D = 4.2 \times 10^4 scm^{-1}$. The salinity profile, averaged over 9 cores from the grid at C4 (figure 2.2), and the derived growth velocities are given in figure 4.11. Salinity data are tabulated in Snellen and Rossiter (1982). The high salinity within the top 5cm of the ice does not imply a particularly high growth rate but rather an increase in brine retention by the fine-grained surface layers (Nakawo and Sinha, 1981). This layer was 20cm thick in our case (figure 1.3) but, since all our measurements are below this level, the resulting error will effect only the absolute times. $F(\tau_3)$, plotted as a function of time derived from the salinity profiles, is shown in figure 4.12. Compared with the results obtained by the previous method, we see that the correlation coefficent is slightly higher (Table 4.1) and that the value of τ_{3o} ($\tau_{3o} = 0.52$) is closer to that for a symmetric girdle. However the times for sea ice to reach 70cm in thickness differ by a factor of three for each method. This discrepancy produces a corresponding factor of three uncertainty in the value of R_τ and both values are used for comparison with the laboratory experiments. Thus in this case, R_τ from the least squares fit to all the data, is 160 hours and by taking minimum and maximum slopes for the data from a single core we find 110hours $< R_\tau <$ 470hours.

4.7.6 The dependence of alignment relaxation time on fluid velocity

We conclude our interpretation of the experiment by suggesting the form of the dependence of R, [10] the alignment relaxation time, on the conditions at the time of solidification. ~~Following Fine (1964), we propose that [11]~~

~~$$R = R_o \exp\left(-\frac{\Delta g}{k_B T}\right) , \qquad [4.25]$$~~

~~and $\Delta g = g - g'$ where g and g' are the Gibbs functions of neighbouring grains. The origin of Δg is the concentration difference at the tips of cells at the growing interface. We saw in sections 4.5.3 to 4.5.6 that this concentration difference, ΔC_{tip}, resulted from the fluid motion and that~~

---

[10] We use R to mean R_f or R_τ.

~~[11] k_B is Boltzmann's constant and R_o is a constant.~~

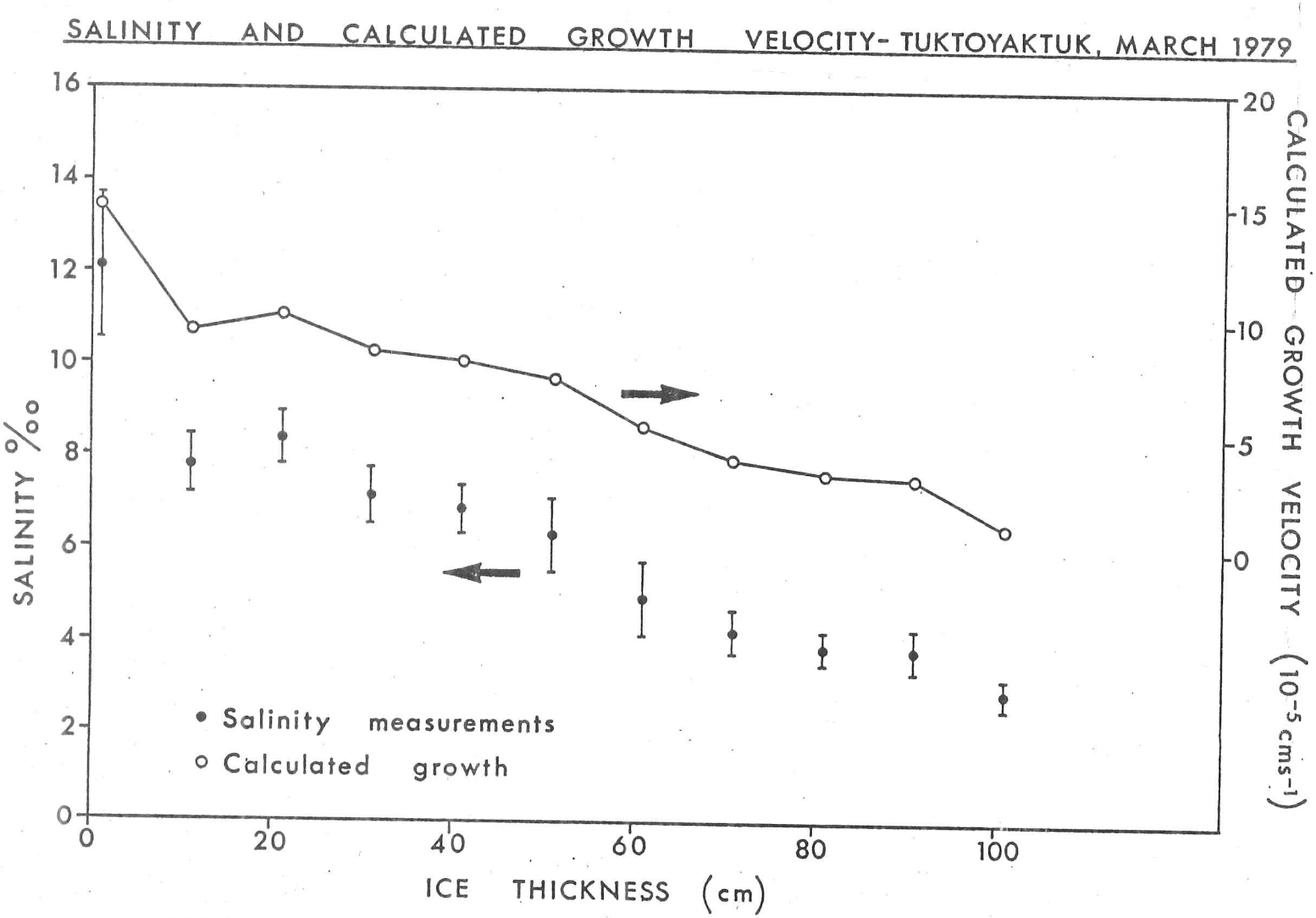

FIGURE 4.11 Diagram showing the average salinity measurements over the C4 grid at Tuktoyaktuk. Using equation [1.7], these salinities are used to calculate the growth velocity at the time the ice formed.

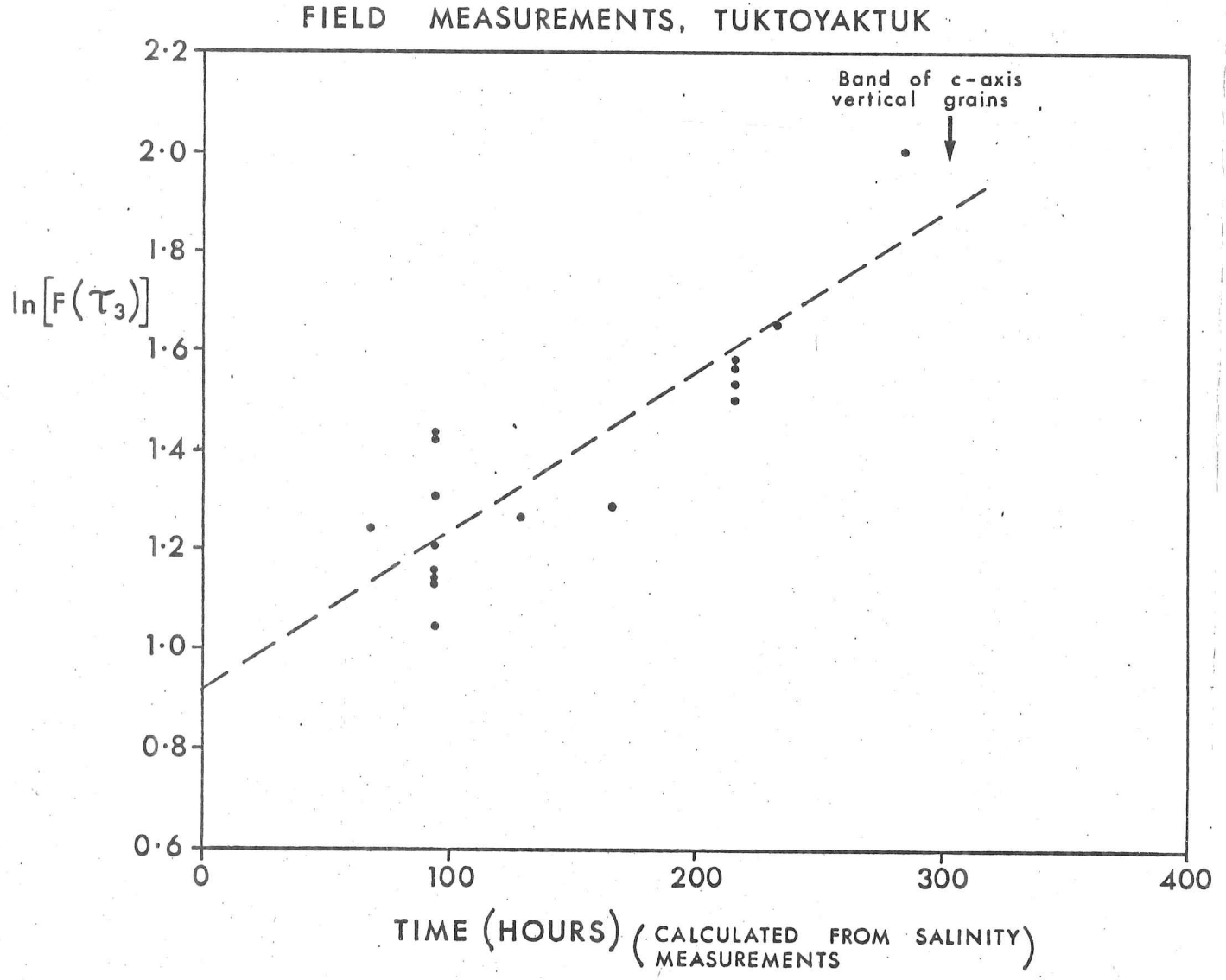

FIGURE 4.12 C-axis alignment data from the field plotted according to equation [4.21]. Times have been estimated from the salinity profile as shown in figure 4.11.

~~the functional dependence between Δc_{tip} and fluid velocity, u, was determined by the flow regime, which in turn, was controlled by the magnitude of the current. For our experiments and in most field situations, we concluded that~~

$$c_{tip}^{\perp} - c_{tip}^{\parallel} = \Delta c_{tip} \propto u_{\infty}$$

~~If we consider the particular case of neighbouring grains with c-axes aligned parallel and perpendicular to the current, then~~

$$\Delta \ell = \ell^{\perp} - \ell^{\parallel} \propto \Delta c_{tip} \propto u_{\infty} \qquad [4.26]$$

~~and equation [4.25] becomes~~ Empirically

$$R = R_o \exp(-\frac{u_{\infty}}{u}) \qquad [4.27]$$

where u is a constant. Figure 4.13 shows that our limited data are consistent with equation [4.27]. The equation of the line in this figure, with R_τ in hours and u_∞ in cms^{-1} is

$$R_\tau = 1200 \exp(-\frac{u_\infty}{1.2}) \qquad [4.28]$$

According to this equation, the field results using growth velocities tabulated by Thorndike and others (1975) lie closest to the laboratory data.

Combining equations [4.23] and [4.27] we finally have

$$F(\tau_3) = F(\tau_{30}) \exp\left(\frac{t \exp(\frac{u_\infty}{u})}{2R\tau_0}\right) , \qquad [4.29]$$

where

$$F(\tau_3) = \frac{1+\tau_3^{\frac{1}{2}}}{(1-\tau_3)^{\frac{1}{2}}} .$$

$\tau_{30} = 0.5$ in most cases for sea ice growth and u and $R_{\tau o}$ are empirically determined constants. $R_{\tau o}$ is the relaxation time for a value of τ_3 indicating significant alignment, to be established when fluid velocites are negligibly small. In the absence of fluid motion, c-axis alignment may

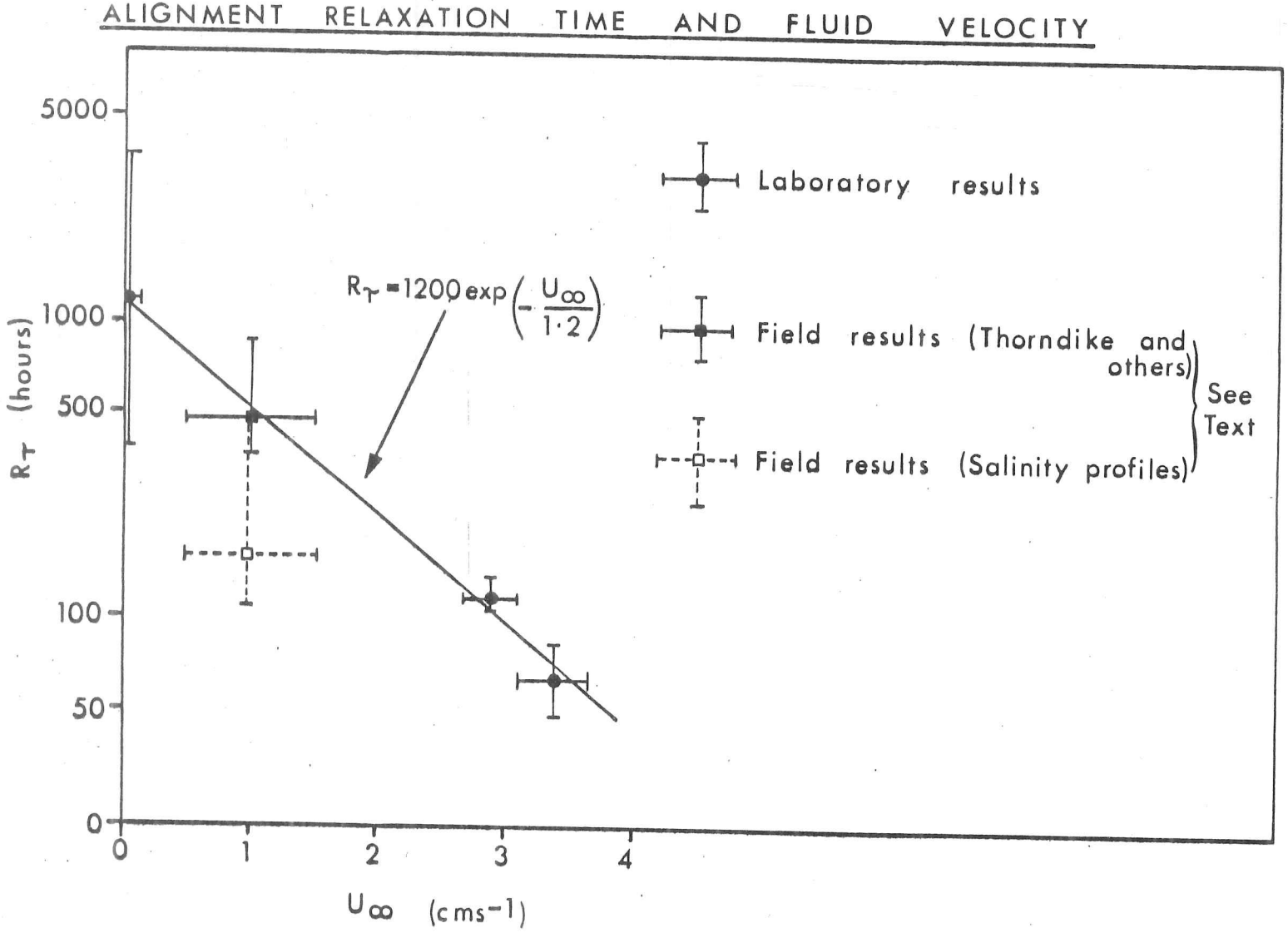

FIGURE 4.13 Empirical dependence of the alignment relaxation time on the fluid velocity outside the boundary layer.

still arise because of the preference of a grain to adjoin its neighbours at a small angle (see section 2.1). u gives an indication of the fluid velocity above which flow produces a distinct effect on the fabric of the sea ice. However more data are required before we may establish whether the values of $R_{\tau o}$ = 1200 hours and u = 1.2cms^{-1} from this study can be applied in the field, since ocean currents are not constant in magnitude or direction and u and $R_{\tau o}$ will respond to the integrated effect of the flow.

However, given $R_{\tau o}$ and u, it is possible to estimate the magnitude and direction of this "effective" current from the texture of the sea ice. The current direction is deduced from the mean c-axis direction of the distribution, and the current magnitude from the strength of this alignment about the mean. Likewise, sea ice fabrics can be inferred from knowledge of the flow.

4.8 Summary of the interpretation of the experiments

The laboratory results of chapter 3 have shown the considerable influence of fluid motion on the grain structure and c-axis alignment of NaCl ice. An investigation of the metallurgical literature suggests that this might be expected, and in this chapter we have compared some of the flow-induced features observed in metals, semiconductors and organics with the observations in our experiment. The cellular to planar transition in Run 5 was compared with a theory for interface stability in the presence of a flowing melt. Qualitative and quantitive agreement were found, indicating that fluid motion stabilises the ice-water interface.

Flow at the interface produces a second order disturbance in the growth velocity, resulting in grains with c-axis parallel to the current growing slightly more rapidly than those with c-axis perpendicular to the flow. We have looked at mutually interacting components of the disturbance separately. Firstly, the cell spacing is only influenced by the fluid motion through the flow modification of the solute gradient at the interface. Secondly, we have identified four regimes of fluid motion and

solute transport in the region of the interface. In most cases of sea ice growth, the concentration difference between the tips of cells oriented with c-axes parallel and perpendicular to the current, is directly proportional to the fluid velocity outside the boundary layer. This concentration difference is of the order of 2 parts per million, indicating the smallness of the effect and the extreme sensitivity of columnar growth to differences in concentration. Finally we have described the development of the preferred texture with time (see equation [4.23]), the rate being determined by the difference in tip concentration between neighbouring grains, and hence by the fluid velocity, through the Gibbs function (see equation [4.25]). Data from our laboratory experiments and field work fit the combined result of these equations (see equation [4.29]) with a relaxation time for alignment with negligible fluid motion of 1200 hours and a characteristic velocity of $1.2 cms^{-1}$.

In the field, the rate of alignment is determined by the integrated effect of the variable currents at the ice-water interface. The magnitude and direction of this effective current can be found from the strength and direction of the preferred fabric of the sea ice. Indeed, using impulse radar, this may be found remotely.

5. CONCLUSIONS

The main aim of this project was to explain the observed alignment of crystal c-axes in sea ice. The principle conclusions which have resulted from this study are given below. The most important of these is listed first, but subsequent conclusions are considered to have equal weight.

1) Our experiments show that, in the presence of a current, the mean direction of a crystal c-axis distribution aligns with the flow vector at the ice-water interface. The average deviation between these quantities was 7^{o} in our experiments. When there was no unidirectional fluid motion, there was a significant reduction in the strength of the alignment.

2) During the saline experiment with forced flow, the columnar axis was deflected in the upstream direction, into the current. The c-axes were inclined from the horizontal in a similar manner so that the columnar axis and dendrite direction still coincided.

3) There is good evidence to suggest that natural convection, forced into a unidirectional pattern by the geometry of the tank, is also efficient at producing an alignment of c-axes.

4) The flow in our flume was laminar but there were convective temperature and velocity fluctuations due to brine rejection at the interface. Speeds outside the boundary layer were 3.4 and 2.9cms^{-1} ($\pm$8%) for experiments with saline and brackish solutions respectively.

5) Horizontal temperature gradients in the range 0 to 0.25^{o}Ccm^{-1} do not control grain alignment. These gradients may be deduced to within 40% from the slope of the ice-water interface and the vertical temperature gradient.

6) Horizontally-oriented stresses and tilting of the sheet of sea ice were absent during the experiments and therefore cannot explain the observed alignment.

7) The thickness versus time data for the sheet of artificial sea ice were fitted to a theory for solidification with a convective heat flux at the ice-water interface. The growth velocity, convective heat flux from the fluid, the thermal conductivity of the ice and the vertical temperature gradient in the solid can be estimated from this fit. Vertical temperature gradients were in agreement with measured values. Heat conduction through the sea ice slab therefore limits the growth velocity.

8) A cellular to planar transition was noted during growth from a solution of 18‰±5‰ with a current speed of $3.4 cms^{-1}$. This transition agreed with the predictions of stability theory in the presence of a laminar velocity profile.

9) After the cellular to planar transition had taken place there was no further increase in the strength of the c-axis alignment, confirming the influence of the transport of solute from the rough, cellular interface on the preferred c-axis direction.

10) Preferred c-axis orientation was observed in the nearshore waters of the Beaufort Sea in agreement with the results of other workers. This alignment causes an anisotropy in the response of the propagation of electromagnetic waves through sea ice, although no directional dependence was observed in the dielectric constant of the surface layers. Using the wide angle reflection and refraction technique, the ice thickness was found and it agreed with the directly measured thickness. Reasonable values for the dielectric constant of sea ice were obtained.

11) The relative growth rates between grains oriented at different angles to the flow is a second order effect and is controlled by the transport of solute from the interface.

12) The rate of alignment of c-axes, in the field and in the laboratory, has been found to follow a relationship of the form

$$F(\tau_3) = F(\tau_{30})\exp(\frac{t}{2R_\tau}) \ ,$$

where

$$F(\tau_3) = \frac{1+\tau_3}{(1-\tau_3)}^{\frac{1}{2}} \ .$$

τ_{3o} describes the initial c-axis distribution which is generally a symmetric girdle, giving $\tau_{3o}=0.5$. R_τ is a relaxation time for alignment which depends on the current velocity outside the boundary layer through

$$R_\tau = R_{\tau o} \exp(-\frac{u_\infty}{u})$$

Empirically, we have found from field and laboratory results that

$$R_{\tau o} = 1200 \text{ hours}$$
$$u = 1.2 \text{cms}^{-1}$$

13) In principle, the strength and mean direction of a crystal c-axis distribution may be found from a knowledge of the current velocity just outside the viscous boundary layer from the equations in 11). Alternatively the effective current velocity may be deduced from a single measurement of the strength and direction of the preferred c-axis orientation.

A1.1 The brackish experiments - Runs 5 and 6

No temperature measurements in the solid were made during these experiments. However a simple, finite element solution of Laplace's equation for the geometry of our system during Run 5 has been computed. If the flow of heat is important and the resulting alignment of c-axes is normal to the direction of the temperature gradient then a cross-tank temperature gradient will produce the same pattern of c-axes as the fluid flow. Thus we are concerned only with the two-dimensional problem of gradients in the cross-tank plane (see figure A1.1 for the geometry of this model).

Figure A1.2 shows the calculated temperature distribution in the ice and in the insulating materials, 1cm from the ice-water interface. This yields gradients ranging from $0.04^{o}Ccm^{-1}$ at the window edge to $0.006^{o}Ccm^{-1}$ at the opposite side. These are in agreement with the estimates quoted by Lewis (1967) for sea ice.

A1.2 Run 7 (Saline - No Forced flow)

A thermistor probe was constructed to measure the vertical temperature gradient in this experiment. The thermocouples used to measure the horizontal temperature gradient are described here but the measurements are dealt with in section 3.5.1.

A1.2.1 Construction of thermistor probe

Five thermistors were set inside a 1cm diameter plastic syringe which was machined to fit a length of plastic tubing. The beads protruded through small holes and epoxy potting compound was forced down the tube to

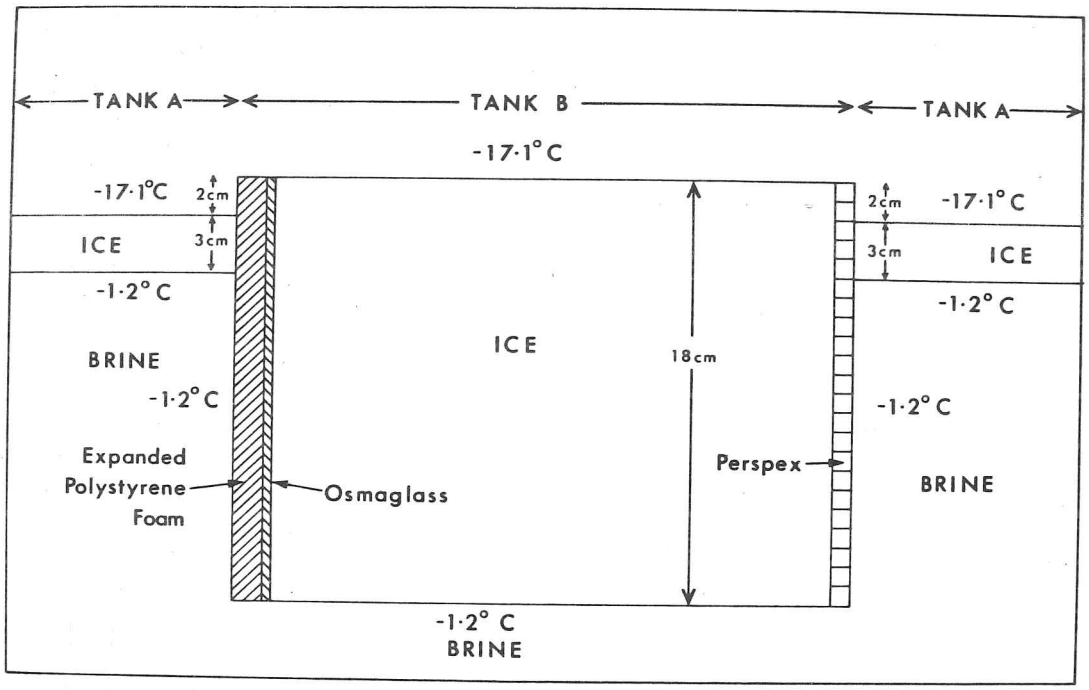

FIGURE A1.1 Diagram of geometry used in the computation of the horizontal temperature gradients for Run 5. The current is pointing into the plane of the page.

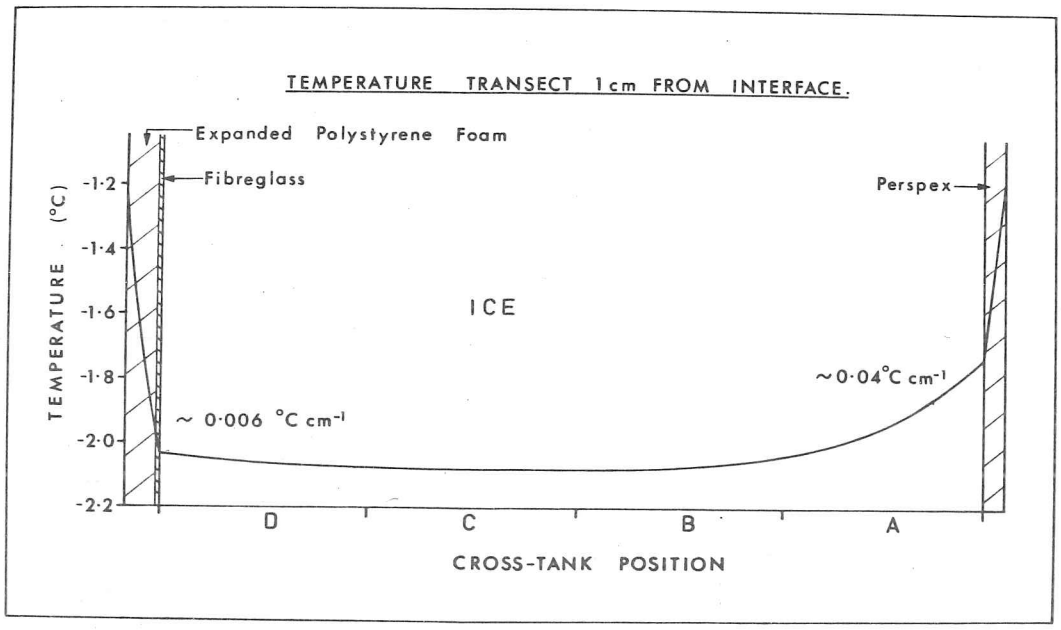

FIGURE A1.2 Calculated temperatures close to the ice-water interface for the conditions during Run 5.

make the probe watertight. The probe was calibrated in an ice-distilled water mixture in a vacuum flask and at the freezing point of solutions of known concentration. Resistance readings were taken directly from a digital Avo and the resolution of the readings was approximately 0.1°C. The relative error between thermistors is 0.15°C although the absolute error in temperature measurement may be larger than this. The probe was inserted 28 hours after initial ice formation and was allowed to settle for 20 hours before readings were taken. The location of the probe close to the centre of the test section is shown in figure 3.3(c).

A1.2.2 Temperature measurements and vertical gradients

The decrease in temperature with time at five depths in the ice is shown in figure A1.3. The vertical temperature profile was found to be linear, [1] for most of the time that the ice was growing and throughout a large proportion of the ice thickness. The change in magnitude of the vertical gradient is shown in figure A1.4 and, as expected, it decreases as the ice thickens. Using these gradients we have extrapolated to find the temperature within the ice at the surface. The time dependence of this is also given in figure A1.3 and this suggests the origin of the fairly large temperature fluctuations which were measured within the ice. Two compressors maintain the temperatures within our cold room, each running for four hours. During this experiment they were set so that there was a temperature difference of approximately 1°C between them, causing a fluctuation in air temperature with a period of 8 hours. Records of the times at which compressors switched over control support this hypothesis.

A1.2.3 Use of thermocouples

The accuracy required in the measurement of the horizontal temperature gradients is greater than for the vertical direction. Since we are interested only in temperature differences, copper-constantan thermocouples are the obvious choice since they measure this difference directly. Standard tables (Scott, 1941;Stallman and Itagaki, 1976) may be used for calibration and, because of the very small range of temperature

---

[1] Coefficients of determination were between 0.993 and 0.999.

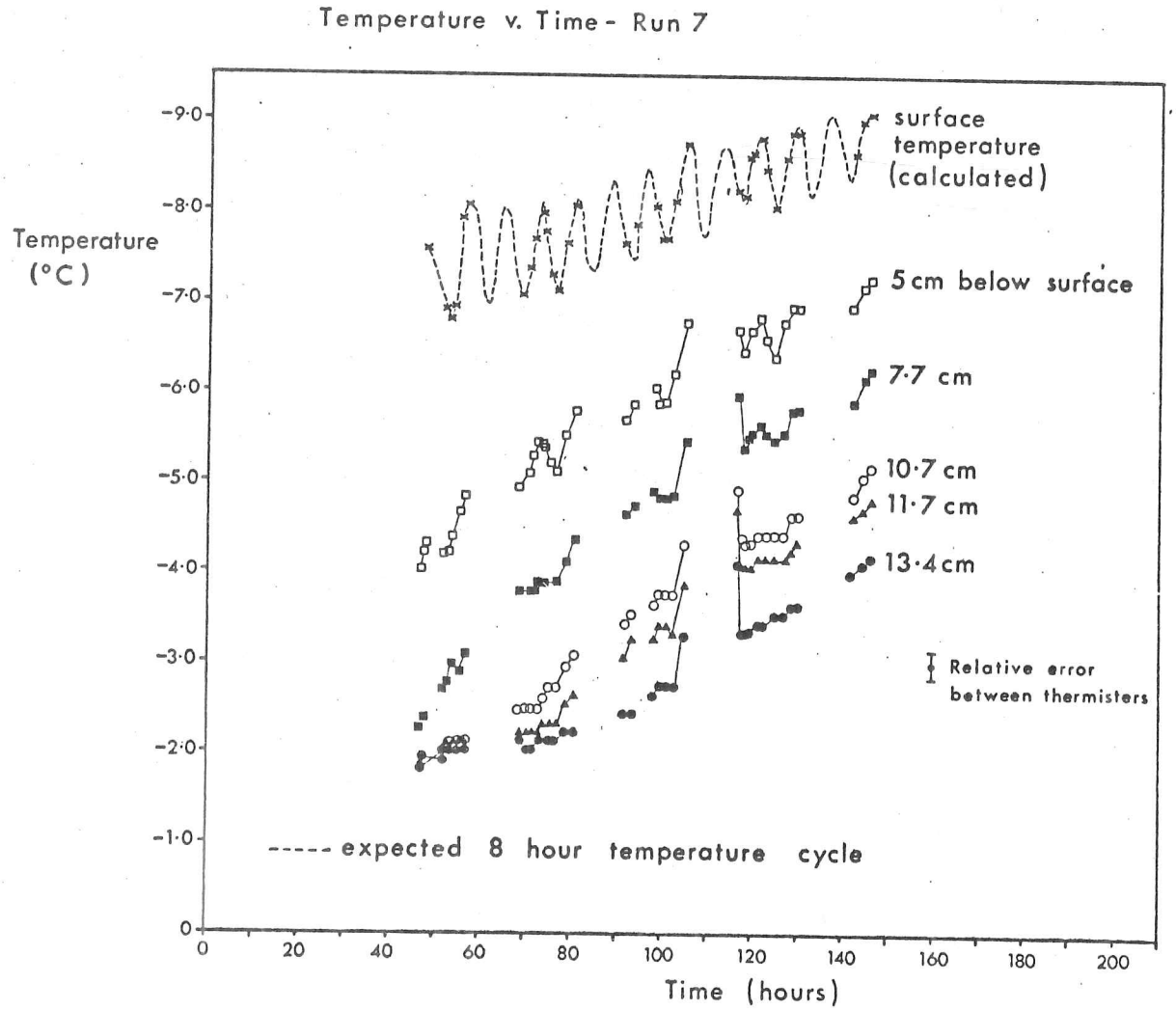

FIGURE A1.3 Temperatures measured with the thermister probe during Run 7. Surface temperature found by extrapolating the vertical temperature gradient to the ice surface. The 8 hour cycle in this surface temperature is due to the cold room control. Temperature increases downwards in this figure.

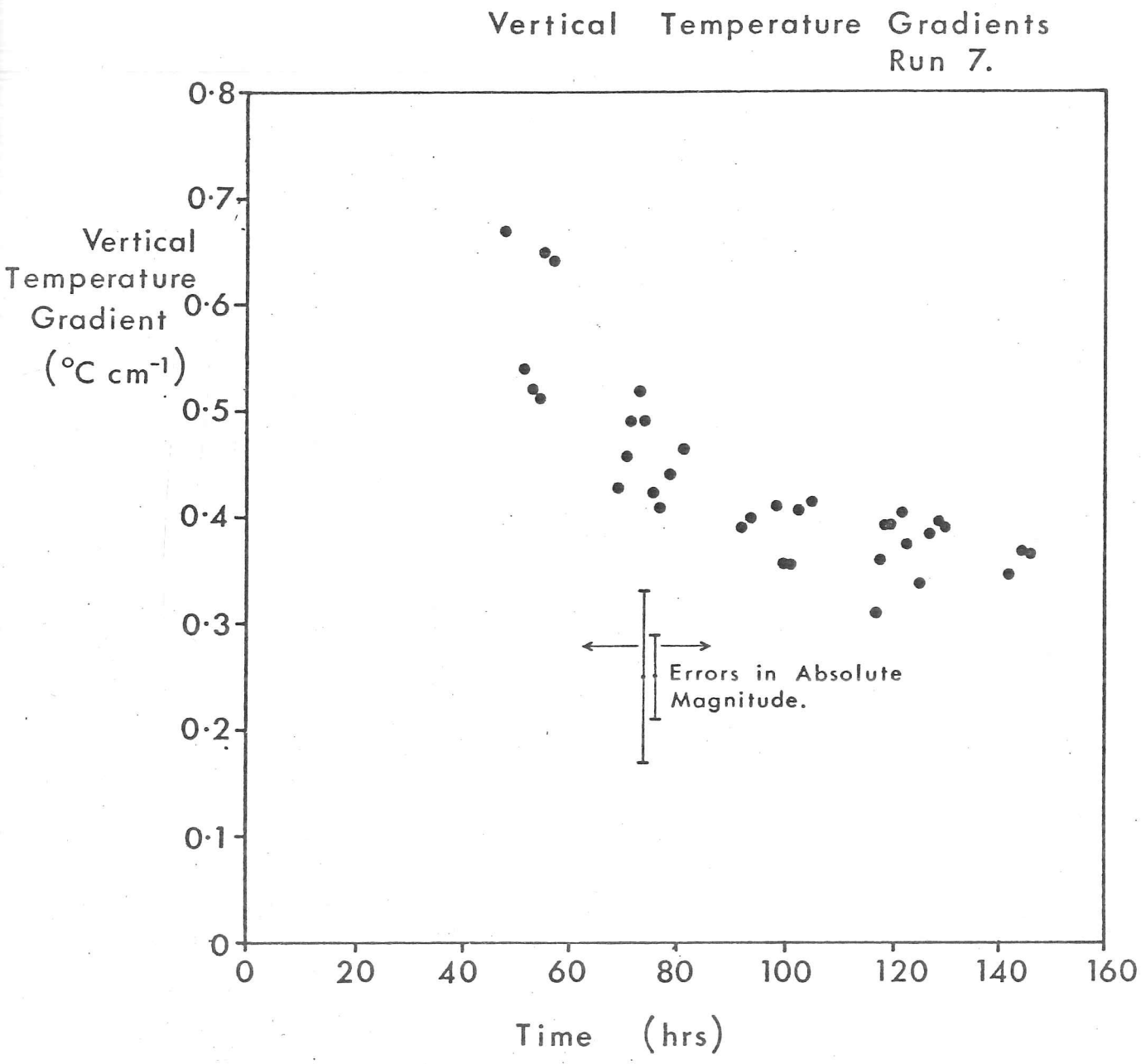

FIGURE A1.4 Measured vertical temperature gradient during Run 7. This is independent of depth in the ice to a good approximation.

differences in this experiment (T = 0.0 to 0.4°C), deviations between thermocouples will be less than 10 μV (Scott, 1941). These deviations are due to inhomogeneities in the thermocouple wire, particularly in the constantan.

The copper-constantan wires were twisted together, soldered to form a junction, varnished with nail polish and placed in 0.2cm diameter tubing to give some rigidity. The insulated copper wires leaving the cold chamber were also twisted together to cut down electromagnetic interference. The output was recorded on a Leeds and Northrup 12 point chart recorder. At the end of the experiment the thermocouples gave no discernible output when all four were placed in a stirred ice-water bath.

A1.3 Run 8 (Saline - Forced Flow)

During this experiment, horizontal and vertical temperature gradients were measured with an array of thermistors. A support, which accurately positioned these in the horizontal plane, was designed and built by Mr. S. Moore. This is shown in place in tank B in figure 3.2.

A1.3.1 Construction of the thermistor array

Thermistors were laid inside 0.5cm diameter perspex tubing which had been machined to form a gutter shape. The beads protruded from the housing and epoxy potting compound and nail polish were used to seal the connecting wires in place. These fine wires were shielded with copper braid and protected with heat shrinkable sleeving at the point where they left the probes. The use of small diameter, insulating tubing ensured a quick response time and minimised the thermal effect of the probes on the ice cover. Three such probes were fixed to a triangular plate, which could be brought into a horizontal position by adjusting the tilt of a shaft supporting it (see figure 3.2). Unfortunately the probes were not rigid and a plastic spacer, placed just above the uppermost thermistor, held them parallel to the shaft. The wires from the thermistors ran to a connector where the fine, high resistance wires were exchanged for wires with a lower resistance per unit length. Thermistor resistance was measured

directly from a Hewlett Packard digital multimeter.

A1.3.2 Calibration and errors

The thermistors were originally calibrated against Beckman thermometers immersed in a constant temperature bath and referenced to an ice-water mixture in a vacuum flask. However, it was obvious during the experiment that the calibration of four of the thermistors had drifted. Fortunately, just prior to and in the early stages of freezing, our system behaves as a constant temperature bath. This fact allowed us to recalibrate all the thermistors against one which was known to be stable. For those thermistors which had not drifted, this gave excellent agreement with the previous determination. There is no evidence of any further drift and we are confident the results are well within the errors we outline below.

(i) Variations in a single thermistor can be determined to $\pm 0.01^{o}C$. This is limited by the resolution of the multimeter. The resistance of the connecting wires was less than the instrument resolution and self-heating effects were not important.

(ii) Temperature determination of one thermistor relative to another has an error of 1% of the difference from $-1^{o}C$. This was estimated graphically from extrapolation from the calibration range, $-0.41^{o}C$ to $-1.72^{o}C$, to the minimum measured value of $-6^{o}C$.

(iii) The absolute calibration of any thermistor has an additional error of $\pm 0.03^{o}C$. We are concerned with absolute measurements only for comparison with freezing points.

A1.3.3 Temperature measurements

Figure 3.2 shows that the probes were mounted in the tank before freezing began with the spacer on the water surface. The uppermost thermistor of probe 1, which will subsequently be referred to as the surface thermistor, was then 0.35cm below the water surface. In the discussion we take this thermistor as our reference for depth since sublimation at the ice surface makes it impossible to find any better

definition. The depths of the thermistors are given below.

	Thermistor Number	Depth (cm)
Probe 1	1	0.00
	2	3.91
	3	7.99
	4	10.06
	5	12.02
Probe 2	6	8.04
	7	10.08
	8	12.06
Probe 3	9	8.05
	10	10.10
	11	12.05

Figure A1.5(a) and (b) show the temperature measurements. The data for probe 2 from 130 hours onwards has been discarded since it appears that the probe was knocked out of thermal contact with the ice. A number of points may immediately be noted from this data.

Firstly we see that activity in the cold room and the additions of cooled brine has a noticable effect on the temperature data; for example, the brine has warmed by 0.1°C when 32 litres of solution were added slowly between t = 75 and 82 hours.

Secondly the measured surface temperatures fluctuate rapidly by 0.5 to 1°C from 70 hours onwards (see figure A1.5(a)) because sublimation exposed this thermistor to the air at approximately 50 hours. At this point, there is also a widening in the difference between the measured temperatures and those found by extrapolating the vertical temperature gradient to the ice surface. These extrapolated values will be rather too high because the release of latent heat within the ice will cause an increase in vertical temperature gradient towards the top of the ice slab. This effect has been illustrated in the laboratory results of Niedrauer and Martin (1979). On the other hand, the temperature measured just above the ice surface will be significantly lower than the actual temperature of the air-ice interface because of the boundary layer in the air and because of the

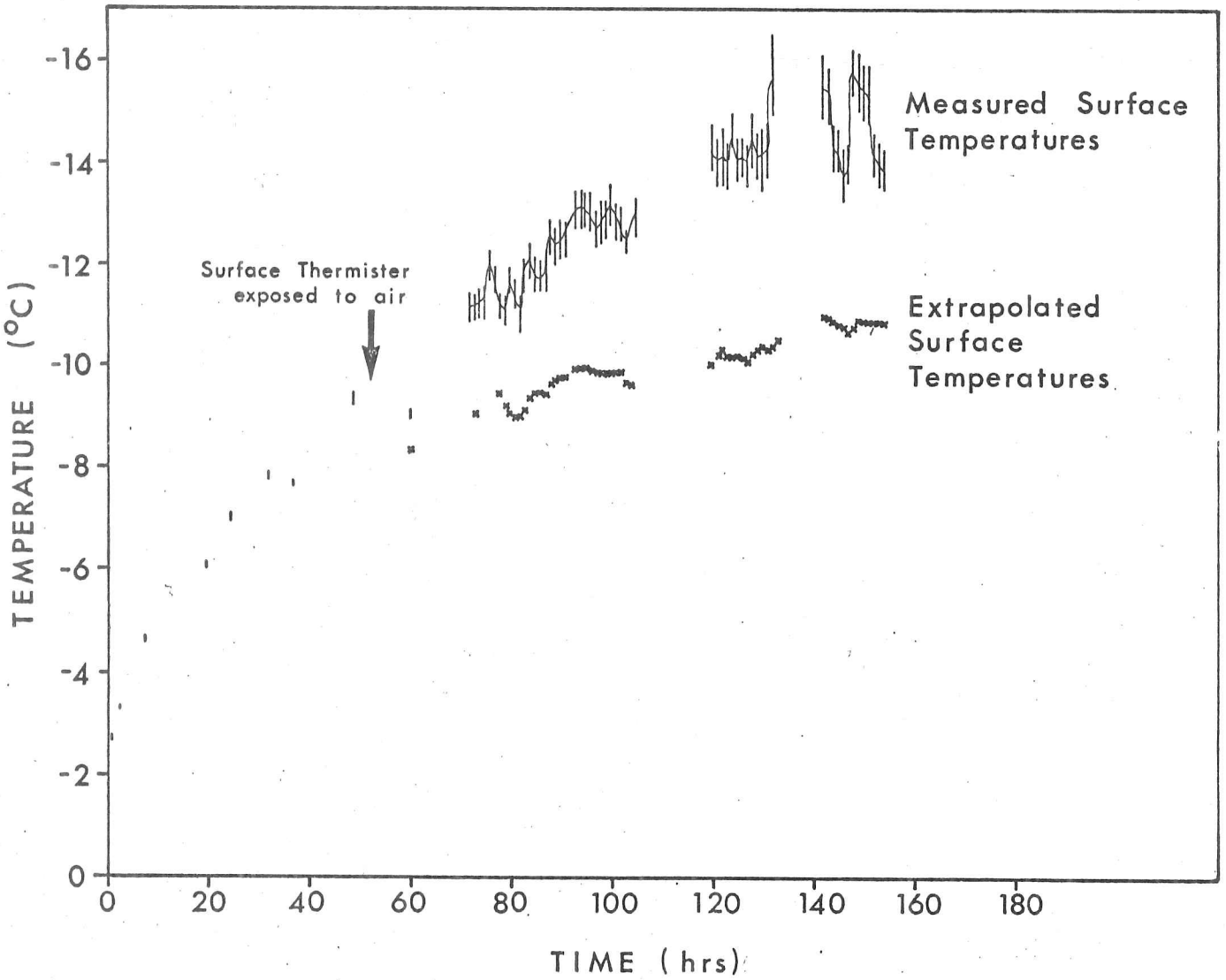

FIGURE A1.5 (a) Range of fluctuation in measured surface temperatures is shown by the length of the line. This thermistor was exposed to the air by sublimation Crosses are the result ofextrapolating the vertical gradient to the surface. The arrow shows the point at which the thermistor left the ice.

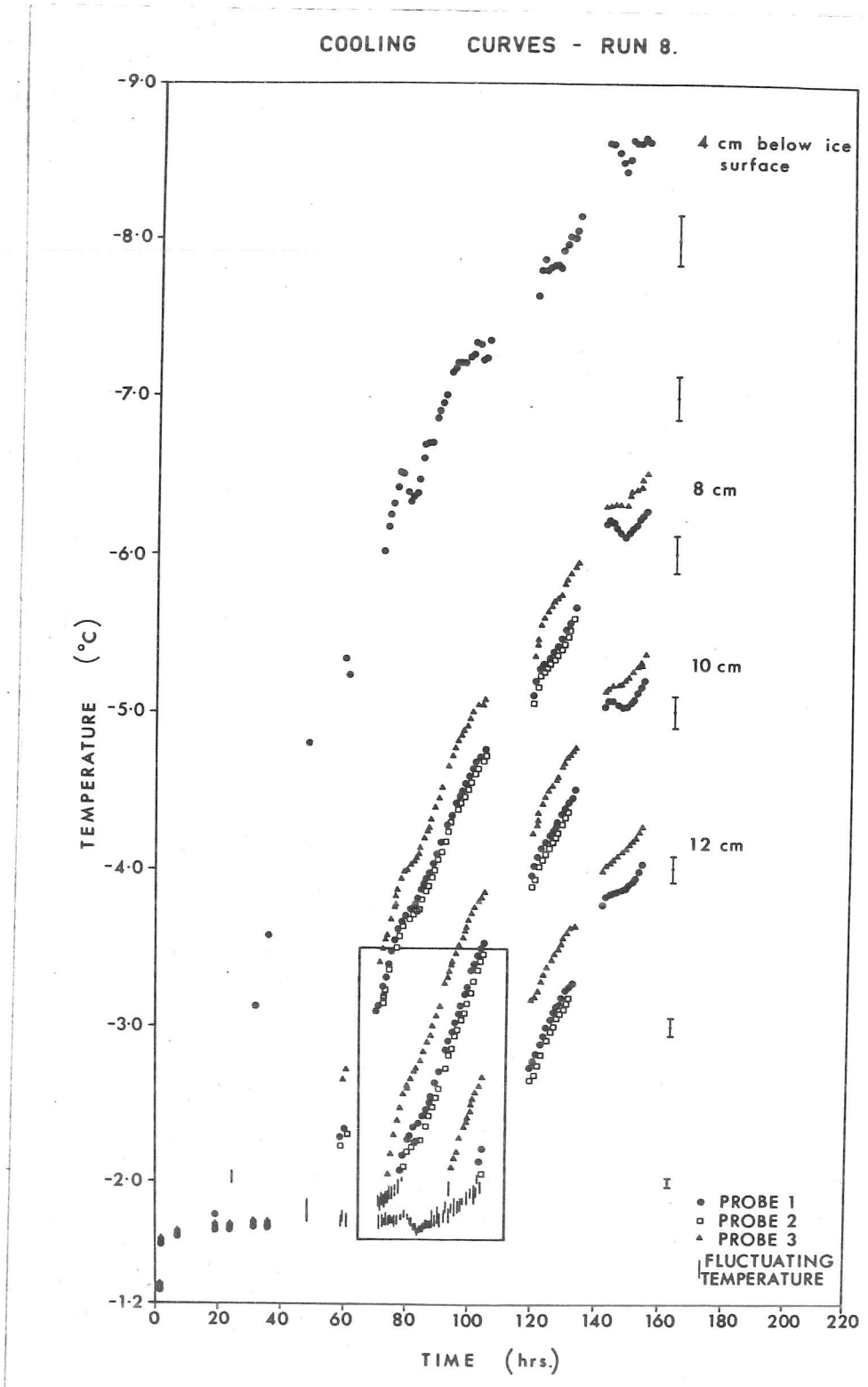

FIGURE A1.5 (b) Diagram showing the rate of change of temperature for the thermistors at approximately 4, 8, 10 and 12cm from the ice surface. The vertical bars show the range over which the temperature was fluctuating at a frequency much greater than 1 hour^{-1}. Error bars are shown for different temperature ranges.

thermal resistance of the surface. [2] The true surface temperature will lie between the "measured" and "extrapolated" values of figure A1.5(a).

A1.3.4 Vertical temperature gradients

The vertical temperature gradients were calculated again by fitting linear temperature profiles. [3] This implies that the decrease in vertical temperature gradient with z, which results from the release of latent heat in the ice, is confined to the upper 4cm and is probably small. Figure A1.6 shows these results for the three probes and where we have sampled hourly the data are joined with a smooth curve. Within the absolute error in magnitude of $\pm 0.03^{o}Ccm^{-1}$ there is no difference in the vertical temperature measured by each of the three probes. The error in the change in gradient is substantially less than this.

A1.3.5 Thermal diffusivity

The thermal diffusivity of the artificial ice can be estimated from the data from probe 1 between 142 and 154 hours. At this time the growth velocity is sufficiently small for there to be negligible ice growth during the time required for the transmission of thermal energy and we thus replace the ice by a slab of constant thickness (Lewis, 1967). Since we do not require the thermal diffusivity with any great accuracy, we make the further approximation that the slab may be replaced by a semi-infinite solid which greatly simplifies the calculation. Figure A1.7 shows the shapes of the temperature wave at depths of 0, 4, 8, 10 and 12 cm in the ice. The amplitude of these are not important for our purposes. Assuming the thermal diffusivity is constant with depth, the velocity of propagation of the minima (joined by a dotted line) is constant and given by (Carslaw and Jaeger, 1959)

---

[2] The thermal resistance of an interface is defined as the reciprocal of the proportionality constant between the heat flux across the interface and the temperature difference between the surface and the surrounding medium. This resistance is 500 to 1000 times greater for a boundary with air than with water (Carslaw and Jaeger, 1959).

[3] This gave correlation coefficients better than 0.9984 and typically 0.9997.

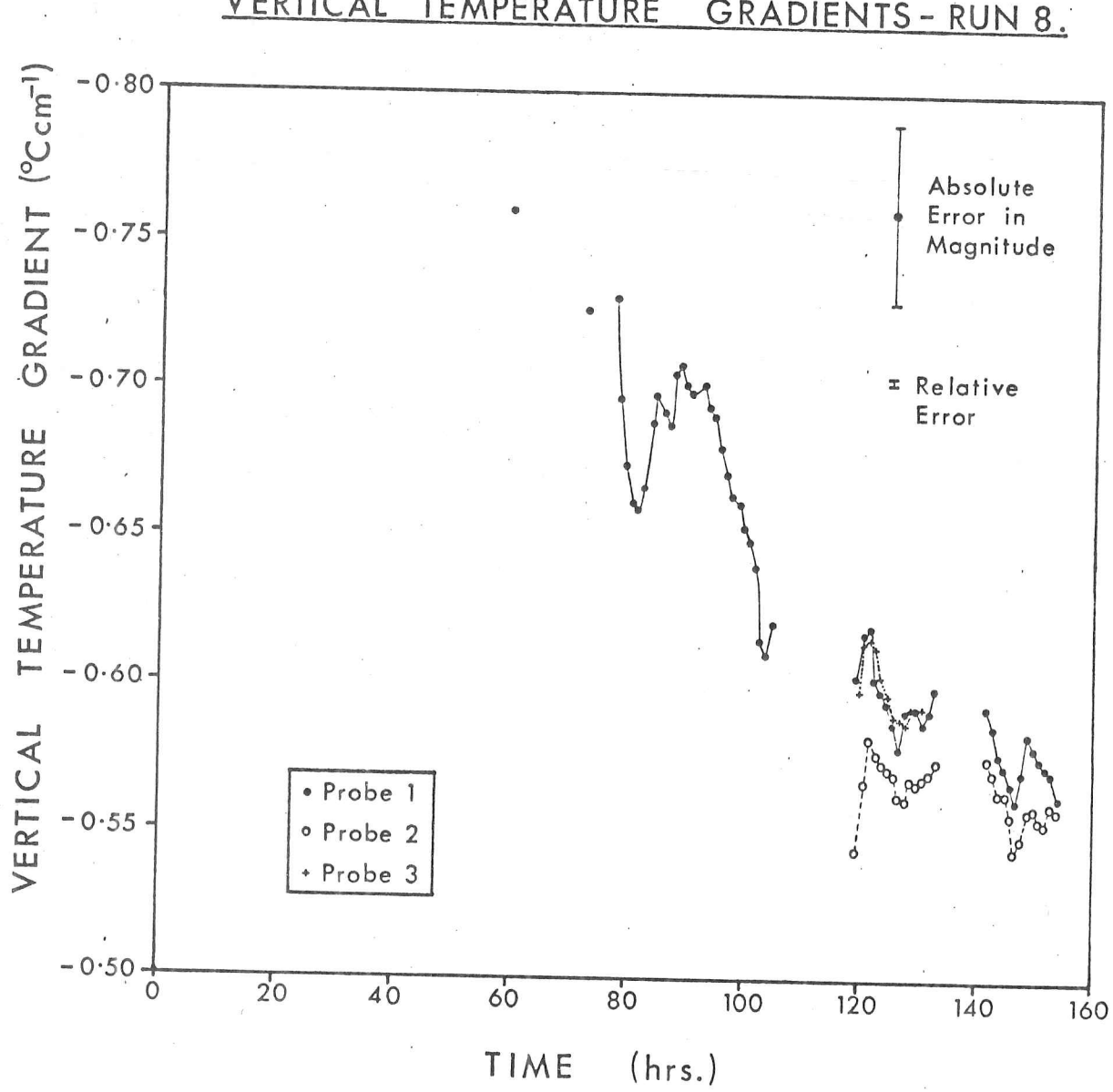

FIGURE A1.6 Measured temperature gradients in the vertical direction on probes 1 to 3 during Run 8.

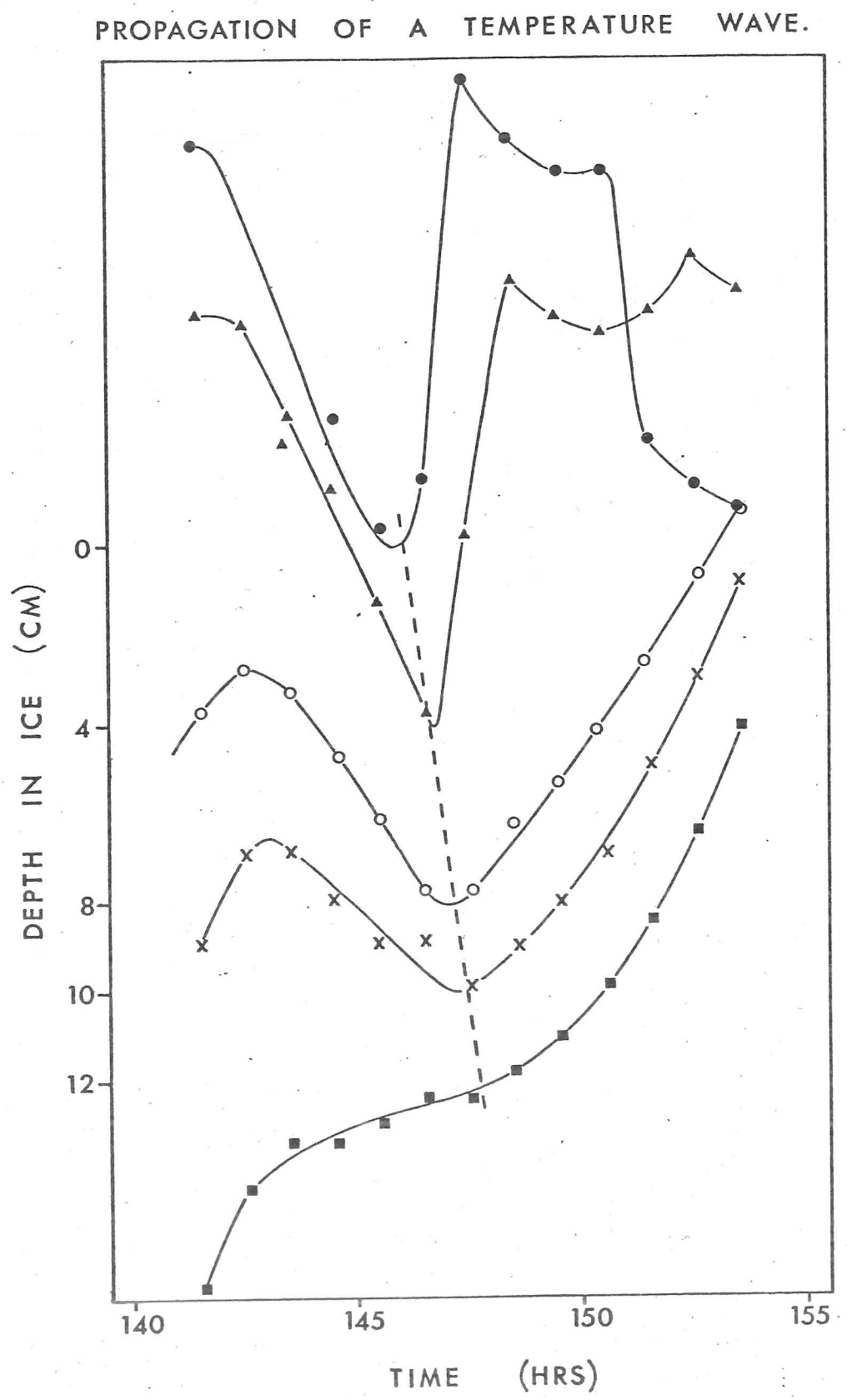

FIGURE A1.7 Diagram showing the temperature wave at 5 depths in the ice. The amplitude of the waves are not to scale. The dotted line shows the progress of the minimum in the z-t plane.

$$(\frac{4\pi K}{\Omega}s)^{\frac{1}{2}} \qquad [A1.1]$$

where Ω= period of the temperature wave. This yields

$$\kappa_s = 9 \pm 3 cm^2 s^{-1}$$

which is close to the value found by Lewis (1967) for thick sea ice. Although the present result and those of Lewis do not agree with the predictions of Schwerdtfeger (1963) for thermal diffusivity, Lewis found reasonable correspondence for other thermal parameters.

BIBLIOGRAPHY

Throughout this bibliography, we use the following abbreviations:

AIDJEX - Arctic Ice Dynamics Joint Experiment, Division of Marine Resources, University of Washington, Seattle, U.S.A.

C-CORE - Centre for Cold Regions Research and Engineering, St John's, Newfoundland, Canada.

CRREL - U.S. Army Cold Regions Research and Engineering Laboratory, Hanover, New Hampshire, U.S.A.

SIPRE - U.S. Army Snow, Ice and Permafrost Research Establishment, as above.

In addition, Problems of the Arctic and Antarctic is translated from Problemy Arktiki i Antarktiki by the Isreal Program for Scientific Translation.

Abe, H. and K. Togano. 1969. Study on the textures of Al-Cu alloy ingots solidified from the flowing liquid. J. Japan Institute of Metals, 33, 970-974.

Abe, H. and K. Togano. 1970. Texture of Zn-Cd alloy solidified from the flowing liquid. J. Japan Institute of Metals, 34, 993-996.

Addison, J.R. 1977. Impurity concentrations in sea ice. J. Glaciol., 18(78), 117-127.

Allen, D.J. and J.D. Hunt. 1979. Temperature gradient zone melting and microsegregation in castings. In Solidification and Casting of Metals, Proceedings of an International Conference on Solidification, Sheffield, U.K., 18-21 July 1977, 39-43.

Annan, A.P. and J.L. Davis. 1976. Impulse radar sounding in permafrost. Radio Science, 11(4), 384-394.

Anderson, D.L. 1958. Model for determining sea ice properties. In Arctic Sea Ice, Proceedings of a Conference, Easton, Maryland, U.S.A., 24-27 Feb. 1958, Publication no. 598, National Academy of Sciences - National

Research Council, Washington, D.C., 106-138.

Anderson, D.L. 1960. The physical constants of sea ice. Research, 13, 310-318.

Anderson, D.L. and W.F. Weeks. 1958. A theoretical analysis of sea-ice strength. Trans. Am. geophys. Un., 39(4), 632-640.

Arakawa, K. 1955. Growth of ice crystals in water. J. Glaciol., 17, 463-464.

Ashton, G.D. 1979. River Ice. Am. Scient., 67(1), 38-45.

Ashton G.D. and J.F. Kennedy. 1970. Temperature and flow conditions during the formation of river ice. Proceedings of an International Symposium on Ice and its Action on Hydraulic Structures, Reykjavic, Iceland, 7-10 Sept. 1970, paper 2.4.

Assur, A. 1958. Composition of sea ice and its tensile strength. In Arctic Sea Ice, Proceedings of a Conference, Easton, Maryland, U.S.A., 24-27 Feb 1958, Publication no. 598, National Academy of Sciences - National Research Council, Washington, D.C., 106-138.

Assur, A. and W.F. Weeks. 1964. Growth,structure and strength of sea ice. CRREL Research Rep. 135, 19pp.

Bardsley, W., J.M. Callan, H.A. Chedzey and D.T.J. Hurle. 1961. Constitutional supercooling during crystal growth from stirred melts - II. Experimental: Gallium - doped germanium. Solid-St. Electron., 3, 142-154.

Bardsley, W., J.B. Mullin and D.T.J. Hurle. Microsegregation and defect generation during the controlled solidification of semiconductors. In The Solidification of Metals, ed. B.W. Berry, Proceedings of a Conference, Brighton, U.K., 4-7 Dec. 1967, Iron and Steel Institute Publication 110, 93-101

Bardsley W., D.T.J. Hurle, M. Hart and A.R. Lang. 1980. Structural and chemical in homogeneities in germanium single crystals grown under conditions of constitutional supercooling. J. Crystal Growth, 49, 612-630.

Beaubouef, R.T. and A.J. Chapman. 1967. Freezing of fluids in forced flow. Int. J. Heat Mass Transfer, 10(11), 1581-1587.

Beeley, P.R. 1979. Solidification and aspects of cast metal quality. In Solidification and Casting of Metals, Proceedings of a Conference on Solidification, Sheffield, U.K., 18-21 July 1977, 319-324.

Belyakov, L.N. 1974. Hydromechanical peculiarities of the underice layer. Problems of the Arctic and Antarctic, 44, 184-191.

Bennington, K.O. 1963a. Some chemical composition studies on Arctic sea ice. In Ice and Snow, Properties, Processes and Applications, ed. W.D. Kingery, M.I.T. Press, Cambridge, U.S.A., 248-257.

Bennington, K.O. 1963b. Some crystal growth features of sea ice. J. Glaciol., 4(36), 669-689.

Bennington, K.O. 1967. Desalination features in natural sea ice. J. Glaciol., 6(48), 845-857.

Bennington, K.O. 1968. Crystal and brine relationships in sea ice. In Arctic Drifting Stations, ed J.E. Sater, Proceedings of a Symposium, Warrenton, Virginia, U.S.A., April 1966, 181-189.

Bolling, G.F. and W.A. Tiller. 1960. Growth from the melt. Part II. Cellular interface morphology. J. appl. Phys., 31(11), 2040-2045.

Budd, W.F. 1972. The development of crystal orientation fabrics in moving ice. Z. Gletscherk. Glazialgeol., Bd VIII, Heft 1-2, 65-105.

Burton, J.A., R.C. Prim and W.P. Slichter. 1953. The distribution of solute in crystals grown from the melt. Part I. Theoretical. J.chem. Phys., 21(11), 1987-1996.

Buynitskiy, V. Kh. 1967. Structure, principal properties and strength of Antarctic sea ice. Soviet Antarctic Expedition Information Bulletin, 6(6), 504-510.

Campbell, K.J. and A.S. Orange. 1974a. A continuous profile of sea ice and freshwater ice thickness by impulse radar. Polar Rec., 17(106), 31-41.

Campbell, K.J. and A.S. Orange. 1974b. The electrical anisotropy of sea ice in the horizontal plane. J. geophys. Res., 79(33), 5059-5063.

Cantor, B. and A. Vogel. 1977. Dendritic solidification and fluid flow. J. Crystal Growth, 41, 109-123.

Carslaw, H.S. and J.C. Jaeger. 1959. Conduction of Heat in Solids, Oxford University Press, London, U.K., 2nd ed., 510pp.

Chayes, F. 1956. Petrographic Modal Analysis, Wiley and Sons, 113pp.

Cherepanov, N.V. 1964. Structure of sea ice of great thickness. Tr. Arkt. i Antarkt. N.-I. Instituta, 267, Translation by E.R. Hope, 13-18.

Cherepanov, N.V. 1968. Role of thermal regime of the water body in formation of crystal structure of ice. Problems of the Arctic and Antarctic, 29, 56-69.

Cherepanov, N.V. 1971. Spatial arrangement of sea ice crystal structure. Problems of the Arctic and Antarctic, 38, 176-181.

Cherepanov, N.V. 1972. Classification of the crystalline structure of Arctic ice. Problems of the Arctic and Antarctic, 40, 75-80.

Cherepanov, N.V. 1973. Main results of an investigation of the crystal structure of sea ice. Problems of the Arctic and Antarctic, 41, 55-68.

Chikovskii, S.S. 1978. The role of Antarctic ice shelves in the formation of frazil ice. Materialy Glyatsiologicheskikh Issledovaniy Khronika Obsuzhdeniya, 34, 205-210, (English summary).

Coachman, L.K. 1966. Production of supercooled water during sea ice formation. ed. J.O. Fletcher. Proceedings of a Conference on Arctic Heat Budget and Atmospheric Circulation, Lake Arrowhead, California, U.S.A., 497-529.

Cole, G.S. 1967. Temperature measurements and fluid flow distributions ahead of solid-liquid interfaces. Trans. metall. Soc. A.I.M.E., 239(9), 1287-1295.

Cole, G.S. 1971. Transport processes and fluid flow in solidification. In Solidification, ed. T.J. Hughel and G.F. Bolling, Seminar of the American Society for Metals, Cleveland, Ohio, 11-12 Oct 1969, 201-266

Cole G.S. and G.F. Bolling. 1965. The importance of natural convection in casting. Trans. metall. Soc. A.I.M.E., 233(8), 1568-1572.

Cole G.S. and G.F. Bolling. 1966. Augmented natural convection and equiaxed grain structure in casting. Trans. metall. Soc. A.I.M.E., 236(9), 1366-1368.

Cole G.S. and G.F. Bolling. 1967. Enforced fluid motion and control of grain structures in metal castings. Trans. metall. Soc. A.I.M.E., 239(11), 1824-1835.

Cole G.S. and G.F. Bolling. 1968. Importance of fluid motion during ingot solidification. In The Solidification of Metals, ed. B.W. Berry, Proceedings of a Conference, Brighton, U.K., 4-7 Dec. 1967, Iron and Steel Institute Publication 110, 323-329.

Copley, S.M., A.F. Giamei, S.M. Johnson and M.F. Hornbecker. 1970. The origin of freckles in unidirectionally solidified castings. Metallurgical Transactions, 1, 2193-2204.

Coriell, S.R., D.T.J. Hurle and R.F. Sekereka. 1976. Interface stability during crystal growth: the effect of stirring. J.Crystal Growth, 32, 1-7.

Coriell, S.R., M.R. Cordes, W.J.Boettinger and R.F. Sekerka. 1980. Convective and interfacial instabilities during unidirectional solidification of

a binary alloy. J. Crystal Growth, 49, 13-28.

Cox, G.F.N. and W.F. Weeks. 1974. Salinity variations in sea ice. J. Glaciol., 13(67), 109-120.

Cox, G.F.N. abd W.F. Weeks. 1975. Brine drainage and initial salt entrapment in NaCl ice. CRREL Research Rep. 345, 85pp.

Dawson, D.A. and O. Trass. 1972. Mass transfer at rough surfaces. Int. J. Heat Mass Transfer, 15, 1317-1336.

Delves, R.T. 1968. Theory of stability of a solid-liquid interface during growth from a stirred melt. J. Crystal Growth, 3,4, 562-568.

Delves, R.T. 1971. Theory of the stability of a solid-liquid interface during growth from a stirred melt II. J. Crystal Growth, 8, 13-25.

Delves, R.T. 1974. Theory of interface stability. In Crystal Growth, ed. B.R. Pamplin, Pergamon Press, 40-103.

Doherty, B.T. and D.R. Kester. 1974. Freezing point of sea water. J.mar. Res., 32(2), 285-300.

Donaghey L.F. and W.A. Tiller. 1968. On the diffusion of solute during the cellular mode of crystallisation. In The Solidification of Metals, ed. B.W. Berry, Proceedings of a Conference, Brighton, U.K., 4-7 Dec. 1967, Iron and Steel Institute Publication 110, 89-92.

Doronin, Yu.P. and D.Ye. Kheysin. 1975. Sea Ice, Published for Office of Polar Programs and National Science Foundation, Washington, D.C. by Amerind Publishing Co., Pvt. Ltd., New Delhi, 1977, 322pp.

Eide, L.I. and S. Martin. 1975. The formation of brine drainage features in young sea ice. J. Glaciol., 14(70), 137-154.

Farhadieh, R. and R.S.Tankin. 1972. Interferometric study of freezing of sea water. J. geophys. Res., 77(9), 1647-1657.

Farhadeih, R. and R.S. Tankin. 1975. A study of the freezing of sea water. J.Fluid Mech., 72(2), 293-304.

Farrar, J. and W.S. Hamilton. 1965. Nucleation and growth of ice crystals. U.S. Department of the Interior, Research and Development Progress Rep. No. 127, 51pp.

Fertuck, L., J.W. Spyker and W.H.W. Husband. 1972. Computing salinity profiles in ice. Can. J. Phys., 50(3), 264-267.

Fine, M.E. 1964. Phase Transformations in Condensed Systems, Macmillan Co., New York, U.S.A., 133pp.

Flemings, M.C. 1974. Solidification Processing, McGraw-Hill, New York, U.S.A., 364pp.

Fletcher, N.H. 1970. The Chemical Physics of Ice, Cambridge University Press, Cambridge, U.K, 271pp.

Foster, T.D. 1965. Stability of a homogeneous fluid cooled uniformly from above. Physics Fluids, 8, 1249-1257.

Foater, T.D. 1968. Haline convection induced by the freezing of sea water. J. geophys. Res., 73(6), 1933-1938.

Foster, T.D. 1969. Experiments on haline convection induced by the freezing of sea water. J. geophys Res., 74(28), 6967-6974.

Foster, T.D. 1972. Haline convection in polynyas and leads. J. Phys. Oceanography, 2(4), 462-469.

Frankenstein G. and R. Garner. 1967. Equations for determining the brine volume of sea ice from -0.5°C to -22.9°C. J. Glaciol., 6(48), 943-944.

Fujino, K., E.L. Lewis and R.G. Perkin. 1974. The freezing point of sea water at pressures up to 100 bars. J. geophys. Res., 79(12), 1792-1797.

Gee, D.L. and R.L. Webb. 1980. Forced convection heat transfer in helically rib-roughened tubes. Int. J. Heat Mass Transfer, 23, 1127-1136.

Giamei, A.F. and B.H. Kear. 1970. On the nature of freckles in nickel base superalloy. Metallurgical Transactions, 1, 2185-2192.

Gilpin, R.R., H. Imura and K.C. Cheng. 1978. Experiments on the onset of longitudinal vortices in horizontal Blasius flow heated from below. J. Heat Transfer, 100, 71-77.

Gilpin, R.R., T. Hirata and K.C. Cheng. 1980. Wave formation and heat transfer at an ice-water interface in the presence of a turbulent flow. J. Fluid Mech., 99(3), 619-640.

Golden, K.M. and S.F. Ackley. 1980. Modeling of anisotropic electromagnetic reflection from sea ice. Proceedings of an International Workshop on Remote Estimation of Sea Ice Thickness, St John's, Newfoundland, 25-26 Sept. 1979, 247-294.

Gow, A.J. 1980. Time priority studies of deep ice cores. In, Ice Cores, compiled by P.K. Mackinnon, World Data Centre A for Glaciology Rep. GD-8, 91-97.

Gow, A.J. and W.F. Weeks. 1977. The internal structure of fast ice near Narwhal Island, Beaufort Sea, Alaska. CRREL Rep. 77-29, 8pp.

Gow, A.J., S.F. Ackley, W.F. Weeks and J.W. Govoni. 1982. Physical and structural characteristics of Antarctic sea ice. Annals of Glaciology, 3, 113-117.

Greenspan, H.P. 1968. The Theory of Rotating Fluids, Cambridge University Press, Cambridge, U.K., 328pp.

Gross, G.W., G. M^{c}Kee and Wu Chen-Lo. 1975. Concentration dependant solute redistribution at the ice/water phase boundary. 1. Analysis. J. chem. Phys., 62 (8), 3080-3084.

Gross, G.W., P.M. Wong and K. Humes. 1977. Concentration dependent solute redisribution at the ice-water phase boundary. III. Spontaneous convection chloride solutions. J. chem Phys., 67(11), 5264-5273.

Hamalainen, M. 1967. Constitutional supercooling in the presence of convection cells. J. Crystal Growth, 1, 125-130.

Hardy, S.C. 1977. A grain boundary groove measurement of the surface tension between ice and water. Phil. Mag., 35(2), 471-484.

Hardy, S.C. and S.R. Coriell. 1968. Morphological stability and the ice-water interfacial free energy. J. Crystal Growth, 3,4, 569-573.

Hardy, S.C. and S.R. Coriell. 1973. Surface tension and interface kinetics of ice crystals freezing anf melting in sodium chloride solutions. J. Crystal Growth, 20, 292-300.

Harrison, J.D. 1965. Solute transpiration pores in ice. J. appl, Phys., 36 (1), 326-327.

Harrison, J.D. and W.A. Tiller. 1963a. Controlled freezing of water. In Ice and Snow, Properties, Processes and Applications, ed. W.D. Kingery, M.I.T. Press, Cambridge, U.S.A., 215-225.

Harrison, J.D. and W.A. Tiller. 1963b. Ice interface morphology and texture developed during freezing. J. appl. Phys., 34(11), 3349-3355.

Healey, D.A. 1971. Oceanographic observations in the Beaufort Sea, July 15-Sept. 4, 1970. Pacific Marine Science Rep. 71-3, Dept. of Fisheries and Forestry, Marine Services Branch, Victoria, B.C., Canada, 36pp.

Herlinveaux, R.H. and B.R. de Lange Boom. 1976. Physical oceanography of the southeastern Beaufort Sea. Beaufort Sea Project Tech. Rep. 18, 96pp.

Herlinveaux, R.H., B.R. de Lange Boom and G.R. Wilton. 1976. Water movements in the Beaufort Sea, summer 1974, spring and summer 1975. Pacific Marine Science Rep. 76-27, Institute of Ocean Sciences, Patricia Bay, Victoria,

B.C., Canada, 69pp.

Hillig, W.B. 1958. The kinetics of freezing of ice in the direction perpendicular to the basal plane. In Growth and Perfection of Crystals, Proceedings of a Conference on Crystal Growth, Cooperstown, New York, 27-29 Aug. 1958, John Wiley, New York, U.S.A., 350-360.

Hirata T., R.R. Gilpin, K.C. Cheng and E.M. Gates. 1979a. The steady state ice layer profile on a constant temperature plate in a forced convection flow -I Laminar regime. Int. J. Heat Mass Transfer, 22, 1425-1433.

Hirata T., R.R. Gilpin and K.C. Cheng. 1979b. The steady state ice layer profile on a constant temperature plate in a forced convection flow -II The transition and turbulent regimes. Int. J. Heat Mass Transfer, 22, 1435-1443.

Hobbs, P.V. 1974. Ice Physics, Clarendon Press, Oxford, UK, 837pp.

Hooke, R.Le B. and P.J. Hudleston. 1981. Ice fabrics from a borehole at the top of the south dome, Barnes Ice Cap, Baffin Island. Bull. geol. Soc. Am., Pt. I, 92(5), 274-281.

Huang, J.S. 1975. The effect of natural convection on ice crystal growth in salt solutions, Ph.D. dissertation, Syracase Univ., U.S.A..

Hunkins, K. 1972. Water stress and ocean current measurements at Camp 200, 1971. AIDJEX Bulletin No.12, 35-60.

Hunkins, K. and M. Fliegel. 1974. Ocean current observations at the AIDJEX 1972 Main Camp. AIDJEX Bulletin No.26, 75-108.

Hunt, J.D. 1979. Cellular and primary dendrite spacings. In Solidification and Casting of Metals, Proceedings of an International Conference on Solidification, 18-21 July 1977, Sheffield, UK, 3-9.

Hunt, J.C.R. 1980. Wind over hills. Amer. Met. Soc. Publication.

Hunt, M.D., J.A. Spittle and R.W. Smith. 1968. Cellular growth in metallic crystals pulled from a stirred melt. In The Solidification of Metals, ed B.W. Berry. Proceedings of a Conference, Brighton, UK, 4-7 Dec. 1967, Iron and Steel Inst. Publication 110, 57-60.

Hurle, D.T.J. 1961. Constitutional supercooling during crystal growth from stirred melts - I Theoretical. Solid-St. Electron., 3, 37-44.

Hurle, D.T.J. 1969. Interface stability during the solidification of a stirred binary-alloy melt. J. Crystal Growth, 5, 162-166.

Hurle, D.T.J. E. Jakeman and C.P. Johnson. 1974. Convective temperature oscillations in molten gallium. J. Fluid Mech., 64(3), 565-576.

James, D.W. 1966. On the nature of the solid/liquid interface at the onset of constitutional supercooling. Trans. metall. Soc. A.I.M.E., 236(6), 936.

Jones, D.R.H. 1973a. The temperature gradient migration of liquid droplets through ice. J. Crystal Growth, 20, 145-151.

Jones, D.R.H. 1973b. The measurement of solid-liquid interfacial energies from the shapes of grain boundary grooves. Phil. Mag., 27(3), 569-584.

Jones, D.R.H. and G.A. Chadwick. 1971. The experimental determination of the kinetics of solid-liquid interfaces in transparent materials using temperature gradient zone migration. Phil. Mag., 24(192), 1327-1345.

Jones, D.R.H. 1978. The migration of grain boundary grooves at the solid-liquid interface. Acta metall., 26, 689-694.

Kader, B.A. and A.M. Yaglom. 1972. Heat and mass transfer laws for fully turbulent wall flows. Int. J. Heat Mass Transfer, 8, 639-653.

Kader, B.A. and A.M. Yaglom. 1977. Turbulent heat and mass transfer from a wall with parallel roughness ridges. Int. J. Heat Mass Transfer, 20, 345-357.

Kaempffer F. and F. Weinberg. 1971. Interdendritic fluid flow in Pb-Sn alloy. Metallurgical Transactions, 2, 3051-3054.

Kamb, B.W. 1959a. Theory of preferred crystal orientation developed by crystallisation under stress. J. Geol., 67(2), 153-170.

Kamb, B.W. 1959b. Ice petrofabric observations from Blue Glacier, Washington, in relation to theory and experiment. J. geophys. Res., 64(11), 1891-1909.

Katsaros, K.B. 1973. Supercooling on the surface of an Arctic lead. J. Phys. Oceanography, 3(4), 482-486.

Kawamura, T. and N. Ono. 1980. Freezing phenomena at sea water surface opening in polar winter III Measurement of crystallographic orientation of newly grown sea ice. Low Temp. Sci Ser. A, 39, 175-180.

Kay, J.M. and R.M. Nedderman. 1974. Fluid Mechanics and Heat Transfer, Cambridge Univ. Press, UK, 3rd ed., 322pp.

Ketcham, W.M. and P.V. Hobbs. 1967. The preferred orientation in the growth of ice from the melt. J. Crystal Growth, 1, 263-270.

Ketcham, W.M. and P.V. Hobbs. 1968. Step growth on ice during freezing of pure water. Phil. Mag., 18(153), 659-661.

Ketcham, W.M. and P.V. Hobbs. 1969a. Direct measurements of the ice-water interfacial temperature for two crystallographic orientations during

the freezing of pure water. J. Crystal Growth, 6, 113-115.

Ketcham, W.M. and P.V. Hobbs. 1969b. An experimental determination of the surface energies of ice. Phil. Mag., 19, 1161-1173.

Kingery W.D. and W.H. Goodnow. 1963. Brine migration in salt ice. In Ice and Snow, Properties, Processes and Applications, ed. Kingery, M.I.T. Press, Cambridge, Mass., U.S.A., 237-247.

Knight, C.A. 1962a. Studies of Arctic lake ice. J. Glaciol., 4(33), 319-336.

Knight, C.A. 1962b. Crystal growth of ice on surfaces. J. appl. Phys., 33(5), 1808-1815.

Knight, C.A. 1966. Grain boundary migration and other processes in the formation of ice sheets on water. J. appl. Phys., 37(2), 568-574.

Knight, C.A. 1967. The Freezing of Supercooled Liquids, Van Nostrand Co., Princeton, New Jersey, U.S.A., 145pp.

Knight, C.A. and N.C. Knight. 1968. Orientation fabrics in sea ice. In Arctic Drifting Stations, ed. J.E. Sater. Proceedings of a Symposium, Warrenton, Virginia, U.S.A., April 1966, 217-225.

Kohnen, H. 1975. On the D.C. resistivity of sea ice. Z. Gletscherk. Glazialgeol., 11(2), 143-154.

Kolmogorov, A.N. 1949. Geometric selection of crystals. Doklady Akademii Nauk SSSR, 65(5), 681-684 (Russian).

Kovacs, A. 1979. Oil pooling under sea ice. Environmental Assessment of the Alaskan Continental Shelf, Annual Rep. of the Principal Investigators, March 1979, Vol. VIII, Transport, 310-353.

Kovacs, A. and R.M. Morey. 1978. Radar anisotropy of sea ice due to preferred azimuthal orientation of the horizontal c-axes of ice crystals. AIDJEX Bulletin No.38, 171-201.

Kovacs, A. and R.M. Morey. 1979. Anisotropic properties of sea ice in the 50-150 MHz range. J. geophys. Res., 84(C9), 5749-5759.

Kvajic, G., V. Brajovic and E.R. Pounder. 1968. Rejection of impurities by growing ice from a melt. In Physics of Ice, ed. N. Riehl, B. Bullemer & H. Engelhardt. Proceedings of an International Conference on the Physics of Ice, Munich, West Germany, Plenum, New York, U.S.A., 120-131.

Kvajic, G. and V. Brajovic. 1970. Segregation of $(^{134}Cs)^{+}$ impurity during growth of polycrystalline ice. Can. J. Phys., 48, 2877-2887.

Kvajic, G. and V. Brajovic. 1971. On anisotropy of growth of polycrystalline ice in constitutionally supercooled water. Can. J. Phys., 49(14),

1861-1864.

Kvajic, G., E.R. Pounder and V. Brajovic. 1971. Instability of smooth-planar solid-liquid interface on an ice crystal growing from the melt. Can. J. Phys., 49(21), 2636-2645.

Kvajic, G., V. Brajovic, M. Milosevic-Kvajic and E.R. Pounder. 1973. Selective growth of ice crystals from dilute water solution. In Physics and Chemistry of Ice, ed. E. Whalley, S.J. Jones & L.W. Gold. Proceedings of a Symposium, Ottawa, Canada, 251-255.

Lake R.A. and E.L. Lewis. 1970. Salt rejection by sea ice during growth. J. geophys. Res., 75(3), 583-597.

Lake, R.A. and E.L. Lewis. 1972. The microclimate beneath growing sea ice. In Sea Ice, Proceedings of an International Conference, Reykjavik, Iceland, 241-245.

Landauer, J.K. and H. Plumb. 1956. Measurements on anisotropy of thermal conductivity of ice. U.S. Army SIPRE Research Rep. 16, 4pp.

Langhorne, P.J. 1980. Crystal anisotropy in sea ice. Proceedings of the International Workshop on Remote Estimation of Sea Ice Thickness, St. Johns, Nfld, 25-26 Sept. 1979, 189-224.

Langhorne, P.J., J.R. Rossiter and T.E. Keliher. 1980. Remote estimation of the properties of sea ice, ice core analysis, Beaufort Sea, March 1979. Scott Polar Research Institute Rep. 80-1, and C-CORE Rep. 80-7, 172pp.

Langway, C.C. 1958. Ice fabrics and the universal stage. US Army SIPRE Tech. Rep. 62, 16pp.

Lapadula, C. and W.K. Mueller. 1966. Heat conduction with solidification and a convective boundary condition at the freezing front. Int. J. Heat Mass Transfer, 9, 702-704.

Lasca, N.P. 1971. River-ice fabrics : Preliminary results. J. Glaciol., 10(58), 151-152.

Lewis, E.L. 1967. Heat flow through winter ice. In Physics of Ice and Snow, ed. H.Oura. International Conference on Low Temperature Science, Sappora, Japan, 1966, 611-631.

Lewis E.L. and R.A. Lake. 1971. Sea ice and supercooled water. J. geophys. Res., 76(24), 5836-5841.

Lewis E.L. and A.R. Milne. 1977. Underwater sea ice formations. In Polar Oceans, ed. M.J. Dunbar. Proceedings of the Polar Oceans Conference, M^{c}Gill Univ., Montreal, Canada, May 1974, 239-245.

Lewis, E.L. and E.R. Walker. 1970. The water structure under a growing ice sheet. J. geophys. Res., 75(33), 6836-6845.

Lewis, E.L. and W.F. Weeks. 1970. Sea ice : Some polar contrasts. Symposium on Antarctic Ice and Water Masses, Tokyo, Japan, 23-34.

Ling, Chi-Hai and N Untersteiner. 1974. On the calculation of the roughness parameter of sea ice. AIDJEX Bulletin No.23, 117-125.

Lofgren, G. and W.F. Weeks. 1969. Effect of growth parameters on substructure spacing in NaCl. J. Glaciol., 8(52), 153-165.

M^{c}Donald, R.J. and J.D. Hunt. 1969. Fluid motion through the partially solid region of a casting and its importance in understanding A-type segregation. Trans. metall. Soc. A.I.M.E., 245, 1969-1993.

M^{c}Phee, M.G. 1980. Physical oceanography of the seasonal ice zone. Cold Regions Science and Technology, 2, 94-118.

M^{c}Phee, M.G. and J. Dungan Smith. 1975. Measurements of the turbulent boundary layer under pack ice. AIDJEX Bulletin No.29, 49-92.

Malmgren, F. 1927. On the properties of sea ice. In The Norwegian North Polar Expedition with the "Maud" 1918-1929. Scientific Results, 1(5), 67pp.

Mardia, K.V. 1962. Statistics of Directional Data, Academic Press, Lond., UK, 357pp.

Martin, S. 1974. Ice stalactites: comparison of a laminar flow theory with experiment. J. Fluid Mech., 63(1), 51-79.

Martin, S. 1979. A field study of brine drainage and oil entrainment in first-year sea ice. J. Glaciol., 22(88), 473-502.

Martin, S. 1981. Frazil ice in rivers and lakes. A. Rev. Fluid Mech., 13, 379-397.

Martin, S. and P. Kauffman. 1981. A field and laboratory study fo wave damping by grease ice. J. Glaciol., 27(96), 315-330.

Martin, S. P. Kauffman and P.E. Welander. 1976. A laboratory study of the dispersion of crude oil within sea ice grown in a wave field. In Science in Alaska, Proceedings of the 27th Alaska Science Conference, Vol.II, Fairbanks, Alaska, U.S.A., 261-287.

Matthews, J.B. 1981a. Observations of surface and bottom currents in the Beaufort Sea near Prudhoe Bay, Alaska. J. geophys. Res., 86(C7), 6653-6660.

Matthews, J.B. 1981b. Observations of under-ice circulation in a shallow lagoon in the Alaskan Beaufort Sea. Ocean Management, 6, 223-234.

Mel'nichenko, N.A., V.I. Mikhaylov and V.I. Chiyhik. 1979. Studies of the temperature-dependence of the brine content of sea ice by the pulse N.M.R. method. CRREL Draft Translation 757, Feb. 1981, 6pp (Transln. from Okianologiya, 19(5), 811-814).

Michaels, A.S., P.L.T. Brian and P.R. Sperry. 1966. Impurity effects on the basal plane solidification kinetics of supercooled water. J. appl. Phys., 37(13), 4649-4661.

Michel, B. and R.O. Ramseier. 1971. Classification of river and lake ice. Can. geotech. J., 8(1), 36-45.

Miksch, E.S. 1969. Solidification of ice dendrites in flowing supercooled water. Trans. metall. Soc. A.I.M.E., 245, 2069-2072.

Morris, L.R. and W.C. Winegard. 1969. The development of cells during the solidification of a dilute Pb-Sb alloy. J. Crystal Growth, 5, 361-375.

Mullins, W.W. and R.F. Sekerka. 1964. Stability of a planar interface during solidification of a dilute binary alloy. J. appl. Phys., 35(2), 444-451.

Nakawo, M. and N.K. Sinha. 1981. Growth rate and salinity profile of first year sea ice in the high Arctic. J. Glaciol., 27(96), 315-330.

Nazintsev, Yu L. 1974. Quantative relations in phase composition of sea ice. Problemy Arktiki i Antarktiki, 45, 76-83.

Neidrauer, T.M. and S. Martin 1979. An experimental study of brine drainage and convection in young sea ice. J. geophys. Res., 84(C3), 1176-1186.

NORCOR Engineering and Research Ltd. 1975. The interaction of crude oil with Arctic sea ice. Beaufort Sea Tech. Rep. No.27.

Paige, R.A. 1966. Crystallographic studies of sea ice in M^{c}Murdo Sound Antarctica. US Naval Civil Eng. Lab. Tech. Rep. R494, Port Hueneme, Calif., U.S.A., 31pp.

Perey, F.G.L. and E.R. Pounder. 1958. Crystal orientation in ice sheets. Can. J. Phys., 36, 494-502.

Perry, A.E., W.H.Schofield and P.N. Joubert. 1969. Rough wall turbulent boundary layers. J. Fluid Mech., 37(2), 383-413.

Peyton, H.R. 1963. Some mechanical properties of sea ice. In Ice and Snow, Properties, Processes and Applications, ed. W.D. Kingery. M.I.T. Press, Cambridge, Mass., U.S.A., 107-113.

Peyton, E.R. 1966. Sea ice strength. Final Rep. for Dept. of Navy, Office of Naval Research, Dec. 1966, Geophysical Inst., Univ. of Alaska, Fairbanks, U.S.A., 273pp.

Peyton, H.R. 1968. Sea-ice strength - effect of load rates and salt reinforcement. In Arctic Drifting Stations, ed. J.E. Sater. Proccedings of a Symposium, Warrenton, Virginia, U.S.A., April 1966, 197-217.

Phillips, O.M. 1977. The Dynamics of the Upper Ocean, Cambridge University Press, Cambridge, UK, 2nd ed., 336pp.

Pounder, E.R. 1963. Crystal growth as a function of orientation. In Ice and Snow, Properties, Processes and Applications, ed. W.D. Kingery. M.I.T. Press, Cambridge, Mass., U.S.A., 12-16 Feb. 1962, 226-231.

Pruppacher, H.R. and J.D. Klett. 1978. Microphysics of Clouds and Precipitation, D. Reidel Publishing Co., Dordrecht, Holland, 714pp.

Ramseier, R.O. 1968. Origin of preferred orientation in columnar ice. J. Crystal Growth, 3-4, 621-624.

Richardson, C. 1976. Phase relationships in sea ice as a function of temperature. J. Glaciol., 17(77), 507-519.

Richardson, C. and E.E. Keller. 1966. The brine content of sea ice measured with a nuclear magnetic resonance spectrometer. J. Glaciol., 6(43), 89-100.

Rohatgi, P.K. and C.M. Adams Jr. 1965. Solidification and separation of ice from saline water. Office of Saline Water, Research and Development Progress Rep. No.142, Dept. of the Interior, 71pp.

Rohatgi, P.K. and C.M. Adams Jr. 1967a. Ice-brine dendritic aggregate formed on freezing of aqueous solutions. J. Glaciol., 6(47), 663-680.

Rohatgi, P.K. and C.M. Adams Jr. 1967b. Freezing rate distributions during unidirectional solidification of solutions. Trans. metall. Soc. A.I.M.E., 239, 830-857.

Rohatgi, P.K. and C.M. Adams Jr. 1967c. Effect of freezing rates on dendritic solidification of ice from aqueous solution. Trans. metall. Soc. A.I.M.E., 239(11), 1729-1736.

Rohatgi, P.K., M.J. Surendar and C.M. Adams Jr. 1968. Dendritic crystallisation of ice from aqueous solutions. Ind. Engng Chem., 7(1), 72-79.

Rohatgi, P.K., S.M. Jain and C.M. Adams Jr. 1974. Effect of magnetic and electric fields on dendritic freezing of aqueous solutions of sodium

chloride. Material Science and Engineering, 5, 283-290.

Rutter, J.W. and B. Chalmers. 1953. A prismatic substructure formed during solidification of metals. Can. J. Phys., 31, 15-39.

Saito, T. and N. Ono. 1980. Percolation of sea ice II - Brine drainage channels in young sea ice. Low Temp Sci Ser. A, 39, 127-132 (English summary).

Samoilovich, Yu A. 1978. Heat exchange between the flow of a melt and the ingot crystallisation front. Fiz. Khim. Obrab. Mater., 6, 28-35 (Russian).

Schlichting H. 1968. Boundary Layer Theory, McGraw-Hill, New York, U.S.A., 6th ed., 748pp.

Schwarzacher, W. 1959. Pack-ice studies in the Arctic Ocean. J. geophys. Res., 64(12), 2357-2367.

Schwerdtfeger. P. 1963. The thermal properties of sea ice. J. Glaciol., 4(36), 789-807.

Scott, R.B. 1941. The calibration of thermocouples at low temperatures. In Temperature - Its Measurement and Control in Science and Industry, Proceedings of a Symposium, New York, U.S.A., Nov. 1939, 206-218.

Seidensticker, R.G. 1972. Partitioning of HCl in the wtare-ice system. J. chem. Phys., 56(6), 2853-2857.

Sekerka, R.F. 1965. A stability function for explicit evaluation of the Mullins-Sekerka interface stability criterion. J. appl. Phys., 36(1), 264-268.

Sekerka, R.F. 1968. Morphological stability. J. Crystal Growth, 3,4, 71-81.

Shumskii, P.A. 1955. Principles of Structural Geology, Dover Publications, New York, Air Force Cambridge Res. Lab., Bedford, Mass., U.S.A., Translation D. Krauss.

Sinha, N.K. 1977. Technique for studying structure of sea ice. J. Glaciol., 18(79), 315-323.

Smith, D.D. 1964. Ice lithologies and structure for ice island ARLIS II. J. Glaciol., 5(37), 17-38.

Smith, J.D. 1971. AIDJEX oceanographic investigations. AIDJEX Bulletin No.4, 1-7.

Smith, J.D. 1974. Oceanographic investigations during the AIDJEX lead experiment. AIDJEX Bulletin No.27, 125-134.

Snellen, J.B. and J.R. Rossiter. 1982. Remote estimation of the properties of sea ice, surfae truth measurements, Beaufort Sea, March 1979, C-CORE Publication (in press).

Sprenger, R.M. 1972. Continuous observations of the structural changes in deforming polycrystalline ice. Scientific Rep. N00014-67-A-0103-0007NR 307-252 Dept. of Atmos. Sci., Univ. of Washington, Seattle, Washington, U.S.A., 69pp.

Stallman, P.E. and K. Itagaki. 1976. Improved millivolt-temperature conversion tables for copper-constantan thermocouples. CRREL Special Rep. 76-18, 66pp.

Stander, E. and G.A. Gidney. 1980. The measurement of finite strain in sea ice by impulse radar. C-CORE Publication No.80-21, Proceedings of the Workshop on Sea Ice Field Measurements, ed. A.J. Allan and D.P.Bazeley, St. Johns, Nfld., Canada, 29 April-1 May 1980, 127-164.

Stehle, N.S. 1965. Ice engineering - Growth rate of sea ice in a closed system. US Naval Engng. Lab. Tech. Rep. 396, Port Hueueme, Calif., U.S.A., 25pp.

Stewart, M.J. and F. Weinberg. 1972. Fluid flow through a solid-liquid dendritic interface. Metallurgical Transactions, 3, 333-337.

Szckely, J. and A.S. Jassal. 1978. An experimental and analytical study of the solidification of a binary dendritic system. Metallurgical Transactions, 9B, 389-398.

Tabata, T. and N. Ono. 1957. On the structure of sea ice. Low Temp Sci Ser. A, 16 197-210 (Japanese with English summary).

Takahashi, T. 1981. Solidification and segregation of steel ingot. Proceedings of Sino-Japanese Symposium on Iron and Steel, Sept. 1981, The Chinese Society of Metals, Beijing, China, 6-10.

Takahashi, T., I. Hagiwara and K. Ichikawa. 1972. Significance of the solidifying zone on ingot solidification. Transctions Iron and Steel Institute Japan, 12, 412-421.

Takahashi, T., K. Ichikawa, K. Masayuki and K. Shimahara. 1976. The effect of fluid flow on the macrosegregation in steel ingot. Transactions Iron and Steel Institute Japan, 16, 283-292.

Takahashi, T., K. Ichikawa and M. Kudou. 1979. Effect of fluid flow on macrosegregation in steel ingots. In Solidification and Casting of Metals, Proceedings of an International Conference on Solidification, 18-21 July 1977, Sheffield, UK, 331-333.

Thorndike, A.S., D.A. Rothrock, G.A. Maykut and R. Colony. 1975. The thickness distribution of sea ice. J. geophys. Res., 80(33), 4501-4513.

Tiller, W.A. and S. O'Hara. 1968. On the mechanisms of crystal multiplication during solidification in the presence of fluid motion Part 2. In The Solidification of Metals, ed. B.W. Berry, Proceedings of a Conference, 4-7 Dec. 1967, Iron and Steel Institute Publication 110, 28-36.

Townsend A.A. 1976. The Structure of Turbulent Shear Flow, Cambridge University Press, Cambridge, UK, 2nd ed., 429pp.

Turnbull D. 1953. The kinetics of precipitation of barium sulphate from aqueous solution. Acta metall., 1, 684-691.

Turner, J.S. 1973. Buoyancy Effects in Fluids, Cambridge University Press, Cambridge, UK, 368pp.

Untersteiner, N. 1967. Natural desalination and equilibrium salinity profile of old sea ice. In Physics of Snow and Ice, ed. H. Oura. Proceedings of International Conference on Low Temperature Science, 14-19 Aug. 1966, Sapporo, Japan, 569-610.

Vant, M. 1976. Combined Theoretical and Empirical Study of the Dielectric Properties of Sea Ice over the Frequency Range 100 MHz - 40 GHz. PhD Dissertation, Carlton Univ., U.S.A.

Vittoratos, E.S. 1979. Existence of oriented sea ice by the Mackenzie Delta. In Port and Ocean Engineering under Arctic Conditions 79, Proceedings of a Conference, 13-18 Aug. 1979, Trondheim, Norway, 643-650.

Wadhams, P. 1980. Ice characteristics in the seasonal sea ice zone. Cold Regions Science and Technology, 2, 37-87.

Wakatsuchi, M. 1974. Experiments on the growth of sea ice and the rejection of brine. Low Temp Sci Ser. A, 32, 195-205 (Japanese with English summary).

Wakatsuchi, M. 1977. Experiments on haline convection induced by freezing of sea water. Low Temp. Sci Ser. A, 35, 249-258, (Japanese with English summary).

Walker, E.R. and P.Wadhams. 1979. Thick sea-ice floes. Arctic, 32(2), 140-147.

Weber, J.E. 1977. Heat and salt transfer associated with the formation of sea-ice. Tellus, 29, 151-160.

Webb, R.L., E.R.G. Eckert and R.J. Goldstein. 1971. Heat transfer and friction in tubes with repeated rib-roughness. Int. J. Heat Mass Transfer, 14, 601-617.

Weeks, W.F. 1958. The structure of sea ice : a progress report. In Arctic Sea Ice, Proceedings of a Conference, Easton, Maryland, 24-27 Feb. 1958,

Publication 598, National Academy of Sciences/National Research Council, Washington D.C., U.S.A., 96-99.

Weeks, W.F. 1962. Tensile strength of NaCl ice. J. Glaciol., 4(31), 25,52.

Weeks, W.F. 1966. Understanding the variations in the physical properties of sea ice. Symposium on Antarctic Oceanography, 13-16 Sept. 1966, Santiago, Chile.

Weeks, W.F. 1982. The physical properties of the sea ice cover of the Greenland Sea. CRREL Tech. Rep., in press.

Weeks, W.F. and D.L. Anderson. 1958. An experimental study of the strength of young sea ice. Trans. Am. geophys. Un., 39(4), 641-647.

Weeks, W.F. and A. Assur. 1963. Structural control of the vertical variation of the strength of sea and salt ice. In Ice and Snow, Properties, Processes and Applications, ed W.D. Kingery, M.I.T. Press, Cambridge, Mass., U.S.A., 258-276.

Weeks, W.F. and A.Assur. 1967. Mechanical properties of sea ice. CRREL Res. II-C3, 80pp.

Weeks, W.F. and G.F.N. Cox. 1974. Laboratory preparation of artificial sea and salt ice. CRREL Special Rep. 206, 10pp.

Weeks, W.F. and A.J. Gow. 1978. Preferred crystal orientations along the margins of the Arctic Ocean. J. geophys. Res., 84(C10), 5105-5121.

Weeks, W.F. and A.J. Gow. 1980. Crystal alignments in the fast ice of Arctic Alaska. J. geophys. Res., 85(C2), 1137-1146.

Weeks, W.F. and A.J. Gow. 1982. The growth, structure and properties of sea ice. Proceedings of NATO Advanced Study Institute on Air-Sea-Ice Interaction, Maratea, Italy, in press.

Weeks, W.F. and W.L. Hamilton. 1962. Petrographic characteristics of young sea ice, Point Barrow, Alaska. Am. Miner., 47, 945-961.

Weeks, W.F. and O.S. Lee. 1958. Observations on the physical properties of sea ice at Hopedale, Labrador. Arctic, 11(3), 135-155.

Weeks, W.F. and O.S. Lee. 1962. The salinity distribution in young sea ice. Arctic, 15(2), 92-108.

Weeks, W.F. and G. Lofgren. 1967. The effective distribution coefficient during the freezing of NaCl solutions. In Physics of Snow and Ice, ed H. Oura, Proceedings of an International Conference on Low Temperture Science, Sappora, Japan, 579-597.

Wilson, H.P. 1974. Winds and currents in the Beaufort Sea. In The Coast and Shelf of the Beaufort Sea, ed J.C. Reed and J.E. Sater, Arctic Institute of North America, Washington, D.C., 13-23.

Wimbush, M. and W. Munk. 1971. The benthic boundary layer. In The Sea Volume 4. Part 1, ed A.E. Maxwell, Wiley and Sons, New York, U.S.A., 791pp.

Winsor, W.D. and B.R. LeDrew. 1978. Ice feature characterisation.- Labrador offfshore. Field data report 14. C-CORE Publication 78-4, 50pp.

Wolf, A.V., G.B. Morden and P.G. Prentiss. 1978. Concentrative properties of aqueous solutions. C.R.C. Handbook of Chemistry and Physics, 59th ed.

Woodruff, D.P. 1973. The Solid-Liquid Interface, Cambridge University Press, Cambridge, U.K., 182pp.

World Meteorological Organisation. 1970. W.M.O. Sea-Ice Nomenclature, Published by the Secretariat of the World Meteorological Society , Geneva, Switzerland.

Wu, R.S. and K.C. Cheng. 1976. Thermal instability of Blasius flow along horizontal plates. Int. J. Heat Mass Transfer, 19, 907-913.

Yaglom, A.M. and B.A. Kader. 1974. Heat and mass transfer between a rough wall and turbulent fluid flow at high Reynolds and Peclet numbers. J. Fluid Mech., 62(3), 601-623.

Zotikov, I.A., V.S. Zagorodnov and J.V. Raikovsky. 1980. Core drilling through the Ross Ice Shelf (Antarctia) confirmed basal freezing. Science, 207(4438), 1463-1465.